Volume 2, No. 1 March 1955

P.7
125
141

RECORDS OF OCEANOGRAPHIC WORKS IN JAPAN

New Series

Being the continuation of the
RECORDS OF OCEANOGRAPHIC WORKS IN JAPAN, Vol. 12, No. 2

Compiled by
Pacific Science Liaison Committee
of
Science Council of Japan

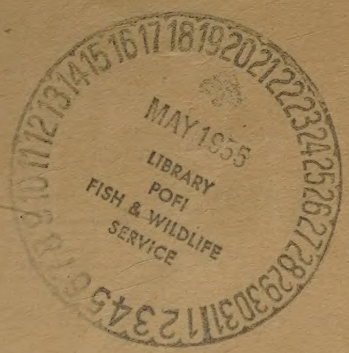

Published by
Japanese National Commission for Unesco
(4-3 Kasumigaseki, Chiyoda-ku, Tokyo, Japan)

BOARD OF EDITORS

Editor-in-Chief

Shinkishi Hatai

Editors

Yoshio Hiyama — Kōji Hidaka
Yasuo Miyake — Hiroshi Niino

With

the Co-operation of

(Physical Oceanography)
Kōji Fukutomi — Shōichirō Hayami
Mashito Nakano — Tadayoshi Sasaki
Kanji Suda — Ryūtarō Takahashi
Michitaka Uda

(Chemical Oceanography)
Masayoshi Ishibashi — Yasuo Matsudaira
Ken Sugawara

(Geological Oceanography)
Shōzaburō Hanzawa

(Biological Oceanography)
Denzaburō Miyadi — Yo K. Okada
Isao Taki — Yukio Yamada

(Fisheries)
Hiroaki Aikawa — Motosaku Fujinaga
Takeo Imai

Secretary

Buei Araya

SUGGESTION TO AUTHORS OF PAPERS FOR THE RECORDS OF OCEANOGRAPHIC WORKS IN JAPAN

An author wishing to contribute a paper to the RECORDS OF OCEANOGRAPHIC WORKS IN JAPAN should submit in compliance with the following suggestions :

1. Manuscripts will be accepted within the scope of
   Physical oceanography
   Geological oceanography
   Chemical oceanography
   Biological oceanography and
   Fisheries
2. An original and a copy of his munuscript should be type-written, doubld-spaced in 21×29.5 cm paper, within 12 sheets, making 6 printed pages including plates and tables.
3. The manuscript should be addressed to the competent editor and mailed to the official in charge of the Japanese National Commission for Unesco, 4-3 Kasumigaseki, Chiyoda-ku, Tokyo, Japan.
4. The author is asked to follow this publication for forms of headings and references, etc.
5. The editors reserve the right to accept the manuscripts and to make minor editorial changes in them, so that all papers may conform to over-all style of this publication.

CONTENTS

A Study on the Foaming of Sea Water–
On the Mechanism of the Decay of Foams and their Size Distribution in Foam Layer of Sea Water ..... ABE, Tomosaburo··· 1

Upwelling induced by a circular wind system ···HIDAKA, Koji and AKIBA, Yoshio··· 7

On the Vertical Distribution of Density and Upwellings in a Cold Water Mass ..... HIKOSAKA, Shigeo··· 19

Decay of the Large Horizontal Eddies in the Ocean..... IWATA, Kenko··· 23

Simple Method of Investigation of Tidal Current in Narrow Channel and its Application to Ki-i Suido, Japan ..... IWATA, Kenko··· 29

On the distribution of the radio activity in the sea around Bikini Atoll in June, 1954··· MIYAKE, Yasuo, SUGIURA, Yoshio and KAMEDA, Kazuhisa··· 34

On the Content of Rudidium and Cesium in Sea-Water ..... ISHIBASHI, Masayoshi and HARA, Tadashi···45

Generation of the Tsunami in Compressible Water (Part II) ··· MIYOSHI, Hisashi··· 49

On the Vertical Distribution of the Intensity of Illumination in the Water and Water Temperature of Lake Ashinoko..... SASAKI, Tadayoshi, OKAMI, Noboru WATANABE, Seiichi and ŌSHIBA, Gohachirō··· 57

On the Antarctic Circumpolar Current ..... TAKANO, Kenzo··· 71

An Example of Thermal Convective Current ..... TAKANO, Kenzo··· 76

Sur la Dimension des Tourbillons Cellulaires dans les Expériences de Henri Bénard ..... TAKANO, Kenzo··· 80

Sur les Tourbillons Thermoconvectifs dans la Nappe Fluide Horizontale Chauffée par en dessous ..... TAKANO, Kenzo··· 87

Sur la Différence Critigue de Température dans les Expérieacse de Douchan Avsec au Sujet des Courants Thermoconvectifs ..... TAKANO, Kenzo··· 93

Sur les Courants Thermoconvectifs dans la Nappe Fluide Horizontale Chauffée par en dessous ..... TAKANO, Kenzo··· 97

The Relation between Chlorinity and Sillicate Concentration of Water Observed in Some Estuaries ..... MAKIMOTO, Hironari, MAEDA, Hiroshi and ERA, Shitoku··· 106

Seasonal Difference in the Amount of the Inorganic Phosphorus in Blood Serum of Fishes ..... ICHIKAWA, Ryushi··· 113

A new species of copepod, *Scolecithricella vespertina* from the Sea of Japan ..... TANAKA, Otohiko··· 117

Preface to the Reports of the Oceanographical and Biological Survey of the Kuroshio ..... HIDAKA, Koji··· 121

Hydrographic Survey in the Equatorial Pacific Ocean, the South China Sea and the Formasa-Satsunan Kuroshio Region ..... ISHINO, Makoto··· 125

Preliminary Report on the Kuroshio in the Eastern Sea of Japan (Currents and Water Masses of the Kuroshio System III) ..... MASUZAWA, Jotaro··· 132

On the Subtropical Convergence and the Currents in the North Western Pacific. ..... UDA, Michitaka··· 141

A Note on Forecasting Ocean Waves Caused by Typhoons ..... UNOKI, Sanae and NAKANO, Mashito··· 151

Markings on a Tidal Flat in Uranouchi Bay, Shikoku ..... HATAI, Kotora and MII, Hideo··· 162

Observations on the Tidal Flats in Uranouchi Bay, Kochi Prefecture, Shikoku, Japan ..... HATAI, Kotora and MII, Hideo··· 168

On a new Pacific flying-fish, *Prognichthys Sealei* retaining five unbranched fin-rays above in the pectoral throughout life ..... ABE, Tokiharu··· 185

Further Notes on the Brachynran Crustacea of the Hachijo Island··· SAKAI, Tsune··· 193

Distribution of Mopalioid Chitons in the Pacific ..... TAKI, Isao··· 202

Marine Plankton Copepods from Hachijo Island, Idzu Is., with Special Reference to their Vertical Distribution ..... MOTODA, Shigeru and ANRAKU, Masateru··· 210

Records of Oceanographic Works
in Japan, Vol. 2, No. 1,
March 1955

A Study on the Foaming of Sea Water.

——On the Mechanism of the Decay of Bubbles and their Size Distribution in Foam Layer of sea Water——

by
Tomosaburo Abe
(Oceanographic Laboratory, Meteorological Research Institute)

§ 1. Introduction

Existence of white-chops produced by wind has an important effect on Beaufort's scale. It is considered from our experimental results that the degrees of white-chops change with chlorinity of sea water, temperature and stability of foam. The experimental relationships among these factors have already been reported by Y. Miyake and T. Abe, and recently the mechanism of the decay of foam layer of sea water has been experimentally studied by the present author.

In the present paper, a discussion will be made on the phenomenon of decay from the standpoint of energy. A discussion will also be made on the frequency distribution of the size of bubbles in the foam layer.

§ 2. *Activation energy*

It has been experimentally obtained by the present author that the type of the decay of the bubbles in foam layer is formally that of the so-called "1-st order chemical reaction", and it seems to be possible to treat this decay phenomenon by means of an analogy with chemical kinetics which has been fully discussed by many authors. Thus we may consider the so-called activation energy in the case of the decay of bubbles, too.

Now consider a certain gaseous reaction, and let its velocity constant be K', say, then the equation of Arrhenius is written as follows;

$$\frac{dl_nK'}{dT}=\frac{A'}{RT^2} \quad \cdots\cdots(1)$$

where T is the absolute temperature, R the gas constant and A' the activation energy (i.e., the minimum disposable energy is a possibly effective reaction).

Integrating Eqn. (1) with respect to T, assuming A' as independent of T as Arrhenius did, we have

$$L_nK'=L_nC-\frac{A'}{RT} \quad \cdots\cdots(2)$$

where C is the characteristic constant of reaction. Plotting log K' against $\frac{1}{T}$

for observations over a sufficient range of temperatures, it is found that Eqn. (2) gives an adequate representation of the facts, that is, we can assume that there is a linear relation between log K' and $\frac{1}{T}$.

Then, from Eqn. (2) we have

$$A' = R \tan \alpha \quad \cdots\cdots (3)$$

Table 1

Concentration / Sea water temp.	Decay const. (k)					
	19.26‰ Cl.	18.46	16.04	14.42	12.82	9.63
29°C	0.143	0.170	0.166	0.137	0.145	0.200
21	0.124	0.128	0.099	0.131	0.109	0.214
14	0.071	0.071	0.084	0.094	–	–
5	0.071	0.047	0.058	0.049	–	0.097
"A"	146×10K	208×10K	150×10K	148×10K	–	100×10K

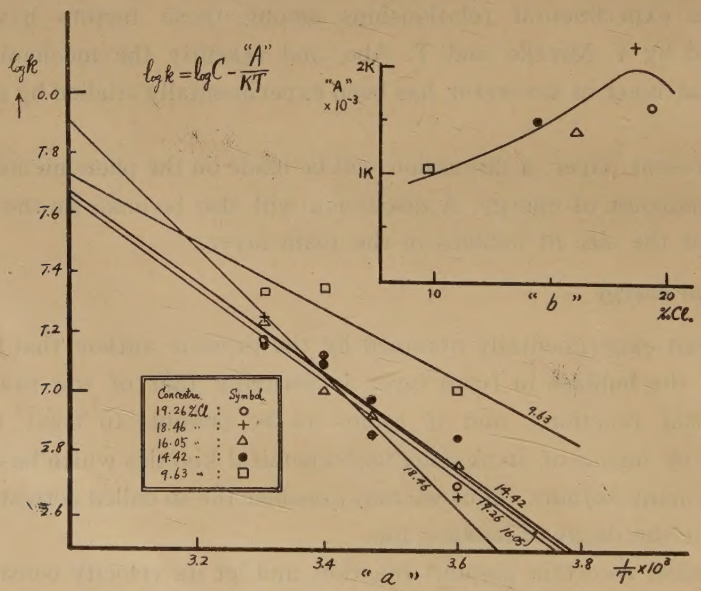

Fig. 1-a: Relation between the decay const. (k) and temp. (T) of sea water,
-b: Change of "A" with the Chlorinity of sea water

where α represents the gradient of the straight line.

We treated the experimental data on sea water in the same manner as mentioned above (Table 1, Fig. 1-a).

Fig. 1-a shows the relation between the decay constant (k) and temperature (T) in the case of sea water, that is, log k for five cases of concentrations have been plotted as functions of $\frac{1}{T}$, and they are mutually in linear relation approximately, and we obtained the values of "A" that correspond to A' in the

gaseous reactions as mentioned above, where R corresponds to K.

The values of "A" increases with increasing Cl concentration up to a certain maximum value and decreases with further increase of the concentration (see Fig. 1-b).

Since "A" is considered as necessary minimum amount of energy which activate a bubble to decay, the larger the Cl concentration of sea water, the smaller the amounts of bubbles which decay, but over a certain concentration they again decay easily.

§ 3. *Theoretical treatments of the frequency distribution of the size of bubbles.*

The author examines the process of forming of bubbles in foam layer in the case of his experiment.

The glass ampule containing sea water, was vibrated up and down by vibrating apparatus about constant frequency and amplitude, that is, energy was given to the system of sea water in a form of vibration. It is supposed that there are numerous micro heterogenious points in the system (i. e., heterogenious points of local density, temperature, concentration of chlorinity and of concentration of dessolved gases etc.) and they are distributed uniformly and at random in the system. Then, when the energy is given to the system, it is divided up in various ways and the various divisions of it accumulate properly into the heterogenious points and innumerable cracks are born in the system. That is, various sizes of bubbles are born in sea water. Though these bubbles react each other and then coagulations, decompositions and breakages sometimes occur, the rates of productions of bubbles become to be equal to that of disappearances, that is, the equilibrium of the state is reached. After this, the state of bubbles is statistically constant.

At the stationary state, the energy E (= ne) is given to the system of sea water for unit time (e is the energy of bubble which is produced in initial stage), and there are N bubbles in it (N is a large number).

From statistical point of view, he considered how to distribute the energy (ne) into the each of N bubbles in the system. The numbers of the ways of the distribution is distinctly $\frac{(n+N-1)!}{n!\,(N-1)!}$ (put $M_N(n)$ to it)

$$M_N(n) = \frac{(n+N-1)!}{n!\,(N-1)!} \quad \cdots\cdots(4)$$

Using this Fqn., the probability $P(x)$ which energy $x\,e$ is distributed to a certain bubble, is calculated ($x \geqq 0$).

Thus

$$P(x) = \frac{M_{N-1}(n-x)}{\sum_{x=0}^{n} M_{N-1}(n-x)} = \frac{M_{N-1}(n-x)}{M_N(n)} \quad \cdots\cdots(5)$$

Now, at the special case ($N \gg 1$, $xe \ll E$), the Eqn. (5) take the following simplified form:

$$P(x) \doteqdot \frac{N-1}{n+N}\left(\frac{n}{n+N}\right)^x \doteqdot \frac{1}{\bar{e}+1}\left(\frac{\bar{e}}{\bar{e}+1}\right)^x \quad \cdots\cdots(6)$$

where $\bar{e}$ is the mean energy of bubbles.

Though he wishes to obtain the actual values of frequencies of bubbles in the system of sea water at initial stage, this is a very difficult work in experiment. And so he satisfies, as the first approximation, with the values of those at the initial layer: those were obtained by extrapolation of the values of each size of bubbles, assuming that each bubble has decayed in exponential type.

Table 2, Frequencies of sizes of Bubbles. Sea water: 14.42‰Cl, 21°C

Range of dia. mm. (medion dia.) / Time sec.	0.~0.2 (0.1)	0.2~0.4 (0.3)	0.4~0.6 (0.5)	0.6~0.8 (0.7)	0.8~1.0 (0.9)	1.0~1.2 (1.1)	1.2~1.4 (1.3)	Total
2	48.1	24.1	17.9	3.65	4.74	–	0.73	
4	25.1	27.1	30.0	14.1	2.20	1.20	0.85	
6	23.2	30.4	20.5$_5$	10.7	4.47	0.89	1.79	
8	21.2	26.9	11.5	9.60	7.69	11.5	3.84	
10	15.0	25.0	10.0	35.0	5.00	–	5.0	
Initial value (obtained by extrapolation)	49.0	28.0	20.0	2.2	1.5	–	–	100.7

Now, the observed values of frequencies of sizes of bubbles of sea water having 14.42‰ Cl at 20 ± 1°C, are shown in Table 2. The values of the lowest column in the Table are those of P_{od} (i. e., initial frequency of bubble having dia. d) obtained by extrapolation of above values.

The bubbles are supposed to be spheres surrounded by thin membranes and energy of bubbles are preserved by those membranes in the form of surface energy (see Fig. 2).

Table 3

Range of dia. mm	median dia (d)	P_{od}	d^2	number (n)	nd^2
0~0.2	0.1	49.0	1×10^{-2}	0.49 N	0.49×10^{-2}N
0.2~0.4	0.3	28.0	9 〃	0.28 〃	2.52 〃
0.4~0.6	0.5	20.0	25 〃	0.20 〃	5.00 〃
0.6~0.8	0.7	2.2	49 〃	0.022 〃	1.08 〃
0.8~1.0	0.9	1.5	81 〃	0.015 〃	1.22 〃
	Total →	100.7		1.007 N	10.3 〃 ($=\Sigma nd^2$)

where N: Large number,
P_{od}: Initial frequency value of Bubble (dia. d).

If the total number of bubbles be N and the total surface energy of the system is equal to E (see Table 3),

$$E=2\sigma\pi\Sigma nd^2=2\sigma\pi\times 0.103\,N\,erg \quad \cdots\cdots(7)$$

where σ is the surface energy per unit area of a bubble.

The calculated value of σ at 21°C is 1.16 erg/mm².

Then, if the mean surface energy of bubble is $\bar{e}$, and its diameter $\bar{d}$,

$$\bar{e}=\frac{E}{N}=0.206\,\sigma\pi=0.75\,erg \quad \cdots\cdots(8)$$

$$\bar{d}=0.321\,mm \quad \cdots\cdots(9)$$

$$\text{or}\quad \bar{d}^2=0.103\,mm^2 \quad \cdots\cdots(9')$$

Accordingly, from Eqn. (6),

$$P(x)=\frac{1}{0.75+1}\left(\frac{0.75}{0.75+1}\right)^x=0.571\times 0.428^x \quad \cdots\cdots(6')$$

§ 4. *Comparison of the observed and theoretical values of* P_{od}

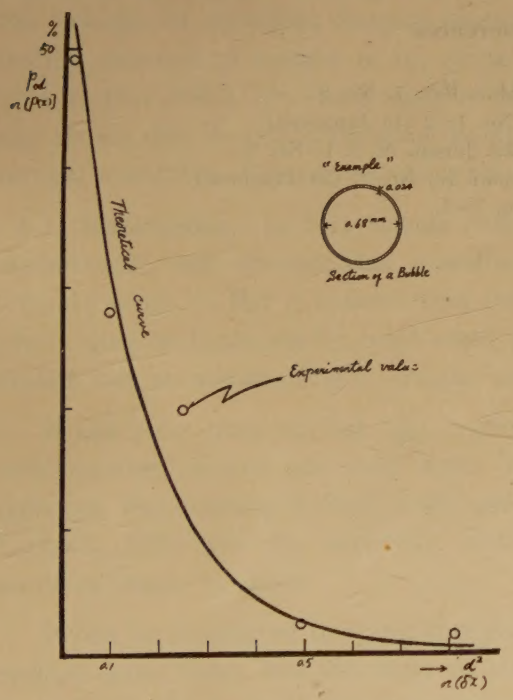

Fig. 2 Frequency Distribution of Theoretical and Experimental values

The quantities x and d^2 mentioned above, are that of proportional to the energy which bubble holds. The value of d^2 at which mean surface energy is $\bar{e}$, is 0.103 mm^2, and the frequency (P_{od}) of it is 29.2%. On the other hand, by the Eqn. (6′) the value of x at this frequency is obtained as follows, $x=0.789$.

The ratio $\delta\#$ of value of d^2 and that of x which holds the same frequency P_{od}, is $\frac{0.103}{0.789}$ or 0.130.

Thus, the relation between the P_{od} and d^2 or x is shown in Fig. 2. It is seen that the theoretical values of the frequencies calculated by statistical method agreed fairly well with those derived from experimental data.

§ 5. *Summary and conclusion*

1. In considering the process of the decay of foam layer of sea water, the author has introduced the same quantity "A" as the activation energy in chemical changes. Thus by using "A" he discussed the phenomenon. The quantity "A" increases with increasing concentration of sea water up to a

certain maximum, and then decreases with further increase of concentration (§ 2).

2. Also he discussed the frequency distribution of the size of bubbles in the foam layer by means of statistical methods; The theoretical values of the frequencies calculated by statistical methods agreed fairly well with those obtained by experiments; Thus it appears that it is possible to deal with the phenomenon of foaming by means of statistical methods or mathematical probability (§ 4).

Acknowledgement—The author wishes to express his sincere thanks to Dr. M. Nakano, Dr. Y. Miyake of this Institute, Prof. Dr. C. Tsuboi of Tokyo University and Prof. Dr. M. Uda of Tokyo University of Fisheries for their interest and encouragement throughout the study and he also wishes to thank to Mr. I. Kanazawa for his assistance in preparing the photographs used in this experiment.

References

Miyake, Y. and Abe, T., 1948 : Journ. Mar. Res. 7, No. 2.
Abe, T., 1953 : Oceanogr. Rep. CMO 3, No. 1~2 (in Japanese)
Abe, T., 1953 : Records. Oceanogr. Works. Japan. N. S. 1, No. 2.
Abe, T., 1954 : Journ. Oceanogr. Soc. Japan. 10, No. 1, (in Japanese)
Abe, T., 1954 : Pap. Met. Geophys. 5. No. 3~4.

Records of Oceanographic Works
in Japan, Vol. 2, No. 1,
March 1955

Upwelling Induced by a Circular Wind System

By

Koji Hidaka and Yoshio Akiba

(Geophysical Institute, Tokyo University)

Abstract: A theory of upwelling induced by a circular wind system is worked out. Assuming a simple distribution of wind stresses and taking the effect of Coriolis forces and both horizontal and vertical mixing into account, the hydrodynamical equations are solved. The results show that in the case of cyclonic wind system, upwelling is induced by convergent wind as well as divergent wind The velocity of upwelling depends upon the angle between the wind direction and the direction of tangent to the circle. And in case of convergent wind, the wind system which has small angle is more effective for the upwelling. It is also shown that vertical circulation occurs in a wide region in r-z plane and vertical variation of horizontal currents is similar to Ekman spiral.

§ 1 **Introduction.** In 1954 Hidaka (1954) treated the problem of upwelling theoretically, and showed that upwelling was induced by a longshore and offshore winds. But it appears that there are some phenomena of upwelling which must be explained by some other causes. As one of them we attempt to explain this phenomenon by a circular wind system.

It has been often noticed that typhoon changes the ocean currents, and anticlockwise vortices and cold water mass often appear after passing of typhoons. For instance, K. Suda (1943) and M. Uda (1949) suggested that Muroto Typhoon (1934) was the important motive of cold water mass located off southern coasts of Japan.

It can be considered that the divergence of surface water occurs where the cyclonic wind blows, and the water of lower layers upwells to compensate it. So, not only the typhoon but a stationary cyclonic wind system staying for some time in the same place due to the effects of topography will induce upwelling.

The present research treats such a problem mathematically and we obtain some quantitative conclusion concerning this process.

§ 2 **The theory of upwelling induced by a circular wind.**

Let us consider a wide homogeneous sea, and take cylindrical coordinates in

which z axis is taken vertically downwards. We assume that a circular wind is blowing steadily, and the wind stresses do not vary in θ-direction. Therefore all the vertical and horizontal components of currents can be determined as functions of r and z only, and the surface of the sea will have a slope in the r direction. We take the effect of the Earth's rotation and frictional forces due to vertical and horizontal mixing into account.

In such a case the hydrodynamical equations are,

$$\left.\begin{aligned} \frac{A_v}{\rho}\frac{\partial^2 u}{\partial z^2}+\frac{A_h}{\rho}\left\{\frac{\partial^2 u}{\partial r^2}+\frac{1}{r}\frac{\partial u}{\partial r}-\frac{u}{r^2}\right\}+2\omega\sin\varphi v-g\frac{\partial \zeta}{\partial r}&=0\\ \frac{A_v}{\rho}\frac{\partial^2 v}{\partial z^2}+\frac{A_h}{\rho}\left\{\frac{\partial^2 v}{\partial r^2}+\frac{1}{r}\frac{\partial v}{\partial r}-\frac{v}{r^2}\right\}-2\omega\sin\varphi u&=0\end{aligned}\right\} \quad (1)$$

where A_v and A_h are the coefficients of vertical and horizontal mixing of the sea water, u and v the horizontal components of the current velocity in r- and θ-directions, ζ the surface elevation, ω the angular velocity of the earth, φ the geographic latitude and ρ the density respectively.

In addition to them the equation of continuity is

$$\frac{\partial u}{\partial r}+\frac{u}{r}+\frac{\partial w}{\partial z}=0 \quad (2)$$

since $\frac{\partial v}{\partial y}=0$. In this equation w is the vertical component of currents and represents the intensity of upwelling.

In the equations (1) we neglect the terms of the centrifugal force, so that the solutions of eqations (1) are not valid at or close to the centre of the circle.

As the distribution of the wind stresses let us assume the following system,

$$\left.\begin{aligned} \tau&=\tau_m\frac{r}{r_m} \qquad \text{for} \quad 0<r<r_m\\ \tau&=\tau_m\frac{r_m}{r} \qquad \text{for} \quad r_m<r<\infty\end{aligned}\right\} \quad (3)$$

Where τ_m is the maximum stress, and r_m is the distance from the centre at which $\tau=\tau_m$. (Fig. 1)

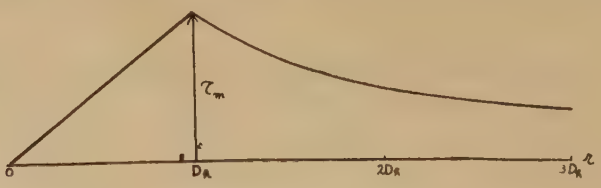

Fig. 1. Distribution of wind stresses

On the surface of the sea, the conditions to be satisfied are

$$\left.\begin{aligned} -A_v\frac{\partial u}{\partial z}&=\tau_r\\ -A_v\frac{\partial v}{\partial z}&=\tau\theta\end{aligned}\right\} \quad (4)$$

where τ_r, τ_θ are the stress components of the wind in r- and θ-directions, considered to be functions of r. At the bottom $z=h$ we must have

$$u = v = 0. \tag{5}$$

Next, we introduce the depth of frictional influence and "frictional distance" as follows

$$D_v = \pi\sqrt{\frac{A_v}{\rho\omega \sin\varphi}} \qquad D_h = \pi\sqrt{\frac{A_h}{\rho\omega \sin\varphi}} \tag{6}$$

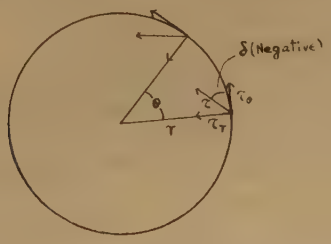

Fig. 2. Tangential and radial velocity

Then eqs. (1) become

$$\left.\begin{aligned} D^2\frac{\partial^2 u}{\partial z^2} + \left\{\frac{\partial^2}{\partial l^2} - \frac{1}{l}\frac{\partial}{\partial l} - \frac{1}{l^2}\right\}u - 2\pi^2 v - \frac{\pi^2 g}{\omega \sin\varphi D_h}\cdot\frac{\partial\zeta}{\partial l} &= 0 \\ D^2\frac{\partial^2 v}{\partial z^2} + \left\{\frac{\partial^2}{\partial l^2} + \frac{1}{l}\frac{\partial}{\partial l} - \frac{1}{l^2}\right\}v - 2\pi^2 u &= 0 \end{aligned}\right\} \tag{7}$$

where $l=r/D_h$.

In order to solve equations (7), we express u, v, $\frac{\partial\zeta}{\partial l}$, τ by the following Bessel-Fourier integrals:

$$\left.\begin{aligned} u &= \int_0^\infty \lambda u_1(z,\lambda)\ J_1(l\lambda)d\lambda \\ v &= \int_0^\infty \lambda v_1(z,\lambda)\ J_1(l\lambda)d\lambda \end{aligned}\right\} \tag{8}$$

$$\frac{\partial\zeta}{\partial l} = \int_0^\infty \lambda\beta(\lambda)\ J_1(l\lambda)d\lambda \tag{9}$$

$$\tau = \int_0^\infty \lambda T(\lambda)\ J_1(l\lambda)d\lambda \tag{10}$$

Let us introduce α such that

$$u_1 + iv_1 = \alpha \tag{11}$$

and substituting equations (8) (9) (10) (11) into equations. (7), the two equations of (7) are combined into

$$D_v^2\frac{d^2\alpha}{dz^2} - (\lambda^2 + 2\pi^2 i)\alpha - \frac{\pi^2 g}{\omega \sin\varphi D_h}\cdot\beta = 0 \tag{12}$$

and the boundary conditions to be satisfied become

$$\alpha = o \qquad \text{at} \quad z = h \tag{13}$$

$$-A_v\frac{d\alpha}{dz} = T(\lambda) \qquad \text{at} \quad z = 0 \tag{14}$$

The solution of (12) subject to the conditions (13) (14) is

$$\alpha = \frac{T(\lambda)}{\sqrt{\lambda^2+2\pi^2 i}} \cdot \frac{D_v}{A_v} \cdot \frac{\sinh\left(\sqrt{\lambda^2+2\pi^2 i}\,\frac{h-z}{D_v}\right)}{\cosh\left(\sqrt{\lambda^2+2\pi^2 i}\,\frac{z}{D_v}\right)}$$

$$+\frac{\pi^2 g\beta(\lambda)}{(\lambda^2+2\pi^2 i)\,\omega \sin\varphi\, D_h}\left\{1-\frac{\cosh\left(\sqrt{\lambda^2+2\pi^2 i}\,\frac{z}{D_v}\right)}{\cosh\left(\sqrt{\lambda^2+2\pi^2 i}\,\frac{h}{D_v}\right)}\right\} \tag{15}$$

and $u+iv \equiv W$ is given by

$$W=\int_0^\infty \lambda\left\{\frac{T(\lambda)}{\sqrt{\lambda^2+2\pi^2 i}} \cdot \frac{D_v}{A_v} \cdot \frac{\sinh\left(\sqrt{\lambda^2+2\pi^2 i}\,\frac{h-z}{D_v}\right)}{\cosh\left(\sqrt{\lambda^2+2\pi^2 i}\,\frac{z}{D_v}\right)}\right.$$

$$\left.+\frac{\pi^2 g\beta(\lambda)}{(\lambda^2+2\pi^2 i)\,\omega \sin\varphi\, D_h}\left\{1-\frac{\cosh\left(\sqrt{\lambda^2+2\pi^2 i}\,\frac{z}{D_v}\right)}{\cosh\left(\sqrt{\lambda^2+2\pi^2 i}\,\frac{h}{D_v}\right)}\right\}\right\} J_1(l\lambda)\,d\lambda \tag{16}$$

Next, we can obtain $T(\lambda)$ by Hankel-transformation of (10) as

$$T(\lambda)=\int_0^\infty l\tau J_1(l\lambda)\,dl \tag{17}$$

Substituting (3) into (17) we have

$$T(\lambda)=\frac{2\tau_m}{\lambda^2} J_1(a\lambda) \tag{18}$$

where $a=r_m/D_h$.

β can be also obtained from equations (2) and (16). If the depth of sea is large, (15) becomes

$$\alpha = \frac{T(\lambda)}{\sqrt{\lambda^2+2\pi^2 i}} \cdot \frac{D_v}{A_v} \cdot e^{-\sqrt{\lambda^2+2\pi^2 i}\; z/D_v}$$

$$+\frac{\pi^2 g\beta(\lambda)}{(\lambda^2+2\pi^2 i)\,\omega \sin\varphi\, D_h}\left\{1-e^{-\sqrt{\lambda^2+2\pi^2 i}\,\frac{(h-z)}{D_v}}\right\} \tag{19}$$

approximately.

Integrating eqation of continuity with respect to z from $z=0$ to $z=h$, we have

$$\frac{\partial}{\partial r}\int_0^h u\,dz+\frac{1}{r}\int_0^h u\,dz=-w\Big|_0^h=0, \tag{20}$$

since there are no vertical motions on the surface and at the bottom of the sea. With (20) and condition that there is no horizontal motion at the centre, we have

$$\int_0^h u\,dz=0. \tag{21}$$

Therefore, integrating (19) with respect to z from the surface down to the bottom, and equating the real part of the result to zero, we have

$$\beta(\lambda)=\frac{\frac{2\tau_m D_v^2}{A_v}}{\frac{\lambda^2}{2\pi^2}\left(h-\frac{P}{P^2+Q^2}D_v\right)+\frac{Q}{P^2+Q^2}D_v}\times\frac{J_1(a\lambda)}{\lambda^2} \tag{22}$$

§ 3 Upwelling in a deep sea.

When the depth of the sea is large enough, we have

$$\beta(\lambda)\to 0 \tag{23}$$

and

$$\alpha=\frac{2\tau_m}{\lambda^2\sqrt{\lambda^2+2\pi^2 i}}J_1(a\lambda)\ e^{-\sqrt{\lambda^2+2\pi^2 i}\frac{z}{D_v}} \tag{24}$$

From (8) (11) (24), we have

$$W=\frac{2D_v\tau_m}{A_v}\int_0^\infty \frac{J_1(a\lambda)\,J_1(l\lambda)}{\lambda}\cdot\frac{1}{\sqrt{\lambda^2+2\pi^2 i}}\cdot e^{-\sqrt{\lambda^2+2\pi^2 i}\frac{z}{D_v}}d\lambda. \tag{25}$$

If we separate the real part P of $\sqrt{\lambda^2+2\pi^2 i}$ from the imaginary Q we have

$$\left.\begin{aligned} P&=\sqrt{\frac{\sqrt{\lambda^4+4\pi^2}+\lambda^2}{2}},\\ Q&=\sqrt{\frac{\sqrt{\lambda^4+4\pi^2}-\lambda^2}{2}}. \end{aligned}\right\} \tag{26}$$

Thus (25) becomes

$$W=\frac{2D_v}{A_v}(\tau_{ml}+i\tau_\theta)\int_0^\infty \frac{J_1(a\lambda)J_1(l\lambda)}{\lambda}\left\{\frac{P}{P^2+Q^2}-i\frac{Q}{P^2+Q^2}\right\}$$
$$\times e^{-P\frac{z}{D_v}}\times\left\{\cos\left(Q\frac{z}{D_v}\right)-i\sin\left(Q\frac{z}{D_v}\right)\right\}d\lambda. \tag{27}$$

Thus the horizontal components of velocity are given by

$$\left.\begin{aligned} u&=\frac{2D_v}{A_v}\tau_{m\theta}K_1+\frac{2D_v}{A_v}\tau_{ml}K_2\\ v&=\frac{2D_v}{A_v}\tau_{m\theta}K_2-\frac{2D_v}{A_v}\tau_{ml}K_1 \end{aligned}\right\} \tag{28}$$

where K_1, K_2 are

$$\left.\begin{aligned} K_1&=\int_0^\infty R(l,\lambda)\ M(z,\lambda)\,d\lambda\\ K_2&=\int_0^\infty R(l,\lambda)\ N(z,\lambda)\,d\lambda \end{aligned}\right\} \tag{29}$$

and R. M. N are

$$R(l,\lambda)=\frac{J_1(a\lambda)J_1(l\lambda)}{\lambda}, \tag{30}$$

$$\left.\begin{aligned} M(z,\lambda)&=e^{-P\frac{z}{D_v}}\frac{\left\{P\sin\left(Q\frac{z}{D_v}\right)+Q\cos\left(Q\frac{z}{D_v}\right)\right\}}{P^2+Q^2},\\ N(z,\lambda)&=e^{-P\frac{z}{D_v}}\frac{\left\{P\cos\left(Q\frac{z}{D_v}\right)-Q\sin\left(Q\frac{z}{D_v}\right)\right\}}{P^2+Q^2} \end{aligned}\right\} \tag{31}$$

Equation of continuity can be rewritten as

$$\frac{1}{D_h}\cdot\frac{\partial}{\partial l}(ul)+\frac{\partial}{\partial z}(wl)=.\ O \tag{32}$$

If we define a function φ as

$$ul=-\frac{\partial\varphi}{\partial z};\qquad wl=\frac{1}{D_h}\cdot\frac{\partial\varphi}{\partial l}\ , \tag{33}$$

φ is given by

$$\varphi=\frac{2D_v^2}{A_v}\tau_{m\theta}\,\phi_\theta+\frac{2D_v^2}{A_v}\tau_{ml}\,\phi_l \tag{34}$$

where ϕ_θ, ϕ_l are

$$\left.\begin{aligned}\phi_\theta&=l\int_0^\infty R(l,\lambda)\ L_1(z,\lambda)d\lambda\\ \phi_l&=l\int_0^\infty R(l,\lambda)\ L_2(z,\lambda)d\lambda\end{aligned}\right\} \tag{35}$$

and L_1, L_2 are

$$\left.\begin{aligned}L_1=\frac{1}{(P^2+Q^2)^2}\Bigg\{&(P^2-Q^2)\left(\cos\left(Q\frac{z}{D_v}\right)e^{-P\frac{z}{D_v}}-1\right)\\&-2PQ\,e^{-P\frac{z}{D_v}}\sin\left(Q\frac{z}{D_v}\right)\Bigg\},\\ L_2=\frac{1}{(P^2+Q^2)^2}\Bigg\{&(P^2-Q^2)\sin\left(Q\frac{z}{D_v}\right)e^{-P\frac{z}{D_v}}\\&+2PQ\left(\cos\left(Q\frac{z}{D_v}\right)e^{-P\frac{z}{D_v}}-1\right)\Bigg\}.\end{aligned}\right\} \tag{36}$$

A function φ is not an ordinary stream function, but we can treat this function like a stream function, for the lines of φ=constant indicate stream lines.

The vertical component of velocity is now given by

$$\left.\begin{aligned}w=&\frac{1}{D_h}\cdot\frac{2D_v^2}{A_v}\tau_{m\theta}\cdot\frac{1}{l}\int_0^\infty R(l,\lambda)\ L_2(z,\lambda)d\lambda\\&+\frac{1}{D_h}\cdot\frac{2D_v^2}{A_v}\tau_{ml}\cdot\frac{1}{l}\int_0^\infty R(l,\lambda)\ L_1(z,\lambda)d\lambda\\&+\frac{1}{D_h}\cdot\frac{D_v^2}{A_v}\tau_{m\theta}\int_0^\infty S(l,\lambda)\ L_1(z,\lambda)d\lambda\\&+\frac{1}{D_h}\cdot\frac{D_v^2}{A_v}\tau_{ml}\int_0^\infty S(l,\lambda)\ L_2(z,\lambda)d\lambda\end{aligned}\right\} \tag{37}$$

where S is

$$S=J_1\ (a\lambda)\ \{J_0\ (l\lambda)-J_2\ (l\lambda)\} \tag{38}$$

§ 4 **Numerical examples.**

In the previous paragraph we obtained the expressions for the motion of water induced by a circular wind, and we can compute u, v, w, φ. from the

equations (28), (34) and (37) for any distance and any depth. We worked out numerical calculations for several cases. Let us take the values of D_v as 100 m, D_h as 100 km respestively, r as 100 km, φ as 30°N and for simplicity we take $\tau_m=1$ *c.g.s.* which corresponds to a wind velocity of 5 to 6 m/s.

At first we shall show values of K_1 K_2 ϕ_θ ϕ_l, for seoeral cases can be treated using these values. The values of K_1 K_2 ϕ_θ ϕ_l for several z/D_v and r/D_h are given in Table 1, 2, 3, 4.

Table 1 Values of $\phi_\theta \times 10^5$

z/D_h / z/D_v	2.	.4	.6	8	1.0	1.2	1.4	1.6	1.8	2.0
2	66	−236	−511	−842	−1146	−1388	−1433	−1514	−1480	−1454
.4	− 99	−384	−824	−1360	−1846	−2239	−2311	−2358	−2349	−2350
.6	−114	−432	−963	−1578	−2139	−2594	−2678	−2715	−2705	−2684
.8	−124	−487	−1040	−1691	−2275	−2726	−2772	−2766	−2704	−2644
1.0	−117	−460	−991	−1620	−2257	−2700	−2710	−2736	−2711	−2688
1.2	−112	−453	−972	−1593	−2155	−2597	−2678	−2685	−2650	−2614
1.4	−111	−446	−964	−1578	−2134	−2561	−2668	−2643	−2612	−2589
1.6	−110	−444	−958	−1570	−2120	−2553	−2654	−2627	−2597	−2562

Table 2. Values of $\phi_l \times 10^5$

r/D_h / z/D_v	.2	.4	.6	.8	1.0	1.2	1.4	1.6	1.8	2.0
.2	−37	−141	−330	−598	−825	−931	−861	−810	−747	−798
.4	−35	−137	−325	−612	−850	−922	−812	−736	−635	−650
.6	−22	−93	−242	−474	−660	−672	−532	−430	−311	−358
.8	−14	−64	−165	−346	−497	−464	−337	−256	− 90	−124
1.0	− 9	−37	−124	−280	−406	−416	−244	−155	+ 37	+ 6
1.2	− 7	−30	−109	−256	−375	−314	−204	− 22	+ 67	+ 36
1.4	− 7	−29	−107	−234	−372	−312	−225	− 21	+ 65	+ 34
1.6	− 7	−30	−109	−237	−376	−319	−237	− 32	+ 56	+ 24

Table 3. Values of $K_1 \times 10^4$

z/D_h / z/D_v	.2	.4	.6	.8	1.0	1.2	1.4	1.6	1.8	2.0
.0	+166	+325	+470	+583	+634	+642	+565	+504	+448	+401
.2	+125	+345	+358	+435	+472	+478	+422	+377	+335	+301
.4	+ 63	+124	+178	+217	+235	+237	+208	+185	+163	+145
.6	+ 22	+ 43	+ 61	+ 73	+ 76	+ 75	+ 64	+ 39	+ 47	+ 40
.8	+ 1	+ 3	+ 4	+ 5	+ 4	+ 1	− 2	− 4	− 6	− 7
1.0	− 5	− 9	− 14	− 15	− 17	− 19	− 19	− 19	− 18	− 17
1.2	− 4	− 6	− 11	− 13	− 15	− 16	− 16	− 15	− 14	− 13
1.4	− 2	− 5	− 6	− 8	− 8	− 10	− 8	− 8	− 7	− 7
1.6	− 1	− 2	− 3	− 3	− 3	− 3	− 3	− 3	− 2	− 2

Table 4. Values of $K_2 \times 10^4$

r/D_h / z/D_v	.2	.4	.6	.8	1.0	1.2	1.4	1.6	1.8	2.0
.0	+143	+334	+511	+696	+781	+733	+519	+506	+447	+398
.2	+ 27	+ 58	+ 98	+129	+143	+125	+ 90	+ 67	+ 50	+ 46
.4	− 24	− 45	− 59	− 67	− 74	− 86	− 92	− 84	− 78	− 74
.6	− 29	− 55	− 74	− 91	− 100	−107	−100	− 95	− 87	− 79
.8	− 18	− 35	− 48	− 58	− 63	− 66	− 61	− 57	− 51	− 46
1.0	− 8	− 18	− 22	− 26	− 27	− 28	− 26	− 23	− 21	− 18
1.2	− 2	− 4	− 6	− 8	− 8	− 6	− 5	− 4	− 3	− 3
1.4	+ 0	+ 1	+ 1	+ 1	+ 2	+ 2	+ 2	+ 3	+ 3	+ 3
1.6	+ 1	+ 2	+ 2	+ 3	+ 3	+ 3	+ 3	+ 3	+ 3	+ 3

Let us consider δ to be the angle between the wind direction and the direction of tangent to the circle, being positive when it is clockwise. Then the motion of water is expected to depend upon this angle (Fig. 2)

In case of $\delta = +90°$ the wind stresses are divergent and upwelling will occur there. If δ is $-90°$, namely, in case of a convergent stress there will occur the sinking of water, but comparing ϕ_θ and ϕ_l, we are aware of the fact that the values of ϕ_θ are larger than that of ϕ_l, so it may be anticipated that upwelling will occur for a negative δ. We shall treat, therefore, two cases $\delta = 0$ and $\delta = 45°$ separately.

Case 1 $\delta = 0$

If the wind blows in positive θ-direction, r-component of wind stress becomes zero, and in this case the lines of $\phi_\theta =$ constant in r-z plane indicate the projective circulation patterns and the lines of $K_2 =$ constant indicate the vertical variatiton of v, the θ-component of the horizontal velocity.

Circulation patterns in this case are illustrated in Fig 3 and Fig. 4

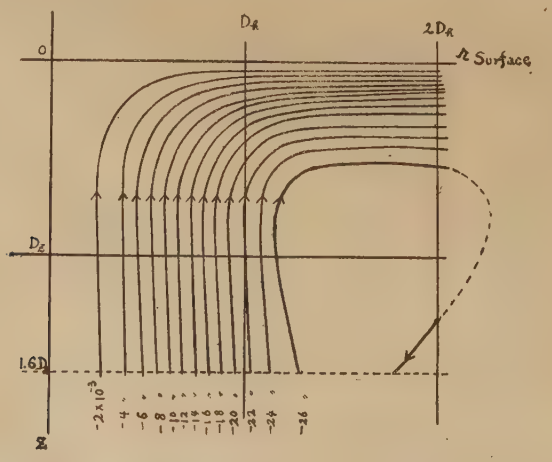

Fig 3. Upwelling as induced by a circular wind ($\delta = o$)

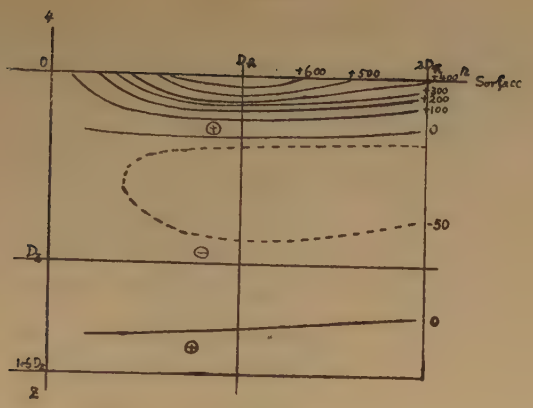

Fig 4. Distribution of horizontal currents

From these figures we can see that the upwelling occurs mainly within the distance $r=D_h$ from the centre of circle. The water in this region upwells along the spiral courses from the layer $z=1.6\,D_v$ or more, and diverges at a point close to the surface. The stream lines outside the distance $r=2D_h$ may go down gradually and a clockwise circulation would be formed in a wide region of the vertical plane.

The values of the vertical velocity component w which represent the intensity of the upwelling can be obtained from the function φ. Table 5 shows the values of w for several r/D_h and z/D_v.

Table 5. Values of $w\times10^3$ cm/sec upward ($\delta=0$, $\tau_m=1\,cgs$)

r/D_h / z/D_v	.2	.4	.6	.8	1.0	1.2
.2	.89	1.15	1.24	1.12	.82	.62
.4	1.34	1.92	1.98	1.81	1.31	.88
.6	1.54	2.15	2.39	2.08	1.51	1.02
.8	1.67	2.32	2.58	2.20	1.58	1.01
1.0	1.58	2.31	2.39	2.21	1.84	.74
1.2	1.51	2.30	2.34	2.16	1.52	.99
1.4	1.51	2.24	2.34	2.10	1.50	.96
1.6	1.50	2.23	2.33	2.08	1.49	.97

The maximum values of w can be seen near at $r=0.6\,D_h$, and its value is about 2.4×10^{-3} cm/sec, which corresponds to 2.1 m/day. This value is reasonable. The horizontal velocity can be calculated from equation (28), and the angle between the wind and the surface currents can also be obtained. Table 6 shows the angle for several distaces from the centre.

Table 6. Angle between the wind and surface currents.

r/D_h	.2	.4	.6	.8	1.0	1.2	1.4	1.6	1.8	2.0
angle	49°.3	44°.2	42°.6	40°.0	39°.3	41°.2	43°.7	44°.9	45°.1	45°.2

The angles decrease from the centre to the maximum stress distance and increase outside this distance. This angle variation may be due to the special structure of the assumed wind system.

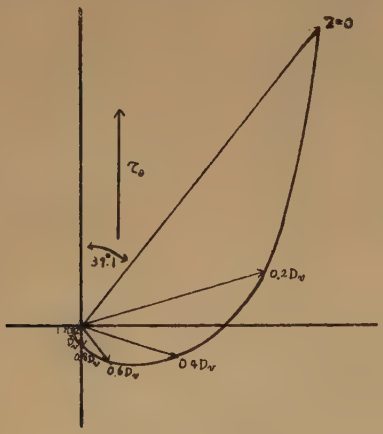

Fig 5. Vertical variation of drift currents.

The vertical variation of the drift currents is known as we can calculate u and v for any depth. As an example, we shall show the variation at $r=D_h$. Figure 5 illustrates how the drift currents change with the depth and the arrows indicate the velocity for $z=0.2\,D_h$, $z=0.4\,D_h$ etc. The pattern of variation is similar to Ekman spiral. For any other distance, the variation shows similar pattern.

Case 2. $\delta=-45°$

In case $\delta=-45°$, namely the wind blows in an inward directison like in a typhoon, the components of stresses in r- and θ-directions have the same values. So we can calculate the values of the function ϕ in this case ($\equiv\phi_{-45°}$), taking τ_r and τ_θ equal in the equations (28), (34). The values of ϕ_{-45}. are given in Table 7.

Table 7. Values of $\phi_{-45°}\times10^5$

r/D_h / z/D_v	.2	.4	.6	.8	1.0	1.2	1.4	1.6	1.8	2.0
.2	−17	− 67	−128	−172	− 228	− 331	− 405	− 498	− 544	− 482
.4	−45	−174	−355	−529	− 704	− 931	−1060	−1147	−1211	−1202
.66	−65	−240	−510	−780	−1044	−1300	−1515	−1558	−1692	−1672
.8	−80	−299	−619	−951	−1259	−1583	−1722	−1774	−1849	−1778
1.0	−76	−299	−613	−947	−1295	−1606	−1744	−1826	−1937	−1889
1.2	−75	−299	−610	−946	−1259	−1614	−1749	−1874	−1921	−1974
1.4	−75	−294	−605	−940	−1246	−1590	−1728	−1854	−1892	−1855
1.6	−74	−291	−600	−932	−1233	−1582	−1709	−1835	−1876	−1872

The circulation patterns are illustrated in Fig. 6.

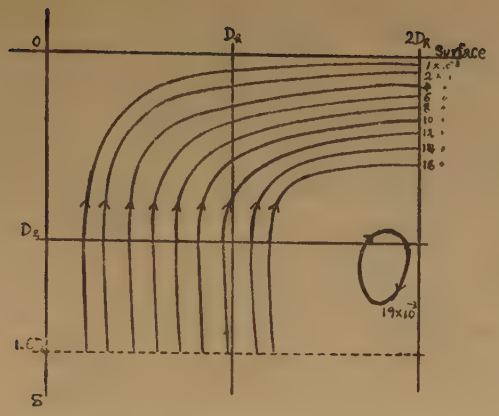

Fig 6. Upwelling as induced by a circular wind ($\delta=-45°$)

In this case, we have the similar circulation patterns as in the former case, but it seems that the region of upwelling extends much further. The velocity of upwelling is smaller than in the former case.

Table 8 shows the velocity of upwelling for $\tau_m=1$ *c.g.s.*

Table 8 Values of $w\times10^3$ cm/sec upward ($\delta=-45°$ $\tau_m=1$ *c.g.s*)

z/D_v \ r/D_h	.2	.4	.6	.8	1.0	1.2
.2	.23	.34	.27	.15	.15	.23
.4	.61	.87	.81	.59	.47	.51
.6	.88	1.18	1.22	.90	.71	.58
.8	1.08	1.48	1.44	1.12	.82	.73
1.0	1.02	1.50	1.43	1.13	.96	.70
1.2	1.03	1.51	1.40	1.14	.85	.80
1.4	1.03	1.48	1.40	1.14	.80	.77
1.6	1.03	1.46	1.40	1.43	.79	.77

The maximum value of upwelling (which appears near at the distance $r=0.6\,D_h$) is 1.5×10^{-3} cm/sec or 1.3 m/day. These are the values for $\tau_m=1$ *c.g.s.*, so these values will be increased if the muximum wind stress take a larger value. In the case of typhoon, the value of maximum stress is by far greater than 1 c. g. s., and the velocity of upwelling may take sometimes a value ten times as large. However, considering the fact that the states of the sea change within rather short time, this value will be consistent.

Comparing both cases, we learn that case 1 is more effective for the upwelling. Generally speaking, in the case of convergent wind, wind system which has smaller δ can be considered to be more effective for the upwelling.

References

Hidaka, K : A contribution to the theory of upwelling and coastal currents. T. A. G. U. 35 (3) pp 431-444, 1954.

Suda, K : "Kaiyo Kagaku" (Oceanography) 1943. pp. 720.

Syôji, D : The variations of oceanic currents in the adjacent seas of Japan. "Suiro Yôhô" (Hydrographic Bulletin) No. 25 pp. 230-244, 1951

Uda, M : On the correlated fluctuation of the Kurosio currents and cold water mass. The Oceanographical Magazine Vol. 1. No. 1 pp. 1-12, 1949.

Gray and Mathews : Treatise on Bessel Function. London, 1922.

Records of Oceanographic Works
in Japan, Vol. 2, No. 1,
March 1955

On the Vertical Distributions of Density and Upwellings in a Cold Water Mass

By

Shigeo Hikosaka

(Hydrngraphic Office, Maritime Safety Board)

Abstract: In this paper, we estimated the mean velocity of upwelling using the observed actual temperature-distributions in a cold waters and then calculated the vertical distributions of density in a upwelling region. The results are in good agreement with the observed density-distributions excepting the layers near the surface.

1. *Introduction* : The many oceanographers in Japan have investigated the cold waters in the Kuroshio. In the previous paper, the present author calculated the velocity of upwelling using the actual temperature distributions in a cold waters and it was found the order was about 10^{-3} assumed the coefficient of vertical diffusion 10. In this paper, we determind the vertical distributions of density in the cold waters existing the upwellings. According to the results, the calculated density distributions are in good agreement with the actual observed values.

2. *Temperature Distributions and Upwellings*: We assume that the vertical distributions of temperature in the cold waters is governed by the following equation

$$w \frac{\partial T}{\partial z} = A_z \frac{\partial^2 T}{\partial z^2} \tag{1}$$

where, w is the vertical velocity,

A_z the coefficient of vertical diffusion,

T water temperature,

and z axis is taken positive downwards.

From the equation (1), we get

$$w \Big/ A_z = \frac{\partial^2 T}{\partial z^2} \Big/ \frac{\partial T}{\partial z} = \frac{\partial}{\partial z} l_n \frac{\partial T}{\partial z} \tag{2}$$

Integrating the above equation with z from z_1 to z_2,

$$l_n \frac{\partial T}{\partial z} \Big/_{z_2} - l_n \frac{\partial T}{\partial z} \Big/_{z_1} = \int_{z_1}^{z_2} \frac{w}{A_z} dz \tag{3}$$

If we write the mean value of w/Az between z_1 and z_2 depth as $\overline{w/Az}$, the equation (3) can be written

$$l_n \frac{\partial T}{\partial z}\Big/_{z_2} - l_n \frac{\partial T}{\partial z}\Big/_{z_1} = (z_2 - z_1)\overline{\frac{w}{Az}} \tag{4}$$

Fig. 1 shows the vertical distribution of temperature at St. 5 (about center of the cold water region) by the Osyoro Maru, in summer, 1939. From the equation (4), we calculated the mean velocities of upwelling and the values are tablated in Table 1. Fig. 2 shows the histogram of the mean velocities of upwelling. The water temperatures near the surface, however, have the diurnal variations, so we omitted this calculations at the layers between the surface and 50 m depth. In general, the vertical velocity at the surface can be considered zero if the surface elevation is neglected in the steady states. So that, we assume the vertical distribution of upwelling is expressed by the equation $\partial z e^{-\alpha z}$. The heavy line in Fig. 2 was determined by the least square method and the curve is expressed by

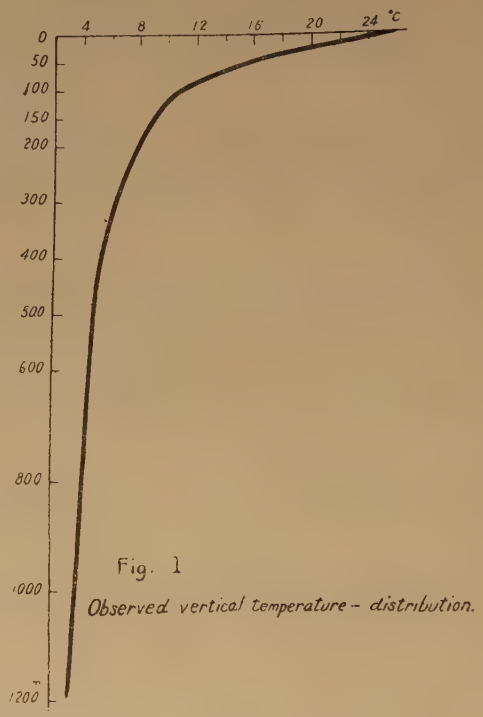

Fig. 1
Observed vertical temperature - distribution.

$$-\frac{w}{Az} = 1.905 \times 10^{-8} z \; e^{-0.682 \times 10^{-4} z} \tag{5}$$

where the units are taken in c. g. s.

3. *Vertical Distributions of Density*: As above mentioned, we neglect the terms of the lateral mixings and the lateral advections. Then, the vertical distributions of density are governed by the following equation

$$w \frac{\partial \sigma_t}{\partial z} = A_z \frac{\partial^2 \sigma_t}{\partial z^2}$$

$$\therefore \quad \frac{w}{Az} = \frac{\partial}{\partial z} l_n \frac{\partial \sigma_t}{\partial z} \tag{6}$$

Substituting from (5) into (6),

$$\frac{\partial \sigma_t}{\partial z} = A a^{e^{-\alpha z}} (\alpha z + 1) \tag{7}$$

where a and α are the constants and A is an integration constant.

Integrating the equation (7) with z from z_1 to z_2,

$$\sigma_t \Big|_{z_2} - \sigma_t \Big|_{z_1} = A \int_{z_1}^{z_2} a^{e^{-\alpha z}(\alpha z+1)}\, dz \qquad (8)$$

It seems to be not able to integrate the right hand side of the equation (8), but the curve of $a^{e^{-\alpha z}}(\alpha z+1)$ can be drawn as shown in Fig. 3. So, we can obtain the value of integration on a diagram. Write the density at the surface and 1200 m depth as $\sigma_t/_0$ and $\sigma_t/_{1200}$ respectively, the value of A can be determined by the equation

$$A = \frac{\sigma_t/_{1200} - \sigma_t/_0}{\int_0^{1200} a^{e^{-\alpha z}}(\alpha z+1)\, dz} \qquad (9)$$

Then, we can calculate the density σ_t at any depth substituting (9) into (8).

In Fig. 4, the full line shows the density-distributions by the such method and × marks are actual observed values of density, and we see the both value is in good agreement excepting the layers near the surface.

Table 1.

layer	$\frac{\overline{w}}{A_z}\times 10^4$	layer	$\frac{\overline{w}}{A_z}\times 10^4$
50—100m	−1.43	300—400m	−0.336
100—150	−1.39	400—500	−0.223
150—200	−1.21	500—600	−0.278
200—300	−0.539	600—800	−0.203

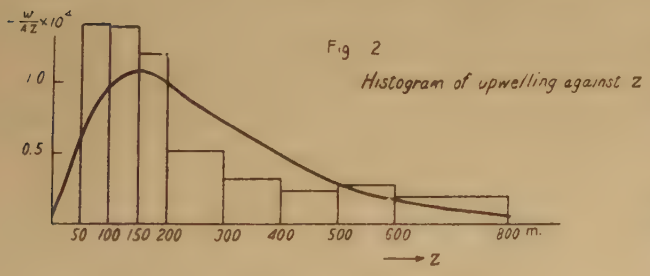

Fig. 2
Histogram of upwelling against z

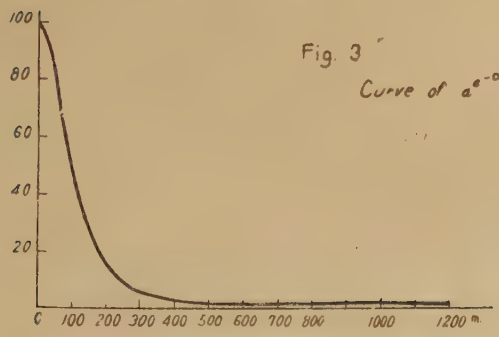

Fig. 3
Curve of $a^{e^{-\alpha z(\alpha z+1)}}$

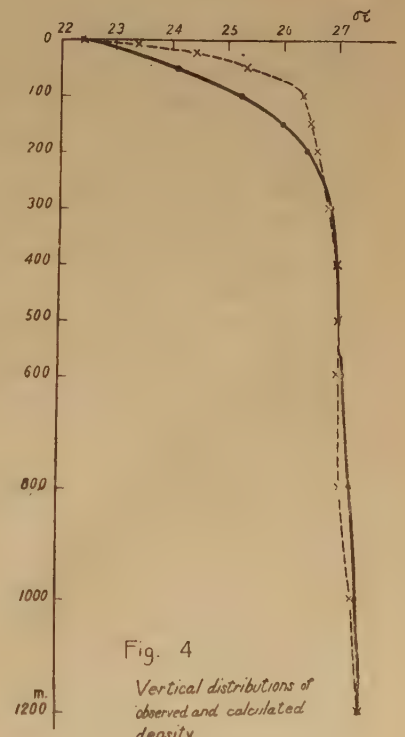

Fig. 4
Vertical distributions of observed and calculated density
• calculated
× observed

4. *Conclusions* : Summerizing the results of this investigation, We have the following conclusions.

1) The ratio of the vertical velocity of upwelling near the center of the cold waters and the coefficient of vertical diffusion is about 10^{-4}.

2) The vertical density-distributions can be explained as the results of the upwellings and vertical diffusions.

3) The discrepancy between the calculated and the observed densities near the surface is seemed to be due to the bad estimations of upwelling and the diurnal or annual variations of temperature. As a matter of course, the steady states are not maintained in the upper layers.

Acknowledgements: The author expresses his hearty thanks to Dr. K. Suda, the Director of Hydrographic Office, M. S. B. and to Mr. S. Miyahara, the Chief of the Oceanographical Section, Hydrographic Office, who kindly reads the manuscript before printing.

References

1. McEwen. G. F. (1939) : Some Calculations of Vertical Turbulence in the North Pacific near Southern California. Commitees Reports & Abstract of Communications.
2. T. Ichiye(1954) : On the Varition of Oceanic Circulation (6). The Geophsical Magazine Vol. 25, No. 3 & 4.
3. S. Hikosaka (1954) : On tbe Upwellings in the Cold water Mass. Hydrographic Bulletin No. 43.

Records of Oceanographic Works
in Japan. Vol. 2, No. 1,
March 1955

Decay of the Large Horizontal Eddies in the Ocean

By

Kenko Iwata

(Hydrographic Office. Maritime Safety Board)

(1) In 1948, G. F. Mcewen published his study[1] about the horizontal eddy circulation of the ocean in the southern California region, and in his paper he attacked the decay of these eddies by solving the vorticity equation in two dimensions, assuming the initial conditions as follows; "the vorticity is constant between the center of the eddies and the difinite distance $r = r_0$, and in the outer region $r > r_0$ is zero", that is, he deduced the general solutio of this vorticity equation under the initial conditions that the transversal velocity increases lineary from the center to the distance $r = r_0$ and decreases hyperbolicaly outside of it, and he carried out the numerical integral in order to obtain the velocities.

The auther, in this paper has obtained the solutions of the velocity equation instead of the vorticity equation under the adequate initial condition in some paticular form, and the solutions obtained in these ways are very simple to calculate the velocities and the elevations.

(2) We assume at first that the eddies take a circular motion and the motion is circular symmetry. Under the above assumptions, equations of motion in cylindrical-polar coordinate in two dimensions are as follows,

$$\left.\begin{aligned} \frac{\partial u}{\partial t} - \lambda v + u\frac{\partial u}{\partial r} - \frac{v^2}{r} &= -\frac{1}{\rho}\frac{\partial p}{\partial r} + \nu\left(\nabla_1^2 u - \frac{u}{r^2}\right) \\ \frac{\partial v}{\partial t} + \lambda u + u\frac{\partial v}{\partial r} + \frac{uv}{r} &= \nu\left(\nabla_1^2 v - \frac{v}{r^2}\right) \end{aligned}\right\} \qquad (1)$$

and the equation of continuity is,

$$\frac{\partial u}{\partial r} + \frac{u}{r} = 0; \qquad (2)$$

where,

$$\nabla_1^2 = \frac{\partial^2}{\partial r^2} + \frac{1}{r}\frac{\partial}{\partial r}, \qquad \lambda = 2\omega \sin\varphi$$

ω represents the angular velocity of the earth φ is the latitude, u and v are the radial and tranversal velocity. From the equation (2), we get directly,

$$u = \frac{C}{r}; \qquad C = Const. \qquad (3)$$

Therefore the radial velocity which is finite at the center of the eddies is zero, so that the equations of motion are rewritten in the following form,

$$\frac{\partial v}{\partial t}=\nu\left(\frac{\partial^2 v}{\partial r^2}+\frac{1}{r}\frac{\partial v}{\partial r}-\frac{v}{r^2}\right) \tag{4}$$

$$\lambda v+\frac{v^2}{r}=\frac{1}{\rho}\frac{\partial p}{\partial r} \tag{5}$$

General solution of the equation (4) is derived easely,

$$v=\int_0^\infty F(\beta)\, J_1(\beta r)\, e^{-\nu\beta^2 t}\, d\beta, \tag{6}$$

where J_1 represents the Bessel function and $F(\beta)$ is the arbitary lunction.

(3) We assume that the initial velocity is given,

$$t=0; \qquad v=are^{-br^2} \tag{7}$$

i. e., this curve increases uniformly up to $r=\frac{1}{\sqrt{2b}}$ and decreases outside then reaches inflexion point at $r=\frac{\sqrt{3}}{\sqrt{2b}}$. As the velocity profils obtained from many observations can be represented by such a curve, we can determine the constants a and b by the "least squares" and can apply to the practical problems approximately. The initial velocity (7) is expanded by the Fourier-Bessel

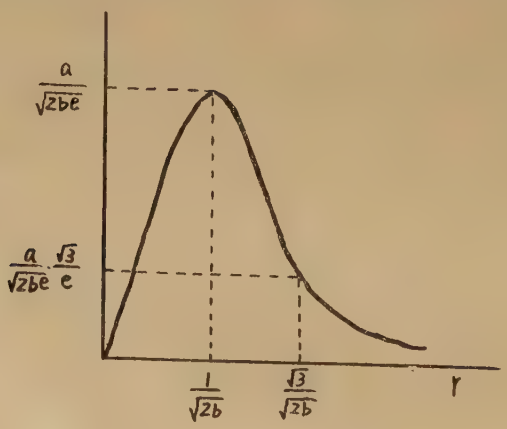

integral formula,

$$are^{-br^2}=a\int_0^\infty \beta J_1(\beta r)\, d\beta \int_0^\infty s^2 e^{-bs^2} J_1(\beta s)\, ds \tag{8}$$

and comparing with (6), we get,

$$F(\beta)=a\beta\int_0^\infty s^2 e^{-bs^2} J_1(\beta s)\, ds \tag{9}$$

By making use of the well known integral formula,

$$\int_0^\infty x^{\nu+1} e^{-px^2} J_\nu(ax)\, dx=\frac{a^\nu}{(2p)^{\nu+1}} e^{-\frac{a^2}{4p}} \quad (\nu>-1)$$

we can write

$$F(\beta) = \frac{a}{4b^2}\beta^2 \; e^{-\frac{\beta^2}{4b}} \tag{10}$$

i. e., the solution satisfying the initial condition is

$$v = \frac{a}{4b^2}\int_0^\infty \beta^2 \; e^{-\frac{(1+4b\nu t)}{4b}\beta^2} J_1(\beta r)\, d\beta \tag{11}$$

and by the same integral formula, we get as the result,

$$v = \frac{ar}{(1+4b\nu t)^2} \; e^{-\frac{br^2}{1+4b\nu t}} \tag{12}$$

The distance from the center at which the transversal velocity u ataines its maximum is deduced from (12) easely,

$$r^m = \frac{1+4b\nu t}{\sqrt{2b}} \tag{13}$$

that is, it increases linearly in proportion to time or eddy viscosity coefficient.

(4) Next we shall consider the elevations of the sea surface. From the equation (5), we get

$$\frac{\partial p}{\partial r} = \rho v\left(\lambda + \frac{v}{r}\right) \tag{14}$$

If we assume that the statical equilibrium is held in the vertical direction, it follows,

$$-\frac{\partial \zeta}{\partial r} = \frac{v}{g}\left(\lambda + \frac{v}{r}\right) \tag{15}$$

where ζ represents the depression. From (12) and (15), we get

$$\zeta = \frac{a}{2bg}\frac{1}{1+4b\nu t} \; e^{-\frac{br^2}{1+4b\nu t}}\left\{\lambda + \frac{a}{2b}\frac{1}{(1+4b\nu t)^2} \; e^{-\frac{br^2}{1+4b\nu t}}\right\}, \tag{16}$$

for example at the center of the eddies,

$$\zeta = \frac{a}{2bg}\frac{1}{1+4b\nu t}\left\{\lambda + \frac{a}{2b}\frac{1}{(1+4b\nu t)^2}\right\}$$

(5) we may take, for example, $\frac{1}{\sqrt{2b}} = 15\ km$ and $\nu = 1.5\times 10^5$ *c. g. s.* which are used in the Mcewen's paper. After the simple calculations, we may find that the time interval to reduce the velocity by half is about 54 days and is in fairly accordance with the Mcewen's research.

(6) Next we shall deal with the same problem in three dimensions. In this case we may neglect the inertia terms and the equations of motion will take the following forms,

$$\left.\begin{aligned} \frac{\partial u}{\partial t} - \lambda v &= -\frac{1}{\rho}\frac{\partial p}{\partial r} + \nu\left(\nabla^2 u - \frac{u}{r^2}\right) \\ \frac{\partial v}{\partial t} + \lambda u &= \nu\left(\nabla^2 v - \frac{v}{r^2}\right) \end{aligned}\right\} \tag{17}$$

where

$$\nabla^2 = \frac{\partial^2}{\partial r^2} + \frac{1}{r}\frac{\partial}{\partial r} + \frac{\partial^2}{\partial z^2}$$

and we get from the above equations denoting $u+iv=W$,

$$\frac{\partial W}{\partial t} + i\lambda W = \nu\left(\nabla^2 W - \frac{W}{r^2}\right) - \frac{1}{\rho}\frac{\partial p}{\partial r} \tag{18}$$

The function $W(z)$ will be transformed by the well known Fourier formula as follows,

$$W(z) = \frac{2}{\pi}\int_0^\infty \cos z\xi \, d\xi \int_0^\infty W(\eta) \cos \xi\eta \, d\eta \tag{19}$$

Therefore by the assumptions

$$\left.\frac{\partial W}{\partial z}\right|_{z=0} = 0\,; \qquad \left.\frac{\partial W}{\partial z}\right|_{z=\infty} = 0,$$

which represent the no wind stress at the surface and the no velocity gradient in the vertical direction at the infinite depth, we get the following equation from (18) and (19).

$$\frac{\partial W}{\partial t} - \nu\left[\frac{\partial^2 W}{\partial r^2} + \frac{1}{r}\frac{\partial W}{\partial r} - \left(\xi^2 + \frac{i\lambda}{\nu}\right)W - \frac{W}{r^2}\right] = -\frac{1}{\rho}\frac{\partial p}{\partial r} \tag{20}$$

(7) In the practical ocean, it may be impermissible to think that the pressure gradient in the horizontal direction is zero, and yet we may take the case $\frac{\partial p}{\partial r} = 0$ for the mathematical model apart from the facts. This assumption is true only in the paticular case when the density ρ is constant and the no gradient of the sea surface exists. In this case the equation (20) becomes homogeneous and the general solution may be obtained as follows, the same as two dimensions,

$$W(\eta) = \int^\infty F(\varphi)\, J_1(\varphi r)\; e^{-\nu t\left(\varphi^2 + \xi^2 + \frac{i\lambda}{\nu}\right)}\, d\varphi \tag{21}$$

where

$$\varphi^2 = \beta^2 - \xi^2 - \frac{i\lambda}{\nu}$$

For the initial condition, we may take similarly,

$$t=0\,; \qquad W_0 = e^{-qz^2}(a_1 r e^{-b_1 r^2} + iare^{-br^2}) \tag{22}$$

then the solution of the equation (20) is obtained,

$$W(z) = \frac{e^{-i\lambda t}}{\sqrt{1+4q\nu t}}\, e^{-\frac{qz^2}{1+4q\nu t}}\left[\frac{a_1 r}{(1+4b_1\nu t)^2}\, e^{-\frac{b_1 r^2}{1+4b_1\nu t}} + \frac{iar}{(1+4b\nu t)^2}\, e^{-\frac{br^2}{1+4b\nu t}}\right] \tag{23}$$

that is, the component velocities are given as follows,

$$u=\left[\frac{a_1}{(1+4b_1\nu t)^2}\,e^{-\frac{b_1r^2}{1+4b_1\nu t}}\cos\lambda t+\frac{a}{(1+4b\nu t)^2}\,e^{-\frac{br^2}{1+4b\nu t}}\sin\lambda t\right]$$
$$\times\frac{r}{\sqrt{1+4q\nu t}}\,e^{-\frac{qz^2}{1+4q\nu t}} \tag{24}$$

$$v=-\left[\frac{a_1}{(1+4b_1\nu t)^2}\,e^{-\frac{b_1r^2}{1+4b_1\nu t}}\sin\lambda t-\frac{a}{(1+4b\nu t)^2}\,e^{-\frac{br^2}{1+4b\nu t}}\cos\lambda t\right]$$
$$\times\frac{r}{\sqrt{1+4q\nu t}}\,e^{-\frac{qz^2}{1+4q\nu t}} \tag{25}$$

In the case of three cimensions, the equation of continuity takes a following form,

$$\frac{\partial u}{\partial r}+\frac{u}{r}+\frac{\partial w}{\partial z}=0, \tag{26}$$

and the vertical velocity is given formaly by the above equation as follows,

$$w=2\int e^{-\frac{qz^2}{1+4q\nu t}}dz\times\left[\frac{a_1}{(1+4b_1\nu t)^2}\,e^{-\frac{b_1r^2}{1+4b_1\nu t}}\left(1-\frac{b_1r^2}{1+4b_1\nu t}\right)\cos\lambda t\right.$$
$$\left.+\frac{a}{(1+4b\nu t)^2}\,e^{-\frac{br^2}{1+4b\nu t}}\left(1-\frac{br^2}{1+4b\nu t}\right)\sin\lambda t\right]\times\frac{1}{\sqrt{1+4q\nu t}}+C \tag{27}$$

(8) Next we shall try to get the formal solution when the equation is not homogeneous, i. e., the term $\frac{1}{\rho}\frac{\partial p(\eta)}{\partial r}$ is not zero and equalls to $f\ (r,\ \eta,\ t)$.

In this case, by performing the Laplace's transformation on the function $W(t)$ and $f(t)$, we get the following equation from (20),

$$\frac{\partial^2\chi}{\partial r^2}+\frac{1}{r}\frac{\partial\chi}{\partial r}-\left(\xi^2+\frac{\alpha+i\lambda}{\nu}\right)\chi-\frac{\chi}{r^2}=\frac{1}{\nu}\left(f-W_0\right) \tag{28}$$

where W_0 is the initial value of the velocity and

$$\chi(\alpha)=\int_0^\infty W(t)\,e^{-\alpha t}\,dt;\quad \bar{f}=\int_0^\infty f(t)\,e^{-\alpha t}\,dt$$

and the general solution of this equation is descrived,

$$\chi=C_1 I_1(\gamma r)+I_1(\gamma r)\int r\,I_1^{-2}(\gamma r)\left\{\int r\,(f-W_0)\,I_1(\gamma r)\,dr+c_2\right\}dr \tag{29}$$

here I_1 represents the modified Bessel function, and $\gamma^2=\xi^2+\frac{\alpha+i\lambda}{\nu}$.

From the function χ obtained in these ways, the function $W\ (r,\ \eta,\ t)$ may be represented as follows,

$$W(r,\ \eta,\ t)=\frac{1}{2\pi i}\int_{c-i\infty}^{c+i\infty}\chi(\alpha)\,e^{\alpha t}\,d\alpha \tag{30}$$

Thus we may get the velocies by introducing (30) into the equation (19).

Neverthless it is difficult to calculate the functions χ and $W\ (r,\ \eta,\ t)$ even

if the function f is comparatively simple.

In conclusion, the author wishes to express his sincere thanks to Dr. K. Suda and Mr. S. Miyahara for their kind suggestions and encouragement.

Refernce

(1) G. F. McEWEN; The Dynamics of Large Horizontal Eddies (Axes Vertical) in the Ocean off Southern California. Scripps Institution of Oceanography, Coutrbutions-1948, No. 383.

Records of Oceanographic Works
in Japan. Vol. 2, No. 1,
March 1955

Simple Method of Investigation of Tidal Current in Narrow Channel and its Application to Ki-i Suido, Japan.

by
Kenko Iwata
(Hydrographic Office, Maritime Safety Board)

(1) It is necessary to reduce the harmonic constants from observation in order to determine the tidal current as well as the tidal elevetion, but it is very labourous and difficult to perform the continuous current observations at many spots where tidal constants are necessary. However in narrow channel, if we reduce harmonic constants from observations at one spot, we can estimate the approximate tidal current at the other spot in that channel by help of the knowledge of tide at coast.

(2) Equation of motion is given regarding the friction to be proportional to the velocity,

$$\frac{\partial u}{\partial t}+\frac{f}{h}u+g\frac{\partial \zeta}{\partial x}=0 \qquad (1)$$

where u, f and ζ is velocity, coefficient of friction and elevation respectively, and the Coriolis term can be neglected so far as the breadth of channel is narrow.

From the equation (1) we get the velocity by simple integration as follows,

$$u=-ge^{-\frac{f}{h}t}\int\frac{\partial \zeta}{\partial x}e^{\frac{f}{h}t}dt \qquad (2)$$

On the other hand, tidal elevation at coast is given by harmonic analysis,

$$\zeta=\sum_r f_r H_r \cos\left(V_{0r}+\sigma_r t-\kappa_r\right) \qquad (3)$$

where r denote the each constituent and f, H, V_0, σ and κ are reduction feacter, amplitude, argument, angular velocity and the lag of phase of tide respectively. Here we may regard that the tidal elevation on the sea surface could be replaced by the value at coast so far as the narrow channel is considered. Therefore, when we take the principal lunar constituent M_2 for example, it follows from (2) and (3),

$$u=\frac{-g}{\sigma^2+\left(\frac{f}{h}\right)^2}\left[\left(\sigma F+\frac{f}{h}G\right)\sin\sigma t-\left(\sigma G-\frac{f}{h}F\right)\cos\sigma t\right] \qquad (4)$$

where

$$F = f\left[\frac{\partial H}{\partial x}\cos(\kappa - V_0) - H\frac{\partial \kappa}{\partial x}\sin(\kappa - V_0)\right],$$

$$G = f\left[\frac{\partial H}{\partial x}\sin(\kappa - V_0) + H\frac{\partial \kappa}{\partial x}\cos(\kappa - V_0)\right] \tag{5}$$

and the time of slack is given,

$$t = \frac{1}{\sigma}\left[\tan^{-1}\frac{\sigma G - \frac{f}{h}F}{\sigma F + \frac{f}{h}G}\right] = \frac{1}{\sigma}\left[\tan^{-1}\left(\frac{h}{\frac{f}{\sigma}}\right) - \tan^{-1}\left(\frac{F}{G}\right)\right] \tag{6}$$

Accordingly the slack water time increases with the depth, i. e., tidal current returns sooner on shallow water than deep water[1], and the space variation of slack water time is represented by the term $\tan^{-1}(F/G)$. But the numerical values of F and G are inaccurate because of the difficulties of the calculations of differential quotients of H and κ, so that the another way must be looked for.

(3) Equation of continuity is,

$$\frac{\partial \zeta}{\partial t} + \frac{1}{b}\frac{\partial}{\partial x}(Su) = 0 \tag{7}$$

where b and S are breadth and sectional area of the channel respectively.

By the integration directly we get,

$$Su = -\int_0^x b\frac{\partial \zeta}{\partial t}dx + S_0 u_0 \tag{8}$$

From (3) and (8), we get for M_2 tide, for example,

$$Su = \sin\sigma t\int_0^x bAdx - \cos\sigma t\int_0^x bBdx + S_0 u_0 \tag{9}$$

where

$$A = \sigma f H\cos(\kappa - V_0), \quad B = \sigma f H\sin(\kappa - V_0) \tag{10}$$

On the other hand, velocity u must be repreesented.

$$u = V\cos(\sigma t - \eta) \tag{11}$$

so that we must have,

$$SV\cos(\sigma t - \eta) = S_0 V_0\cos(\sigma t - \eta_0) + \sin\sigma t\int_0^x bAdx - \cos\sigma t\int_0^x bBdx \tag{12}$$

that is,

$$\left.\begin{aligned} SV\cos\eta &= S_0 V_0\cos\eta_0 - \int_0^x bBdx \\ SV\sin\eta &= S_0 V_0\sin\eta_0 + \int_0^x bAdx \end{aligned}\right\} \tag{13}$$

i. e.,

$$\gamma_l = \tan^{-1} \frac{S_0 V_0 \sin \gamma_0 + \int_0^x bA dx}{S_0 V_0 \cos \gamma_0 - \int_0^x bB dx} \tag{14}$$

$$SV = \left(S_0 R_0 \cos \gamma_0 - \int_0^x bB dx \right) \sec \gamma_l \tag{15}$$

where S_0, V_0 and γ_0 are sectional area, mean velocity and mean value of lag of phase at the section $x = 0$ and γ_l given by (14) is the sectional mean of lag of phase at each section. from these eqnations we can determine the mean velocity and lag of phase easely.

(4) Thereafter numerical calculations must be practised as follows;

1. At first, we must compute sectional mean value, V_0 and γ_0 for each tidal constituent at the section $x = 0$, using the results of harmonic analysis of observed data

2. Sectional mean value of lag γ_l is calculated from (14) using the harmonic constants of tide at coast at each section fer each constituent.

3. Deviation of lag from the above mean value at the each section are given by the equation (6)

4. Similarly, we can derive the velocity at each spot from the equation (15) and (4).

In these ways we can determine the tidal current at any spot for each constituent.

(5) According to the results of A. Defant's reseach[2], values of $f/h\sigma$ are given as follows,

h (in meter)	100	50	30	10 or under
$f/h\sigma$ about	0.1-0.2	0.5	0.5-1.0	1.2-2.0

and the mean value of f/σ is about 2×10^3, which is used in the case of Ki-i Suido.

When we denote the sectional mean velocity and time-lag by u_0 and t_0 and corresponding mean depth by h_0, we may get from the equation (4) and (6),

$$\left(\frac{u}{u_0} \right) = \frac{h_0^2 + \left(\frac{f}{\sigma} \right)^2}{h^2 + \left(\frac{f}{\sigma} \right)^2} \left(\frac{h}{h_0} \right)^2 \quad \frac{h_0^2 + 4\times10^6}{h^2 + 4\times10^6} \left(\frac{h}{h_0} \right)^2 \tag{16}$$

$$\sigma (t - t_0) = \tan^{-1} \left(\frac{h}{2\times10^3} \right) - \tan^{-1} \left(\frac{h_0}{2\times10^3} \right) \tag{17}$$

By these formulae we can estimate the velocity-ratio and the difference of time-lag at any spot.

(6) In the case of Ki-i Suido, we took almost two week's continuous record of currents at the spot z_0. we found that the velocity vector was almost northward

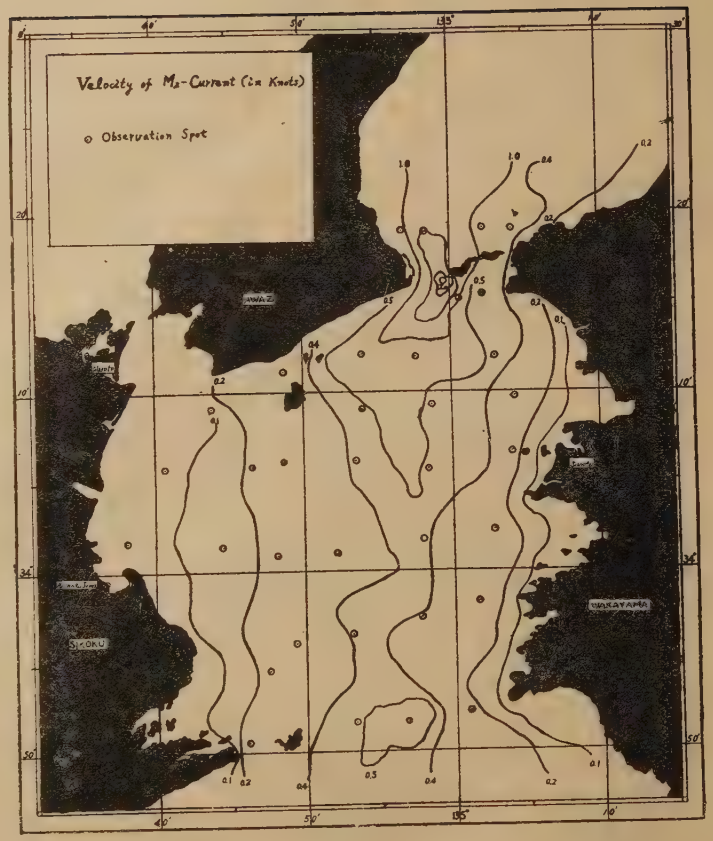
Velocity of Ma-Current (in Knots)
⊙ Observation Spot
AWAZI
SHIKOKU
WAKAYAMA
40'
50'
135°
10'
20'
30'
10
34
50

Slack Water Time Calculated
from the Mean Moon's Transit
upper the Meridien 135° E
⊙ Observation Spot
AWAZI
SHIKOKU
WAKAYAMA
4h 20m
4h 10m
4h 00m
3h 50m
3h 40m
3h 30m
3h 20m
3h 10m
3h 00m
40'
50'
135°
10'
20'
30'
10
34
50

and the east-west component was negligible small. Moreover, at the other spots, about 35, we took almost 25 hour's continuous record, and found that the ratio of minor axis to major axis of current ellipse is small. Therefore we took x-axis southward and the origin at the parallel of latitude involving the spot z_0.

When we take M_2-tide, for example, the above numerical calculations lead to the results shown in the figure.

The results obtained in these ways are in fairy good agreement with the obserbations carried out at the spots shown in the figure.

In conclusion, the author wishes to express his best thanks to Dr. K. Suda, and Mr. S. Miyahara for their kind suggestions and encouragement.

Reference

(1) W. Hansen ; 1950, Gezeitenstoroeme im Englischen Kanal. Deutsche Hydrographische Zeitschrift, Bd. 3, Heft 3/4

(2) A. Defant ; 1925, Gezeitenprobleme des Meeres in Landnaehe. Probleme der Kosmischen Phsik, Bd. 4.

Records of Oceanographic Works
in Japan, Vol. 2, No. 1,
March 1955

On the distribution of the radioactivity in the sea around Bikini Atoll in June, 1954

by

Y. Miyake, Y. Sugiura and K. Kameda

(Meteolorogical Research Institute, Tokyo)

Introduction

Leaving Tokyo Harbour on 15th May, 1954, the observation were carried out until 4th July aboard the survey boat the "Shunkotsu-maru" belonging to the Ministry of Agriculture and Forestry in the sea area near Bikini Atoll where H-bomb tests had been done by U. S. Atomic Energy Commision, to make clear the state of the radioactive contamination to living matter, sea water, the air etc. The purpose of this "Japanese Bikini Expedition" wasto obtain a counter-plan against the serious damage fell on the Japanese pelagicfisheries due to the radioactivity carelessly scattered in this sea area since theunfortunate affair of the fishing boat the "Fuku-ryu-maru", the "Lucky Dragon"on 1st March.

In this expedition the present authors took charge of making a plan and observations on the radioactive contamination of sea water and the air. Two of the authors (Sugiura and Kameda) participated in the expedition as observers. The fairly strong radioactivity was detected in wide area around Bikini Atoll, though U. S. Atomic Energy Commission had declared that the presence of the radioactivity in the area was negligible[1]. In this paper the authors intend to report the results of observations and some oceanographic discussions regarding the distributions of the radioactivity near Bikini Atoll.

1. The method of measurement of the radioactivity in sea water

It is difficult to measure the radioactivity in sea water directly by simple evaporation method owing to its high salinity, therefore, the carrier method has been adopted. After adding 2 gr of solid ammonium chloride, 1 ml of the aqueous solution of iron alum (86.3 gr/1) and 1 ml of barium chloride solution (17.8 gr/1) to 1 litre of sea water, water is heated to 60~70°C stirring well. A few drops of an alcoholic solution of phenol-phthalein (1%) are added as an indicator, then ammonium hydroxide solution (1 : 1) is carefully dropped in with a pipet until a faint pink colour appears. After two minutes boiling, the precipitate is settled on standing for a couple of hours at room temperature. The precipitate is filtered under suction on a round filter paper (dia. 3.5 cm)

laying on the glass filter. The precipitate remained on a filter paper is dried in a air bath or a desiccator holding in a small brass case to avoid the folding of the surface. Measurements of radioactivity are done by putting the precipitate kept in a brass case under a mica window of G-M counter. The G-M counter used aboard the "Shunkotsu-maru" is Radiation Counter, Model 32 manufactured by Science Research Institute Ltd., Tokyo. The thickness of mica window is 3.7 mg/cm^2 and the distance between the mica window and the surface of the precipitate is 1.5 cm. After the measurement has been done, the precipitate is covered by a polyethylene film to protect the surface. It was confirmed that at least 70~80 % of the total activity in sea water could be transfered to the precipitate by preliminary tests using the fission materials fell aboard the fishing boat the "Fuku-ryu-maru". Therefore, the actual activities might be 25~40 % higher than observed values. To obtain the counting efficiency the aqueous solution containing Ce 144 of which activity had been referred to the standard RaE was treated chemically as mentioned above, and its radio-activity was measured under the same geometrical conditions. Thus, the efficiency of the measurement was found to be 7.7 %, that is, 1000 counts per minute is equivalent to about 5.9 mμC. The maximum activity in sea water obtained aboard by this method was 7025 cpm/l which was found at the depth of 75 m, at 570 km west of Bikini Atoll on 21st June.

The second was 6050 cpm/l found at the depth of 20 m at 150 km west of the atoll on 12th June. It was confirmed that most parts of the radioactive materials were dispersed in water as true solution, ionic or eucolloidal, since more than 99 % of the radioactivity passed through a filter paper (pore size 0.5μ, No. 4 Filter Paper, Tōyō Filter Paper Manufacturing Co., Tokyo).

It is rather surprising that the activity in sea water near Bikini and Eniwetok Atolls was often stronger than, or at least comparable to, that of White Oak Lake receiving waste effluent from nuclear reactors of Oak Ridge National Laboratory USA. The latter was 2710~5190 cpm per litre on an average[2].

2. The distribution of the radioactivity in sea water around Bikini Atoll

a. Horizontal distribution

Fig. 1 shows the horizontal distribution of the activity in the surface water near Bikini Atoll. There must have been some changes in the activity due to the time variation of the sea condition, the natural decay and the loss of the radioactivity during the course of observation. However, since the causes of changes were much complicated, and the correction were almost impossible, the distribution was drawn by using directly the observational data without giving any correction.

As shown in Fig. 3 the radioactive water extended on the WNW direction leaving near Bikini Atoll while a branch spread out to WSW. The cause of this branching is not clear. But, as explained below, it seems that there was a

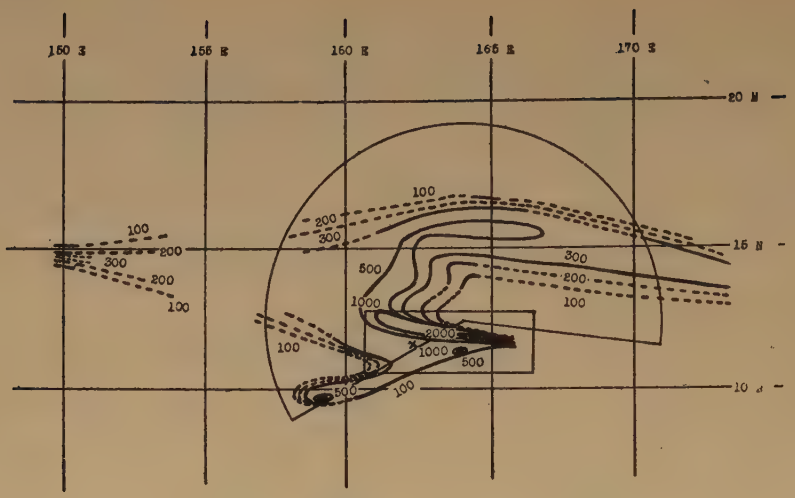

Fig. 1 The horizonal distribution of radioactivity in the surface water near Bikini Atoll. (cpm/l)

weak discontinuous boundary along the line passing Bikini and Eniwetok Atolls. The water B_1 (Fig. 2) on the northern side of this line had on an average the temperature, 27.1°C, the chlorinity, 19.23‰ and σt, 22.51 at 50 m depth. On the other hand, the water system B_2 on the southern side of the line had T, 27.0°C, Cl, 19.04‰ and σt, 22.29: Thus, it seems that there was a slight but definite jump in the properties between two water systems, which might be one of the causes of the branching.

The radioactive water flowing on the main direction of the North Equatorial Current extended sooner toward the west than in the southern part where the flow rate was smaller because the latter was near the boundary between the North Equatorial Current and Equatorial Counter Current and there was also the oppression due to the north-eastward inclination of the Equatorial Counter Current. Thus, on the WNW direction the activity of 100 cpm/l reached as far as 2000 km from Bikini Atoll, while on the WSW direction the extension was only 1000 km.

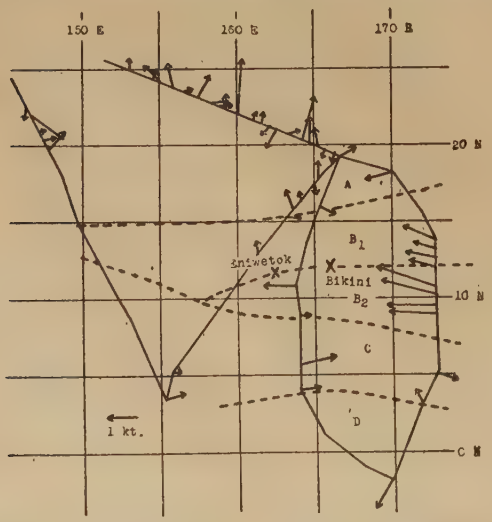

Fig. 2 The course of the cruise of "Shunkotsu-maru". Arrows represent current. A, B_1, B_2, C, D are the water systems.

It is to be noted that the radioactivity was also detected at the position 700~800 km from

Bikini on the NNE direction. This is the end part of the radioactivity distribution turning to the east at about 350 km north of Bikini Atoll (Fig. 2). To clarify the cause of this turning on the backward direction of North Equatorial Current may be one of the important problems.

Though it is not clear at present, whether it was the extention of the easterly current along the northern boundary of the North Equatorial Current which was found recently between 180°E～140°W[3] or it was only the local eddy. Several discussions will be done below on this point.

When we investigate the horizontal distribution of water system near Bikini Atoll by using the T-S diagrams of waters at the depth of 50 m below the surface, we can find out that there are at least four different types of waters (Fig. 2). The first one (A) is highly saline water (chlorinity, 19.3‰, water temperature, 27.5°C, σt, 22.77) covering the area northern than 15°N.

In the southern part of the atoll there is the second type of water (C) which belongs to the Equatorial Counter Current with smaller chlorinity (Cl, 18.9‰) and higher temperature (T, 28.0°C). The third one (B) belongs to the North Equatorial Current representing the intermediate property between A and C. In the southern part of the water C, there extends the water (D) of the South Equatorial Current with higher chlorinity (Cl, 19.6‰) and higher temperature (T, 28.0°C).

The water B may be classified into two sub-groups B_1 and B_2 as mentioned above. As shown in Fig. 2 the east part of B was comparatively broad and it

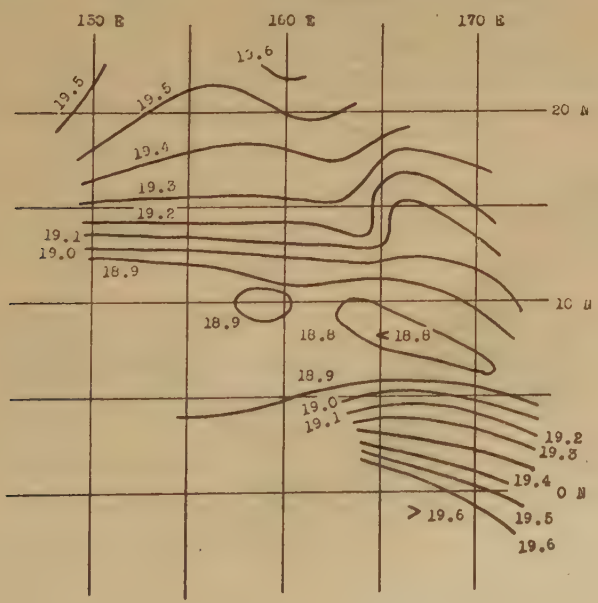

Fig. 3 The surface distribution of chlorinity near Bikini Atoll in ‰

became narrower on approaching to the west. It was probably due to that at the time the boundary between waters B and C somewhat inclined to the north. Therefore, the North Equatorial Current was pressed by the Equatorial Counter Current and the backward current flowing toward the north-east direction of Bikini Atoll would have been resulted.

The observation of the current direction obtained *in situ* also suggests the presence of counter or eddy current in the same area. It is, however, not sure whether this current would form the origin of the general easterly current as mentioned above.

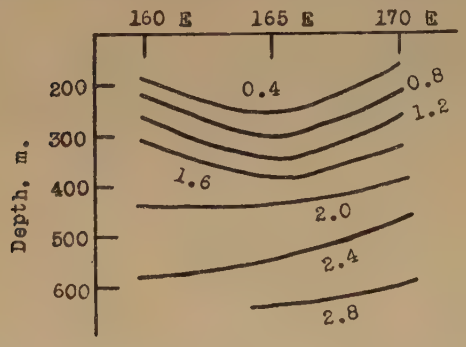

Fig. 4 The vertical distribution of phosphate in P μg atoms/1. along 15°N

On the other hand, a remarkable loop of the isochlor lines shown in the surface distribution of the chlorinity (Fig. 3) in the northern area of Bikini also indicates the presence of eddy flow.

As shown in Figs. 4 and 5, in the vertical distributions of phosphate and the dissolved oxygen along 15°N, there was the subsidence in the area near 15°N, 165°E which was probably due to the anticyclonic eddy.

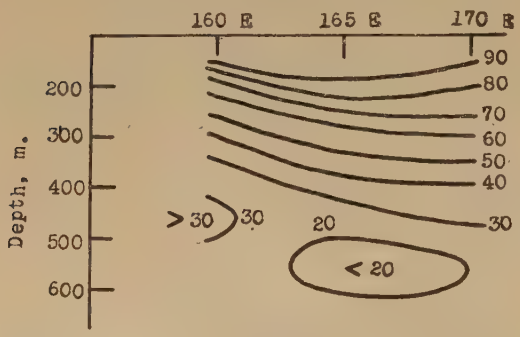

Fig. 5 The vertical distribution of degree of saturation of dissolved oxygen in %. along 15°N

b. Vertical distributions of the radioactivity in sea water

Figs. 6, 7 and 8 show the distributions of radioactivity of

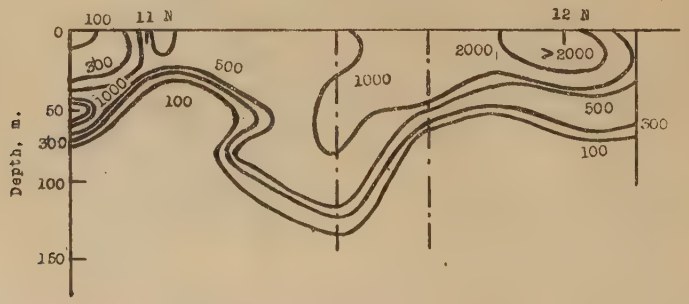

Fig. 6 The distribution of radioactivity in sea water on the vertical section perpendicular to the North Equatorial Current along the lines 150 km west of Bikini Atoll.

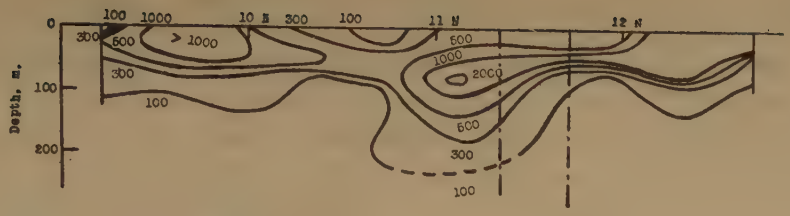

Fig. 7 The distribution of radioactivity in sea water on the vertical section perpendicular to the North Equatorial Current along the lines 570 km west of Bikini Atoll.

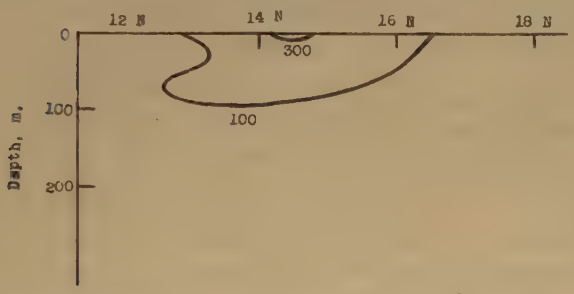

Fig. 8 The distribution of radioactivity in sea water on the vertical section perpendicular to the North Equatorial Current along the lines 1300 km west of Bikini Atoll.

sea water on the vertical section perpendicular to the North Equatorial Current along the lines respectively at 150 km, 570 km and 1300 km west of Bikini Atoll. The profile at 150 km west of Bikini shows already the branching of the activity in the direction of N-S. The dotted lines in the figures represent respectively the latitude of the sites of Bikini and Eniwetok Atolls. The strong activity is separated on both sides of these dotted lines and the distance of two maxima is about 100 km. The depth which shows the activity of 100 cpm/l is at about 80 m below the surface in the northern and southern parts and in the middle part it sinks down to about 120 m. It is noteworthy that the activity decreases rapidly down to only 28 cpm/l at 200 m depth. This corresponds to the depth of thermocline which was about 150 m in this area.

The estimated amount of flow of radioactivity was about 1×10^5 curie/hour passing through this section. The vertical section at 570 km west of Bikini the distance of branching became broader and also the depth of 100 cpm/l activity was 200 m below the sea surface on an average. The flow of radioactivity was about 0.6×10^5 curie/hour. The distance between the former and the latter section was about 400 km and assuming that the speed of current was about 0.7 knots on the direction perpendicular to the sections it would have taken about 2 weeks to flow between them. Thus, the activity passing through both sections would have been about the same when the rate of decay during two weeks was taken into consideration.

3. The relation between radioactivity in water and radioactive fallout

The fishing boat the "Fuku-ryu-maru" was situated at the position 150 km east of Bikini Atoll in the early morning on 1st March when her crews recognized small, white dust particles falling on the deck. The amount of dusts covered the surface of the deck was not clearly known, however, it may be supposed that it was about 0.5 gr/m^2 or so. On the other hand, the radioactivity of the dust particles was regarded as about 1.4 curie/gr at the time of falling (3 hours after the detonation)[4]. Assuming that the mean diameter of dust particles was 0.1 mm, the rate of sinking of such particles in sea water is about 30m/hour. Then, it takes about 1~1.5 sec. to pass the water layer of 1 cm. Here, if we assume that at most 0.01 % of the radioactive substances in the dusts could dissolve into sea water in one second, most part of radioactive materials would have remove to water from dusts before they reached 100 m depth below the sea surface. Thus, the mean activity in water near the sea surface around there would have been 3.1×10^{-6} curie/l at the time five or six hours after detonation. Needless to say, this was the activity of sea water in the area about 150 km apart from Bikini Atoll, therefore, the activity near and in the atoll would have been much more stronger. On the other hand, it was confirmed by the records of micro-barographs and tide gauges obtained in Japan[5] that the detonations had been carried out four or five times since 1st March (1st March, 27 th March 6th Apr., 26th Apr. and 5th May), it would be no wonder the wide sea area far from Bikini Atoll had been contaminated by fission materials as strongly as it was actually observed aboard the "Shunkotsu-maru" in June, 1954.

4. The property on the radioactive substances in sea water

The relation between the gross radioactivity ($A_{(t)}$) of the fission materials and the time after detonation may be simply expressed by the next equation,

$$A_{(t)}=ct^{-\alpha}$$

where c and α are constants. From the decay curve of the radioactivity of the precipitates prepared aboard the "Shunkotsu-maru", it has been found that α is confined within the comparatively narrow limits of 1.3~1.6 (mean, 1.5) assuming the date of detonation was 5 th May. In normal cases, α is about 1.2[6], whereas it was 1.37 for the radioactive dusts fell on the deck of the "Fuku-ryu-maru".

In sea water some of the radioactive elements contained in the original fission materials might be preferentially precipitated owing to pH of sea water, (about 8.2~8.3). Therefore, the chemical composition should be somewhat different from the original fission materials, which might be the cause of change in the value of α.

The radiochemical analysis of the fission materials in sea water have

been furnished also by the present authors which will be reported in near future. In Table 1 the full data of the gross activity of sea water observed aboard the observation vessel is given.

References.

(1) AECD 3446–Radiobiological Survey of Bikini, Eniwetok and Likiep Atolls. July-August 1949 ; July 12 (1950) AEC.

(2) Radioisotope Uptake by Aquatic Plants and Animals living in waste Effluents of Oak Ridge National Laboratory ; A paper presented to U. S.–Japan Radiobiological Conference held in Tokyo, 1954.

(3) Cromwell. T., 1953 : Circulation in a Meridional Plane in the Central Equatorial Pacific. Jour. Mar. Res., 12, 196–213. Barnes, C. A., Bumpus, D. F. and Lyman, J., 1948 : Ocean Circulation in Marshall Island Area. Trans. Am. Geophys. Union, 29 (6).

(4) Kimura, K. *et al*, 1954 : On the Radioactive Substances having Precipitated on the Fishing Boat the 11, Fuku–ryu–maru". Japan Analyst, 3, 335–348 (in Japanese).

(5) Yamamoto, R., 1954 : The Microbarographic Oscillations Produced by the Explosions of H-bombs. Bulletin of the Institute for chemical Research, Kyoto Univ. The Radioactive Dust from the Nuclear Detonation.

Central Meteorological Odservatory, 1954 : A preliminary report of oscillations on atomospheric oscillations caused by H-bomb tests (in Japanese).

(6) Hunter, H. F. and Ballou, N. E. 1951 : Fission-Product Decay Rates. Nucleonics, 9, C–2～C–7.

Table 1

Radioactivity of Sea Water at Various Depths

1000 cpm is cquivalent to about 5.9mμc.

Date	St. No.		Latitude	Longitude	Depth m	Activity cpm/1
May,	31	6	13–51N	172°–56'E	0	450
					100	34
					210	5
					430	0
June,	1	7	10–44	173–03	0	25
					5	27
					10	27
					20	27
					30	27
					49	36
					92	0
	12	17–1	10–55	163–51	0	84
					25	262
					54	5780
					75	67
					98	25
					210	28
					300	23
		17–2	11–07.3	163–49.3	0	1610
					20	982
					40	169
					50	50
					60	23
					94	12
					105	8
					192	27

June.	12	17–3	11°–18′N	163°–50′E	0	566
					20	810
					40	1160
					50	503
					60	273
					83	1283
					101	368
					194	11
		17–4	11–29	163–51	0	859
					20	641
					40	1563
					50	1683
					85	840
					100	939
					195	59
		17–5	11–39	163–52	0	1539
					20	1841
					40	1792
					50	1221
					60	517
					86	182
					105	25
					202	65
		17–6	11–49	163–52.5	0	1792
					20	1875
					40	516
					50	470
					62	216
					80	48
					95	20
					200	50
					290	110
					475	116
		17–7	11–59	163–53	0	5540
					20	6050
					40	923
					50	356
					60	375
					86	55
					105	15
					200	64
		17–8	12–09	163–57.3	0	260
					20	1091
					40	452
					50	580
					60	346
					82	39
					102	32
					196	49
	13	18	13–23	164–25	0	70
					20	57
					40	61
					50	84
					60	58
					83	38
					101	10
					193	59
	14	19	15–57	165–22	0	654
					25	603
					50	420
					100	24
					213	64
					394	16
					576	0

June,	19	20	15°-03′ N	163°-15′E	0	478
					25	426
					50	408
					75	22
					106	8
					199	0
					480	0
	20	21-1	12-42	161-26	0	1260
					25	1233
					50	331
					75	187
					106	24
					193	34
					489	48
		21-2	12-18	161-03.5	0	1829
					25	1684
					50	1237
					74	1840
					93	343
					175	20
		21-3	11-54	160-46	0	457
					25	680
					50	1242
					79	19
					102	14
					195	83
		21-4	11-30	160-29	0	421
					25	487
					48	1056
					70	879
					98	168
					180	105
	20	21-5	11-05	160-12.5	0	360
					24	480
					48	1400
					82	7025
					103	1620
					194	231
		21-6	10-42	159-55	0	93
					25	46
					49	390
					81	464
					104	55
					206	130
	21	22-1	10-21	159-35	0	208
					10	208
					25	235
					48	775
					70	330
					80	60
					115	44
					200	95
					280	38
					360	6
					405	13
					485	22
					715	43
		22-2	09-58.5	159-15	0	425
					25	905
					50	1225
					75	295
					96	240
					184	97

June,	21	22–3	09°–35′N	158°–57′E	0	1890
					25	2016
					48	1349
					76	349
					99	120
					198	25
		22–4	09–13	158–41	0	78
					25	850
					49	394
					73	157
					95	157
					175	0
					455	2
	23	23	05–03	155–53	0	16
					26	7
					50	9
					72	6
					99	5
					189	13
					500	13
	24	24	03–24.5	155–31	0	0
					25	0
					49	5
					72	9
					106	7
					170	0
					515	0
	26	25	08–59	152–51	0	10
					25	10
					49	0
					73	0
					95	tr.
					180	tr.
					565	0
	27	26	12–00	151–10	0	10
					25	7
					50	9
					75	69
					102	7
					193	tr.
					485	tr.
	28	27	14–46	149–56	0	350
					25	185
					49	184
					72	180
					106	0
					185	0
					450	0
	29	28	18–00	148–38.5	0	7
					27	3
					51	3
					74	3
					110	3
					186	2
					495	0
	30	29	21–00	147–21	0	0
					25	7
					50	10
					74	5
					98	0
					198	0
					525	0

Records of Oceanographic Works
in Japan, Vol. 2, No. 1,
March 1955

On the Content of Rubidium and Cesium in Sea-Water

Masayoshi Ishibashi and Tadashi Hara

(Faculty of Science, Kyoto University)

As for the amounts of rubidium and cecium dissolving in see-water we cannot find good data, and some data by several persons···200 γ/L of rubidium and $2\gamma/L$ of cesium by H. Wattenberg[3] and $35\gamma/L$ of rubidium and of $2\sim10\times10^{-3}\gamma/L$ of cesium by M. Ishibashi and Y. Harada[4] are remarkably different from one another, and morever, they seem to be inadequate.

The authors determined the amounts of rubidium and cesium in the sea-waters sampled at the following places; Kaganoura Shizuoka Pref., 6 miles in the west of Shirahama, Wakayama Pref., and Suma, Hyogo Pref., Japan. And $250\sim400\gamma$ of rubidium and $3.3\sim4.3\gamma$ of cesium were respectively found in one litre of those sea-waters.

Concentration of Rubidium and Cesium in Sea-Water[1]

The content of rubidium and cesium is so little that it is difficult to directly determine their amounts in sea-water.

In order to adequately concentrate the rubidium and cesium in sea-water, the authors utilized the co-precipitation method as follows; using the potassium dissolving in sea-water as a carriers the rubidium and the cesium were thrown down with potassium cobaltinitrite by means of $Na_3\ Co\ (No_2)_6$.

The co-precipitation of rubidium and cesium with potassium cobaltinitrite was comparatively incomplete when the amount of $Na_3Co(No_2)_6$ was little and the temperature of sea-water was high, whereas it became almost complete in case more than 200ml. of $Na_3\ Co\ (No_2)_6$ solution was added to 10 litres of sea-water at less than 10°C.

Separation of Rubidium and Cesium from Potassium

The chemical Behaviors of potasium, rubidium and cesium are so resemble that it is difficult so quantitatively seperate rubidium and cesium from a large amount of potassium. In order to selectively and quantitatively seperate rubidium and cesium from potassium, the authors utilized a modified Ball's Reagent (hereafter it is denoted as M. B. R.) containing silver nitrate.

By means of M. B. R., rubidium and cesium are selectively and quantitatively precipitated as orange crystalline presiptates in the presence of a large amount

of potassium. In cace of potassium alone, no precipitate takes place even from its saturated solution by M. B. R. Whereas in their mixtures, a small amount of potassium is co-precipitated with rubidium of cecium salts. Then the orange precipitates of rubidium and cesium are recrystallized. Thus the M. B. R. salts of rubidium and cesium which contain no potassium are obtained as yellow precitates.

Gravimetric Determination of Rubidium[1),5)]

At present, the following methods can be used for the gravimetric determination of a small amount of rubidium ; hexanitrodipicrylaminate method, hexanitrocobaltinitrite method, and hexanitrodipicrylaminate method[6)] in which the content of rubidium is smaller than any other rubidium salts.....here chemical factor is equal to 0.1629.

If 10 litres of sea-water is sampled, the rubidium amount in it is exactly obtained by weighing as the hexanitrodipicrylaminate using a semi-micro-balance. In this case the found sum of rubidium and cecium is locked for to be equal to the amount of rubidium alone, because the cesium amount in sea-water is very small comparing with that of rubidium.

Colorimetric Determination of Cesium[7)]

During the course of an investigation[8),9)10)] of the chemical methods of seperation and estimating cesium with $KBiI_4$ reagent, which is a specific rea-gent for cesium with exception of thallous thallium, in the presence of large amounts of rubidium, it was found that the amount of rubidium co-precipitain range of rubidium amount. This fact was applied for the micro-determination of cesium in co-presence of rubidium.

Then, a new method has been established for the indirect estimation of small amounts of cesium in the presence of large amounts of rubidium, based upon a precipitation of the cesium as $Cs_3\ Bi_2\ I_9$ ($3CsI.\ 2BiI_3$), followed by a photometric determination of the bismuth.

The bismuth was determined by dithizon method. As the rubidium amout is easily found from the sum of rubidium and cesium dipicrylaminates, the amount of cesium is almost exactly estimated by means of the calibration curve which has been obtained in the presence of the rubidium near that in sea-nater.

Measurement of Recovery

About 2μC. of radioactive Cs^{137} was utilized for a measurement of the efficient recovery of cesium in sea-water and its radio-activity was measured by a GM counter. It was theoretically revealed from its specific activity that the mass of Cs^{137} as a tracer did not give any effect to that of the cesium coming from sea-water.

Determination Rubidium and Cesium in Sea-Water

After adding of about 2 μC. of Cs^{137} to 10 litres of the sea-water, 200 ml. of $Na_2Co(No_2)_6$ solution was added at the solution temperature less than 10°C.

Thus the rubidium and the cesium were co-precipitated with the potassium. The supernatant liquid was siphoned off and the precipitate were dissolved in mineral acid. Cobalt was removed as hydroxide and from the alkaline filtrate, the dipicrylaminates of potassium, rubidium and cesium were obtained with dipicrylamine. After removal of the dipicrylamine with acetone and hydrochloric acid, the most part of potassium was seperated from rubidium and cesium by the modified Well-Steven's Method.

Then the alkali chlorides were converted to their nitrates with nitricacid. The rubidium and the cesium were separated from the potassium by means of the above mentioned procedure. The M. B. R. salts of rubidium and cesium were dissolved in a little nitric acid. Then the silver and the bismuth were removed with hydrochloric acid and hydrogen sulfide as their precipitates. From the filtrate, the sum of rubidium and cesium which is approximately equal to the rubidium amount in sea-water was found out by means of the coventional method using O.1N-calsium dipicrylaminate reagent. The amine was removed with hydro- chloric acid and acetone, and the filtrate was diluted to a constant volume with distilled water. Then the efficient recovery was measured by the comparison of the radioactivity in the solution with that of the Cs^{137} standard solution under the same conditions. Then cesium was determined photometrically. The results obtained are shown in Table 1. and Table 2.

Table 1. Surface Sea-Water at Suma(March. 3. 1953)

Sea-Water Taken		10 L
Chlorinity	‰	17.64
Rb Found	γ/L	250 260
Cs Found	γ/L	3.5 4.1

Table 2. Sea-water at Koganoura and 6 Miles in the West of Shirahama (Jan. 10. 1953)

Sampled Place		the offshore of Shirahama				Koganoura
Experimnt Number		I	II	III	V	IV
Depth from Surface	m	0	5	20	45	5
Chlorinity	‰	18.95	18.48	18.61	18.99	18.22
Rb Found	γ/L	380	382	400	316	278
Cs Found	γ/L	–	3.4	4.1	4.3	3.5

As seen from Table I and Table 2, the rubidium and the cesium content of

the sampled sea-water are respectively 250～400γ/L and 3.4～4.3γ/L. being in average 330γ/L and 4γ/L. These both values are larger than those which have been estimated. Considering that the before data have been obtained from the karnalite or the brine produced from sea-water, these values seem to be more appropriate.

Acknowledgment

The authors are indebted to Mr. I. Yamaji, of the Seto Marine Research Institute of Kyoto University, for the sampling of sea-water and to Mrs. Y. Kusaka and M. Oyabu for the measuring of radio-activity.

Reference

1). It was read in the First Annual Congress, Japan Society for Analytical Chemistry, Oct, 1952. "Chemical Studies on the Rare Alkali Elements" (Part 10).
2). It was read in the Second Annual Congress, Japan Society for Analytical Chemistry, Oct. 1953. "Chemical studies on the Rare Alkali Elements" (Part 12).
3). H. Wattenberg, Z. anorg. allgem. Chem, *236*, 339 (1938)
ibid, *251*, 86 (1943)
4). M. Ishibashi and Y. Harada, J. Chem. Soc. Japan, *63*, 211 (1942)
ibid *64*, 1049 (1943)
5). It was read in the First Annual Congress, Japan Society for Analytical Chemistry, Oct. 1952. "Chemical Studies on the Rare Alkali Elements" (Part 9).
6). I. M. Kolthoff and G. H. Bendix, Ind. Eng. Chem., Anal. Ed., *11*, 94 (1939)
S. Sato, J. Chem. Soc. Japan. 72. 181 (1951)
7). It was read in the Debating Society for Analytical Chemistry, May, 1953. "Chemical Studies on the Rare Alkali Elements" (Part 11)
8). It was read in the meeting of Kinki Division, Chem. Soc. of Japan, Feb. 1950.
9). It was read in the Fourth Annual Congress, Chem. Soc. of Japan, April, 1950.
10). It was read in the meeting of Kinki Division, Chem. Soc. of Japan, March, 1950.

Records of Oceanographic Works
in Japan, Vol. 2, No.1,
March 1955

Generation of the Tsunami in Compressible Water (Part II)

By

Hisashi Miyoshi

(Tokyo University of Fisheries)

Abstract: Soon after the bottom deformation, the disturbances due to the waves of expansion propagate much faster than the tsunami, and form the rings of interference. This interference pattern is characteristic for the time interval during which the bottom deformation continued, and not for the shape of the deformation. And the surface elevations and depressions due to the disturbances are included inside a very thin oblate spheroid, the axis of rotation of which is the vertical line at the center of the origin. This means that the energy of the compressional waves, being considered to be comparable order as that of the (gravitational) tsunami waves, does not concentrate anywhere.

§ 4. *Analysis of the Wave Form due to the Compressional Disturbances.*

The equations of the surface elevations due to the compressional waves, which accompany the generation of the tsunami were given in Part I as follows.

$$\zeta_0=\frac{1}{T}[\xi_0(t)-\xi_0(t-T)] \qquad t>T$$

$$=\frac{1}{T}[\xi_0(t)-\xi_0(0)] \qquad t<T$$

where

$$\frac{\pi a^2}{V}\xi_0=\frac{\pi}{z_0^2}\int_0^\infty \sum_{n=1}^{\infty} \frac{(-1)^n(2n-1)\sin\gamma_{no}t\cdot J_0\left(m\frac{r}{a}\right)J_1(m)}{\gamma_{no}^3}\,dm \qquad (19),$$

$$(1-\Delta\gamma_{no}/\gamma_{no})\times\frac{t}{T}\Big\}=\begin{cases}1\\ \Xi\end{cases},\quad \Delta\gamma_{no}/\gamma_{no}=\delta\frac{(m^2-b_n^2)}{(m^2+b_n^2)}+\cdots\cdots,\quad \delta=\frac{1}{2}\left(\frac{C}{U}\right)^2,\quad b_n=\frac{(2n-1)}{2h}\pi,$$

$h=H/a$, $\gamma_{no}=\frac{h}{z_0}\sqrt{(m^2+b_n^2)}$ and $z_0=H/U$. Here, H, C and U are the depth of the sea, velocity of the long wave and that of the sound wave in water, respectively. And a, t and T are the radius of the bottom deformation area, time and the time duration during which the deformation continued.

Now we transform (19), using the relations

$$J_1(m)=m\int_0^1 sJ_0(ms)\,ds, \qquad J_0\left(m\frac{r}{a}\right)J_0(ms)=\frac{1}{\pi}\int_0^\pi J_0(m\Omega)\,d\omega$$

$$\Omega=\sqrt{\left(\frac{r}{a}\right)^2+s^2-2\left(\frac{r}{a}\right)s\cos\omega} \tag{26}$$

as follows

$$\frac{\pi a^2}{V}\xi_0=\frac{1}{z_0{}^2}\int_0^1 sds\int_0^\pi d\omega\int_0^\infty\sum_{n=1}^{\infty}\frac{(-1)^n(2n-1)\sin\gamma_{no}\,t\cdot J_0(m\Omega)mdm}{\gamma_{no}{}^3} \tag{27}$$

This integral is intractable, except for the large value of t, when the Debye's method or the Kelvin's method can be applied. We shall use the latter method, expanding (27) in the asymptotic formula and adding some variation, and obtain the next equation,

$$\frac{\pi a^2}{V}\xi_0=\frac{z_0}{\sqrt{2\pi}\,h^3}\Re\left\{\frac{e}{i}^{-\pi/4\cdot i}\int_0^1 sds\int_0^\pi d\omega\,[I_1-I_2]\right\} \tag{28}$$

where

$$I_{1,2}=\int_0^\infty\sum_{n=1}^{\infty}\frac{\sqrt{m}\,(-1)^n(2n-1)}{\sqrt{\Omega}\,(m^2+b_n{}^2)^3}\,e^{i\Omega(m\pm K\sqrt{m^2+b_n{}^2})}dm \tag{29}$$

and

$$K=\frac{ht}{z_0\Omega}=\frac{Ut}{a\Omega} \tag{30}$$

Now I_2 has the stationary point, so we put them m_s and assume that $m=m_s+\varepsilon$, then

$$m-K\sqrt{m^2+b_n{}^2}=m_s-K\sqrt{m_s{}^2+b_n{}^2}-\frac{K}{2}\frac{b_n{}^2\varepsilon^2}{(m_s{}^2+b_n{}^2)\sqrt{m_s{}^2+b_n{}^2}}+\frac{K}{2}\frac{m_s b_n{}^2\varepsilon^3}{(m_s{}^2+b_n{}^2)^2\sqrt{m_s{}^2+b_n{}^2}}+\cdots\cdots\cdots$$

where

$$m_s=\frac{b_n}{\sqrt{K^2-1}}\quad\therefore\quad m_s{}^2+b_n{}^2=\frac{b_n{}^2K^2}{K^2-1}.$$

When the front of the disturbances is approached, K tends 1--0 and the accuracy of the calculation drops, if we adopt the term of ε^2. And we cannot utilize, similarly, the terms of ε^3, ·····. But, in this case, as $m_s\longrightarrow\infty$, the amplitude of (29) becomes small enough, when m is near m_s. Consequently, the disturbances due to the compressional waves are very small near the front.

Except the above case, we will integrate I_2 for $K\neq 1$, as follows.

$$I_2=\int_{-\infty}^{\infty}\sum_{n=1}^{\infty}\frac{\sqrt{m_s}\,(-1)^n(2n-1)}{\sqrt{\Omega}\,(m_s{}^2+b_n{}^2)^3}e^{\,i\Omega(m_s-K\sqrt{m_s{}^2+b_n{}^2})}\times e^{-\frac{\Omega K b_n{}^2}{2(m_s{}^2+b_n{}^2)^{3/2}}i\varepsilon^2}d\varepsilon \tag{31}$$

By the way, as is well-known,

$$\int_{-\infty}^{\infty}e^{-ai\varepsilon^2}d\varepsilon=\sqrt{\frac{\pi}{a}}e^{-\pi/4\cdot i} \tag{32}$$

(31) becomes

$$I_2 = \sqrt{2\pi}\, e^{-\pi/4 \cdot i} \sum_{n=1}^{\infty} \frac{(-1)^n (2n-1)}{\Omega \sqrt{K} (m_s^2 + b_n^2)^{3/4}} \cdot \frac{\sqrt{m_s}}{b_n} e^{i\Omega(m_s - K\sqrt{m_s^2 + b_n^2})} \quad (33).$$

$$\therefore \quad \frac{\pi a^2}{V} \bar{\xi}_0 = \frac{z_0}{h^3} \Re \left\{ \int_0^1 s\,ds \int_0^{\pi} d\omega \sum_{n=1}^{\infty} \frac{(-1)^n (2n-1) \sqrt{m_s}}{\Omega \sqrt{K} (m_s^2 + b_n^2)^{3/4} \cdot b_n} \right.$$

$$\left. \times e^{i\Omega(m_s - K\sqrt{m_s^2 + b_n^2})} \right\} \quad (34)$$

$$= \frac{2 z_0^3}{\pi h^4 t^2} \int_0^1 s\,ds \int_0^{\pi} d\omega \left[\Omega \sqrt{K^2 - 1} \sum_{n=1}^{\infty} \frac{(-1)^n}{b_n} \cos (b_n \Omega \sqrt{K^2 - 1}) \right] \quad (35).$$

As

$$\Omega = \frac{r}{a} - s \cos \omega + \cdots\cdots$$

$$\Omega \sqrt{K^2 - 1} = \frac{1}{a} \sqrt{(U t)^2 - r^2} + \frac{rs \cos \omega}{\sqrt{(U t)^2 - r^2}} + \cdots\cdots \quad (36).$$

Neglecting the small modifications on the amplitude,

$$\frac{\pi a^2}{V} \bar{\xi}_0 = \frac{2 z_0^3 \sqrt{(U t)^2 - r^2}}{\pi h^4 t^2 a} \int_0^1 s\,ds \int_0^{\pi} d\omega \left[\sum_{n=1}^{\infty} \frac{(-1)^n}{b_n} \right.$$

$$\left. \times \cos b_n \left\{ \frac{1}{a} \sqrt{(U t)^2 - r^2} + \frac{rs \cos \omega}{\sqrt{(U t)^2 - r^2}} \right\} \right] \quad (37).$$

Now we define the parameter

$$\vartheta = \frac{r}{U t} = \frac{1}{K} \left(1 + \frac{a}{r} s \cos \omega + \cdots\cdots \right) \quad (38),$$

and integrate (37) as follows

$$\frac{\pi a^2}{V} \bar{\xi}_0 = \frac{2 z_0^3 r (1 - \vartheta^2)}{\pi h^4 t^2 a \vartheta^2} \int_0^{\pi} \left[-\frac{\cos \omega}{h} F\left(\frac{\pi}{2h} \frac{r}{a} \sqrt{\frac{1}{\vartheta^2} - 1} + \frac{\pi}{2h} \frac{\cos \omega}{\sqrt{\frac{1}{\vartheta^2} - 1}} \right) \right.$$

$$\left. + \frac{2}{\pi} \sqrt{\frac{1}{\vartheta^2} - 1} \left\{ H\left(\frac{\pi}{2h} \frac{r}{a} \sqrt{\frac{1}{\vartheta^2} - 1} + \frac{\pi}{2h} \frac{\cos \omega}{\sqrt{\frac{1}{\vartheta^2} - 1}} \right) - H\left(\frac{\pi}{2h} \frac{r}{a} \sqrt{\frac{1}{\vartheta^2} - 1} \right) \right\} \right] \frac{d\omega}{\cos^2 \omega} \quad (39),$$

where

$$\left. \begin{aligned} F(x) &= \frac{4}{\pi^2} \left(\frac{\sin x}{1^2} - \frac{\sin 3x}{3^2} + \cdots\cdots \right) \\ H(x) &= \frac{\pi}{8} - \frac{4}{\pi^2} \left(\frac{\cos x}{1^3} - \frac{\cos 3x}{3^3} + \cdots\cdots \right) \end{aligned} \right\} \quad \text{then} \quad H' \equiv F \quad (40).$$

These periodic functions are shown in Figs. 7 and 8.

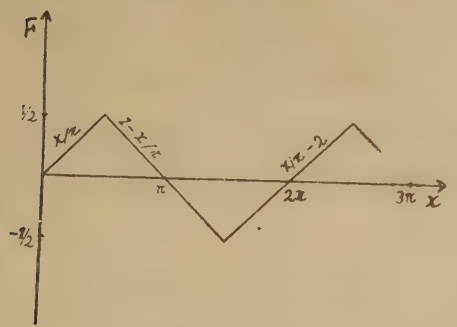

Fig. 7

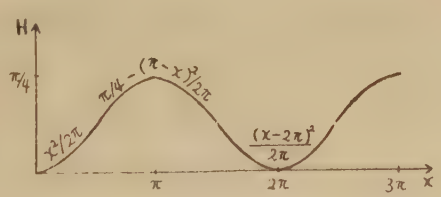

Fig. 8

Let us fix the value of r, and consider about some value of time $t=t_0$, which is large enough. Then we put $\vartheta_0=\frac{r}{Ut_0}$, and $\frac{t-t_0}{t_0}=\varepsilon\ll 1$. And we obtain the following relationship.

$$\vartheta \fallingdotseq \vartheta_0\ (1-\varepsilon)$$

Then we derive the following equation

$$\frac{r}{H}f(\vartheta)=\frac{r}{H}f(\vartheta_0)-\frac{r}{H}\varepsilon\vartheta_0 f'(\vartheta_0)+\cdots\cdots \qquad (41),$$

in which, the second term being equal to $\frac{\Delta t}{z_0}\vartheta_0^2 f'(\vartheta_0)$, so the approximation (41) is accurate enough as far as $\Delta t\ (\equiv t-t_0)\sim z_0$.

$$\therefore\quad \frac{\pi a^2}{V}\xi_0(t)=\frac{4z_0^2\ (1-\vartheta_0^2)^{3/2}}{\pi^2 t_0\vartheta_0^2}\int_0^{\pi}\Big[-\delta_0\cos\omega\cdot F\{f(t)+\delta_0\cos\omega\}$$
$$+H\{f(t)+\delta_0\cos\omega\}-H\{f(t)\}\Big]\frac{d\omega}{\cos^2\omega} \qquad (42),$$

where another parameter $\delta_0=\frac{\vartheta_0\pi}{2h\sqrt{1-\vartheta_0^2}}$ is defined, and then

$$f(t)=\frac{\pi}{2}\left(\frac{r}{H}\frac{\sqrt{1-\vartheta_0^2}}{\vartheta_0}-\frac{t_0}{z_0\sqrt{1-\vartheta_0^2}}\right)+\frac{\pi}{2}\frac{t}{z_0\sqrt{1-\vartheta_0^2}}=\frac{\pi\delta_0\Delta t}{a\vartheta_0}+\frac{\pi r(1-\vartheta_0^2)}{a\vartheta_0^2}\delta_0 \qquad (43).$$

If we remove the zero point of time by the way in which $f(t_0)=2l\pi$, l being an integer, we get from (42) the following relations,

$$\frac{\pi U^2 t_0}{V\sqrt{1-\vartheta_0^2}}\xi_0(t)=\frac{1}{\delta_0^2}\int_0^{\pi}\Big[-\delta_0\cos\omega\cdot F\Big(\frac{\pi\Delta t}{2z_0\sqrt{1-\vartheta_0^2}}+\delta_0\cos\omega\Big)$$
$$+H\Big(\frac{\pi\Delta t}{2z_0\sqrt{1-\vartheta_0^2}}+\delta_0\cos\omega\Big)-H\Big(\frac{\pi\Delta t}{2z_0\sqrt{1-\vartheta_0^2}}\Big)\Big]\frac{d\omega}{\cos^2\omega} \qquad (44)$$
$$=\frac{1}{\delta_0^2}\int_{-1}^{1}\Big[-\delta_0 x F\Big(\frac{\pi\Delta t}{2z_0\sqrt{1-\vartheta_0^2}}+\delta_0 x\Big)+H\Big(\frac{\pi\Delta t}{2z_0\sqrt{1-\vartheta_0^2}}+\delta_0 x\Big)$$
$$-H\Big(\frac{\pi\Delta t}{2z_0\sqrt{1-\vartheta_0^2}}\Big)\Big]\frac{dx}{\sqrt{1-x^2}} \qquad (44'),$$

considering that

$$\frac{F}{H}\{f(t)+k\}=\frac{F}{H}\Big\{\frac{U\delta_0}{a\vartheta_0}\Delta t+k\Big\} \qquad (45)$$

Now, ξ_0 will be determined by the combination of four parameters (H, δ_0, ϑ_0, Δt), instead of that of (H, a, r, t). And we find the parameter which determines the character of integration of (44) is δ_0, because the forms of functions F and H vary every interval of π; that is, when $\frac{(l-1)}{2}\pi<\delta_0\leqq\frac{l}{2}\pi$, the integrand in (44) may spread over l or $(l+1)$ regions in which the forms of the integrand differ each other. As the simplest case, we will perform the integration, when $0<\delta_0\leqq\frac{\pi}{2}$ or $l=1$.

(1) In the time interval during which the following relation is satisfied,

$\frac{\Delta t}{\sqrt{1-\vartheta_0^2}}\varepsilon\left[0,\left(1-\frac{2}{\pi}\delta_0\right)z_0\right]$,

$$\left.\begin{aligned} F\left(\frac{\pi\Delta t}{2z_0\sqrt{1-\vartheta_0^2}}+\delta_0 x\right)&=\left(\frac{\pi\Delta t}{2z_0\sqrt{1-\vartheta_0^2}}+\delta_0 x\right)/\pi, \\ H\left(\frac{\pi\Delta t}{2z_0\sqrt{1-\vartheta_0^2}}+\delta_0 x\right)&=\left(\frac{\pi\Delta t}{2z_0\sqrt{1-\vartheta_0^2}}+\delta_0 x\right)^2/2\pi, \\ H\left(\frac{\pi\Delta t}{2z_0\sqrt{1-\vartheta_0^2}}\right)&=\left(\frac{\pi\Delta t}{2z_0\sqrt{1-\vartheta_0^2}}\right)^2/2\pi \end{aligned}\right\} \quad (46),$$

$\therefore$ (44′) becomes $\dfrac{1}{\delta_0^2}\displaystyle\int_{-1}^{1}\frac{-\delta_0^2}{2\pi\sqrt{1-x^2}}dx=-\frac{1}{2}$ (46′).

(2) When $\dfrac{\Delta t}{\sqrt{1-\vartheta_0^2}}\varepsilon\left[\left(1-\dfrac{2}{\pi}\delta_0\right)z_0, z_0\right]$,

$$\left.\begin{aligned} F\left(\frac{\pi\Delta t}{2z_0\sqrt{1-\vartheta_0^2}}+\delta_0 x\right)&=\left(\frac{\pi\Delta t}{2z_0\sqrt{1-\vartheta_0^2}}+\delta_0 x\right)/\pi, && x<x_{1/2} \\ &=1-\left(\frac{\pi\Delta t}{2z_0\sqrt{1-\vartheta_0^2}}+\delta_0 x\right)/\pi, && x>x_{1/2} \\ H\left(\frac{\pi\Delta t}{2z_0\sqrt{1-\vartheta_0^2}}+\delta_0 x\right)&=\left(\frac{\pi\Delta t}{2z_0\sqrt{1-\vartheta_0^2}}+\delta_0 x\right)^2/2\pi, && x<x_{1/2} \\ &=\pi/4-\left(\frac{\pi\Delta t}{2z_0\sqrt{1-\vartheta_0^2}}+\delta_0 x-\pi\right)^2/2\pi, && x>x_{1/2} \\ H\left(\frac{\pi\Delta t}{2z_0\sqrt{1-\vartheta_0^2}}\right)&=\left(\frac{\pi\Delta t}{2z_0\sqrt{1-\vartheta_0^2}}\right)^2/2\pi \end{aligned}\right\} \quad (47),$$

then (44′) becomes

$$\frac{1}{\delta_0^2}\int_{-1}^{x_{1/2}}\frac{-\delta_0^2 dx}{2\pi\sqrt{1-x^2}}+\frac{1}{\delta_0^2}\int_{x_{1/2}}^{1}\frac{(\delta_0^2x^2-2\delta_0^2x_{1/2}^2)}{2\pi x^2\sqrt{1-x^2}}dx$$
$$=\left(-\frac{\sin^{-1}x_{1/2}}{\pi}-\frac{x_{1/2}\cdot\sqrt{1-x_{1/2}^2}}{\pi}\right) \quad (47'),$$

here

$$x_{1/2}=\frac{1}{\delta_0}\frac{\pi}{2}\left\{1-\frac{\Delta t}{z_0\sqrt{1-\vartheta_0^2}}\right\} \quad (48).$$

(3) And we get further

$$\frac{\pi U^2 t_0}{V\sqrt{1-\vartheta_0^2}}\xi_0(t)=\left(-\frac{\sin^{-1}x_{1/2}}{\pi}-\frac{x_{1/2}\cdot\sqrt{1-x_{1/2}^2}}{\pi}\right) \text{ when } \frac{\Delta t}{\sqrt{1-\vartheta_0^2}}\varepsilon\left[z_0,\left(1+\frac{2}{\pi}\delta_0\right)z_0,\right],$$
$$=1/2 \quad \text{when} \quad \frac{\Delta t}{\sqrt{1-\vartheta_0^2}}\varepsilon\left[\left(1+\frac{2}{\pi}\delta_0\right)z_0,\left(3-\frac{2}{\pi}\delta_0\right)z_0\right],$$
$$=\left(\frac{\sin x_{3/2}}{\pi}+\frac{x_{3/2}\sqrt{1-x_{3/2}^2}}{\pi}\right) \quad \text{when} \quad \frac{\Delta t}{\sqrt{1-\vartheta_0^2}}$$

and
$$\varepsilon\left[\left(3-\frac{2}{\pi}\delta_0\right)z_0,\left(3+\frac{2}{\pi}\delta_0\right)z_0\right],$$
$$=-1/2 \quad \text{when} \quad \frac{\Delta t}{\sqrt{1-\vartheta_0^2}}\varepsilon\left[\left(3+\frac{2}{\pi}\delta_0\right)z_0, 4z_0\right] \quad (49).$$

Here, $x_{3/2}=\dfrac{1}{\delta_0}\dfrac{\pi}{2}\left(3-\dfrac{\Delta t}{z_0\sqrt{1-\vartheta_0^2}}\right)$ (50).

Now we will show, for example, the figure of $\frac{\pi U^2 t_0}{V\sqrt{1-\vartheta_0^2}}\,\xi_0(t) \fallingdotseq \frac{\pi U^2 t_0}{V}\,\xi_0$ in which $\vartheta_0=1/50$ and $\delta_0=1$, in Fig. 9.

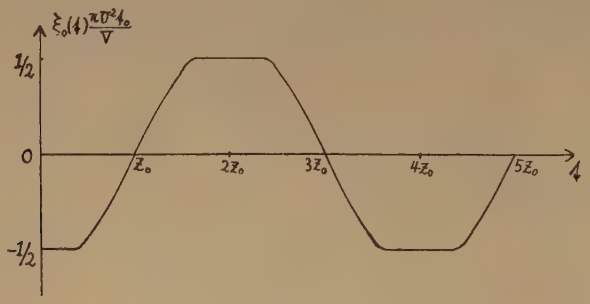

Fig. 9.

In this case, as $\vartheta_0=\frac{r}{U t_0}=1/50$, the considered place is almost at the center of the origin. And as $\delta_0=1$, $\vartheta_0\pi=\pi/50=2h\sqrt{1-\vartheta_0^2} \fallingdotseq 2h$, then $h \fallingdotseq \pi/100 \fallingdotseq 1/30 \ll 1$. Through our analysis in this paragragh, t is required not to be a function of n. This requirement is equivalent, from (19), to the condition that $h=H/a \ll 1$ or $\gg 1$. This condition is satisfied in the above case. Then, as $a \fallingdotseq 30H$, the radius of the deformed area is thirty times as long as the water depth. When the depth is 3 *km*, the radius is 90 *km*. These are natural values.

§ 5. *Characters of the above Waves.*

Through the complicated analysis in § 4, we can point out the several interesting characters of the waves caused by the compressional disturbances.

(1) From (44), we can easily find out that the period and the wave length are $4z_0\sqrt{1-\vartheta_0^2}$ and $4H\sqrt{1-\vartheta_0^2}/\vartheta_0$, respectively. They would be both monotone-decreasing, if one would look over the sea surface from the origin towards the front.

(2) We become aware of from (44) and (46) ····· (49′), that the amplitude is proportional to $\sqrt{1-\vartheta_0^2}$. This means that the elevations or the depressions inscribe or are included inside a thin oblate spheroid, the axis of rotation of which is the vertical line at the center of the origin. Of course, the skirts of this spheroid is the wave front. We know from this fact that *the energy of the compressional waves, being considered to be comparable as that of the (gravitational) tsunami waves, does not concentrate anywhere.*

(3) Finally, if we put $\frac{\pi\mathfrak{T}}{2z_0\sqrt{1-\vartheta_0^2}}=2M\pi$ in (44), and consider that $\mathfrak{T} \fallingdotseq 4z_0N$, we get

$$\vartheta_0 \fallingdotseq \sqrt{1-N^2/M^2} \qquad (51).$$

As the elevation is given as $\zeta_0=\frac{1}{T}\left[(\xi_0(t)-\xi_0(t-\mathfrak{T})\right]$, we find that the distur-

bance takes its nodes where M are integers, and its loops where M are semi-integers. For two examples, we will take $N=3$ and $N=2.5$ and $H=3km$ (this is the mean depth where Japanese famous tsunamis occurred). These values mean that the bottom deformations continued during the time durations of 24 sec. and 20 sec., respectively. From (51), the relative positions of the nodes and the loops are constant for any time. But the pattern of the interference rings is characteristic for the time duration during which the bottom deformation continued. These patterns (in Figs. 10 and 11) differ from those of the Newton's rings.

Fig. 10 $N=3$;
Black regions are nodal bands.

Fig. 11 $N=2.5$;
Black regions are nodal bands.

Table 1. For $N=3$ (and 2.5).

ϑ_n	(0.5528)	(0.6614) (0.7806	(0.8000) (0.8660)	(0.8660) (0.9091)	(0.9035) (0.9340)	·····
ϑ_l	0.5151 (0)	0.7454 (0.6999)	0.8381 (0.8315)	0.8871 (0.8907)	0.9165 (0.9230)	·····

Actually, the sound waves, their orthogonals of which are inside the critical angle (at the rock-water boundary) lose the considerable parts of their energies absorbed into the elastic bottom. And the waves outside the critical angle change their phases every reflexion at the bottom. Then, the secondary front will progress by the velocity less than half the sound wave velocity in water and no disturbance will appear behind this front.

§ 6. *The Case of an Arbitrary Shape of the Bottom Deformation.*

We know easily from Figs. 10 and 11 that the pattern of the interference rings is characteristic for the time duration of the bottom deformation. We will further investigate whether it is characteristic for the shape of the bottom deformation. Let us take an arbitrary function $f(r)$ ($\lim_{r\to\infty} f(r)=0$) to represent

the shape of the bottom deformation, and define the function

$$F(a,m)=\int_0^\infty J_0(k\lambda)\,f(\lambda)\,\lambda d\lambda=a^2\int_0^\infty J_0(m\lambda)\,f(a\lambda)\,\lambda d\lambda \qquad (52),$$

here a is the effective radius of the region of the bottom deformation and $m=ka$. Then we get

$$a^2\xi_0=\frac{\pi}{z_0{}^2}\int_0^\infty \sum_{n=1}^{\infty}\frac{(-1)^n(2n-1)\sin\gamma_{no}t\cdot J_0\left(m\frac{r}{a}\right)m\cdot F(a,m)}{\gamma_{no}{}^3}dm$$

$$=\frac{4a^2\sqrt{U^2t^2-r^2}}{U^{5/2}t^{3/2}r^{1/2}\pi}\sum_{n=1}^{\infty}\frac{(-1)^nF(a,m_s)}{(2n-1)}\cos(2n-1)\frac{\pi\sqrt{U^2t^2-r^2}}{2H} \qquad (53).$$

We can know from (53) that the wave form varies according to $f(r)$. But its wave length, period, and the pattern of its interference rings don't differ from what were treated in § 4 and § 5.

§ 7. *Conclusions.*

Omitting the conclusions in Part I, we obtained in Part II the following ones. (1) The disturbances due to the compressional waves form the rings of interference. This interference pattern is characteristic for the time duration of the bottom deformation, and not for the shape of the deformation.
(2) The crests and troughs of the compressional disturbances inscribe or are included inside a thin oblate spheroid. So, the energy of the compressional disturbances, being considered to be comparable as that of the (gravitational) tsunami (10^{23} ergs for larger ones), does not concentrate anywhere and will not be found out from the ships, except those at the origins. This will not also be perceived along the coast, because it is absorbed along the continental slope.

Acknowledgement.

The author should like to express his many thanks to the people of Geophysical Institute and Professor R. Takahashi of the Earthquake Research Institute, Tokyo University, for their kindness to discuss with him with valuable suggestions.

References

Ergin, K. (1952): "Energy Ratio of the Seismic Waves Reflected and Refracted at a Rock-Water Boundary", Bull. Seism. Soc. Amer. **42** (4), p. p. 349~372.
Lamb, H. (1932): Hydrodynamics.
Lord Rayleigh (1909): "On the Instantaneous Propagation of Disturbance in a Dispersive Medium, Exemplified by Waves on Water Deep and Shallow", Phil. Mag. (XVIII) p. p. 1~6.
Miyoshi. H. (1954): "Generation of the Tsunami in Compressible Water (Part I)," Journ. Oceanogr. Soc. Jap. **10** (1), p. p. 1~9.
Pidduck, F. B. (1912): "The Wave-Problem of Cauchy and Poisson for Finite Depth and Slightly Compressible Fluid," Proc. Roy. Soc. Lond. Vol. 86, p. p. 396~
Watson, G. N. (1922): "A Treaties on the Theory of Bessel Functions".

Records of Oceanographic Works
in Japan. Vol. 2, No. 1,
March 1955

On the Vertical Distributions of the Intensity of Illumination in the Water and Water Temperature of Lake Ashinoko

by

Tadayoshi Sasaki,* Noboru Okami,** Seiichi Watanabe,**
and Gohachirō Ōshiba**

I. Introduction

A considerable amount of experimental work has been carried out in the last few years on the deep scattering layer appeared on the fathogram. The scattering layer is believed to be due inlarge part to the following phenomena: (1) plankton having the negative phototropism which migrate vertically from hour to hour according to the intensity of illumination in the sea. (2) schools of fish looking for the plankton, (3) combination of these phenomena. From the point of view that the scattering layer should be corespond to the discontinuity of the water temperature and the intensity of illumination, we have been investigating the cause of the scattering layer by measuring these physical properties.

As the first step of the investigation, the vertica ldistributions of the intensity of illumination and the water temperature in Lake Ashinoko, Hakone, were measured by a highly sensitive underwater illuminometer and thermistor thermometer both constructed in our laboratory.

II. Explanation of the Apparutas

In the previous work, as the illuminometer a phototube (MATSUDA, PG 50V) with one or two stage D. C. amplifier was used. In the practical use the reliability of the reading of the illuminometer was restricted by lack of stability, in high sensitivity range. The minimum value of the intensity of illumination observed was 6×10^{-3} lux. A highly sensitive illuminometer used in the present investigation was constructed with a photomultiplier, and had perfect characters both in its sensitivity and stability. Formaly the filters were changed directly by hauling up the illuminometer on boad. In the present case, they were changed indirectly by remote controle system making a special design not to increase the number of the lead wire.

1. Electric circuit of the illuminometer.

* Tokyo University of Fisheries , Scientific Research Institute.
** Scientific Research Institute, Tokyo.

The illuminometer is constructed with the following parts: A light receiver mounted in a watertight case, a filter changer, an ammeter, a controler, a 12V battery, cabtire cable, and an earth plate. The inverter and the battery can be replaced by 100 V A. C. (50 or 60 c.p.s.).

The circuit diagram is shown in Fig. 1.

The filters are easily changed by switching on the filter circuit. Time required to measure the intensity of illumination using the six filters is 30-40 seconds.

The high tention electric source consists of an automatic voltage stabiliser, an ordinary smoothing circuit and a potential devider. The out put voltage of the source is ranging from 400V to 1000V.

The intensity of illumination is directly read by a microammeter having four scales : 300, 100, 30, and 10 μA.

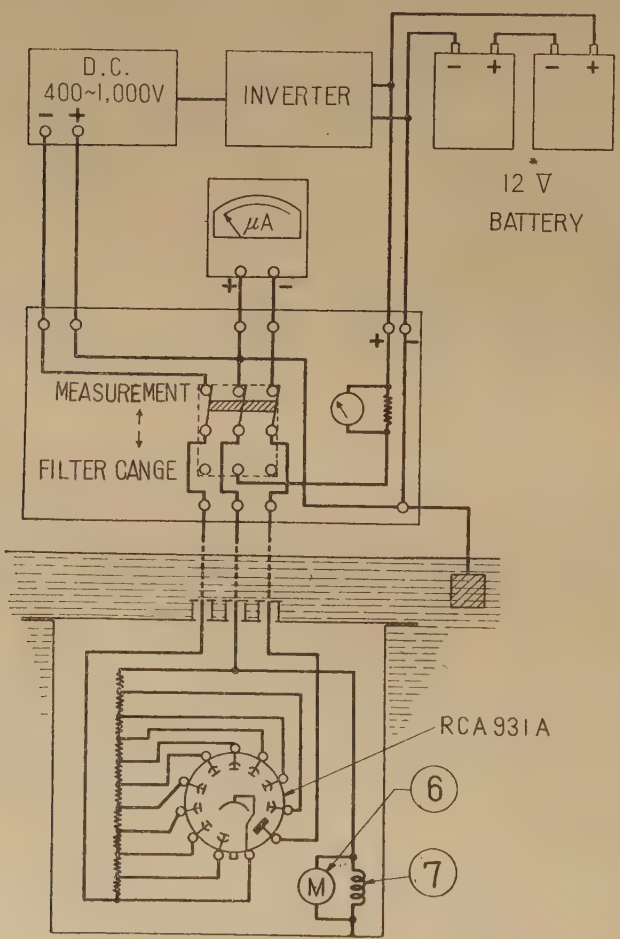

Fig. 1 Schematic circuit diagram of the illuminometer.

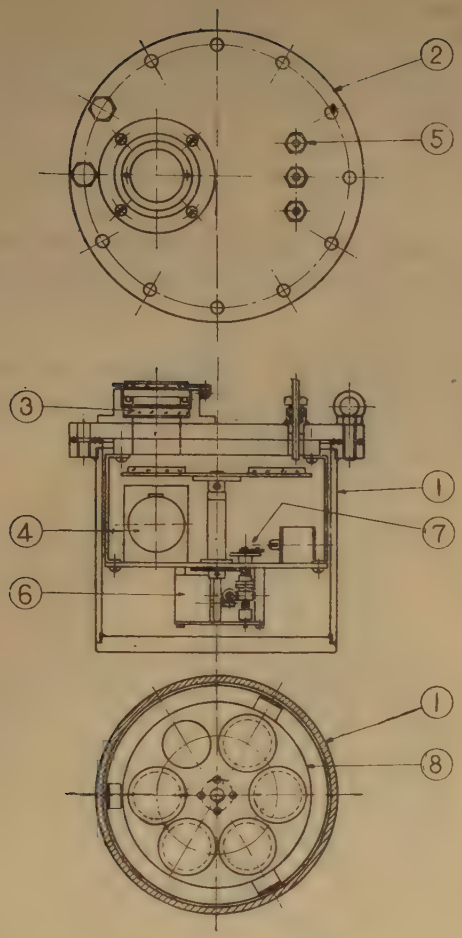

Fig. 2 Water tight case of the illuminometer.

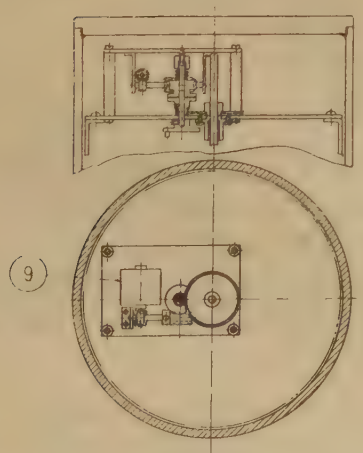

Fig. 3 Moter driven mechanism.

2. Main part of the watertight case.

As shown in Fig. 2. the watertight case is constructed with the following parts : a cap of the case ②, a watertight case ①, a glass window (8mm in thickness) ③, an inlet of cabtire cable ⑤, a filter disk ⑧, a photomultiplier (RCA, 931A) ④, a filter changing mechanism ⑦, and a moter driven mechanism ⑥, the watertight case which is made of blass plate and jointless blass pipe have been tested under a hydraulic pressure of 20 Kg/cm^2. In the present case four filters were mounted on the filter plate : "MATSUDA" V-V_1, V-G_1, V-Y_1, V-R_3.

A opal glass is mounted out side of the glass window to receive the light beams from all directions frontward of the plane of the glass.

It is desirable to use a strong cabtire cable capable of hanging the illuminometer. In the present case three vinyl-coated cupper wires for the fluorescent lamp was used and the illuminometer was hanged by a wire rope independently.

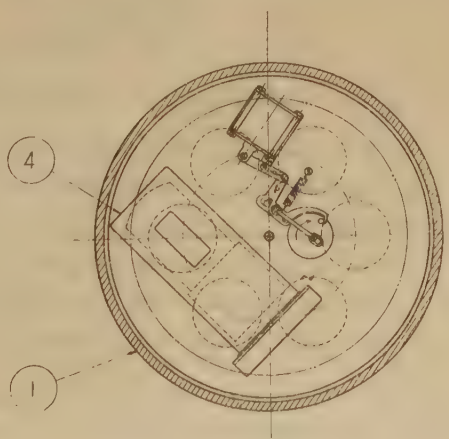

Fig. 4 Trigger mechanism.

3. Filter changing mechanism.

The moter driven mechanism and the trigger mechanism are shown in Figs. 3 and 4 respectively. Using these mechanism the filters can easily and surely be changed by remote controle.

4. Deck photometer.

Deck photometer having relatively low sensitivity has been made to observe the intensity of illumination on boad and to correct the data of underwater measurement.

Details of the photometer are shown in Figs. 5 and 6. The photometer was so carefully designed as to resist rolling of the ship. This meter can also be used for a underwater illuminometer of moderate sensitivity.

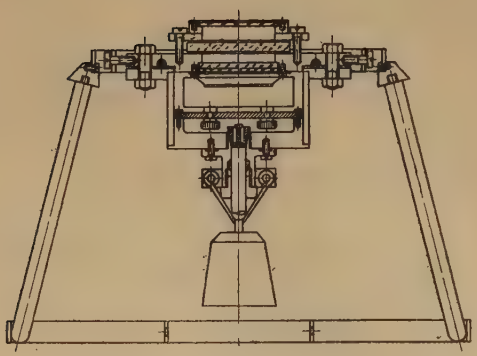

Fig. 5 Side-view of the deck photometer.

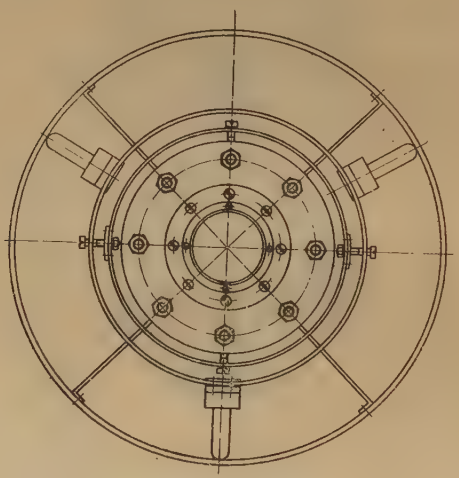

Fig. 6 Plane figure of the deck phtometer.

III. Results and discussion

1. Vertical distributions of the intensity of illumination under water.

From 6: 45 A.M. to 5: 30 P.M. on the 27th of September in 1954, the vertical distributions of the intensity of illumination in Lake Ashinoko (Fig. 7) were measured for every wave length at intervals of tow hours. The results of 9:30 to 10:40 A.M. are shown in Table 1 and Fig. 8. The extinction coefficients of the water in each layer for every wave length were calculated from the measured data are shown in Fig. 9.

From Fig. 8 it is concluded that, in general, the minimum value of the extinction coeficient is obtained at the wave length of about 4500 Å. This means the optical property of the water had the character of pure water in

its extinction coefficient. The result agrees with an observation of transparency made at the same lake.

Fig. 7 Location of stations where observations were made.

Table 1

Percentage of surface light and water temperature obtained at the station 1. September 27, 1954.

Time: 0930-1040 A. M. Surface of water: Calm
Altitude oi sun: 43°10′–51°30′ Transparency: 9 m
Amount of clouds: O

Depth(m) \ Filter	V–V1 (3200–4400Å)	V–G1 (4200–6400Å)	V–Y1 (4600–7000Å)	No Filter (3000–7000Å)	Temp. (°C)
0	100	100	100	100	19.8
2	61	80	71	69	19.1
4	37	63	51	47	19.8
6	18.5	50	36	27	19.1
8	9.2	35	23.5	15.5	19.4
10	4.4	24.5	15.0	9.0	19.4
12	2.3	17.0	10.0	5.1	19.4
14	1.15	11.8	6.5	2.95	19.1
16	0.76	8.3	4.2	1.70	15.3
18	0.51	5.8	2.8	0.98	13.4
20	0.34	4.3	2.0	0.65	11.8
22	0.26	3.2	1.4	0.45	11.4
24	0.20	2.35	0.96	0.30	10.0
26	0.155	1.75	0.68	0.205	8.8
28	0.125	1.27	0.48	0.140	9.1
30	0.096	0.94	0.33	0.098	8.8
32	0.081	0.70	0.24	0.068	8.5
34	0.074	0.54	0.175	0.048	8.0
36	0.068	0.41	0.130	0.038	7.9
38	0.062	0.31	0.094	0.024	7.5
40	0.056	0.24	0.068	0.017	7.7

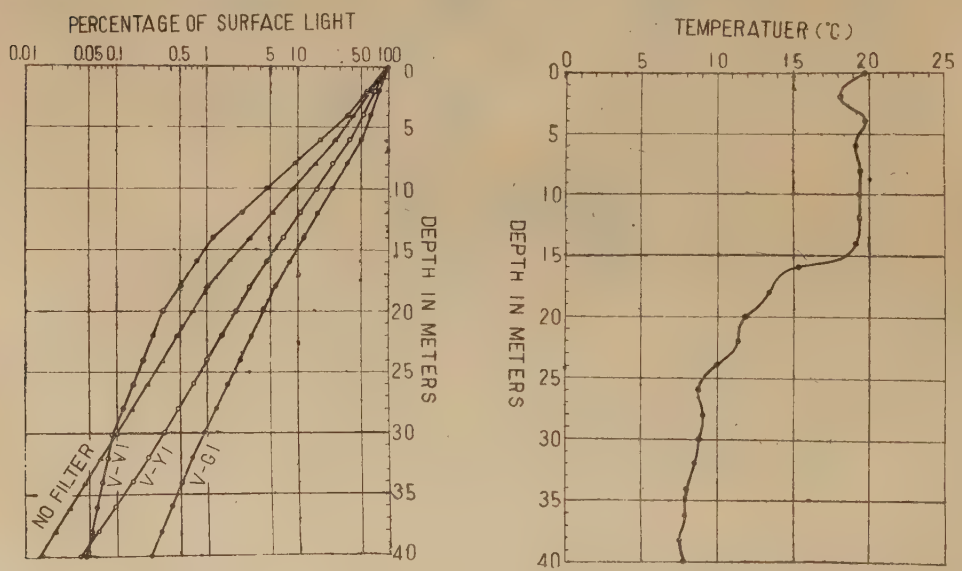

Fig. 8 Percentage of surface light and water temperature obtained at the Station 1. September 27, 1954.

2. Relation between the extinction coefficient and the altitude of the sun.

The extinction coefficients of the water in the surface layer measured at different times with a filter for 5000 Å are tabulated in Table 2. From the table it is noticed that the changes in extinction coefficients against the observed times are larger for the O-4 m layer than for the 4-16 m layer and the value of the extinction coefficient of the O-4 m layer becomes large at sunrise and sunset[1]. When the effect of the altitude of the sun on the extinction coefficient of the surface layer is discussed a care must be taken on the migration of the plankton, because extinction coefficient are largely affected by the suspensoids in the water.

Cloudiness, wind force, transparency of the water and the condition of the water surface observed at the same time are summerized in Table 3. The distribution of the water temperature are tabulated in Table 4.

The table 2 shows that the extinction coefficients of the 0-4 m layer observed between 15 : 00 and 15 : 40 P. M. take small value nevertheless the decrining sun.

Table 2

Relation between the extinction coefficients for the surface layer in 5000 Å and altitude of sun obtained at the station 1. September 27, 1954. (Sun rise : 0532, Sun set : 1732.)

Altitude of Sun	13°10′–22°20′	43°10′–51°30′	52°20′–51°30′	49°30′–44°30′	32°30′–22°30′	1°~3′
Time	0645–0730	0930–1040	1225–1230	1300–1230	1500–1540	1700–1730
0~ 4m	0. 173	0. 119	0. 190	0. 253	0. 081	0. 299
4~16m	0. 147	0. 140	0. 160	0. 163	0. 170	0. 187

Table 3

Amout of clouds, surface, force of wind and transparency corresponding each observating time at the station 1. September 27, 1954.

Time	Amaunt of clouds	Surface	Force of wind	Transparency
0645–0730	7	calm	2	9m
0930–1040	0	〃	2	9
1225–1230	2	〃	2	9
1330–1335	3	〃	2	9
*1550–1540	6	〃	1	9
1700–1730	4	〃	0	9

This anormality may be due to the passing phenomenon of the clauds that shut out the sun's rays. As shown in Table 5 the same effect was observed in the next day when the clouds hung low : the extinction coefficient of the surface layer calculated with the data shown in the table is 0.073 m^{-1} and is smaller than that obtained at the same hour on the day before.

Table 4

Vertical distributions of water temperature obtained at the station 1. September 27, 1954.

Time	0915—1027	1200—1236	1300—1333	1500—1532	1700—1739
Depth (m)	Temperature (°C)				
0	19.8	19.1	20.6	20.3	19.1
2	19.1	18.9	20.4	19.8	19.1
4	19.8	19.1	19.8	20.0	19.1
6	19.1	19.2	19.8	19.8	19.8
8	19.4	19.1	19.8	19.8	19.1
10	19.4	19.2	17.0	19.8	19.8
12	19.4	19.6	18.5	19.8	19.4
14	19.1	17.5	18.0	17.0	18.2
16	15.3	14.3	15.9	15.1	16.1
18	13.4	12.7	13.6	13.5	15.3
20	11.8	11.8	12.3	11.0	12.7
22	11.4	10.0	11.2	10.5	11.8
24	10.0	9.2	10.0	9.5	11.0
26	8.8	9.0	9.9	9.0	10.0
28	9.1	9.0	8.9	8.8	8.5
30	8.8	8.9	8.9	8.5	8.9
32	8.5	8.7	8.9	8.3	9.0
34	8.0	8.3	8.8	8.0	8.0
36	7.9	8.1	8.0	8.5	8.0
38	7.5	8.0	8.0	8.0	8.0
40	7.7	7.9	8.0	7.9	7.9

	Air Temperature (°C)				
	0930 1010	1200 1230	1300	1500 1530	1700 1730
Temp. (°C)	20.6 21.5	20.3 19.8	22.0	22.5 19.8	17.4 17.0

Figs. 10 and 11 show the extinction coefficients of the surface layer obtained at different times against the wave length of the incident light.

The fluctuations of the extinction coefficients in the 0-4 m layer are believed to be due to the altitude of the sun. As clearly seen from the figure 9, (1) the amount of fluctuations are larger in a region of long wave length, (2) the wave length which corresponds to the minimum value of the extinction coefficient varies as time goes by. The cause of the variation may be attributed to change in distribution of the turbidity.

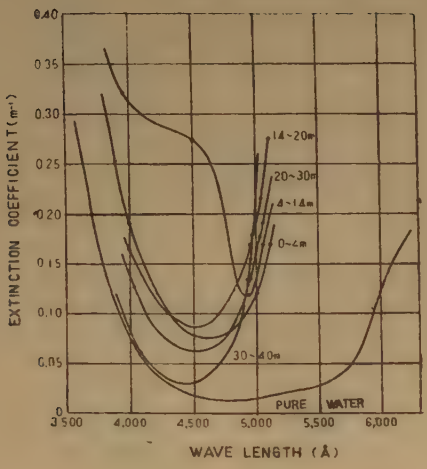

Fig. 9 Extinction coefficients of the water in each layer and for every wave length obtained at the Station 1 Septemder 27, 1954.

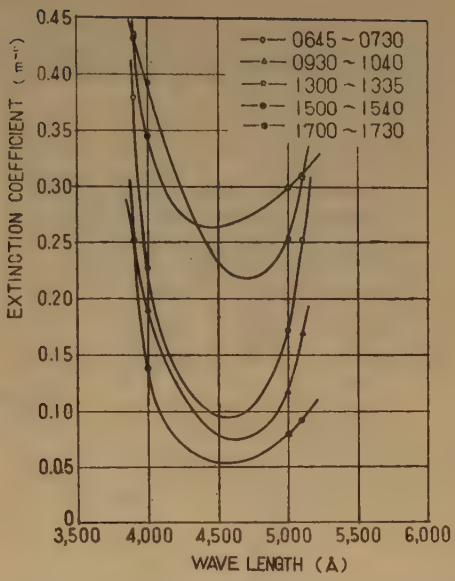

Fig. 10 Relation between the extinction coefficients of the surface layer (0-4 m) obtained at different times and wave legth of the incident light. September 27, 1954.

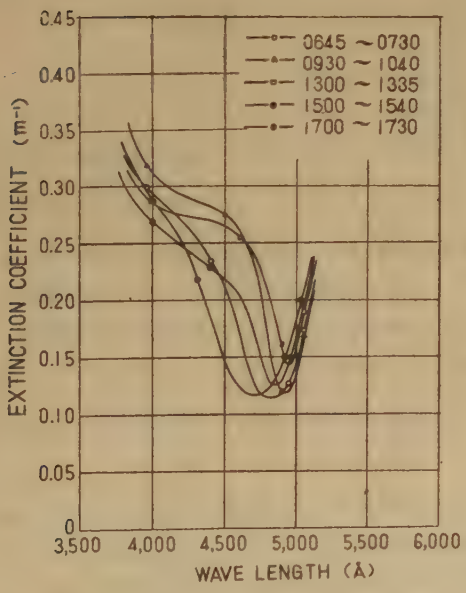

Fig. 11 Relation between the extinction coefficients of tha surfce layer (4-16m) obtained at diferent times and wave lengh of the incident light. September 27, 1954.

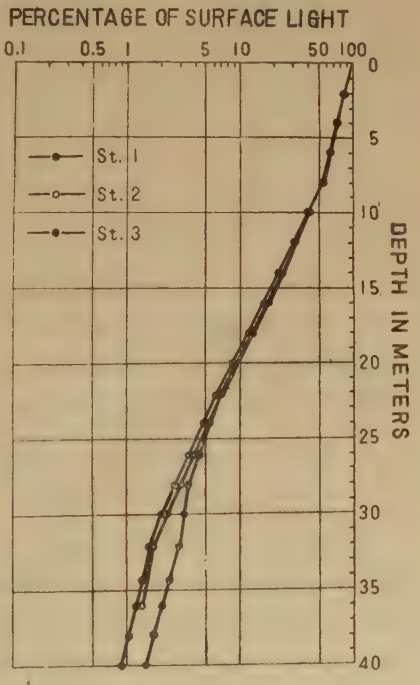

Fig. 12 Percentage of surface light obtained at the stations 2 and 3. September 28, 1954.

Table 5

Percentage of surface light and water temperature obtained at the station 1. September 28, 1954.

Time: 0820–0830
Altitude of sun: 32°50′–33°20′
Amount of clouds: 10 overcast
Surface of water: Calm
Transparency: 7.6 m
Filter: V–G1

Depth (m)	Illumination (%)	Temperature (°C)
0	100	20.4
2	86	20.6
4	74	20.6
6	64	20.6
8	55	21.0
10	43	20.7
12	33	21.0
14	25	20.6
16	18.5	15.3
18	13.2	12.3
20	9.6	12.0
22	7.0	11.0
24	5.6	10.0
26	4.4	9.6
28	3.6	9.0
30	3.3	8.9
32	3.0	8.6
34	2.6	8.8
36	2.2	8.2
38	1.9	8.2
40	1.6	8.0

From these observations it is concluded that the results obtained at 9 : 30 A. M. are considered to represent the true extinction coefficient of the water of Lake Ashinoko at this season of the year, because at the time the altitude of the sun has small influence on the measurements.

3. Relation between the extinction coefficient and the vertical distribution of the plankton.

To study the relation between the extinction coefficient of each layer and the vertical distribution of plankton, the plankton were collected from layer to layer at the same time when the optical measurements were made. The numbers of the plankton were counted under a microscope. The results are listed in Table 6.

The table shows that there is a striking parallelism between the extinction coefficient and the number of the phytoplankton except the surface layer.

Table 6

Relation between the extinction coefficients and the plankton distribution obtained at the station 1. September 28, 1954.

Time: 0820–0830

Filter: V–G1

Layer	Extinction coefficient(m^{-1})	Layer	Amount of Plankton/l	
			Phytoplankton	Zooplankton
0～ 8m	0.073	0～ 6m	6.1	–
8～14	0.133	6～12	2.8	–
14～22	0.158	12～18	3.3	1
22～28	0.111	18～24	4.5	0.5
28～32	0.045	24～30	1.1	0.16
32～36	0.078	30～35	1.6	–
		35～40	3.1	–

Table 7

Extinction coefficients of the water in each layer obtained at the stations 1, 2 and 3. September 28, 1954.

	St. 1	St. 2	St. 3
Time	0820～0830	1025～1036	1112～1119
Altitude of sun	32°51′～33°20′	49°45′～50°36′	52°20′～52°35′
Amount of cloud	10 (Rain)	10(Overcast)	10(Overcast)
Surface	Slight	Slight	Calm
Force of wind	4	3	1
Transparency	7.6m	7.1m	9.5m

Layer	Extinction coefficients (m^{-1})		
0～ 8m	0.073	0.073	0.073
8～14	0.133	0.137	0.142
14～22	0.158	0.156	0.154
22～28	0.111	0.136	0.143
28～30	0.045	0.136	0.143
30～32	0.045	0.136	0.072
32～36	0.078	0.068	0.072

The abnormal behavior of the surface layer correspond to the fact mentioned above: the extinction coefficient of the surface layer is largely affected by the altitude of the sun and the weather condition.

4. Variation of the distribution of the intensity of illumination in the water among different places.

All the measurements mentioned in the preceeding sections were carried out at the station 1 (the center of the lake). To investigate the variation of the distribution of the intensity of illumination in the water among different points other two stations were selected.

Results obtained at the two places are shown in Fig. 12 and Table 7. From Table 7 it is noticed that the extinction coefficients obtained in the surface layer (0-22 m) of the stations 1, 2 and 3 increase with increasing depth while those in the deep layer (28-36 m) decrease with increasing depth at the station 2 and 3, and increase with increasing depth at the station 1. Large value of the extinction coefficient in the deep layer have been attributed to detritus and iron contained in the water, and the phenomena have been observed only in the lake where the water is rich in chemical components. There have been little report on the chemical components contained in the deep water layer of Lake Ashinoko.

Any way, Fig. 12 suggests that the properties of the deep layer at the station 1 are different from those of the surface layer and of the deep layer at the stations 2 and 3.

Table 8 shows the results of the unique examination of the water that have been made at the station 1 by KANAGAWA Fisheries Experiment Station in 1933 and 1935. As noticed from the Table the contents of inorganic matter in the deep layer of the station 1 is different from those of the station 2. This examination can be understand hand by hand with the results of the extinction coefficient and the water temperature: as shown in Figs. 1 and 2, abnormal moderate temperature have been observed in the deep layer of the station 1.

The origin of the abnormal properties of the water in the deep layer at the center of the lake should be considered as follows: (1) under water spring just above the deep layer, water of which is rich in inorganic matter (2) formation of a layer having certain biochemical characters during a summertime.[2]

The complete explanation of the phenomena have not yet been made. It is considered accurate measurements of the properties of the water must be carried out again to solve the problems.

Table 8 (A)

Examination of the water the have been made at the stations 1 and 2 by KANAGAWA Fisheries Experiment Station in 1933 and 1935.

Station of water sampling: The center of the Lake (Station 1)

Date	November 4, 1943.					February 22, 1945			
Weater and others	Clear, Air Temp, 10.7°C Water Color 4					Overcast. Air Temp, 6.7°C Water color 5, Frasparency 11m			
Depth	0m	15	20	25	33 (bottom)	0m	10	25	37 (bottom)
Water Temp. (°C)	15.1	14.9	9.3	8.4	7.8	5.3	5.3	5.3	5.3
O_2 cc/L	6.39	6.54	7.40	6.94	6.13	7.87	7.67	7.99	7.72
O_2 %	99	100	100	93	81	99	97	100	97
PH	7.1	7.2	7.0	6.9	6.6	7.1	7.1	7.1	7.1
Free CO_2 mg/l	0.44	0.78	1.11	1.11	1.33	0.48	0.48	0.48	0.51
Fixed CO_2 mg/l	15.4	–	–	–	13.2	7.7	7.7	6.6	7.7
SiO_2	13.75	12.85	11.21	12.60	14.45	14.45	12.00	13.20	13.10
Ca	6.77	6.12	6.78	6.68	6.51	5.85	5.95	6.25	6.15
Mg	2.01	1.75	1.76	1.92	1.96	1.01	0.97	1.05	1.14
Na	1.71	1.68	1.49	1.47	1.64				
Fe	0.060	0.060	(0.060)	0.060	0.068				
SO_4	10.1	10.8	9.9	9.2	10.4				
Cl	2.04	1.97	2.04	2.10	1.97	2.65	2.99	3.17	3.52
Consump. $KMnO_4$	2.9	2.2	2.2	2.5	4.1	3.9	3.9	4.5	3.6

5. Summary

The vertical distributions of the intensity of illumination, water temperature and number of the plankton were measured. Details of a specially designed highly sensitive underwater illuminometer used in the measurements were fully explained. At the center of the lake, a deep layer having abnormal physical properties was found and the possible explanation were made.

6. Acknowledgement

The authers wish to express their hearty thanks to Mr. Yoshikazu Kokubu, Chief of KANAGAWA Fisherries Experiment Station, Mr. Hiroyuki Watanabe of the station, and HAKONE Shipping Office of SUNZU Railway Co., for their kind assistance in carring out the measurement.

Table 8 (B)

Station of water Sampling: Kojiri (Station 2)

Date	November 3, 1943					February 21, 1945				
Weather and others	Clear. Air Temp. 7.2°C					Clear Air Temp. 6.8 Water color 5, Transparency 11.2m				
					(bottom)					(bottom)
Depth	0m	10	15	18	20	0	5	10	15	18
Water Temp. (°C)	15.1	15.0	15.0	10.9	9.3	5.8	5.5	5.5	5.5	5.4
O_2 cc/L	6.30	–	6.69	7.20	6.81	8.15	7.92	7.92	7.82	7.73
O_2 %	97	–	101	101	96	102	99	99	98	96
PH	7.1	7.0	7.1	6.9	6.7	7.1	7.1	7.1	7.2	7.2
Free CO_2 mg/l	–	–	–	–	–	0.46	0.73	0.68	0.66	0.69
Fixed CO_2 mg/l	–	–	–	–	–	8.8	–	7.3	–	6.0
SiO_2	16.04	–	14.04	14.90	14.40	12.50	12.00	12.50	12.00	10.00
Ca	6.31	–	6.69	6.46	6.60	6.25	6.00	6.86	(6.36)	5.85
Mg	2.11	–	2.09	2.28	2.04	8.81	0.97	0.86	(0.87)	0.87
Na	1.78	–	1.60	1.60	1.42	–	–	–	–	–
Fe	0.060	–	(0.067)	0.067	0.067	–	–	–	–	–
SO_4	11.9	–	10.3	10.9	9.3	–	–	–	–	–
Cl	2.02	–	2.17	2.37	1.97	2.65	2.65	2.65	2.65	2.65
Consump. $KMnO_4$	2.9	–	2.1	4.3	4.2	3.6	3.8	3.8	5.1	6.5

References

(1) Takenouchi, Y., 1939. Angular distribution of submarine solar radiation and the effecf of altitude of sun upon the vertical extinction coefficient. Bulletin of the Japanese Society of Scientific Fisheries. Vol. 8, P. 213.

(2) Yoshimura, S., 1937. Abnormal thermal Stratification of Inland Lakes. Proc. Imp. Acad. Japan. Vol. 13, P. 316.

Records of Oceanographic Works
in Japan, Vol. 2, No. 1,
March 1955

On the Antarctic Circumpolar Current

By

Kenzo Takano

(Geophysical Institute, Tokyo University)

Abstract: This is an attempt to obtain the vertical structure of velocity in the wind-driven current in the Antarctic Ocean in consideration of the variation in density. The surface velocity, the surface slope and the mass transport are satisfactorily explained provided the large coefficient of horizontal mixing is assumed. It is also found that below the depth of frictional resistance both the vertical and lateral mixing have no influence upon the velocity distribution and the pressure gradient is completely balanced by Coriolis forces alone.

Introduction.

As is shown in the previous paper, it is obliged to take the unreasonably large coefficient of vertical mixing in order to get the vertical distribution of current velocity progressively decreasing downward to negligible values, so far as a homogeneous ocean is assumed.

In the present paper, we intend to obtain more reasonably such a vertical structure, specifying the variation in density so that the density distribution in the Antarctic Ocean is approximately represented. The variation of the Coriolis forces is not taken into account.

Theoretical Consideration.

Let the x-axis be positive eastward along the southern boundary of the ocean and the y-axis northward and the z-axis vertically downward from the undisturbed surface. If the nonlinear terms and the term including the vertical motion are neglected, the equations of motion are given by

$$A_h\frac{\partial^2 u}{\partial y^2}+A_v\frac{\partial^2 u}{\partial z^2}-\rho f v=0, \tag{1}$$

$$A_h\frac{\partial^2 v}{\partial y^2}+A_v\frac{\partial^2 v}{\partial z^2}+\rho f u=\frac{\partial p}{\partial y}. \tag{2}$$

Here u, v are the components of the current velocity in the x- and y-directions, p the pressure, ρ the density, A_h and A_v the coefficients of horizontal and vertical mixing. f is givin by $-2\omega\sin\varphi$ where ω the angular velocity of the earth and φ the latitude.

The distribution of density is specified as follows:

$$\rho=\rho_0+\left(\Delta\rho_0+\Delta\rho_1\cos\frac{\pi}{l}y\right)\left(1-\frac{z}{d}\right), \tag{3}$$

where d is the depth of the ocean, ρ_0, $\Delta\rho_0$ and $\Delta\rho_1$ are constants.

Then, we have

$$p=g\int_{-\zeta}^{z}\rho dz=g\left(\rho_0+\Delta\rho_0+\Delta\rho_1\cos\frac{\pi}{l}y\right)(z+\zeta)-g\frac{\Delta\rho_1}{2d}(z^2-\zeta^2)\cos\frac{\pi}{l}y, \tag{4}$$

$$\frac{\partial p}{\partial y}=g\rho_0\frac{\partial\zeta}{\partial y}+g\left(z+\zeta-\frac{z^2-\zeta^2}{2d}\right)\frac{\partial}{\partial y}\left(\Delta\rho_1\cos\frac{\pi}{l}y\right), \tag{5}$$

where $-\zeta$ represents the surface elevation.

The supposition that the horizontal pressure gradient vanishes at the bottom leads to

$$\rho_0\zeta=\rho_0\zeta_0-\frac{d}{2}\Delta\rho_1\cos\frac{\pi}{l}y, \tag{6}$$

where ζ_0 is a constant of integration.

The substitution of (6) into (5) gives

$$\frac{\partial p}{\partial y}=-g\frac{\partial}{\partial y}\left(\Delta\rho_1\cos\frac{\pi}{l}y\right)\cdot\frac{(d-z)^2}{2d}. \tag{7}$$

When ρ_0 is taken 1, the equations of motion are approximately reduced to

$$\left(A_h\frac{\partial^2}{\partial y^2}+A_v\frac{\partial^2}{\partial z^2}\right)^2u+f^2u=f\frac{\partial p}{\partial y}, \tag{8}$$

which further becomes by (7)

$$\left(A_h\frac{\partial^2}{\partial y^2}+A_v\frac{\partial^2}{\partial z^2}\right)^2u+f^2u=-gf\Delta\rho_1\frac{(d-z)^2}{2d}\frac{\partial}{\partial y}\left(\cos\frac{\pi}{l}y\right). \tag{9}$$

The boundary conditions are given by

$$u=v=0 \qquad \text{at the bottom} \quad z=d, \tag{10}$$

$$\left.\begin{aligned}A_v\frac{\partial u}{\partial z}&=-\tau\sin\frac{\pi}{l}y\\ A_v\frac{\partial v}{\partial z}&=0\end{aligned}\right\} \qquad \text{at the surface} \quad z=-\zeta. \tag{11}$$

These can be replaced by

$$\left.\begin{aligned}A_v\frac{\partial u}{\partial z}&=-\tau\sin\frac{\pi}{l}y\\ A_v\frac{\partial v}{\partial z}&=0\end{aligned}\right\} \qquad \text{at } z=0, \tag{12}$$

taking $z=0$ for $z=-\zeta$.

Then, the solution of the equation (9) takes the form:

$$\begin{aligned}u=\frac{fg\pi\Delta\rho_1}{2dl}\sin\frac{\pi}{l}y\Big[&\frac{e^{p(z-d)}}{2pq}\{-(E_2d^2+E_1d+E_0)(p^2-q^2\sin q\sqrt{d-z}\\ &+2pq\cos q\sqrt{d-z})+2E_2\sin q\sqrt{d-z}\}\\ &+e^{-pz}(B_2\sin qz-B_3\cos qz)+E_2z^2+E_1z+E_0\Big],\end{aligned} \tag{13}$$

where

$$E_0=\frac{d^2\left(A_h^2\frac{\pi^4}{l^4}+f^2\right)+4A_vA_h\frac{\pi^2}{l^2}}{\left(A_h\frac{\pi^4}{l^4}+f^2\right)^2},\qquad B_2=\frac{(T+E_1)(p^2-3q^2)-\frac{A_h\pi^2}{A_vl^2}T}{2q(p^2+q^2)},$$

$$E_1=-\frac{2d}{A_h^2\frac{\pi^4}{l^4}+f^2},\qquad B_3=\frac{(T+E_1)(q^2-3p^2)+\frac{A_h\pi^2}{A_vl^2}T}{2p(p^2+q^2)},$$

$$E_2=\frac{1}{A_h^2\frac{\pi^4}{l^4}+f^2},\qquad T=\frac{\tau}{A_v}\frac{2dl}{fg\pi J\rho_1}, \tag{14}$$

and $\pm(p\pm iq)$ $(p,\ q>0)$ are the roots of the equation

$$A_v^2\xi^4-2A\,A_h\frac{\pi^2}{l^2}\xi^2+\left(A_h^2\frac{\pi^4}{l^4}+f^2\right)=0.$$

From the equation (1) and the solution (13), we have

$$v=\frac{g\pi J\rho_1}{2dl}\sin\frac{\pi}{l}y\left[\frac{e^{p(z-d)}}{2pq}\left\{\frac{f}{A_v}(E_2d^2+E_1d+E_0)(-f\sin qd-z\right.\right.$$

$$\left.+A_h\frac{\pi^2}{l^2}\cos qd-z)-2E_2f\cos q(d-z)\right\}-fe^{-pz}(B_2\cos qz+B_3\sin qz)$$

$$\left.-A_h\frac{\pi^2}{l^2}(E_2z^2+E_1z+E_0)+2E_2A_v\right]. \tag{15}$$

The equation of continuity is given by

$$\frac{\partial}{\partial y}(\rho v)+\frac{\partial}{\partial z}(\rho w)=0, \tag{16}$$

which is approximately transformed into

$$W_{-\zeta}-W_a=-\int_{-\zeta}^{a}\frac{\partial v}{\partial y}dz=-\frac{\partial}{\partial y}\int_{-\zeta}^{a}vdz+v_{-\zeta}\frac{\partial\zeta}{\partial y}. \tag{17}$$

As the vertical velocity vanishes at both the surface and the bottom and the volume transport in the y-direction has to vanish at the north and south boundaries, the above equation is reduced to

$$\int_{-\zeta}^{a}vdz=0, \tag{18}$$

provided $v_{-\zeta}\frac{\partial\zeta}{\partial y}$ is negligible.

On the assumption that the surface may be approximately defined by $z=0$ instead of $z=-\zeta$, we have

$$\int_0^a vdz=0, \tag{19}$$

which gives, by the use of the solution (15),

$$\frac{1}{2pq}\left[(E_2d^2+E_1d+E_0)\left\{-A_vq(p^2+q^2)+A_h\frac{\pi^2}{l^2}q\frac{3p^2-q^2}{p^2+q^2}\right\}-2E_2A_vq\right.$$

$$\left.-\frac{2E_2}{l^2}\frac{A_h\pi^2q}{p^2+q^2}\right]+2E_2A_vd-\frac{E_2}{3}A_h\frac{\pi^2}{l^2}d^3-\frac{E_1}{2}A_h\frac{\pi^2}{l^2}d^2-E_0A_v\frac{\pi^2}{l^2}d$$

$$+A_v(T+E_1)-\frac{A_h\pi^2}{2l^2(p^2+q^2)^2}\left\{4(T+E_1)(p^2-q^2)-\frac{2A_h\pi^2T}{A_vh^2}\right\}=0. \qquad (20)$$

This equation determines $\Delta\rho_1$, and when $A_h\frac{\pi^2}{l^2}$ is very small in comparison with $|f|$, $\Delta\rho_1$ is given by

$$\Delta\rho_1=\frac{2lf\tau}{g\pi\left(\frac{A_h\pi^2}{3l^2}d^2+\frac{\sqrt{2}A_v^{3/2}}{\sqrt{f}d}\right)}. \qquad (21)$$

If we take the Antarctic Ocean as a zonal ocean of which the south and north boundaries are defined by 70°S and 45°S respectively, the mean value of the Coriolis parameter and the width l are

$$-f=1.22\times10^{-4}\ \text{sec},^{-1}$$
$$l=2780\ km.$$

Putting $d=4\times10^5\ cm$, $\tau=2\ dyne/cm^2$ $A_v=2\times10^3\ g\ cm^{-1}\ \text{sec}^{-1}$ and $A_h=1.1\times10^{10}\ g\ cm^{-1}\ \text{sec}^{-1}$, we have

$$\Delta\rho_1=60\times10^{-5},$$

which agrees with observations.

In this case, according to (6) the range of the surface slope is 240 cm which agrees also with observations.

The velocity distribution at $y=\frac{l}{2}$ is represented in the fig. 1 by the full lines.

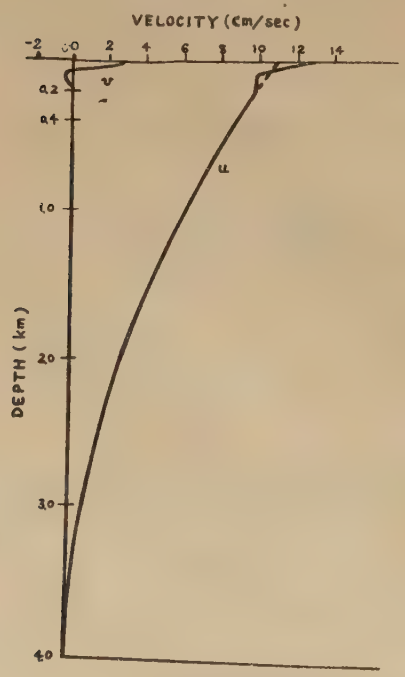

Fig 1 Vertical Distribution of Veloctiy.
full lines: solutions (13) and (15)
broken line: solution (23)

The geostrophic approximation gives the equations of motion

$$\left.\begin{aligned}-fv&=0,\\ fu&=\frac{1}{\rho}\frac{\partial p}{\partial y}.\end{aligned}\right\} \qquad (22)$$

From the pressure gradient (6), we have

$$u=\frac{\pi\Delta\rho_1}{2dfl}(d-z)^2, \qquad (23)$$

$$v=0. \qquad (24)$$

The broken line in the fig. 1 represents the solution (23) for the values of $\Delta\rho_1$, f, d and l obtained above.

Conclusions.

The above results lead us to the follwing conclusions:

(1) The solution in geostrophic approximation agrees very well with that

obtained in consideration of vertical and horizontal eddy viscosity except the surface layer of a thickness $\pi\sqrt{\frac{A_h}{\rho\omega\sin\varphi}}$ or the "depth of frictional resistance". Below this level the effects of both vertical and lateral mixing are negligible. However, as is shown in the equation (21), the coefficient of horizontal mixing plays a leading rôle in the determination of $\Delta\rho_1$ which gives half the range of the density difference at the surface.

(2) The vertical structure of the current is more probable than that in the previous studies which represent appreciable velocity near the bottom.

(3) The actual mass transport in the Antarctic Ocean is about 1.5×10^{14} g sec^{-1}. Our result fairly agrees with it. The assumed coefficient of horizontal mixing 1.1×10^{10} gives the solution compatible with observations with reference to the surface velocity, the surface slope, the difference of density at the surface and the mass transport. This value of the coefficient is far larger than that assumed for other parts of the oceans. It seems, however, that the large coefficient of horizontal mixing has to be assumed in order to obtain the reasonable results so far as a zonal ocean is concerned, and it may be due to the neglect of the variation in the east-west direction.

Acknowledgment.

The author wishes to express his sincere thanks to Professor K. Hidaka, who has encouraged him during this work.

References

Hidaka, Koji (1950)
Circulation in a Zonal Ocean Induced by a Planetary Wind System. Geophy. Notes (Geophys. Inst., Tokyo Univ.) **3** (10): 1-8

Hidaka, Koji and K. Takano (1952)
Wind-Driven Current and Lateral Mixing in a Zonal Ocean. Geophy. Mag., **23** (4): 487-495

Hidaka, Koji and M. Tsuchiya (1953)
On the Antarctic Circumpolar Current. Journ. Mar. Res., **12** (2); 214-222.

Munk, W. H. and E. Pálmen (1951)
Note on Dynamics of the Antarctic Circumpolar Current. Tellus, **3** (1): 53-55.

Sverdrup, H. U. et al (1949)
The Oceans. Prentice-Hall, New York.

Takano, Kenzo
On the Vertical Distribution of Wind-Driven Current in a Homogeneous Ocean. in press

Records of Oceanographic Works
in Japan. Vol. 2, No. 1,
March 1955

An Example of Thermal Convective Current

By

Kenzo Takano

(Geophysical Institute, Tokyo University)

Abstract: On the assumption that the vertical distribution of the temperature is approximately linear and there is no variation in the Coriolis forces, is presented an example of thermal circulation due to temperature differences given at the surface in a rectangular canal of water.

Introduction.

It is well known that a thermal convective circulation is induced in a basin of water by temperature differences maintained at the surface. Henry Stommel has obtained this circulation on a very small scale. In the present note, we intend to get the velocity field in a rectangular canal extending infinitely in the east-west direction, which is 6500*km* in width and 4000*m* in depth, assuming the temperature constant at the bottom and its vertical distribution approximately linear and neglecting the variation of the Coriolis forces with latitude.

Theoretical Consideration.

Taking the origin on the equator, the x- and y-axis positive eastward and northward respectively, the z-axis vertically downward, and neglecting the variations in the east-west direction, the terms concering the vertical eddy viscosity and other small quantities, we have the approximate equations

$$\frac{A_l}{\rho}\frac{\partial^2 u}{\partial y^2}+fv=0, \tag{1}$$

$$\frac{A_l}{\rho}\frac{\partial^2 v}{\partial y^2}-fu=\frac{1}{\rho}\frac{\partial p}{\partial y}, \tag{2}$$

$$0=\frac{1}{\rho}\frac{\partial p}{\partial z}-g, \tag{3}$$

$$\frac{\partial v}{\partial y}+\frac{\partial w}{\partial z}=0, \tag{4}$$

$$v\frac{\partial \Theta}{\partial y}+w\frac{\partial \Theta}{\partial z}=A_l\frac{\partial^2 \Theta}{\partial y^2}+A_v\frac{\partial^2 \Theta}{\partial z^2}, \tag{5}$$

where u, v and w are the three components of the current velocity, p the pressure, f the Coriolis parameter, A_v and A_l the coefficients of vertical and

lateral mixing respectively, ρ the density and Θ the temperature.

Putting $\Theta=-\beta z+\theta$ we have from the equation (5)

$$v\frac{\partial\theta}{\partial y}+w\left(-\beta+\frac{\partial\theta}{\partial z}\right)=A_l\frac{\partial^2\theta}{\partial y^2}+A_v\frac{\partial^2\theta}{\partial z^2}, \tag{6}$$

which is further transformed into

$$-w\beta=A_l\frac{\partial^2\theta}{\partial y^2}+A_v\frac{\partial^2\theta}{\partial z^2}, \tag{7}$$

provided $|\beta\gg\left|\frac{\partial\theta}{\partial z}\right|$.

When the thermal expansion is supposed linear and the stream function ψ is introduced so that $v=\frac{\partial\psi}{\partial z}$ and $w=-\frac{\partial\psi}{\partial y}$, the equations (1) to (4) and (7) are reduced to

$$\left\{g\alpha\beta\frac{\partial^4}{\partial y^4}+\left(A_l\frac{\partial^2}{\partial y^2}+A_v\frac{\partial^2}{\partial z^2}\right)\left(A_l\frac{\partial^4}{\partial y^4}+\frac{f^2}{A_l}\right)\frac{\partial^2}{\partial z^2}\right\}\psi=0, \tag{8}$$

where α is the coefficient of thermal expansion.

The boundary conditions are given by

$$\left.\begin{aligned}&\psi=0 \quad \text{at} \quad y=z=0, \quad y=l \quad \text{and} \quad z=h,\\ &\theta=0 \quad \text{at} \quad z=h,\\ &\theta=\theta_0\cos\frac{\pi}{l}y \quad \text{at} \quad z=0.\end{aligned}\right\} \tag{9}$$

Here h denotes the depth of the cannal, l its width and θ_0 half the range of temperature difference at the surface.

Then, we have the temperature and the stream function

$$\theta=\frac{\theta_0}{D_2^2-D_1^2}\left(-D_1^2\cosh D_1z+D_2^2\cosh D_2z+D_1^2\coth D_1h\sinh D_1z\right.$$
$$\left.-D_2^2\coth D_2h\cdot\sinh D_2z\right)\cos\frac{\pi}{l}y, \tag{10}$$

$$\psi=\frac{g\alpha\pi^3\theta_0}{l^3(D_2^2-D_1^2)}\frac{A_l}{\left(A_l\frac{\pi^2}{l^2}\right)^2+f^2}\left(\cosh D_1z-\cosh D_2z-\coth D_1h\sinh D_1z\right.$$
$$\left.+\coth D_2h\sinh D_2z\right)\sin\frac{\pi}{l}y, \tag{11}$$

where D_1 and D_2 are determined by

$$D_1=\sqrt{\frac{A_l\frac{\pi^2}{l^2}\left(f^2+A_l\frac{\pi^2}{l^2}\right)+\sqrt{A_l^2\frac{\pi^4}{l^4}\left(f^2+A_l\frac{\pi^2}{l^2}\right)^2-4g\alpha\beta A_v\left(A_l\frac{\pi^4}{l^4}+\frac{f^2}{A_l}\right)}}{2A_v\left(A_l\frac{\pi^2}{l^2}+\frac{f^2l^2}{A_l\pi^2}\right)}}, \tag{12}$$

$$D_2=\sqrt{\frac{A_l\frac{\pi^2}{l^2}\left(f^2+A_l\frac{\pi^2}{l^2}\right)-\sqrt{A_l^2\frac{\pi^4}{l^4}\left(f^2+A_l\frac{\pi^2}{l^2}\right)^2-4g\alpha\beta A_v\left(A_l\frac{\pi^4}{l^4}+\frac{f^2}{A_l}\right)}}{2A_v\left(A_l\frac{\pi^2}{l^2}+\frac{l^2f^2}{A_l\pi^2}\right)}}. \tag{13}$$

Putting $l=6500\,km$, $h=4000\,m$, $\theta_0=1°C$, $g=980\,cm\ \sec^{-2}$, $\beta=2.5\times10^{-5}cm^{-1}$ degree, $\alpha=2\times10^{-4}$ degree^{-1} and $f=6.962\times10^{-5}\ \sec^{-1}$, we will work out the following numerical examples: (1) $A_l=10^7 gcm^{-1}\sec^{-1}$, $A_v=10^2 gcm^{-1}\ \sec^{-1}$; (2) $A_l=10^8$, $A_v=10^2$; (3) $A_v=10^7$, $A_v=1$; (4)$A_l=10^8$, $A_v=1$. In every case, the temperature difference between the surface and the bottome is 11°C at the southern boundary (the equator) and 9°C at the northern boundary and the Coriolis parameter is taken the mean value in this region.

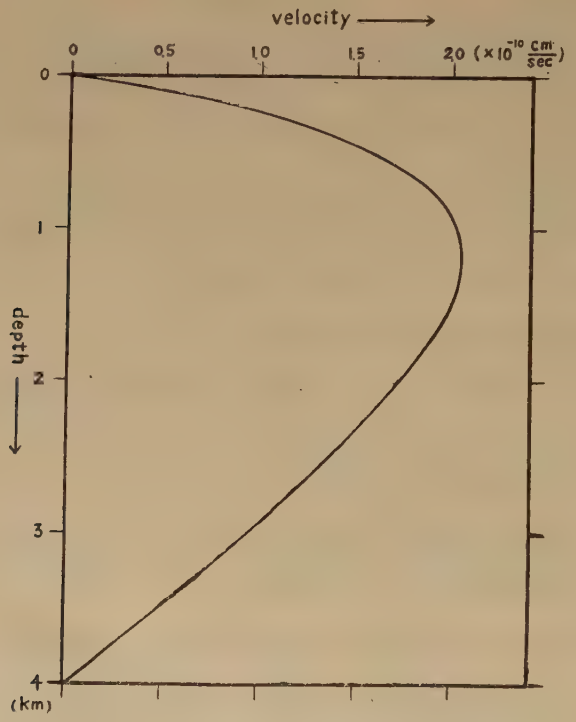

Fig. 1 Vertical Velocity at the Northern Boundary.

The two components of the surface velocity thus calculated are represented in the Table 1 and is illustrated in the Fig. 1 the vertical velocity at the northern boundary in the case (3).

Table 1

Two components of the surface velocity

Cace	A_l	A_v	v (cm/sec)	u (cm/sec)
1	10^7	10^2	0.605×10^{-6}	1.78
2	10^8	10^2	5.03×10^{-6}	1.48
3	10^7	1.0	0.253×10^{-6}	0.744
4	10^8	1.0	0.949×10^{-6}	0.279

Even if β is taken $5\times10^{-5}cm^{-1}$deg, that is, the temperature difference between the surface and the bottom is 21°C at the southern boundary and 19°C at the northern, the results are scarcely affected.

Concluding Remarks.

The essential assumption is that $\left|\frac{\partial\theta}{\partial z}\right|$ is negligible in comparison with β. Under this restriction the maximum value of θ_0 is at the most about 3°C in the case $\beta=2.5\times10^{-5}$. When θ_0 is taken 3°C as is seen in the solutions (10) and (11), the results are three times those which are represented in the Table 1. In the case $\beta=5\times10^{-5}$ the maximum of θ_0 is at the most about 6°C. In order to simplify the calculation the terms concerning the vertical eddy viscosity are neglected and the lateral eddy diffusivity is supposed to be equal to the lateral eddy viscosity. It may be perphaps improbable that these effects modify considerably the above results. Of course, our results can not be applied to the actual ocean circulation.

Acknowledgment

The author expresses his best thanks to professor Koji Hidaka for encouragement.

References

Rayleigh, J. W. S., 1916 : On convection current in a horizontal layer of fluid, when the higher temperature is on the upper side. Phil. Mag. **32**, 529

Stommel, H., 1950 : An example of thermal convection. Trans. Amer. Geophys. Union. **31**, 553

Records of Oceanographic Works
in Japan. Vol. 2, No. 1,
March 1955

Sur la Dimension des Tourbillons Cellulaires dans les Expériences de Henri Bénard

Par

Kenzo Takano

(Institut Géophysique, Université de Tokio)

Résumé; La dimension des tourbillons thermoconvectifs dans la nappe liquide horizontale chauffée par en dessous est étudiée d'une manière approximative à condition que le gradient vertical de la température soit constant à la surface libre et la température soit constante au fond rigide. La dimension ainsi obtenue est de bon accord avec celle qui a été montrée par les expériences de Henri Bénard. Quant à la différence critique de deux températures extêmes à l'instant de l'établissement du régime permanent, elle est environ la moitié de celle obtenue au cas que la température est constante à chaque surface limite.

Introduction.

La convection thermique donne naissance à une circulation tourbillonnaire exactement du même type dans la nappe fluide horizontale chauffée par en dessous. La nappe fluide entière, à une température suffisamment élevée, se divise en prismes verticaux à base polygonale. A l'état final, ce réseau polygonal est composé d'hexagones réguliers rigoureusement alignés et en chaque cellule le liquide chaud s'élève dans la partie voisine de l'axe et le liquide refroidi descend dans la partie périphérique. Les expériences de Henri Bénard montrent, en effet, que tel est le régime permanent. En régime permanent, le rapport de la longueur du côté de l'hexgone régulier à l'épaisseur de la nappe liquide est à peu près constant; plus exactement, en variant en fonction de la température et de l'épaisseur il devient 2.27 au maximum et 1.86 au minimum, mais, quelle que soit l'épaisseur, il est égal à 2.06 au moment où, par le refroidissment du liquide divisé en cellules à une température élevée, la surface libre devient plane, ce qui montre la disparition du réseau polygonal dû aux courants thermoconvectifs et le repos du liquide.

Depuis ses expériences, on s'est attaché à obtenir théoriquement la condition de l'instabilité, c'est-à-dire la différence critique de deux températures extrêmes et la dimension des cellules. Dans ces recherches, on a supposé que la

température soit constante aux surfaces limites. Le tableau 1 représente ces résultats précédents. On verra plus loin que R appelé "nombre de Rayleigh" donne la différence critique de température.

Tableau 1

conditions aux limites	rapport	R
libre-lible	1.89	657.5
libre-rigide	1.56	1100.7
rigide-rigide	1.34	1707.8

Cependant, ils n'expliquent pas le rapport indiqué ci-dessus par les expériences de Henri Bénard où la surface est considérée libre et le fond rigide. En effet, en ce qui concerne la dimension des cellules la théorie et les expériences ne sont pas enocore d'accord jusqu'à présent, et des vérifications expérimentales n'ont porté que sur une seule valeur 1707.8 parmi ces résultats.

Nous essayons alors d'obtenir le rapport 2.06 en supposant que le gradient vertical de la température est constant à la surface libre, car il est très probable que la répartition réelle des températures n'y soit pas uniforme.

Condition de l' Instabilité et Dimension des Cellules.

A l'état stationnaire. les équations du mouvement, l'équation de continuité et l'équation de la chaleur s'écrivent :

$$u_0\frac{\partial u_0}{\partial x}+v_0\frac{\partial u_0}{\partial y}+w_0\frac{\partial u_0}{\partial z}-\nu\nabla^2 u_0=-\frac{1}{\rho}\frac{\partial p_0}{\partial x}, \tag{1}$$

$$u_0\frac{\partial v_0}{\partial x}+v_0\frac{\partial v_0}{\partial y}+w_0\frac{\partial v_0}{\partial z}-\nu\nabla^2 v_0=-\frac{1}{\rho}\frac{\partial p_0}{\partial y}, \tag{2}$$

$$u_0\frac{\partial w_0}{\partial x}+v_0\frac{\partial w_0}{\partial y}+w_0\frac{\partial w_0}{\partial z}-\nu\nabla^2 w_0=-\frac{1}{\rho}\frac{\partial p_0}{\partial z}-g, \tag{3}$$

$$\frac{\partial}{\partial x}(\rho u_0)+\frac{\partial}{\partial y}(\rho v_0)+\frac{\partial}{\partial z}(\rho w_0)=0, \tag{4}$$

$$u_0\frac{\partial \theta_0}{\partial x}+v_0\frac{\partial \theta_0}{\partial y}+w_0\frac{\partial \theta_0}{\partial z}=\kappa\nabla^2\theta_0, \tag{5}$$

dans lesquelles u_0 et v_0 sont les deux composantes de la vitesse horizontale, w_0 la composante suivant la verticale positive vers le haut, p_0 la pression, ρ la densité g l'accélération de la pesanteur, ν le coefficient de viscosité cinématique, θ_0 la température, κ la conductibilité thermométrique et $\nabla^2=\frac{\partial^2}{\partial x^2}+\frac{\partial^2}{\partial y^2}+\frac{\partial^2}{\partial z^2}$.

Pour simplifier les équations, on suppose que, 1°) le fluide est incompressible, la variation de la densité par l'expansion thermique ne modifie que le terme concernant l'accélération de la pesanteur ; 2°) dans l'état fondamental, le fluide est en repos et le gradient vertical de la température est constant partout, ce qui permet de poser $\theta_0=\beta z$ ($\beta<0$) ; 3°) l'expansion thermique est linéaire ; 4) les déviations u, v, w, θ et p en sont si petites que les termes non linéaires sont

négligeables.

Par suite, les équations (1)-(4) se transforment en

$$\upsilon\nabla^2\left(\frac{\partial u}{\partial z}-\frac{\partial w}{\partial y}\right)=g\alpha\frac{\partial\theta}{\partial x}, \tag{6}$$

$$\upsilon\nabla^2\left(\frac{\partial v}{\partial z}-\frac{\partial w}{\partial y}\right)=g\alpha\frac{\partial\theta}{\partial y}, \tag{7}$$

$$\frac{\partial u}{\partial x}+\frac{\partial v}{\partial y}+\frac{\partial w}{\partial z}=0, \tag{8}$$

α étant le coefficient d'expansion theremique,
d'où il vient :

$$\upsilon\nabla^4 w=-g\alpha\nabla_1{}^2\theta, \tag{9}$$

où $\nabla_1{}^2=\frac{\partial^2}{\partial x^2}+\frac{\partial^2}{\partial y^2}$.

Après avoir adjoint à l'équation (9) celle de la chaleur :

$$\kappa\nabla^2\theta=\beta w, \tag{10}$$

on arrivera à

$$\kappa\upsilon\nabla^6 w=-g\alpha\beta\nabla_1{}^2 w. \tag{11}$$

Nous posons $w=F(x, y)\ W(z)$ et introduisons ζ comme nouvelle variable et un nombre caractéristique a de sorte que $z=h\zeta$ et le fond et la surface sont définis par $\zeta=0$ et $\zeta=1$ respectivement et de plus,

$$h^2\nabla_1{}^2F=-a^2F, \tag{12}$$

où h désigne l'épaisseur de la nappe fluide.

Cela posé, l'équation (11) prend la forme :

$$\begin{aligned}(D^2-a^2)^3W&=\frac{g\alpha\beta h^4}{\kappa\upsilon}a^2W\\&=-Ra^2W,\end{aligned} \tag{13}$$

où $R\left(=-\frac{g\alpha\beta h^4}{\kappa\upsilon}\right)$ est le nombre de Rayleigh et $D=\frac{d}{d\zeta}$.

Les conditions aux limites s'écrivent :

$$u=v=w=0, \tag{14}$$

au fond rigide

$$\theta=0, \tag{15}$$

$$\frac{\partial u}{\partial\zeta}=\frac{\partial v}{\partial\zeta}=w=0, \tag{16}$$

à la surface libre

$$K(\theta_0-\theta_a)=\frac{k}{h}\frac{\partial\theta_0}{\partial\zeta}, \tag{17}$$

où θ_a est la température de l'air ambiant et K et k des constantes.

La dernière condition se ramènera à

$$K\theta=\frac{k}{h}\frac{\partial\theta}{\partial\zeta}. \tag{18}$$

Cependant, comme on ne saurait évaluer la constante K de la nappe du spermaceti utilisée par H. Bénard, supposons, ce qui est légitime pourvu que K

soit négligeable par rapport à $\frac{k}{h}$,

$$\frac{\partial\theta}{\partial\zeta}=0, \tag{19}$$

qui est considérée comme condition à la surface non conductrice.

Alors les conditions (14), (15), (16) et (19) sont remplacées par celles par rapport à W en vertu des équations (8), (9) et (10):

$$W=DW=(D^2-a^2)^2W=0, \quad \text{au fond rigide conducteur} \tag{20}$$

$$W=D^2W=D\,(D^2-a^2)^2W=0, \quad \text{à la surface libre non conductrice.} \tag{21}$$

L'équation (13) a été étudiée par quelques méthodes. Nous y utiliserons la méthode adoptée par H. Jeffreys.
On peut écrire approximativement:

$$\left.\begin{aligned}
DW_0&=\frac{1}{2d}(W_1-W_{-1}),\\
D^2W_0&=\frac{1}{d^2}(W_1-2W_0+W_{-1}),\\
D^3W_0&=\frac{1}{2d^3}(W_2-2W_1+2W_{-1}-W_{-2}),\\
D^4W_0&=\frac{1}{d^4}(W_2-4W_1+6W_0-4W_{-1}+W_{-2}),\\
D^5W_0&=\frac{1}{2d^5}(W_3-4W_2+5W_1-5W_{-1}+4W_{-2}-W_{-3}),\\
D^6W_0&=\frac{1}{d^6}(W_3-6W_2+15W_1-20W_0+15W_{-1}-6W_{-2}+W_{-3}),
\end{aligned}\right\} \tag{22}$$

d étant la distance entrè deux points voisins.

En posant $d=\frac{1}{2}$ en première approximation et en désignant les valeurs de W à $\zeta=\frac{1}{2}$ et $\zeta=2$ par b et c, on obtient le tableau 2 en vertu des conditions aux limites et (22).

Tableau 2

ζ	-1	$-\frac{1}{2}$	0	$\frac{1}{2}$	1	$1\frac{1}{2}$	2	$2\frac{1}{2}$
W	$b(8+a^2)$	b	0	b	0	$-b$	c	$\frac{b}{8}(a^4+16a^2+88)+\frac{c}{2}(8+a^2)$

De l'équation (13) il vient alors:

$$\left(\frac{a^4}{2}+8a^2+48\right)b-(a^2+8)\,c=0,$$
$$(768+224a^2+24a^4+a^6-Ra^2)\,b-64c=0,$$

d'où

$$\begin{vmatrix} \frac{a^4}{2}+8a^2+48 & -(a^2+8) \\ 768+224a^2+24a^4+a^6-Ra^2 & -64 \end{vmatrix}=0, \qquad (23)$$

pour que le liquide se mette en mouvement.

Le déterminant (23) se réduit à

$$R=\frac{3072+2048a^2+384a^4+32a^6+a^8}{8a^2+a^4}, \qquad (24)$$

d'où on trouve le minimum de R,

$$R=409 \quad \text{avec} \quad a=1.89 \qquad (25)$$

Puis, nous avons le tableau 3, posant $d=\frac{1}{3}$.

Tableau 3

ζ	$-\frac{2}{3}$	$-\frac{1}{3}$	0	$\frac{1}{3}$	$\frac{2}{3}$	1	$1\frac{1}{3}$	$1\frac{2}{3}$	2
W	$\frac{4}{9}b(a^2+8)-c$	b	0	b	c	0	$-c$	d	$\frac{1}{81}\{(d-b)(18a^2+324)+c(2a^4+72a^3+810)\}$

De même, il vient le déterminant suivant :

$$\begin{vmatrix} -13122-(1377-R)a^2-54a^4-a^6 & 9477+972a^2+27a^4 & 0 \\ 11664+972a^2+27a^4 & -10206-(1215-R)a^2-54a^4-a^6 & 729 \\ -\frac{5}{3}a^2-30 & \frac{2}{27}a^4+\frac{8}{3}a^2+30 & -\frac{a^2}{3}-6 \end{vmatrix}=0 \qquad (26)$$

d' où on arrivera à

$$\begin{aligned} R &= 518, \\ a &= 1.96 \end{aligned} \qquad (27)$$

Afin de déduire les résultats définitifs de (25) et (27), on suppose, comme l'a fait H. Jeffreys, que l' erreur est proportionnelle à d^2, ce qui permet d'écrire

$$\left.\begin{aligned} a-1.89 &= P_1\left(\frac{1}{2}\right)^2 \\ a-1.96 &= P_1\left(\frac{1}{3}\right)^2 \end{aligned}\right\}$$

$$\left.\begin{aligned} R-409 &= P_2\left(\frac{1}{2}\right)^2 \\ R-518 &= P_2\left(\frac{1}{3}\right)^2 \end{aligned}\right\}$$

P_1 et P_2 étant des constantes.

Donc, il résulte de là que

$$\left.\begin{aligned} R &= 605, \\ a &= 2.02. \end{aligned}\right\} \qquad (28)$$

Quand le réseau est composé d'hexagones réguliers, le rapport r de la longueur du côté à l'épaisseur est exprimé par a sous la form:

$$r=\frac{4\pi}{3a}, \tag{29}$$

d'où, selon (28),

$$r=2.07.$$

D'autre part, les expériences de Bénard montrent,

$$r=2.06.$$

Il s'agit de la précision de cette méthode. H. Jeffreys en a obtenu $a=2.33$, $R=540$ pour $d=\frac{1}{2}$, et $a=2.69$, $R=793$ pour $d=\frac{1}{3}$, ce qui donne $a=2.98$ et $R=995$. D'après un calcul plus exact, on a $a=3.0$ et $R=1051$. Cette méthode est donc suffisamment valable dans ce cas-là.

Malgré que les conditions aux limites en soient différentes, on pourrait approximativement déterminer

$$a = 2.07$$
$$R = 600.$$

Conclusions.

Les expériences constatent que le rapport r est égal à 2.06 au moment où le liquide en mouvement se met au repos, tandis que dans cette étude il s'agit du rapport et de la différence critique de deux température extrêmes au moment où le liquide en repos se met en mouvement. Il n'est donc pas improbable que la concordance soit casuelle, mais en tout cas ce rapport expérimental doit prendre une valeur entre le minimum 1.86 et le maximum 2.27 et les études théoriques précédentes ne peuvent l'expliquer. En supposant la surface libre non conductrice au lieu de la surface conductrice, nous avons obtenu le résultat qui s'accorde mieux avee les expériences.

Il est aussi remarquable que la différence critique de température est environ la moitié de celle qui est obtenue par la surface libre conductrice. Il résulte de là que la surface non conductrice grandit la dimension des cellules et facilite l'instabilité.

Remerciements.

Nous tenons à remercier le Professeur Koji Hidaka pour l'intérêt qu'il a porté à ce travail.

Bibliographie

Bénard, H., 1900 : Les Tourbillons Cellulaires dans une Nappe Liquide. Rev. Gén. Sci. Pur. Appl. **12**, 1291, 1309

Bénard, H., 1901 : Les Tourbillons Cellulaires dans une Nappe Liquide Transportant de la Chaleur par Convection en Régime permanent. Ann. Chim. Phys. **23**, 62

Rayleigh, J. W. S., 1926 : On Convection Current in a Horizontal Layer of Fluid, When the Higher Temperature is on the Upper Side. Phil. Mag. **32**, 529

Jeffreys, H., 1926 : The Stability of a Layer of Fluid Heated Below. Phil. Mag. **2**. 833

Jeffreys, H., 1928 : Some cases of Instability in Fluid Motion. Proc. Roy. Soc. London A **118**, 195

Pellew, A. and Southwell, R. W., 1940 : Convection Motion in a Fluid. Proc. Roy. Soc. London A **176**, 312

Records of Oceanographic Works
in Japan, Vol. 2, No. 1,
March 1955

Sur les Tourbillons Thermoconvectifs dans la Nappe Fluide Horizontale Chauffée par en dessous

Par

Kenzo Takano

(Institut Géophysique, Université de Tokio)

Résumé: Au sujet de la condition de 1' instabilité et de la dimension des cellules dans la nappe fluide horizontale chauffée par en dessous, nous avons envisagé les trois cas suivants: 1°) le fond et la surface sont rigides et non conducteurs, 2°) le fond et la surface sont libres et non conducteurs, 3°) le fond est rigide et conducteur et la surface est libre et non conductrice. Ces résultats montrent que le fluide devient facilement instable et de grandes cellules ont lieu par rapport à ceux que 1'on a obtenus en supposant la surface conductrice ou le fond conducteur. D'ailleurs, on constate le résultat précédent trouvé par une méthode approximative et celui des expériences de Henri Bénard.

Introduction.

En régime permanent, la convection divise toutes les nappes fluides horizontales chauffées par en dessous en cellules hexagonales parfaitement régulières. Supposant la surface libre non conductrice, nous avons déjà expliqué la dimension des cellules thermoconvectives obtenue par les expériences de Henri Bénard. Cependant, la méthode y utilisée a été tout approximative. Pour vérifier ce résultat trouvé dans l'étude précédente aussi bien que pour estimer l'effet de la surface non conductrice ou du fond non conducteur, nous allons étudier les trois cas suivants: 1°) le fond et la surface sont rigides et non condnc teurs, 2°) le fond et la surface sont libres et non conducteurs, 3°) le fond est rigide et conducteur et la surface est libre et non conductrice.

Condition de 1' Instabilité et Dimension des Cellules.

Les équations du mouvement, l'équation de continuité et l'équation de la chaleur se réduisent à

$$(D^2-a^2)^3\ w=-Ra^2w, \tag{1}$$

où R est le nombre de Rayleigh, w représente la vitesse verticale, a la dimension des cellules et $D=\frac{d}{d\zeta}$.

Les conditions aux limites s'écrivent :

à la surface libre, $w=D^2w=0,$ (2)

à la surface rigide, $w=Dw=0,$ (3)

à la surface conductrice, $(D^2-a^2)^2\ w=0,$ (4)

à la surface non conductrice, $D\ (D^2-a^2)^2\ w=0.$ (5)

On introduit alors λ^3 de sorte que

$$(D^2-a^2)^3\ w=-\lambda^3 a^6 w, \tag{6}$$

posant $\lambda^3=\dfrac{R}{a^4}$.

La solution de cette équation est de la forme :

$$w=A_1\cosh 2\mu_1\zeta+A_2\cosh 2\mu_2\zeta+A_3\cosh 2\mu_3\zeta+B_1\sinh 2\mu_1\zeta \\ +B_2\sinh 2\mu_2\zeta+B_2\sinh 2\mu_3\zeta, \tag{7}$$

où

$$\left.\begin{aligned} \mu_1&=\frac{a}{2}\sqrt{1-\lambda\omega_1}, & \omega_1&=1,\\ \mu_2&=\frac{a}{2}\sqrt{1-\lambda\omega_2}, & \omega_2&=\frac{-1+\sqrt{3}\ i}{2},\\ \mu_3&=\frac{a}{2}\sqrt{1-\lambda\omega_3}, & \omega_3&=\frac{-1-\sqrt{3}\ i}{2}. \end{aligned}\right\} \tag{8}$$

Nous prenons l'origine de ζ de sorte que la surface et le fond sont désignés par $\zeta=\dfrac{1}{2}$ et $\zeta=-\dfrac{1}{2}$ respectivement, ce qui permet de diviser la solution (8) en partie paire et partie impaire.

cas 1°) :

Les conditions aux limites s'écrivent :

$$w=Dw=D\ (D^2-a^2)^2\ w=0. \tag{9}$$

Il est très probable que la solution paire représente les premiers courants thermoconvectifs. Par suite, d'après la partie paire de la solution (7) et les conditions (9), on arrive à

$$\left.\begin{aligned} &A_1\cosh\mu_1+A_2\cosh\mu_2+A_3\cosh\mu_3=0,\\ &A_1\mu_1\sinh\mu_1+A_2\mu_2\sinh\mu_2+A_3\mu_3\sinh\mu_3=0,\\ &A_1\mu_1\ (4\mu_1^2-a^2)^2\sinh\mu_1+A_2\mu_2\ (4\mu_2^2-a^2)^2\sinh\mu_2\\ &\qquad\qquad +A_3\mu_3\ (4\mu_3^2-a^2)^2\sinh\mu_3=0, \end{aligned}\right\} \tag{10}$$

d'où

$$\begin{vmatrix} \cosh\mu_1 & \cosh\mu_2 & \cosh\mu_3\\ \mu_1\sinh\mu_1 & \mu_2\sinh\mu_2 & \mu_3\sinh\mu_3\\ \mu_1\ (4\mu_1^2-a^2)^2\sinh\mu_1 & \mu_2\ (4\mu_2^2-a^2)^2\sinh\mu_2 & \mu_3\ (4\mu_3^2-a^2)^2\sinh\mu_3 \end{vmatrix}=0, \tag{11}$$

Or, on pose :

$$\left.\begin{aligned}\mu_1&=\gamma i,\\ \mu_2&=A-Bi,\\ \mu_3&=A+Bi,\end{aligned}\right\} \qquad (12)$$

où,

$$\left.\begin{aligned}\gamma&=\frac{a}{2}\sqrt{\lambda-1},\\ A&=\frac{a}{4}\sqrt{2+\lambda+2\sqrt{1+\lambda+\lambda^2}},\\ B&=\frac{\sqrt{3}}{4}a\sqrt{\lambda}\frac{1}{\sqrt{2+\lambda+2\sqrt{1+\lambda+\lambda^2}}}.\end{aligned}\right\} \qquad (13)$$

Cela posé, le déterminant (11) se transforme en

$$\gamma\tan\gamma=\frac{(A^2+B^2)(\cosh 2A-\cos 2B)}{(\sqrt{3}B-A)\sinh 2A+(\sqrt{3}A+B)\sin 2B}. \qquad (14)$$

Après avoir résolu graphiquement cette équation en fonction de a et de γ, on pourra déterminer a et R qui se montrent dans le tableau 1.

Tableau 1

a	γ	R	a	γ	R
0.10	0.6930	720.02	0.80	1.336	735.68
0.20	0.8697	720.18	0.90	1.380	738.97
0.30	0.9910	720.92	1.00	1.420	744.91
0.40	1.086	723.31	1.10	1.456	751.88
0.50	1.163	725.39	1.20	1.490	756.72
0.60	1.229	728.78	1.50	1.569	786.05
0.70	1.286	732.04	2.00	1.659	845.96

Il en résulte que R s'approche de 720.0 en diminuant avec a.

cas 2°) :

Il vient les conditions aux limites :

$$w=D^2w=D\,(D^2-a^2)^2\,w=0, \qquad (15)$$

d'où

$$\begin{vmatrix}\cosh\mu_1 & \cosh\mu_2 & \cosh\mu_3\\ \mu_1^2\cosh\mu_1 & \mu_2^2\cosh\mu_2 & \mu_3^2\cosh\mu_3\\ \mu_1(4\mu_1^2-a^2)^2\sinh\mu_1 & \mu_2(4\mu_2^2-a^2)^2\sinh\mu_2 & \mu_3(4\mu_3^2-a^2)\sinh\mu_3\end{vmatrix}=0, \qquad (16)$$

d'où

$$\gamma\tan\gamma=2\frac{A\sinh 2A-B\sin 2B}{\cosh 2A+\cos 2B}. \qquad (17)$$

De même, on a le tableau 2. Il semble que R s'approche de 119.0.

a	γ	R	a	γ	R
0.01	0.2390	119.43	0.40	0.7979	123.74
0.10	0.5128	119.71	0.50	0.8526	125.94
0.20	0.6424	120.82	0.60	0.8991	128.90
0.30	0.7303	122.14	0.70	0.9410	133.76

cas 3°) :

Les conditions aux limites s'écrivent :

$$w=Dw=(D^2-a^2)^2\ w=0 \qquad \text{au fond,}$$

$$w=D^2w=D\ (D^2-a^2)^2\ w=0 \qquad \text{à la surface.}$$

Pour faciliter le calcul, on change l'origine de ζ de façon que le fond et la surface sont définis par $\zeta=0$ et $\zeta=\frac{1}{2}$.

Il vient alors le déterminant :

$$\begin{vmatrix}
1 & 1 & 1 \\
0 & 0 & 0 \\
(4\mu_1^2-a^2)^2 & (4\mu_2^2-a^2)^2 & (4\mu_3^2-a^2)^2 \\
\cosh\mu_1 & \cosh\mu_2 & \cosh\mu_3 \\
\mu_1^2\cosh\mu_1 & \mu_2^2\cosh\mu_2 & \mu_3^2\cosh\mu_3 \\
\mu_1(4\mu_1^2-a^2)^2\sinh\mu_1 & \mu_2(4\mu_2^2-a^2)^2\sinh\mu_2 & \mu_3(4\mu_3^2-a^2)^2\sinh\mu_3 \\
0 & 0 & 0 \\
\mu_1 & \mu_2 & \mu_3 \\
0 & 0 & 0 \\
\sinh\mu_1 & \sinh\mu_2 & \sinh\mu_3 \\
\mu_1^2\sinh\mu_1 & \mu_2^2\sinh\mu_2 & \mu_3^2\sinh\mu_3 \\
\mu_1(4\mu_1^2-a^2)^2\cosh\mu_1 & \mu_2(4\mu_2^2-a^2)^2\cosh\mu_2 & \mu_3(4\mu_3^2-a^2)^2\cosh\mu_3
\end{vmatrix} =0, \quad (19)$$

d'où

$$-\gamma\tan\gamma=\frac{1}{A^2+B^2+4\sqrt{3}\,AB+\dfrac{4(A^2+B^2)+\cos 2B(A^2+B^2-4\sqrt{3}\,AB)}{\cosh 2A}}$$

$$\times\Big[(A^2+B^2)(A+\sqrt{3}\,B)-2A(A^2-3B^2-\gamma^2)$$

$$+\frac{\sin 2B}{\sinh 2A}\Big\{(A^2+B^2)(\sqrt{3}\,A-B)-2B(3A^2-B^2+\gamma^2)\Big\}$$

$$+\frac{\cos B}{\cos\gamma\cosh A}\Big\{A(A^2+5B^2)-\sqrt{3}\,B(3A^2-B^2)-\gamma^2(A-\sqrt{3}\,B)\Big\}$$

$$-\frac{\sin B}{\cos\gamma\sinh A}\Big\{B(5A^2+B^2)-\sqrt{3}\,A(A^2-3B^2)+\gamma^2(\sqrt{3}\,A+B)\Big\}\Big]. \quad (20)$$

La solution de cette équation se montre dans le tableau 3.

Tableau 3

a	γ	R	a	γ	R
3.80	3.1385	10808.0	4.30	3.1550	10718.4
4.00	3.1452	10724.6	4.40	3.1575	10738.2
4.10	3.1484	10706.5	4.60	3.1630	10819.2
4.20	3.1517	10705.9			

Il vient alors:

$$\left.\begin{aligned} R &= 10704.5 \\ a &= 4.14 \end{aligned}\right\} \qquad (21)$$

Cependant, dans ce cas 1' épaisseur est égale à $\frac{h}{2}$, donc les valeurs correspondant à l'épasseur h deviendront

$$\left.\begin{aligned} R &= \frac{10704.5}{16} = 669.0 \\ a &= \frac{4.14}{2} = 2.07 \end{aligned}\right\} \qquad (22)$$

Quand la nappe fluide se divise en cellules hexagonales, le rapport r de la longueur du côté de l'hexagone à l'épasseur est lié à a par la relation suivante:

$$r = \frac{4\pi}{3a}. \qquad (23)$$

D'après les résultats obtenus plus haut, nous avons:

$$\left.\begin{aligned} r &= \infty && \text{dans le cas 1°,} \\ &= \infty && \text{dans le cas 2°,} \\ &= 2.02 && \text{dans le cas 3°.} \end{aligned}\right\} \qquad (24)$$

Conclusions.

Dans le tableau 4 sont montrés nos résultats (colonne A) et ceux (colonne B) au cas que la température est constante aux deux surfaces.

Tableau 4

conditions aux limites	r		R	
	A	B	A	B
rigide-rigide	∞	1.34	720.0	1707.8
libre-libre	∞	1.89	119.0	657.5
libre-rigide	2.02	1.56	669.0	1170.7

Il en résulte que, si l'on suppose la surface ou le fond non conducteurs, le fluide se met en mouvement plus facilement et les cellules thermoconvectives deviennent plus grandes. Ce qui est intéressant, c'est que la dimension des cellules est infinie dans la nappe fluide dont les deux surfaces limites sont

rigides et non conductrices ou libres et non conductrices.

Il semble que le rapport r soit égal à 2.06 dans les expériences de Henri Bénard. D'autre part il est égal à 2.02 sous les conditions aux limites envisagées dans cette étude. Malgré que la valeur expérimentale soit plus près de 2.02 que de 1.56, il ne se trouve pas la concordance parfaite entre la première et notre résultat 2.02. Cela tient peut-être au fait que le fond dans ses expériences n'etait pas parfaitement conducteur.

La méthode approximative précédente a donné R=605 et a=2.02. Elle est suffisamment précise en comparaison de (22).

Remerciements.

Nous sommes reconnaissant au Professeur Koji Hidaka pour l'intérêt qu'il a porté à ce travail.

Bibliographie

Bénard, H., 1900 : Les Tourbillons Cellulaires dans une Nappe Liquide. Rev. Gén. Sci. Pur. Appl., **12**, 1261, 1309

Bénard, H.,1901 : Les Tourbillons Cellulaires dans une Nappe Liquide Transportant de la Chaleur par Convection en Régime Permanent. Ann. Chim. Phys. **23**, 62

Pellew, A. and Southwell, R. W., 1940 : Convection Motion in a Fluid. Proc. Roy. Soc. London A **176**, 312

Takano. K., 1955 : Sur la Dimension des Tourbillons Cellulaires dans les Expériences de Henri Bénard. Rec. Oceanogr. Works Japan, **2** (1). 80

Records of Oceanographic Works
in Japan, Vol. 2, No. 1,
March 1955

Sur la Différence Critique de Température dans les Expériences de Douchan Avsec au Sujet des Courants Thermoconvectifs

Par

Kenzo Takano

(Institut Géophysique, Université de Tokio)

Résumé ; C' est une étude théorique sur la condition pour que les premiers courants thermoconvectifs se déclanchent dans une couche horizontale chauffée par en dessous. En supposant le fond conducteur et la surface non conductrice, on obtient la différence critique de deux températures extrêmes qui est de bon accord avec celle des expériences de Douchan Avsec.

Introduction.

Les courants thermoconvectifs se déclanchent à une différence de deux températures extrêmes dans la couche fluide horizontale chauffée par en dessous. Dans les études précédentes nous avons déjà montré qu'au cas de supposer la surface ou le fond non conducteurs le fluide se met facilement en mouvement et de grandes cellules apparaissent par rapport au cas de les supposer conducteurs, et que se trouve la bonne concordance entre la dimension des cellules thermoconvectives ainsi obtenue et celle qui a été déterminée par les expériences de Henri Bénard.

Douchan Avsec a expérimentalement montré que la différence critique de deux températures extrêmes de l'air enfermé entre les plaques d'acier et de glace est plus petite que celle que l'on a obtenue en supposant les surfaces rigides et conductrices de la chaleur. Cela tient probablement au fait que cette condition ne soit pas valable dans ses expériences. Il est probable que la surface de glace ne soit pas parfaitement conductrice de la chaleur.

Si l'on suppose la surface non conductrice au lieu de la surface conductrice, les résultats expérimentaux seront bien confirmés. Nous allons essayer de déterminer la différence critique de température d'une façon approximative par la même méthode que dans notre étude précédente.

Détermination de la Condition de l' Instabilité.

L'équation à résoudre s'écrit :

$$(D^2-a^2)^3 w = -\frac{g\alpha \Delta T h^3}{\kappa \upsilon} a^2 w$$
$$= -Ra^2 w \ , \qquad (1)$$

où w représente la composante verticale de la vitesse, a est un nombre caractéristique représentant la dimension des tourbillons, g l'accélération de la pesanteur, α le coefficient d'expansion, h l'épaisseur de la couche fluide, ΔT la différence de deux températures extrêmes, κ le coefficient de viscosité cinématique, υ le conductibilité thermométrique, R donné par $\frac{g\alpha \Delta T h^3}{\kappa \upsilon}$ s'appelle "nombre de Rayleigh", le fond et la surface sont désignés par $\zeta=0$ et $\zeta=1$ et $D=\frac{d}{d\zeta}$.

Les conditions aux limites sont de la forme;

au fond rigide conducteur $\qquad w=Dw=(D^2-a^2)^2 w=0, \qquad (2)$

à la surface rigide non conductrice $\qquad w=Dw=D(D^2-a^2)^2\ w=0. \qquad (3)$

Les dérivées se substituent en approximative par

$$\left.\begin{aligned}
Dw_0 &= -\frac{1}{2d}(w_1-w_{-1}),\\
D^2 w &= \frac{1}{d^2}(w_1-2w_0+w_{-1}),\\
D^3 w &= \frac{1}{2d^3}(w_2-2w_1+2w_{-1}-w_{-2}),\\
D^4 w &= \frac{1}{d^4}(w_2-4w_1+6w_0-4w_{-1}+w_{-2}),\\
D^5 w &= \frac{1}{2d^5}(w_3-4w_2+5w_1-5w_{-1}+4w_{-2}+w_{-3}),\\
D^6 w &= \frac{1}{d^6}(w_3-6w_2+15w_1-20w_0+15w_{-1}-6w_{-2}+w_{-3}),
\end{aligned}\right\} \qquad (4)$$

d étant la distance entre deux points.

Si l'on prend $d=\frac{1}{2}$ en première approximation, la distribution de w montrée dans le tableau 1 satisfait aux conditions aux limites.

Tableau 1

ζ	-1	$-\frac{1}{2}$	0	$\frac{1}{2}$	1	$1\frac{1}{2}$	2	$2\frac{1}{2}$
W	$b(a^2+8)$	b	0	b	0	b	c	$b+c\left(\frac{a^2}{2}+4\right)$

D'après le tableau 1, (1) et (4), il vient:

$$\left.\begin{aligned}
&b\ (-1536-320a^2-24a^4-a^6+Ra^2)+64c=0\\
&b\ (256+48a^2+3a^4)-2c(a^2+8)=0.
\end{aligned}\right\} \qquad (5)$$

Afin que b et c ne soient pas en même temps nuls, il faut le déterminant suivant:

$$\begin{vmatrix} -1536-320a^2-24a^4-a^6+Ra^2 & 64 \\ 256+48a^2+3a^4 & -2(a^2+8) \end{vmatrix}=0 \qquad (6)$$

d'où

$$R=\frac{4096+2560a^2+416a^4+32a^6+a^8}{8a^2+a^4} \qquad (7)$$

De là vient le minimum de R

$$R = 485$$

avec $$a = 2.03 \qquad (8)$$

En posant $d=\frac{1}{3}$ nous avons le tableau 2.

Tableau 2

ζ	$-\frac{2}{3}$	$-\frac{1}{3}$	0	$\frac{1}{3}$	$\frac{2}{3}$	1	$1\frac{1}{3}$	$1\frac{2}{3}$	2
W	$b\left(\frac{4}{9}a^2+8\right)-c$	b	0	b	c	0	c	d	$\left(\frac{4}{9}a^2+4\right)(d-b)$

De même, on arrive à

$$\begin{vmatrix} -13122-1539\,a^2-54a^4-a^6+Ra^2 & 10935+972a^2+27a^4 & 0 \\ 11664+972a^2+27a^4 & -18954-1701a^2-54a^4-a^6+Ra^2 & 729 \\ -270-15a^2 & 810+72a^2+2a^4 & -54-3a^2 \end{vmatrix}=0, \qquad (9)$$

d'où vient

$$R=781,$$
$$a=2.24. \qquad (10)$$

Pour déduire les valeurs de R et a des résultats (8) et (10), on suppose que l'erreur est proportionnelle à d^2, ce qui permet d'écrire

$$\left.\begin{aligned} a-2.03 &= K_1\left(\frac{1}{2}\right)^2, \\ a-2.24 &= K_1\left(\frac{1}{3}\right)^2, \end{aligned}\right\} \qquad (11)$$

$$\left.\begin{aligned} R-485 &= K_2\left(\frac{1}{2}\right)^2, \\ R-781 &= K_2\left(\frac{1}{3}\right)^2, \end{aligned}\right\} \qquad (12)$$

K_1 et K_2 étant des constantes.

Il en résulte que

$$a = 2.41,$$
$$R = 1020 \qquad (13)$$

Dans la figure 1 sont montrées la figure dessinée par D. Avsec et la courbe indiquée par (13). La courbe I montre le résultat théorique (R=1708) dans la couche dont les deux surfaces limites sont rigides et conductrices, la courbe II notre résultat et la courbe III celui (R=657.5) correspondant aux surfaces libres

conductrices. La courbe II s'accorde bien avec les expériences.

Quand la couche se divise en bandes longitudinaux, le rapport r de la distance entre deux paires de bandes à l'épaisseur prend la forme:

$$r = \frac{2\pi}{a}. \tag{14}$$

Nous avons donc:

$$r = 2.61. \tag{15}$$

D'après les expériences de D. Avsec, ce rapport est le plus fréquemment supérieur à 2, ce qui n'est pas en contradiction avec notre résultat.

Conclusion.

En tant que la plaque de glace est cosidérée comme surface parfaitement conductrice de la chaleur, c'est-à-dire la température y est supposée constante, les expériences de D. Avsec ne sont pas expliquées. Cependant, pourvu que l'on considère cette plaque comme surface non conductrice, la concordance de la différence critique de température est suffisante et de plus il n'y a aucune contradiction entre la théorie et les expériences au sujet de la dimension des bandes longitudinaux.

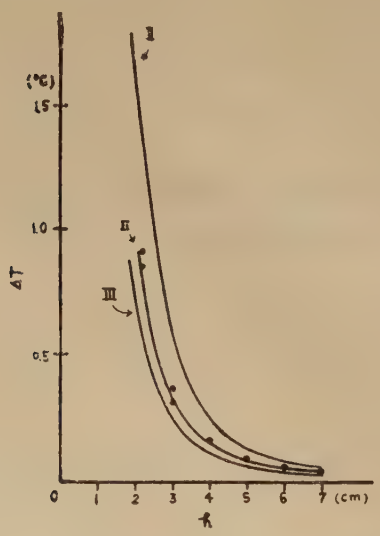

Fig. 1. Relation entre l'Epaisseur et la Différence Critique de Tempérarure. courb I : le cas où les deux surfaces limites sont rigides et conductrices ; courbe Ⅱ : le cas où une est rigide et conducrice et l'autre rigide et non conductrice ; coube Ⅲ : le cas où les deux sont libres et conductrices; cercles noirs : expériences de Douchau Avsec.

Bibliographie

Bénard, Henri et Douchan Avsec (1938) : Travaux Récents sur les Tourbillons Cellulaires et les Tourbillons en Bandes. Applications à l'Astrophysique et à la Météorologie. Journ. de Phys. **9**. 486

Takano, Kenzo (1955) : Sur la Dimension des Tourbillons Cellulaires dans les Expériences de Henri Bénard. Rec. Oceanogr. Works. Japan, **2** (1), 80

Takano, Kenzo (1955) : Sur les Tourbillons Themoconvectifs dans la Nappe Liquide Horizontale Chauffée par en dessous. Rec. Oceanogr. Works. Japan, **2** (1), 87

Records of Oceanographic Works
in Japan, Vol. 2, No. 1,
March 1955

Sur les Courants Thermoconvectifs dans la Nappe Fluide Horizontale Chauffée par en dessous

Par

Kenzo Takano

(Institut Géophysique, Université de Tokio)

Résumé: Nous avons trouvé la condition de l'instabilité de la nappe fluide horizontale limitée entre deux surfaces rigides et chauffée par en dessous dans les cas suivants: 1°) une surface limite est conductrice et l'autre non conductrice; 2°) toutes les deux sont conductrices; 3°) toutes les deux sont non conductrices. Il en résulte que sont bien confirmées les expériences de Douchan Avsec au sujet de la différence critique de deux températures extrêmes au moment où la nappe de l'air se met en mouvement et que des transitions du transfert de la chaleur dans l'expérience de W. V. R. Malkus sont grossièrement expliquées.

Introduction

Dans les expériences de Douchan Avsec, les courants thermoconvectifs se déclenchent beaucoup facilement par rapport au résultat théorique que l'on trouve en supposant les deux limites rigides et conductrices. Nous avons déjà montré d'une manière approximative que celui-ci s'accorde bien avec celles-là par l'hypothèse que la surface limite supérieure de la plaque de glace est non conductrice, c'est-à-dire le gradient vertical de la température y est constant. Un but de ce travail consiste à constater ce résultat approximatif précédent.

Des expériences indiquent qu'ont lieu des transitions discontinues du transfert de la chaleur dû à la convection en raison de l'augmentation de la différence de deux températures extrêmes dans la nappe liquide horizontale chauffée par en dessous, ce qui permet d'en déduire des transitions du régime des courants, c'est-à-dire quand on continue à chauffer la nappe fluide divisée en cellules par une circulation, elle doit prendre brusquement un autre type de la circulation que le premier et cette circulation nouveau-née engendre une transition discontinue du transfert de la chaleur vers le haut. On peut théoriquement déterminer la différence de deux températures extrêmes à chaque transition, mais y intervient une hypothèse que la nappe fluide est en repos et le gradient vertical de la

température est constant partout, avant que la circulation d'un type prenne naissance. En ce qui concerne la première transition elle est valable, cependant quand la deuxième a lieu, elle ne l'est plus, parce que le fluide n'est plus en repos et le gradient vertical de la température n'est plus constant partout à cause de la perturbation des premiers courants. Donc, des résultats expérimentaux ne sont pas nécessairement confirmés par ceux qui sont obtenus par l'hypothèse ci-dessus et ceux-là s'accorderont plus ou moins avec ceux-ci si la perturbation d'une circulation n'a pas l'influence considéuable sur la transition prochaine.

Conditions des Transitions

Les équations du mouvement, l'équation de continuité et l'équation de la chaleur se transforment en

$$(D^2-a^2)^3\ w=-Ra^2w, \tag{1}$$

où w représente la composante verticale de la vitesse, R est le nombre de Rayleigh, a un nombre caractéristique représentant la dimension des cellules et on désigne la surface inférieure et supérieure par $\zeta=-\frac{1}{2}$ et $\zeta=\frac{1}{2}$ respectivement et $\frac{d}{d\zeta}$ par D.

Les conditions aux limites s'écrivent :

$w=Dw=(D^2-a^2)^2\ w=0$ à la surface rigide conductrice, (2)

$w=D^2w=D(D^2-a^2)^2\ w=0$ à la surface rigide non conductrice. (3)

La solution de l'équation (1) prend la forme :

$$w=A_1\cosh 2\mu_1\zeta+A_2\cosh 2\mu_2\zeta+A_3\cosh 2\mu_3\zeta+B_1\sinh 2\mu_1\zeta$$
$$+B_2\sinh 2\mu_2\zeta+B_3\sinh 2\mu_3\zeta, \tag{4}$$

où

$$\mu_1=\frac{a}{2}\sqrt{1-\lambda\omega_1}, \qquad \lambda^3=\frac{R}{a^4}, \qquad \omega_3=\frac{-1-\sqrt{3}\,i}{2},$$

$$\mu_2=\frac{a}{2}\sqrt{1-\lambda\omega_2}, \qquad \omega_1=1,$$

$$\mu_3=\frac{a}{2}\sqrt{1-\lambda\omega_3}, \qquad \omega_2=\frac{-1+\sqrt{3}\,i}{2},$$

A_1, A_2, A_3, B_1, B_2 et B_3 sont des constantes.

Alors nous allons étudier les trois cas suivants : 1°) une surface limite est rigide et non conductrice et l'autre rigide et conductrice ; 2°) toutes les deux sont rigides et conductrices ; 3°) toutes les deux sont rigides et non conductrices. cas 1° :

D'après les conditions (2) et (3), on arrive à

$$
\left.\begin{aligned}
&A_1\cosh\mu_1+A_2\cosh\mu_2+A_3\cosh\mu_3=0,\\
&\mu_1A_1\sinh\mu_1+\mu_2A_2\sinh\mu_2+\mu_3A_3\sinh\mu_3=0,\\
&B_1\sinh\mu_1+B_2\sinh\mu_2+B_3\sinh\mu_3=0,\\
&\mu_1B_1\cosh\mu_1+\mu_2B_2\cosh\mu_2+\mu_3B_3\cosh\mu_3=0,\\
&(4\mu_1^2-a^2)^2A_1\cosh\mu_1+(4\mu_2^2-a^2)^2A_2\cosh\mu_2+(4\mu_3^2-a^2)^2A_3\cosh\mu_3\\
&\quad+(4\mu_1^2-a^2)^2B_1\sinh\mu_1-(4\mu_2^2-a^2)^2B_2\sinh\mu_3-(4\mu_3^2-a)^2B_3\sinh\mu_3=0,\\
&\mu_1(4\mu_1^2-a^2)^2A_1\sinh\mu_1+\mu_2(4\mu_2^2-a^2)^2A_2\sinh\mu_2+\mu_3(\mu_3^2-a^2)^2A_3\sinh\mu_3\\
&\quad+\mu_1(\mu_1^2-a^2)^2B_1\cosh\mu_1+\mu_2(4\mu_2^2-a^2)^2B_2\cosh\mu_2\\
&\quad+\mu_3(4\mu_3^2-a^2)B_3\cosh\mu_3=0,
\end{aligned}\right\}
$$

d'où

$$
\begin{vmatrix}
\cosh\mu_1 & \cosh\mu_2 & \cosh\mu_3\\
\mu_1\sinh\mu_1 & \mu_2\sinh\mu_2 & \mu_3\sinh\mu_3\\
0 & 0 & 0\\
0 & 0 & 0\\
(4\mu_1^2-a^2)^2\cosh\mu_1 & (4\mu_2^2-a^2)^2\cosh\mu_2 & (4\mu_3^2-a^2)^2\cosh\mu_3\\
\mu_1(4\mu_1^2-a^2)^2\sinh\mu_1 & \mu_2(4\mu_2^2-a^2)^2\sinh\mu_2 & \mu_3(4\mu_3^2-a^2)^2\sinh\mu_3
\end{vmatrix}
$$

$$
\begin{vmatrix}
0 & 0 & 0\\
0 & 0 & 0\\
\sinh\mu_1 & \sinh\mu_2 & \sinh\mu_3\\
\mu_1\cosh\mu_1 & \mu_2\cosh\mu_2 & \mu_3\cosh\mu_3\\
-(4\mu_1^2-a^2)^2\sinh\mu_1 & -(4\mu_2^2-a^2)^2\sinh\mu_2 & -(4\mu_3^2-a^2)\sinh\mu_3\\
\mu_1(4\mu_1^2-a^2)^2\cosh\mu_1 & \mu_2(4\mu_2^2-a^2)^2\cosh\mu_2 & \mu_3(4\mu_3^2-a^2)^2\cosh\mu_3
\end{vmatrix}
=0, \quad (5)
$$

pour que le fluide se mette en mouvement.

Ce déterminant se transforme en

$$
\begin{aligned}
&-\frac{\sin 2\gamma}{2\gamma}\\
&\cos 2\gamma\cdot(A^2-B^2)\left(1-\frac{\cos 4B}{\cosh 4A}\right)+2(A^2+B^2)\left(\frac{\cos 2\gamma}{\cosh 4A}+\frac{\sqrt{3}\sin 2B}{2\cosh 2A}-\frac{\cos 2B}{2\sinh 2A}\right)\\
=&\\
&A(\gamma^2-A^2-B^2)\left(1+\sqrt{3}\,\frac{\sin 4B}{\sinh 4A}\right)-B(\gamma^2+A^2+B^2)\left(\sqrt{3}-\frac{\sin 4B}{\sinh 4A}\right),
\end{aligned}
\qquad (6)
$$

dans laquelle

$$
\begin{aligned}
A&=\frac{a}{4}\sqrt{2+\lambda+2\sqrt{1+\lambda+\lambda^2}},\\
B&=\frac{\sqrt{3}\,a\lambda}{4\sqrt{2+\lambda+2\sqrt{1+\lambda+\lambda^2}}},\\
\gamma&=\frac{a}{2}\sqrt{\lambda-1}.
\end{aligned}
\qquad (7)
$$

On peut résoudre graphiquement cette équation comme fonction de a et de

γ et déterminer le nombre de Rayleigh. Dans le tableau 1 se montrent les résultats ainsi obtenus.

Tableau 1

transition	a	γ	R_{cnc}	transition	a	γ	R_{cnc}
1	2.40	1.8580	1300.9	4	8.00	6.590	2.099×10^5
	2.50	1.8600	1297.0		9.00	6.590	2.042×10^5
	2.55	1.8606	1296.0		10.00	6.589	2.049×10^5
	2.60	1.8611	1296.0		11.00	6.585	2.110×15^5
	2.65	1.8618	1297.7				
	2.70	1.8622	1299.8	5	10.00	8.161	4.919×10^5
	2.80	1.8630	1307.5		11.00	8.162	4.807×10^5
2	4.00	3.450	1.609×10^4		12.00	8.160	4.798×10^5
	5.00	3.447	1.526×10^4		13.00	8.158	4.876×10^5
	6.00	3.440	1.608×10^4	6	12.00	9.733	10.023×10^5
	7.00	3.430	1.809×10^4		13.00	9.733	9.731×10^5
3	6.00	5.020	7.112×10^4		14.00	9.732	9.693×10^5
	7.00	5.020	6.861×10^4		15.00	9.730	9.778×10^5
	8.00	5.018	6.983×10^4				
	9.00	5.010	7.369×10^4				

On en trouve les minima de R qu'indique le tableau 2. Dans ce tableau les valeurs de a sont un peu incertaines tandis que les nombres de Rayleigh sont comparativement précis.

Tableau 2

transition	a	R_{cc}
1	2.58	1296
2	5.0	1.52×10^4
3	7.0	6.86×10^4
4	9.4	2.03×10^5
5	11.7	4.79×10^5
6	13.8	9.69×10^5

cas 2° :

La solution est composée d'une partie paire et d'une partie impaire et de même on arrive à

$$-\gamma\tan\gamma=\frac{A(\sqrt{3}\sin 2B+\sinh 2A)+B(\sqrt{3}\sinh 2A-\sin 2B)}{\cosh 2A+\cos 2B},$$

pour la partie paire, (8)

$$-\frac{\tan\gamma}{\gamma}=\frac{\cosh 2A-\cos 2B}{A(\sqrt{3}\sin 2B-\sinh 2A)-B(\sqrt{3}\sinh 2A+\sin 2B)},$$

pour la partie impaire. (9)

Celle-là détermine les 1ère, 3e et 5e transitions et celle-ci les 2e, 4e et 6e

Tableau 3

transition	a	γ	R_{cc}	transition	a	γ	R_{cc}
3	6.00	5.173	7.716×10^4	5	11.00	8.298	5.149×10^5
	7.00	5.154	7.637×10^4		12.00	8.288	5.100×10^5
	8.00	5.135	7.605×10^4		13.00	8.275	5.141×10^5
	9.00	5.115	7.900×10^4		14.00	8.263	5.267×10^5
4	8.00	6.741	2.319×10^5	6	13.00	9.870	10.318×10^5
	9.00	6.727	2.221×10^5		14.00	9.860	10.208×10^5
	10.00	6.712	2.200×10^5		15.00	9.850	10.242×10^5
	11.00	6.697	2.240×10^5		16.00	9.840	10.399×10^5

transtions. Quant aux 1ère et 2e transitions elles ont été déjà étudiées et nous avons les tableaux 3 et 4.

Tableau 4

transition	a	R_{cc}
1	3.13	1708
2	5.36	17620
3	8.0	7.60×10^4
4	10.0	2.20×10^5
5	12.0	5.06×10^5
6	14.5	10.19×10^5

cas 3° :

Nous trouvons aussi deux équations ; une est dérivée de la partie paire et détermine les 1ère, 3e et 5e transitions, l'autre est dérivée de la partie impaire et détermine les 2e, 4e et 6e transitions. Elles s'écrivent :

$$\gamma \tan \gamma = \frac{(A^2+B^2)(\cosh 2A-\cos 2B)}{(\sqrt{3}\,B-A)\sinh 2A+(\sqrt{3}\,A+B)\sin 2B} \qquad (10)$$

et

$$\frac{\tan \gamma}{\gamma} = \frac{(A-\sqrt{3}\,B)\sinh 2A+(\sqrt{3}\,A+B)\sin 2B}{(A^2+B^2)(\cosh 2A+\cos 2B)} . \qquad (11)$$

Les tableaux 5 et 6 représentent les résultats, sauf la condition de la première transition qui a été déjà obtenue.

Tableau 5

transition	a	γ	R_{ncnc}	transition	a	γ	R_{ncnc}
2	3.0	3.260	1.519×10^4	3	5.0	4.848	6.743×10^4
	4.0	3.300	1.321×10^4		6.0	4.873	6.243×10^4
	5.0	3.326	1.328×10^4		7.0	4.892	6.187×10^4
	6.0	3.339	1.454×10^4		8.0	4.904	6.424×10^4

4	7.00	6.427	2.006×10^5
	8.00	6.445	1.905×10^5
	9.00	6.460	1.881×10^5
	10.00	6.470	1.913×10^5
5	10.00	8.018	4.556×10^5
	11.00	8.028	4.492×10^5
5	12.0	8.039	4.528×10^5
	13.0	8.045	4.636×10^5
6	12.0	9.588	9.305×10^5
	13.0	9.598	9.188×10^5
	14.0	9.607	9.211×10^5
	15.0	9.615	9.352×10^5

Tableau 6

transition	a	R_{cnc}
1	(0)	720
2	4.5	1.31×10^4
3	6.7	6.17×10^4
4	9.0	1.44×10^5
5	11.0	4.49×10^5
6	13.4	9.17×10^5

Tableau 7

transition	a	R_0
1	2.22	657.5
2	4.44	1.052×10^4
3	6.66	5.326×10^4
4	8.89	1.683×10^5
5	11.10	4.109×10^5
6	13.33	8.521×10^5

Si les deux surfaces limites sont libres et conductrices, on arrive facilement à

$$R_0=\frac{27}{4}n^4\pi^4 \qquad (12)$$

et

$$a=\frac{n\pi}{\sqrt{2}}, \qquad (13)$$

où n désigne la n^e transition.

Dans le tableau 7 se montrent les résultats dans ce cas.

C'est la figure 1 qui indique les rapports $\frac{R_{cnc}}{R_0}$, $\frac{R_{ncnc}}{R_0}$ et $\frac{R_{cc}}{R_0}$. Chacun semble s'apporocher d'une constante propre et il est aussi possible que les trois rapports se rapprochent d'une constante mais nous ne pouvons conclure cela, n'ayant calculé que jusqu'à la 6^e transition.

Les expériences de Douchan Avsec montrent que dans une nappe de l'air limitée par deux surfaces rigides l'air se met en mouvement régulier au nombre de Rayleigh égal à 1050 ± 50 environ et le rapport de la distance entre deux paires de bandes à l'épaisseur de la nappe est le plus fréquemment supérieur à 2, lorsque la nappe se divise en bandes longitudinaux.

D'autre part, on trouve théoriquement :

$$\begin{aligned} R_{cnc} &= 1296 \quad \text{dans le cas } 1° \\ R_{cc} &= 1708 \quad \text{dans le cas } 2,° \\ R_{ncnc} &= 720 \quad \text{dans le cas } 3°, \end{aligned} \qquad (14)$$

et le rapport ci-dessus r s'écrit :

$$\begin{aligned} r&=2.43 \quad \text{dans le cas 1°,} \\ r&=2.01 \quad \text{dans le cas 2°,} \\ r&=\infty \quad \text{dans le cas 3°,} \end{aligned} \tag{15}$$

comme il est exprimé par la relation suivante :

$$r=\frac{2\pi}{a}.$$

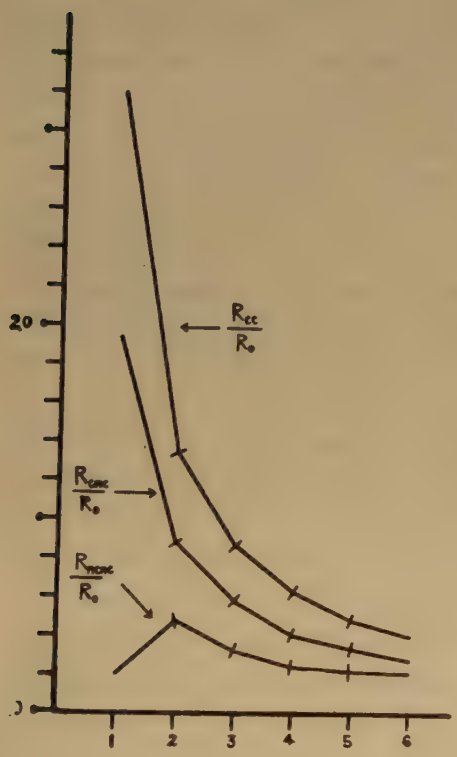

Fig. 1. Variations des trois rapports $\frac{R_{cc}}{R_0}$, $\frac{R_{cnc}}{R_0}$ et $\frac{R_{ncnc}}{R_0}$.
abscisse : transition

A la rigueur, la condition à la limite par rapport à la température prend la forme :

$$K\theta=\frac{\kappa}{h}\frac{\partial\theta}{\partial\zeta}, \tag{16}$$

où θ est la déviation de la température de l'état équilibré, κ la conductibilité de la chaleur, h l'épaisseur et K une constante. Si la constante $\frac{\kappa}{h}$ est suffisamment grande, elle aboutira à la condition $\frac{\partial\theta}{\partial\zeta}=0$ et si $\frac{\kappa}{h}$ est suffisamment petite, elle aboutira à $\theta=0$. Celle-là s'applique à la surface non conductrice et celle-ci à la surface conductrice. La condition à la surface réelle sera tantôt plus près de celle-ci, tantôt plus près de celle-là. Il en résulte donc que si la surface superiéure (plaque de glace) est presque non conductrice et la surface inférieure (plaque d'acier) n'est pas parfaitement conductrice, les résultats expérimentaux de D. Avsec seront bien expliqués. D'après une de ses figures, la surface inférieure est, en effet, loin de représenter l'isotherme le plus élevé. Aucun résultat dans les trois cas n'est en contradiction avec la dimension des bandes dans ses expériences.

Dans une nappe fluide horizontale limitée par deux surfaces rigides, W. V. R. Malkus a observé des transitions du transfert de la chaleur vers le haut qui sont montrés dans le tableau 8.

Tableau 8

transiton	R
1	1700 ± 80
2	11000 ± 2000
	18000 ± 1000
	26000 ± 5000
3	55000 ± 4000
4	170000 ± 15000
5	425000 ± 20000
6	860000 ± 30000

Malgré que ces résultats ne soient pas

d'accord avec ceux qui sont obtenus plus haut, ils sont bien près des résultats dans le cas 3°, ce qui permet de conclure que la perturbation d'une circulation n'a pas l'influence importante sur la transition prochaine.

Conclusions

1°) : Supposé que la surface inférieure n'est pas parfaitement conductrice et la surface supérieure est presque non conductrice, on peut bien expliquer les expériences de Douchan Avsec. Depuis l'étude de Rayleigh sur les courants thermoconvectifs dans la nappe fluide horizontale chauffée par en dessous, on a développé sa méthode jusqu'à la convection dans la sphère qui est ou en repos ou en mouvement rotatoire ou soumis au champs magnétique. Les expériences de K.Chandra, de R. J. Schmidt et S. Milverton, de R. J. Schmidt et O. A. Saunders, de D. T. E. Dassanayake et de W. V. R. Malkus ont montré la validité de sa méthode pour la convection dans une nappe fluide horizontale en repos. Mais ceux de Henri Bénard et de Douchan Avsec ont été en contradiction avec les résultats qu'on trouve en supposant les deux limites conductrices. Cependant nous avons montré dans les travaux présent et précédents que ces expériences sont bien constatées par l'hypothèse que les deux limites sont plus ou moins non conductrices. Bien que des vérifications expérimentales ne portent pas encore sur les résultats théoriques dans des cas compliqués, du moins en ce qui concerne les courants cellulaires dans la nappe horizontale en repos il n'y a peut-être aucune expérience qui n'indique pas la validité de la méthode de Rayleigh.

2°) : Le résultat expérimental de W. V. R. Malkus est, sauf les 1ère et 2^{e} transitions, très près des résultats théoriques dans le cas où les deux limites sont non conductrices. Mais on ne peut en expliquer l'expérience de R. J. Schmidt et O. A. Saunders où les courants deviennent parfaitement turbulents au nombre de Rayleigh égal à 45000 environ.

Remerciements

Nous tenons à remercier le Professeur Koji Hidaka pour l'intérêt qu'il a porté à cette étude, ainsi que Monsieur Kiheiji Ogawa qui a bien voulu revoir une partie des calculs.

Bibliographie

Bénard, Henri et Douchan Avsec (1938) : Travaux Récents sur les Tourbillons Cellulaires et les Tourbillons en Bandes. Applications à l'Astrophysique et à la Météorologie., Journ. de Phys. **9**, 486

Chandra, Krishna (1938) : Instability of Fluid Heated from Below., Proc. Roy. Soc. A **164**, 231

Malkus, W.V. R. (1954) : Discrete Transitions in Turbulent Convection., Proc. Roy. Soc. A **225**, 185

Schmidt, R. J. and S. Milverton (1935) : On the Motion of a Fluid Heated from Below., Proc. Roy. Soc. A **152**, 586

Schmidt, R. J. and O. A. Saunders (1938) : On the Mot on of a Fluid Heated from Below., Proc. Roy. Soc. A **165**, 216

Pellew, A. and Southwell, R. W., (1940) : Convection Motion in a Fluid, Proc. Roy. Soc. A **176**, 312

Sutton, O. G. (1950) : On the Stability of a Fluid Heated from Below., Proc.Roy. Soc. A **204**, 297

Takano, Kenzo (1955) : Sur les Tourbillons Thermoconvectifs dans la Nappe Fluide Horizontale Chauffée par en dessous. Rec. Oceanogr. Works. Japan. **2** (1), 87

Takano, Kenzo (1955) : Sur la Différence Critique de Température dans les Expériences de Douchan Avsec au Sujet des Courants Thermoconvectifs. idem. 93

Records of Oceanographic Works
in Japan, Vol. 2, No. 1,
March 1955

The Relation Between Chlorinity and Silicate Concentration of Water Observed in Some Estuaries, III.

(The [CL]-[SiO_2] relation formula obtained in the estuarine region of the river Chikugo and the amended formula representing the relation between the two constants of the [CL]-[SiO_2] relation formula.*)

Hironari Makimoto, Hiroshi Maéda and Shitoku Era
(Shimonoseki College of Fisheries)

To increase the amount of production of oyster and laver in the estuarine region of the river Chikugo, both suitable organisms to the brackish environment, a series of oceanographichal observations have been carried out by the Ariake Fisheries Laboratory of Fukuoka Prefecture. In these observations, the influence of the river water upon the sea water must be analysed as well as the chemical constituents, when we wish to understand the characteristics of the water of this region and their changes. According to **Yoshimura**, the amount of dissolved silicate determinable easily and exactly is considered to be the most suitable indicator to show the mixing ratio of river water to sea water. The second author (**Maéda**, '52 and '53) reported already that the relation between chlorinity and silicate concentration of estuarine water is represented by the following formula:

$$[SiO_2]+A[CL]=B \cdots\cdots (1)$$

and the relation batween two constants of the above-mentioned formula is shown as follows:

$$B=0.807+15.9A \cdots\cdots (2)$$

Using the data obtained during the period from Nov. '53 to Feb. '54, we estimated the [CL]-[SiO_2] relation formulae of the river Chikugo in Ariake-Sea and examined whether the relation between two constants follows the given formula (2) or not. In consequence, we found that the [CL]-[SiO_2] relation formulae are attributable to the given formula (1) $[SiO_2]+A[CL]=B$ and the relation between two constants of this formula follows the formula (2), but the constants must be changed in this time as follows:

$$B=0.0037+17.665\ A \cdots\cdots (3)$$

* Contributions from the Shimonoseki College of Fisheries, No. 108

Before entering the subject, we must express our sincere thanks to Messrs. Matsuo, Matsunaga and Otsu who afforded us much facilities for carrying out this work.

Method

Observations were made at high-tide of each spring or neap-tide during the period from Nov. '53 to Feb. '54. Water was sampled from surface and bottom layers at each of stations shown in Fig. 1. Chlorinity (‰) was determined by **Mohr**'s silver titration method, and silicate concentration (mg/*l*) by **Dienert-Wandenbulck**'s colorimetric method. The data thus obtained were treated by the same method as described in the second report of this series (**Maeda**, '53).

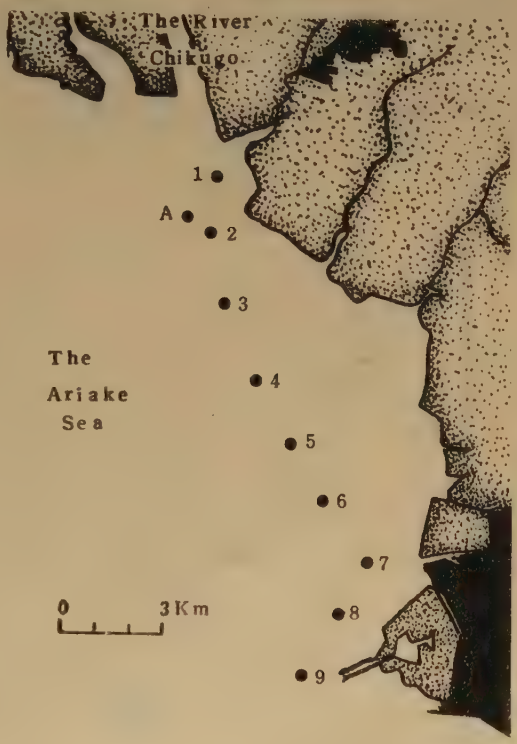

Fig. 1. Map of the estuarine region of the River Chikugo, showing the stations.

Results

The results are shown in table 1 and Figs. 2 and 3. From these table and figures it may be perceived that all formulae are attributable to the fundamental formula $[SiO_2]+A[CL]=B$ and the influence of river water is extending to the bottom layer in a considerable degree in all observations as in the case of the river Ohashi in Nakano-umi (**Maeda**,'53).

Table 1. Constants, A and B, of the $[CL]$-$[SiO_2]$ relation formula obtained from the estuarine water of the river Chikugo.

Date	Layer	A	B	F_0	n_1	n_2	Level of Significance
9, Nov. '53	Surface	1.25	22.53	37.84			<0.005
	Bottom	1.47	26.27	182.43			<0.005
30, Nov. '53	Surface	1.50	25.61	629.17			<0.005
	Bottom	1.41	24.22	250.75			<0.005

8, Dec. '53	Surface	1.25	21.92	81.43			<0.005
	Bottom	1.15	20.29	364.95			<0.005
15, Dec. '53	Surface	1.18	21.91	21.86			<0.005
	Bottom	2.10	37.38	40.86	1	8	<0.005
21, Jan. '54	Surface	1.38	24.70	3368.22			<0.005
	Bottom	1.41	25.39	218.65			<0.005
27, Jan. '54	Surface	1.16	21.11	739.21			<0.005
	Bottom	1.11	20.27	178.63			<0.005
4, Feb. '54	Surface	1.41	25.76	490.15			<0.005
	Bottom	1.46	26.47	254.53			<0.005
11, Feb. '54	Surface	1.79	32.04	588.29			<0.005
	Bottom	1.52	27.74	211.85			<0.005

Note: $[SiO_2]$: mg/*l*, [CL]: ‰
$[SiO_2]+A\ [CL]=B$, $F_8\ (0.05)=14.688$

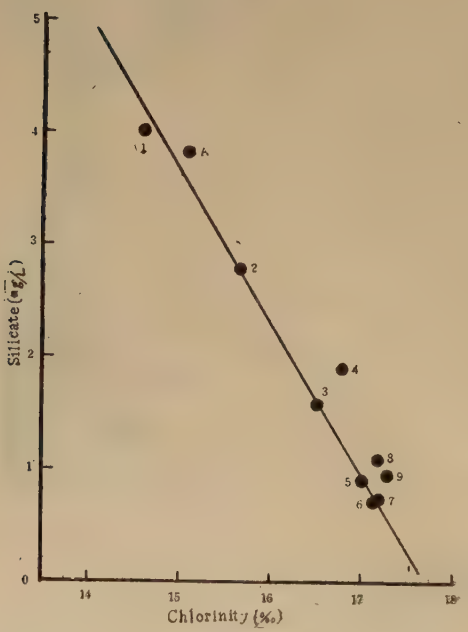

Fig. 2. Silicate-chlorine relation graph drawn on the data observed on November 9th, 1953. (surface layer).

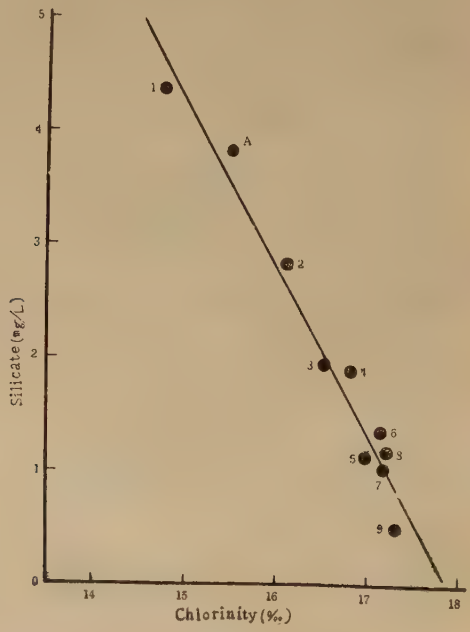

Fig. 3. Silicate-chlorine relation graph drawn on the data observed on November 9th, 1953. (bottom layer).

Discussion and Conclusion

Maèda ('53) reported that the relation between two constants, A and B, was shown by the formula (2) in regions studied previously. Therefore, we examined whether two constants obtained from the [CL]-$[SiO_2]$ relation formulae in the

estuarine region of the river Chikugo are distributed in the rejective zone of the formula (2) or not, using the following formula as that of the rejective zone.

$$\frac{\{(B-9.770)-15.9\ (A-0.56)\}^2}{1.195\{1+\frac{1}{23}+(A-0.56)^2/1.9175\}}=F_0 \quad \cdots\cdots(4)$$

$(n_1=1,\ n_2=21)$

Results of the examination are shown in table 2. And we find that all points, showing values of two constants of the [CL]-[SiO_2] relation formulae in the estuarine region of the river Chikugo, are distributed in the rejective zone of the formula (2) at 0.05 level of significance.

Thus, we estimated newly values of two constants and afforded the following formula as that representing the relation between A and B.

Table 2. F_0-values, computed by the formula (4)

Date	Layer	F_0
9, Nov. '53	Surface	1.810
	Bottom	2.316
30, Nov. '53	Surface	0.431
	Bottom	0.502
8, Dec. '53	Surface	0.887
	Bottom	0.873
15, Dec. '53	Surface	3.468
	Bottom	3.497
21, Jan. '54	Surface	2.123
	Bottom	2.574
27, Jan. '54	Surface	2.178
	Bottom	2.134
4, Feb. '54	Surface	3.566
	Bottom	3.121
11, Feb. '54	Surface	3.306
	Bottom	3.974

Note: formula (4) is

$$\frac{\{(B-9.770)-15.9\ (A-0.56)\}^2}{1.195\{1+\frac{1}{23}+(A-0.56)^2/1.9175\}}=F_0$$

$F'_{21}\ (0.05)=4.3248$

$$B=0.0037+17.665\ A \quad \cdots\cdots(5)$$

Next, we examined whether all points, including those found in previous reports together with newly obtained ones, are distributed in the rejective zone of the formula (5) or not, using the following formula as that of the rejective zone.

$$\frac{\{(B-16.112)-17.665\,(A-0.912)\}^2}{0.9872\{1+\frac{1}{39}\,(A-0.912)^2/9.7092\}}=F_0 \quad \cdots\cdots(6)$$

$(n_1=1,\ n_2=37)$

Results of these examinations are shown in table 3. This table shows that no point is distributed in the out-side of the rejecive zone. Thus, we consider that the following conclusion may be allowed at the present state of the investigation.

Table 3. F_0-values, computed by the formula (6)

Date	Name of river or Lake	F_0
19, Mar. '50	Noda	0.1310
10-12, May '50	Noda	0.1825
30, Sept.-1, Oct. '50	Noda	2.0429
26-30, May, '51	Sasagase	0.4800
	Asahi	0.0256
	Yoshii	0.2012
26-27 Feb. '52	Sasagase	0.1838
	Asahi	1.3973
	Yoshii	1.1480
24-26, Oct. '51	Nakanoumi	1.7633
	Hino	2.3067
27, Oct. '51	Ohashi (surface)	1.2850
	Ohashi (bottom)	0.3363
1, Nov. 34	Fuji	0.6853
6, Sept. '35	Miyakoda	1.7008
12-17, Nov. '34	Hamana	2.7437
	Miyakoda	2.9509
		0.9653
29, Jan.-2, Feb. '35	Hamana	2.5854
	Miyakoda	1.5357
18-22, April, '35	Miyakoda	2.4576
	Inohana	0.0022
22-28, July, '35	Hamana	0.0993
9, Nov. '53	Chikugo(surface)	0.0989
	(bottom)	0.0795
30, Nov. '53	(surface)	0.8107
	(bottom)	0.4537
8, Dec. '53	(surface)	0.0601
	(bottom)	0.0031
15, Dec. '53	(surface)	0.8796
	(bottom)	0.0464
21, Jan. '54	(surfacc)	0.0983
	(bottom)	0.1208

27, Jan. '54	(surface)	0.2224
	(bottom)	0.2537
4, Feb. '54	(surface)	0.4358
	(bottom)	0.3677
11, Feb. '54	(surface)	0.1589
	(bottom)	0.5576

Note: formula (6) is

$$\frac{\{(B-16.112)-17.665\ (A-0.912)\}^2}{0.9872\{1+\frac{1}{39}(A-0.912)^2/9.7092\}}=F_0$$

$F'_{37}\ (0.05)=4.1106$

1) The A-B relation is shown more adequately in the following formula:

$$B=0.0037+17.665\ A$$

2) The above-mentioned formula is applicable in the range of A-value from 0.06 to 21.0.

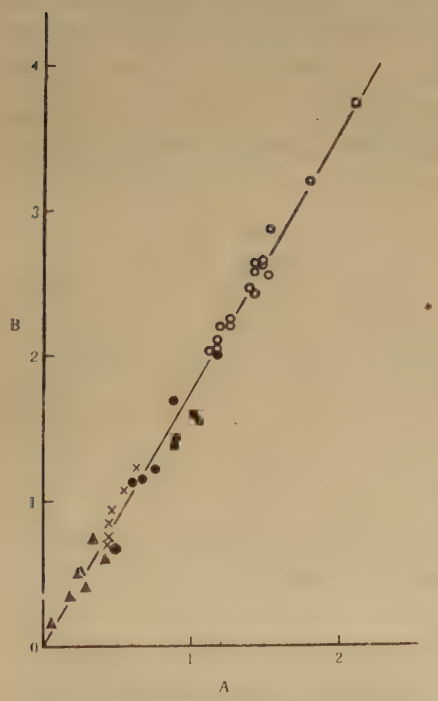

Fig. 4. Relation graph of both constants A and B.
Remarks:
▲ : Japan Sea Group
× : Seto-naikai Group
● : Pacific Group
○ : Ariake Sea Group

3) (a) If the silicate concentration in river water is high or low, the point showing values of the two constants of the relation formula will appear in the right or left side of the A-B relation line. (b) When $[SiO_2]/[CL]$ of sea water in a certain area is larger than in other bays, the point will appear in the upside of the relation line, while (c) when the ratio is smaller, the point will be found in the lower side.

As newly obtained situations in the graph are all found in the case of (a), it may be said safely that silicate concentration of water of the river Chikugo is higher as compared with those of other rivers, although $[SiO_2]$ /[CL] of Ariake-Sea is not unusual but stays in the range of general degree. Higher silicate concentration may seem as if it is a characteristic of the estuarine water of the river Chikugo. However it is not an essential feature but only a superficial one; [CL]-$[SiO_2]$ and A-B relations in the estuarine region of the river Chikugo are fundamentally ascribable to the formulae available to those

in estuarine of other rivers.

The distribution of points in Fig. 4 shows that both or each of the two constants in surveyed regions are arranged as follows in the order of values from lower to higher.

Japan Sea Group (rivers flowing into Yosa-naikai and Miho Bay)···Seto-Naikai Group (rivers flowing into Kojima Bay)···Pacific Ocean Group (rivers flowing into Suruga Bay and Lake Hamana)···Ariake Sea Group (rivers flowing into Ariake Sea).

Summary

1. Observations were pursued at high-tide of each spring or neap-tide during the period from Nov. '53 to Feb. '54, at the stations shown in Fig. 1.

2. [CL]-[SiO_2] relation formulae in the estuarine region of the river Chikugo at each time are shown in Table 1 and Figs. 2 and 3.

3. [CL]-[SiO_2] relation formulae in the estuarine region of the river Chikugo, at both surface and bottom layers, were represented fundamentally by the formula $[SiO_2]+A\,[CL]=B$. The influence of the river water was extending to the bottom in a considerable degree in all observations.

4. A-B relation formula estimated on all calculated values, including those already reported and also newly obtained ones about the river Chikugo, is:

$$B=0.0037+17.665\ A$$

5. Both or each of the two constants, A and B, are arranged in the order of values from lower to higher as follows:

Japan Sea Group···Seto-Naikai Group···Pacific Ocean Group···Ariake Sea Group.

References

1. MAÉDA, H., 1952, The relation between chlorinity and silicate concentration of water observed in some estuaries, publ. Seto Mar. Biol. Lab., 2 (2) 249-255.

2. MAÉDA, H., 1953, The relation between chlorinity and silicate concentration of water observed in some estuaries II, Jour. Shimonoseki Coll. Fish., 3 (2) 167-180.

3. MASUYAMA, G., 1949, Statistical methods of treating samples and methods of planning the experiments···for the people who are engaged in clinics (in Japanese). 3rd Ed. KAWADE-SHOBO (Tokyo).

4. YOSHIMURA, S., 1931, Soluble silicate as indicator of extent of inflow of river water into a sea, Gerlands Beitr. z. Geophys., 34, 393-399.

5. YOSHIMURA, S., 1936 Sci. Rep. Tokyo Bunrika Daigaku, Ser. C, 1 (3), 127-155.

Records of Oceanographic Works
in Japan, Vol. 2, No. 1,
March 1955

Seasonal Difference in the Amount of the Inorganic Phosphorus in Blood Serum of Fishes.

Ryushi Ichikawa

(Fisheries Institute, Faculty of Agriculture, Tokyo University)

Introduction

Annual rings and spawning marks appearing on scale, fin ray, otolith, vertebra and other hard tissues of fish have been well studied by various biologists as to be the special marks expressing the temporary retardation of their calcification process. And this retardation is supposed to be caused by the seasonal change of external and internal factors either directly or indirectly. That is the environmental or hydrological conditions and the physiological conditions of fish body itself. Apparently, the lowering of water temperature would cause the inactivity of metabolism, and the maturing of gonad, malnutrition or disease would cause the retardation of calcification in these tissues.

Here, to clarify the mechanism of the annual ring formation, the author investigated the seasonal change in calcium metabolism of fishes, by measuring the amount of inorganic phosphorus in blood serum of fishes. As far as human body concerned, seasonal change in calcium metabolism was already found to be very slight (McCance 1943). However, as fish is supposed to have more remarkable seasonal change in physiology than human being, the author had interest to investigate this. And as far as the amount of calcium and phosphorus in blood of fish, Fontaine (1931,1932) already found the considerable difference between Teleostei and Selachie, not in the amount of total calcium in blood serum but in the amount of inorganic phosphorus in blood serum. Of course, in Selachie it was surely less than in another. He mentioned, that this lesser amount of inorganic phosphorus would cause the mal-calcification of skeletal system of Selachie.

Considering these facts, the author analysed the amount of inorganic phosphorus in blood serum of fishes comparing this in winter and summer, in order to clarify the mechanism of annual ring formation.

Material and Method

The experiments were carried on in July and August 1953 and January and Februaly 1954 in fisheries laboratory in Tokyo university, using the carp, *Ciprinus carpio,* and the eel, *Anguilla japonica,* as the material. Carps were obta-

ined from the culture pond of Mizumoto branch of Tokyo metropolitan fisheries experimental station, from the culture pond of Hongo in Tokyo and from the Tokyo fish markets. Eels were all obtained from the Tokyo fish markets. Body weight of carp in summer was from ca. 120 gr. to 160 gr. and thatin winter ca. 700 gr. to 900 gr. That of eels in both season was from ca. 150 gr. to 200 gr.

The method of the quantitative analysis of the inorganic phosphorus in blood serum was as follows:-

(1) The fish was stuck on a wooden plate by pins lying on its back. The heart of fish was exposed by the dissection of its pectral region. The ventral aorta was cut off at the point of about 2 or 3 cm from the heart and the blood pouring out from it was received by a glass tube.

(2) Immediately after this, blood obtained was centrifuged at the velosity of 3000 cycle per minutes during five minutes. And the serum was separated from it by a small pippet. The blood which haemolysis occured was excluded for the test material because the blood corpuscle containes a pretty amount of phosphorus. The haemolysis of blood of carp actually occurred sometimes.

(3) The colorimetric analysis of the amount of inorganic phosphorus was carried out by the modified method of Fiske-Subbarow (Saito, 1950). The amount of serum used in each individual was 0.5 cc and the amount of inorganic phosphorus was measured by photo-electoric calorimeter of Itō chōtampa seisakusho (Itō ultra-short wave manufactory).

Results and Discussion

In case of eel, as it is shown in table 1, A, the amount of inorganic phosphorus in blood serum was from 8.2 to 13.5 mgr. per deci-litre and the mean value of them was 11.1 mgr. per deci-litre during summer. On the contrary, during winter this value was from 3.5 to 9.2 mgr. per deci-litre and 6.6 the mean value. In case of carp, as it is shown in table 1, B, this value was from 8.8 to 19.5 mgr. per deci-litre and the mean was 13.4 during summer. On the contrary during winter, this was from 3.3 to 9.8 and the mean was 6.8. From these results, it is sure, during winter time both species have much fewer amount of inorganic phosphorus in their blood serum than that in summer. (table 1)

Table 1. The amount of inorganic phosphorus in blood serum of fish.

(A) Eel *Anguilla japonica* (from Tokyo fish markets)

Summer			Winter		
No.	Date	P(mg/d.l.)	No.	Date	P(mg/d.l.)
1	Jul. 6	10.6	1	Dec. 8	6.4
2	〃	12.0	2	〃	9.2
3	Jul. 23	8.2	3	Dec. 14	5.9
4	〃	10.3	4	〃	5.0
5	Aug. 17	13.5	5	〃	3.6
6	〃	11.9	6	Dec. 24	8.6
7	〃	10.1	7	〃	8.0
8	〃	11.8	8	〃	6.2
9	〃	11.7			
	Mean	11.1		Mean	6.6

(B) Carp *Ciprinus carpio*

Summer (from Mizumoto culture pond)			Winter (No.1–6 markets No.7–11 Hongo pond)		
No	Date	P (mg/d.l.)	No	Date	P(mg/d.l.)
1	Jul. 28	10.9	1	Jan. 11	8.9
2	〃	10.4	2	〃	8.1
3	〃	10.0	3	〃	6.9
4	Aug. 4	12.7	4	Jan. 19	9.8
5	〃	18.6	5	〃	8.7
6	〃	8.8	6	Jan. 22	8.7
7	〃	16.2	7	Jan. 25	4.9
8	Aug. 12	13.0	8	〃	3.3
9	〃	16.2	9	〃	5.6
10	〃	19.5	10	〃	4.1
11	〃	9.5	11	〃	5.3
12	〃	15.1			
	Mean	13.4		Mean	6.8

Fontaine (1932) cited above investigated the relationship between the true bone formation and the amount of inorganic phosphorus in blood serum of fish. He used *Labrus berggylta, Trigla lineata, Conger vulgaris, Pleuronectes platessa* representing Teleostei and *Scylliorhincus canicula, Mustellus asterias, Raja batis, Raja clavata* representing Selachie and *Lamproie marine* representig Cyclostome. Each mean value of Selachie and cyclostome was both less than half of Teleostei though his report did'nt state the season when the investigation carried out. (table 2)

Table 2. The comparison among Teleostei, Selachie and Cyclostome in their inorganic phosphorus in blood serum. (abridged from Fontaine 1932)

Fishes investigated	Mean value of p(mg/d.l.)
Teleostei (4 species, 8 individuals)	15.8
Selachie (4 species, 9 individuals)	7.8
Cyclostome (1 species, 3 individuals)	5.6

It is interested by the auther that his data is quite comparable to these. That in my cases of both eel and carp, the figures obtained in summer fairly correspond with the mean value of Teleostei and those in winter with that of Selachie.

This tells during winter time the phosphate ion concentration in blood serum of Teleostei decreases to the low value nearly equal to that of Selachie. Thus this decrease of this amount is supposed to be the one of the causes of the retardation of calcification in hard tissues of fishes in winter just like the rachitic condition in case of mammals which is often followed by low value of the inorganic phosphorus in blood serum. Therefore, as it had been supposed to be so, the auther thinks he can conclude by his experiments that there were definite relationship between the seasonal change in amount of the inorganic phosphorus in blood serum of fishes and that of the calcification process of their hard tissues, which makes the annual ring on them.

The author wishes to express his thanks to Dr, Yoshio Hiyama professer of Tokyo university for his advice and criticism and to Mr. Kazuo Kanzaki the chief of Mizumoto branch of Tokyo metropolitan fisheries experimental station for his kindness in obtaining the material fishes and to Mr. Aritsune Saiki assistant professer of Tokyo university for his kindness in using the photo-electoric calorimeter

References

Fontaine, M. 1931 Sur 1a teneur en calcium du sang des poissons marins. C.R. Acad. Sci. 193.

————, 1932 Sur 1a relation existant chez 1es poisson marins et potomatoques entre 1a teneur en phosphore inorganique du serum et 1'ossification du squelette. ibid. 194.

McCance, R.A. and Widdowson, E.M. 1943 Seasonal and annual changes in the calcium metabolism of man. J. physiol. 102.

Saito, M. 1950 The method of clinical chemistry by photo-electric calorimeter. (in Jap.) Nanzando., Tokyo

Records of Oceanographic Works
in Japan, Vol.2, No. 1,
March 1955

A new species of copepod, *Scolecithricella vespertina*, .sp. from the Sea of Japan*

Otohiko Tanaka

(Faculty of Fisheries, Kyushu University)

Female. Length, 1.09 mm. The Cephalothorax oval. The Head fused with the 1st thoracic segment. The frontal margin of the head narrory rounded. The 4th and the 5th thoracic segments are fused. The lateral margin of the last thoracic segment is slightly emarginate. The Rostrum consists of two fine filaments attached to a wide difurcated base.

The Abdomen 4-Jointed, and is contained about 4-times in the length of the cephalothorax. The abdominal segments and furca are in the proportional lengths:

1+2	3	4	5	Furca
40	20	17	6	17 =100

The furcal rami 1.5 -times as long as wide. The genital segment is slightly swollen at the middle of the lateral margin when viewed from the dorsal; the ventral surface of the segment slightly produced below.

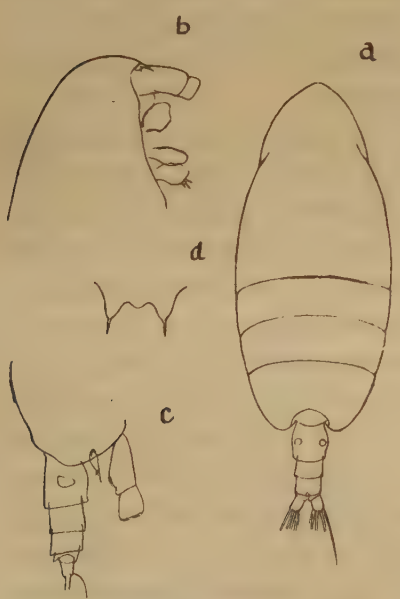

Fig. 1. a, body, dorsal view, X26; b, head, lateral view X 33; c, last thoracic segment and abdomen, lateral view, X 33; d, rostrum, X 131.

Fig. 2. a, 2nd antenna, X131; b, mandible, X131; c, lst maxilla, X131.

The 1st antenna 21-jointed, extends to the posterior margin of the last thoracic segment. The joints 1 and 2, 8 to 10, and 24 and 25 are fused. The joints 12 and 13 are fused on the posterior margin. The joints are in the following propotional lengths:

1-2 3 4 5 6 7 8-9-10 11 12 13 14 15 16 17 18 19 20 21 22 23 24-25
99 25 25 25 25 25 64 25 25 29 39 44 44 49 49 49 49 54 64 84 108=1000.

The 2nd antenna well developed. The exopodite is adout 1.3-times (37 : 28) as long as the endopodite. The 2nd joint of the endopodite is swollen on the outer margin, and is furnished with hairs on the outer margin. The Mandible small, but well developed. The exopodite about 2-times as long as the endopodite (11 : 6). The 3rd joint of the exopodites the longest (8 : 7 : 12 ; 3 : 2). The teeth of the cutting edge are slender. The Maxilla is small. The spinulation on the various parts are as follows: the outer lobe, 6 long and 3 short setae; the exopodite, 5 setae; the endopodite, 6 setae; the 2nd basal joint, 2 setae; the 3rd inner lobe, 2 setae; the 2nd inner lobe, 1 seta; the 1st inner lobe, 8 long and 1 short spines. The 2nd maxilla has 4 inner lobes, of which the distal one is the strongest; it is furnished with a strong spine, a slender one and a wormlike sensory filament. The endopodite of the 2nd maxilla is furnished with 9 sensory filaments of which the middle 4 are bud-like. The Maxillipede well developed. The basal joints are of about equal lengths. The 1st basal joint has a bud-like sensory filament on the inner margin about the middle of the joint. The 4th and the 5th joints of the endopodite have each an outer marginal seta.

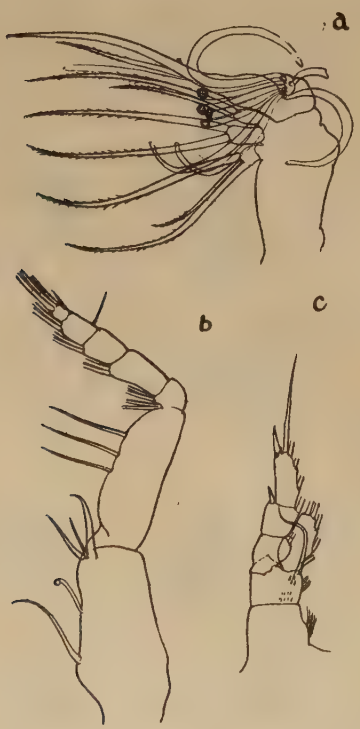

Fig. 3. a, 2nd maxilla, X131; b, maxillipede, X 131; c, lst leg, posterior aspect, X 52.

The 1st leg has 3-jointed exopodite and 1-jointed endopodite. The 1st joint of the exopodite is devoid of outer edge spine. The 2nd basal joint is furnished with two groups of minute spinules on the posterior surface. The 2nd leg has 3-jointed exopodite and 2-jointed endopodite. The 1st basal joint of the 2nd leg has small spines on the proximal outer margin, and a row of minute spinules on the posterior surface about the middle of the joint. The inner distal margin of the 2nd basal joint is produced into an acute angle. The 1st joint of the exopodite has the outer edge spine reaching the middle of the 2nd joint of

the exopodite. The posterior surface of the joint is furnished with a longitudinal row of spinules. The 2nd joint of the exopodite has a strong outer edge spine which extends to the middle of the proximal outer edge spine of the 3rd joint. The posterior surface of the joint is furnished with two rows of spinules. The 3rd joint of the exopodite has 3 outer marginal spines. The terminal spine is finely serrated; the teeth are about 40 in number. The posterior surface of the 3rd joint is furnished with 4 transverse rows of spinules as shown in the figure. The endopodite is broad The 1st joint is pointed at the distal outer edge. The 2nd joint has 6 remarkable spines on the anterior surface and a longitudinal row of minute spinules on the posterior surface. The 3rd leg has 3-jointed exopodite and endopodite. The 1st basal joint has a row of spines on the proximal outer margin; the posterior surface is furnished with groups of spinules; the inner marginal seta short. The 2nd and 3rd joints of the exopodite are each furnished with rows of minute spinules on the posterior surface. The 2nd and 3rd joints of the endopodite are each furnished with remarkable spines on the anterior surface, and with a longitudinal row of minute spinules on the posterior surface as shown in the figure. The 4th leg has the similar structure as in the 3rd leg. The outer margin of the 1st basal joint smooth. The inner marginal seta absent. There is on the posterior surface a row of strong spines, 5 in number, at the distal margin of the joint, and a group of minute spinules about the middle of the joint. The 2nd joint of the exopodite has a very short outer edge spine and a transversal row of minute spinules on the posterior surface. The 3rd joint of the exopodite has 3 rows of minute spinules on the posterior surface. The terminal spine is very finely serrated. The 2nd and 3rd joints of the endopodite are each furnished with longitudinal rows of spinules on the posterior surface. The 5th leg is 1-jointed. The inner margin has on the middle of the joint a serrated spine which is about half as long as the joint. The distal margin of the joint is furnished with a short spine. The outer margin has a small spine on the distal one-fourth of the joint.

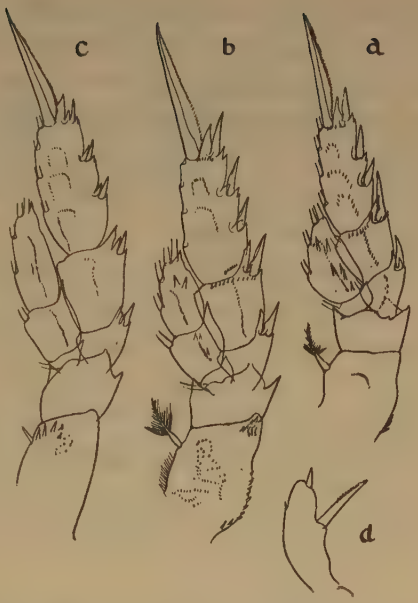

Fig. 4. a, 2nd leg, anterior aspect, X 52; b, 3rd leg, posterior aspect, X 52; c, 4th leg, posterior aspect, X 52; d, 5th leg, X 131.

Mori (1937) recorded the occurrence of th following species from the adjacent waters of Japan: *Scolecithricella minor* (Brady), *S. bradyi* (Giesbrecht), *S. abyssalis*

(Giesbrecht), *S. orientalis* Mori, and *S. spinipedata* Mori. These were taken chiefly from the surface layers. Among those *S. minor* is the cold water species, and has been recorded from the northern waters; the remainings have been reported from the warm waters. *S. orientalis*, though I have not found it in my collections, appears to be valid. But *S. spinicauda* seems to be identical with *S. ctenopus* (Giesbrecht) in having the 2nd, 3rd, and 5th pair of legs quite similar in structure to those of *S. ctenopus*.

The writer (1953) has reported 23 species of the genus Scolecithricella from the Pacific coast of the Middle Japan. Most of them appear to be bathypelagic, except *S. bradyi* and *S. ctenopus* which have been taken from the surface in the region. It is astonishing that the night haul made in the surface layer of the Japan Sea by the Kyoto Fisheries Experimental Station in July of 1953 caught *S. beata* which was one of the deep-water species of the Pacific, and was described by the writer (the description and figures yet unpublished). The present species may probably be an inhabitant of deep layers, and must have come up to the surface in the evening.

The specimen, though much smaller in size than *S. valida* (Farran), has the The 5th pair of legs quite similar in structure to those of *S.valida*. However, the spinulation on the 1st basal joint of the 3rd and 4th legs are quite different from those of the other species which have hitherto been observed by the writer.

Two specimens was taken in the surface night hauls in July of 1953 at the station 40 miles north of Maizuru.

*Foot Note. This paper is a result of the study carried out by the financial aid of grant from the Scientific Research Fund of the Ministry of Education.

Records of Oceanographic Works
in Japan, Vol. 2, No. 1,
March 1955

Preface to the Reports of the Oceanographical and Biological Surveys of the Kuroshio

By Koji Hidaka

(Geophysical Institute, Tokyo University)

Since the termination of the World War II the entire world has paid a special attention to the utilization of marine resources. Many oceanographic laboratories were established along the coasts of civilized countries. In the United States of America, the already existing institutions like the Scripps, Woods Hole and the University of Washington have been largely expanded and more than five laboratories were newly established along both the Atlantic and Pacific coasts. An oceanographic institute was attached several years ago to the University of British Columbia, Canada. In the United Kingdom, the National Institute of Oceanography was just established at Wormley, England, and a department of oceanography was added to the University of Liverpool.

Shortly after the restoration of peace, Hans Pettersson directed the Swedish Deep-Sea Expedition on board the "Albatross" in 1947-48 and obtained many exciting results on the features of the ocean floor, the thickness of its sediment carpet, the geochronology of the ocean beds and the current system in the equatorial waters. Anton Bruun of Denmark was the leader of the Danish Deep-Sea Expedition with the "Galathea" in 1950-52. Thomas Gaskell found many interesting oceanographic features during his British "Challenger" Expedition 1950-52. The United States also sent several ships on the Mid-Pacific, Shelback, Capricorn and the Trans-Pacific Expeditions between 1950 and 1953. As the results of these expeditions the least hetherto explored Pacific Ocean revealed many fascinating oceanographic features, especially with respect to the ocean floor.

The population of the world is increasing year by year, and the natural resources, fresh water and minerals are gradually coming short to feed the people. The best and most efficient solution for this problem is to explore the ocean and to produce more marine resources. The United States is a nation having the largest amount of land resources and so would feel the least necessity of relying upon the marine resources. Still they are paying special efforts to the oceanographic research and the exploration of marine resources.

The nations having meagrest natural resources are now concentrated into the southeastern corner of Asia, Japan being one of them, of course. In this area,

the Indo-Pacific Fisheries Council (IPFC) was established several years ago under the Food and Agricultural Organization (FAO). Since 1951 these nations are anxious to initiate an international institute of oceanography under the sponsorship of the UNESCO and to begin some basic oceanographic studies for exploring the marine resources and to improve the living standards of the people in this area. In the fall of 1953 specialists in oceanography met at Manila in a conference and discussed the possibility and necessity of such an institute.

Under these circumstances Japan cannot be indifferent alone. Japan is, as well known, surrounded by the waters on all sides and has a very prominent geographical position on the margin of the Pacific Ocean. It has a center of scientific research faced on this gigantic expanse of water, the most unexplored and the most fascinating part of the world's oceans.

In addition to these circumstances, Japanese fisheries has an unrivalled position among the Pacific countries. Its amount of fish catch occupies almost 25 percents of the world's production. About half of the world's fisheries people belong to ours. Now oceanography is related to fisheries as the natural sciences to engineering. Oceanography furnishes the fisheries with necessary basis for its advance and improvement. This is the reason why Japan has to pay a special attention to the basic oceanographic research.

The phenomena going on in the ocean are manifold. They cover the subjects of attack in almost all fields of natural sciences and these phenomena are all interrelated one another. This fact inevitably requests that all fields in the natural sciences should cooperate in attacking the phenomena going on in the oceans. For this reason a modern oceanographic institute should involve research sections of physics, chemistry, botany, zoology, geology, geography and marine meteorology at the same time. Therefore, most of the newly established oceanographic institutions adopt this systen.

Judging from this situation, Japan has to have a well equipped national organization responsible for the synthetic oceanographic research. Indeed we have a lot of oceanographers in all fields of oceanography. We have many eminent specialists in fisheries. But we don't have even a single oceanographic institution involving physical, chemical, geological, and biological studies in its regime. This situation is rather astonishing for a country like Japan for which the exploration of marine research is so urgently needed.

For this reason Japanese oceanographers are requesting their government to establish a national synthetic oceanographic institution for the said purpose and to maintain the future population in this country. This movement is still going on actively and its success would depend upon the activities and efforts of Japanese oceanographers.

Very fortunately the recent UNESCO policy is largely inclined to help the

advance of oceanography in the south-eastern part of Asia in order to promote the living standards of the people in this area. For this reason a UNESCO fund was bestowed to the Standing Committee on Oceanography of the Pacific Science Association, one of UNESCO's advisory agencies, when the Eighth Pacific Science Congress was held at Manila, Philippines in November 1953. These meetings also initiated among the Pacific oceanographers an atmosphere to meet in an international oceanographic organization temporarily called the "Pacific Oceanographic Institute", though its date of materialization would be considerably ahead.

In connection with the UNESCO's policy of cultivation of arid zones for the nations suffering from the shortage of food and other resources, Japan requested the UNESCO to help Japanese people in exploring marine resources for the same reason. This proposal was approved in 1952 and the Japanese National Commission for UNESCO in Tokyo has been eager since then to help Japanese oceanographers in their basic research. By the efforts of this commission, small funds have been issued by the Japanese Government for the fiscal years 1953 and 1954. And I was fortunate enough to be appoint a chairman in operating the studies with a part of the funds issued for the fiscal year beginning on April 1, 1954.

Early in 1954 I was asked by the Japanese Commission for UNESCO to spend these funds in a most efficient way in the basic oceanographic research. After ample consideration I came to the conclusion that the oceanographic and biological studies of the Kuroshio, or the Japan Current would be most urgently needed for us. It is a mighty warm ocean current which transports about sixty five million tons of water per second from the south with its immense amount of heat and minerals. This current has a very important influence upon the everyday life of Japanese people, bestowing a mild climate to their islands. Though this is very familliar to our people like the Gulf Stream is to the United States and Europe, still this current is far less studied than is its equal in the Atlantic. So I had to make haste in organizing the group. I was fortunate to be able to secure the cooperation of almost all agencies in Japan responsible for the oceanographic observations.

The observations were mostly carried out in August 1954 by the Hydrographic Office of the Maritime Safety Agency, Tokyo, the Tokyo and other Fisheries Laborataries, Tokyo Fisheries University, Tokyo, and the Central Meteorological Observatory, Tokyo and its subordinate marine observatories.

The present volume involves the results of these Kuroshio surveys together with other research worked out by Japanese oceanographers. A part of the Kuroshio surveys is still going on in Tokyo Fisheries University during February 1955 and the results will be published on later opportunities.

Japanese oceanographers are now cooperating with the United States of America and Canada in the "NorPac" project which is an international joint oceanographic observations to be carried out in the North Pacific north of the Tropic of Cancer by the oceanographers of Japan, America and Canada. Japan is expecting to explore the area west of the international date line in August 1955 with about 15 boats.

According to the information of the Japanese delegation who attended at the UNESCO General Meeting held last November at Montevideo, Urguay, the International Union of Geodesy and Geophysics (IUGG) and the International Council of the Scientific Unions (ICSU) proposed last fall that an advisory committee on oceanography consisting of outstanding oceanographers of the world should be initiated under the sponsorship of the UNESCO and discuss the local oceanographic problems such as the establishment of an international oceanographic institute in the Indo-Pacific area, the fisheries problems now urgent off the Pacific coasts of South America etc. They further reports that UNESCO meetings of such an advisory committee may be held next fall in Tokyo together with an oceanographic symposium also sponsored by UNESCO.

I should be greatly pleased if these papers would contribute to the developement and advance of the Pacific and world's oceanography and to serve in promoting the living standards of the Pacific people.

Finally I have to express my deepest feeling of gratitude to Mr. Tadakatsu Suzuki, Secretary-General of the Japanese National Commission for UNESCO and the staff members of the organizations responsible for the oceanographic observations, who took charge in the Kuroshio surveys last August for their kind cooperation.

Records of Oceanographic Works
in Japan, Vol. 2, No. 1,
March 1955

Hydrographic Survey in the Equatorial Pacific Ocean, The South China Sea and the Formosa-Satsunan Kuroshio Region.

Makoto Ishino

(Tōkyō University of Fisheries)

This reprot is based on the observations during the period from June 21 to August 11 in 1954 by Umitaka-Maru (754 tons), the training ship of the Tōkyō University of Fisheries. Observations at forty-five stations (see Fig. 1) carried out in the Equatorial Pacific Ocean, the South China Sea and the Formosa-Satsunan Kuroshio region.

The profiles of water temperature, chlorinity, density and saturation pcrcentage of dissolved oxygen (%) are shown in Fig. 2, 3 and 4. The arrows shown in Fig. 1 represent the surface current measured by the drift of ship and the inclined direction of sounding wire, in addittion to them by the current float used.

1. Hydrographic Conditions of Equatorial Pacific Ocean

In this area two main currents (Sourth Equatorial Current and North Equator ial Current), the Equatorial Counter Current, the Kuroshio Current and other currents are shown.

Hydrographic observations at fifteen stations were taken in this region. Between St. 1 and St. 3 the waters indicated the temperature of about 20°C and high chlorinity (about 19.40‰) at the depths from 200 m to 250 m. The intermediate water at the depths from 400m to 600m shows somewhat lower chlorinity (19.00‰). Those features are the same pattern as found in the Kuroshio proper waters.

In the region from St. 4 to St. 9, the spring layer of temperature and dissolved oxygen were found, however not found the above mentioned intermediate waters. Accordingly, referring to the direction of the current, it was considered that the region lies in Equatorial Counter Current, and σ_t profile represents the considerable high speed of current.

Since north-easterly currents were observed at St. 10 and St. 12, the waters with higher chlorinity at the 150 m depth might be a thrusting block originated in South Equatorial Current, and as the result of it, it might reduce the convergent sinking at about St. 11. Thus the remarkable higher temperature of nearly 10°C even at the 600 m depth, and abundant oxygen in the deeper layer would indicate the sinking of watermass.

In the far southern region the coastal waters of lower chlorinity extend over the surface layer.

2. Hydrographic Conditions of South China Sea

Sampling and observation were taken at seventeen stations in this region. First of all, with exception of St. 24, the physical and chemical conditions repre-

Fig. 1. Stations occupied by Umitaka-Maru. June 21~Aug. 11 in 1954. Arrow···Surface Current.

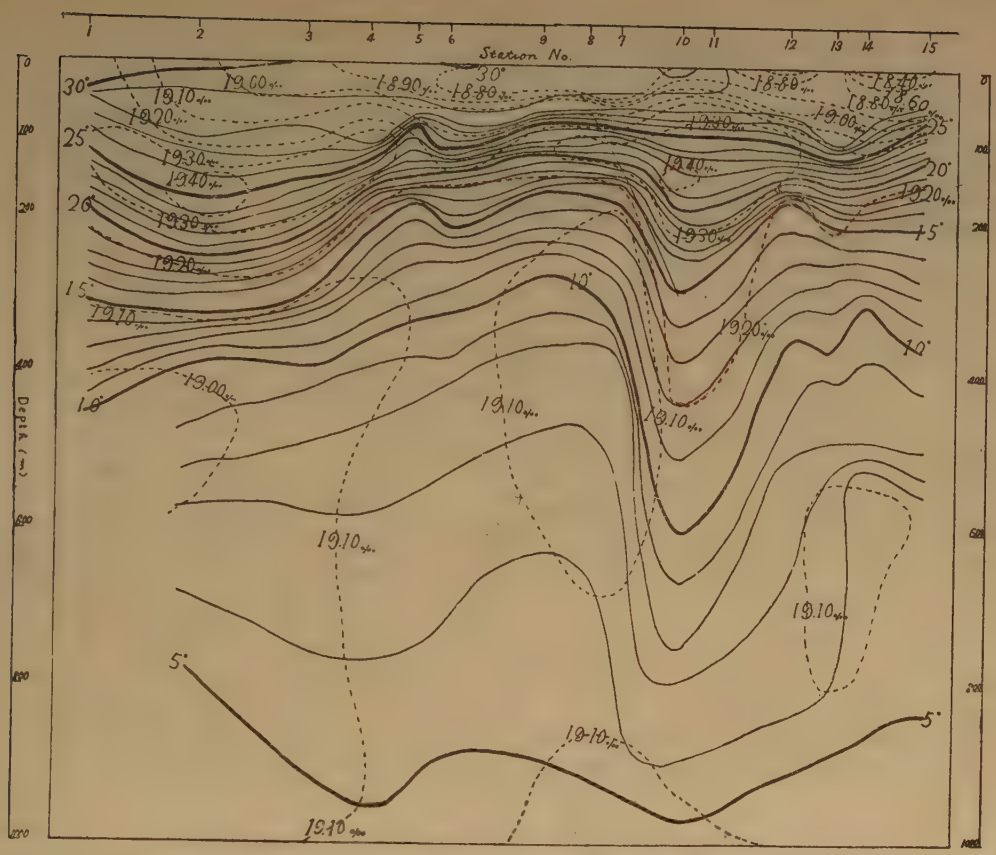

Fig. 2-A. Hydrographic section–isotherms(°C), isohalines (‰)–in the Equatorial Pacific Ocean. Real line ···Water temp. Dotted line···Cl.

sent almost homogeneous state as shown in figures (Fig. 3-A and 3-B), i.e. the water temperature about 20°C, and the chlorinity keeping 19.00‰ at the depth of about 100 m.

However, at St. 24 10°C isotherm lies at about 500 m depth, which is somewhat different from those at other stations. Inspecting in the surface currents of adjacent stations, an extensive eddy and as its consequence the downward sinking of the watermass in the upper layer can be proved. Whereas the warmer and saline waters of 200 m depth at St. 32 may represent the waters of Kuroshio system inflowed through the Bashi Channel.

3. Hydrographic Conditions of Formosa-Satsunan Kuroshio Region

Observations at thirteen stations were taken in the areas from the east off Formosa toward Kyūshū (Japan) along the Kuroshio Current. Between St. 33 and St. 41, the waters with the water temperature of 20°C-25°C and the chlorinity over 19.20‰ exist in 100m-250 m layer, corresponding to the core of Kuroshio. Everywhere the surface currents flow in the north-easterly direction. And the dissolved oxygen shows comparatively abundant in the considerable

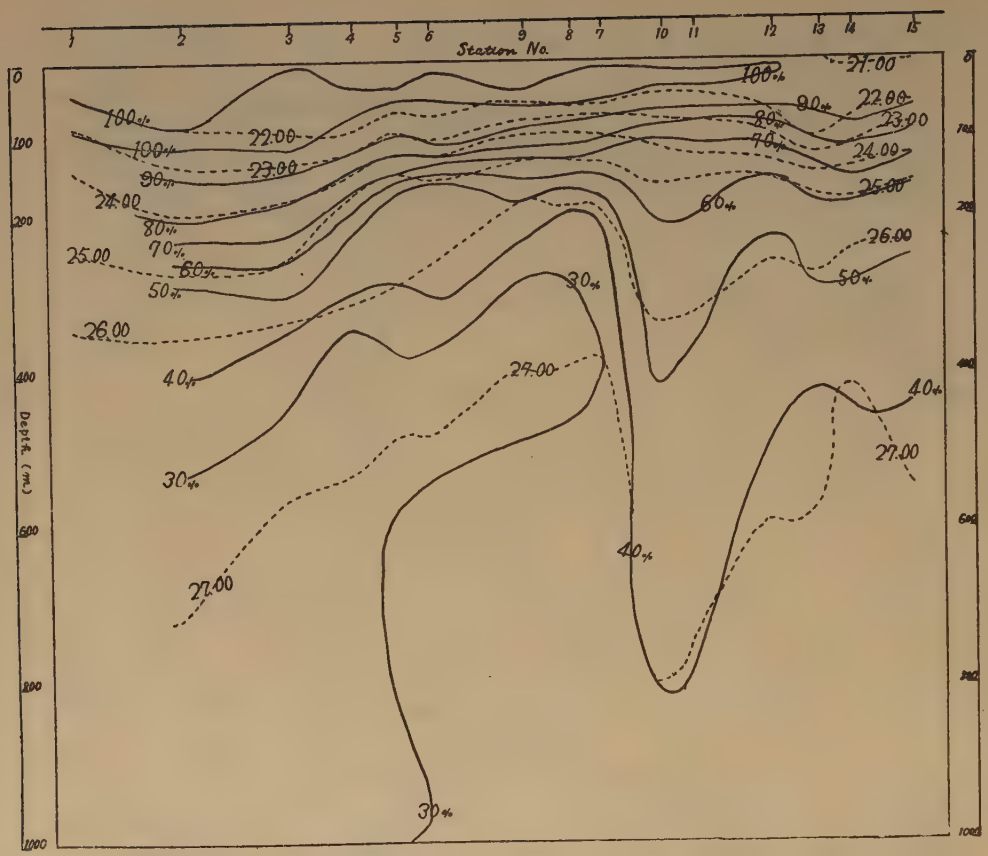

Fig. 2-B. Hydrographic section-iso-lines of O_2/O_2'(%), isophycnic lines-in the Equatorial Pacific Ocean. Real line···O_2/O_2' Dotted line···σ_t

deep layer. However, the intermediate waters are not found clearly.

On the other hand, peculiar feature is found at northerly situated St. 35, where the water of different system (coastal water originated from Eastern Sea) dominates.

In the areas adjacent to Kyūshū, the surface waters with the lower chlorinity extend over and the isothermal line of 20°C had an ascending tendency to 100m depth, and intermediate waters seems to lie in the deeper layers.

Concluding Remarks

In above, basing on the investigation during June 21 to August 11 in 1954, we have found the actual hydrographical states of several sea regions in the Western Pacific and its neighbouring.

Finally, the author wishes to express his thanks to the kindly aids of Dr. M. Uda, and to the cooperation of Mr. J. Hattori, the crews of Umitaka-Maru (Captain-Mr. M. Nagayama), and thd members of the Oceanographical Dept. of Tōkai-Regional Reseach St.

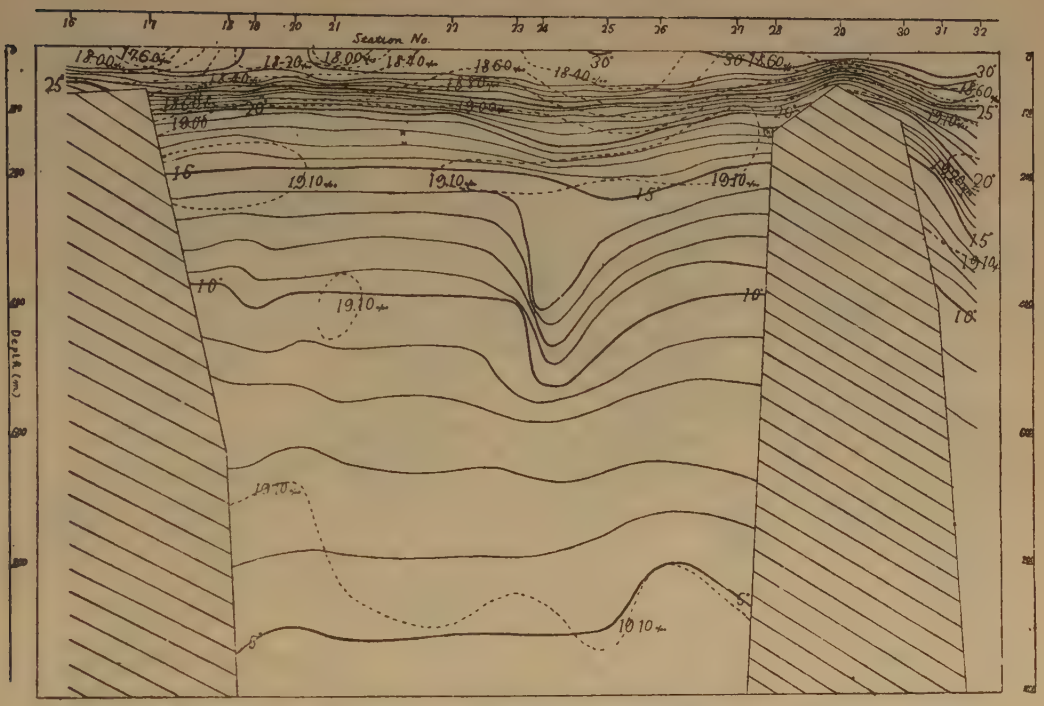

Fig. 3–A. Hydrographic section-isotherms(°C), isohalines(‰)–in the Southe China Sea. Real line···Water temp. Dotted line···Cl.

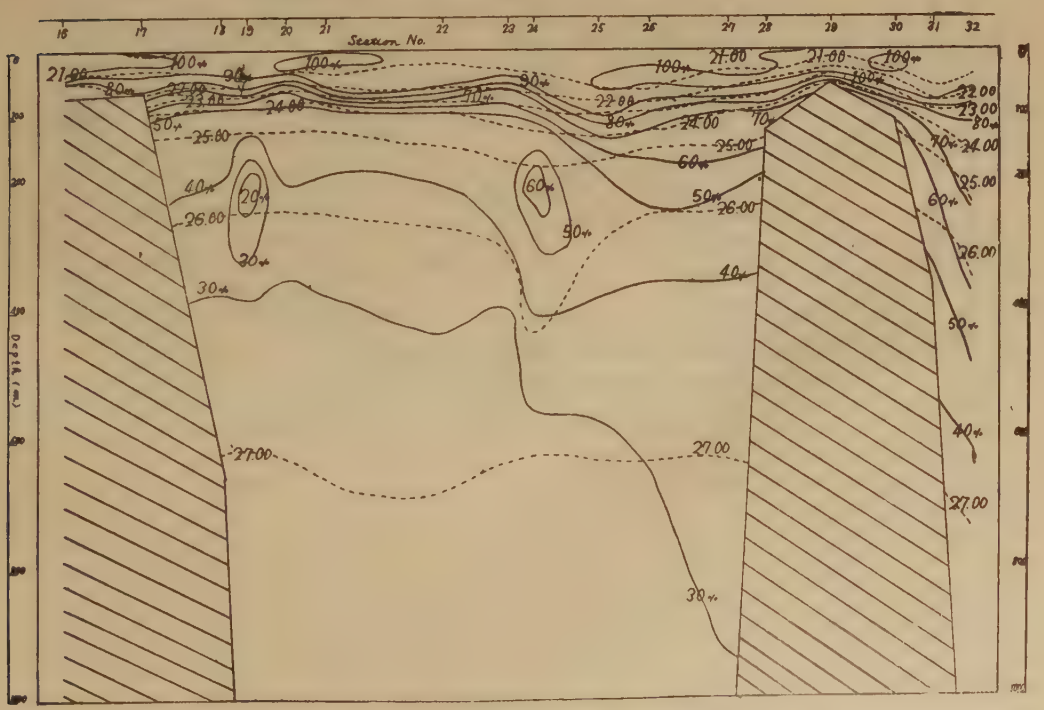

Fig. 3–B. Hydrographic section-iso-lines of $0_2/0_2'$(%), isophycnic lines-in the South China Sea. Real line—$0_2/0_2'$ Dotted line···σ_t

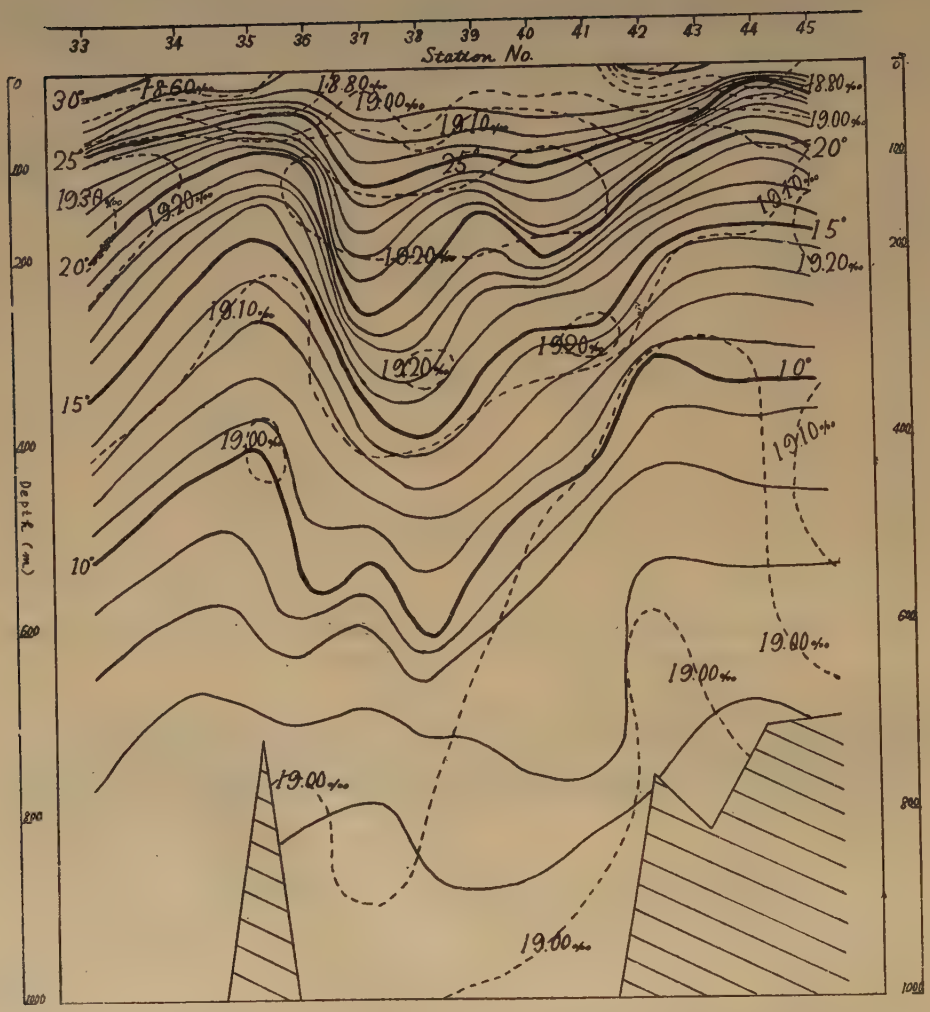

Fig. 4-A. Hydrographic section-isotherms(°C), isohalines(‰)-in the Formosa-Satsunan Kuroshio Region. Real line···Water temp. Dotted line···Cl.

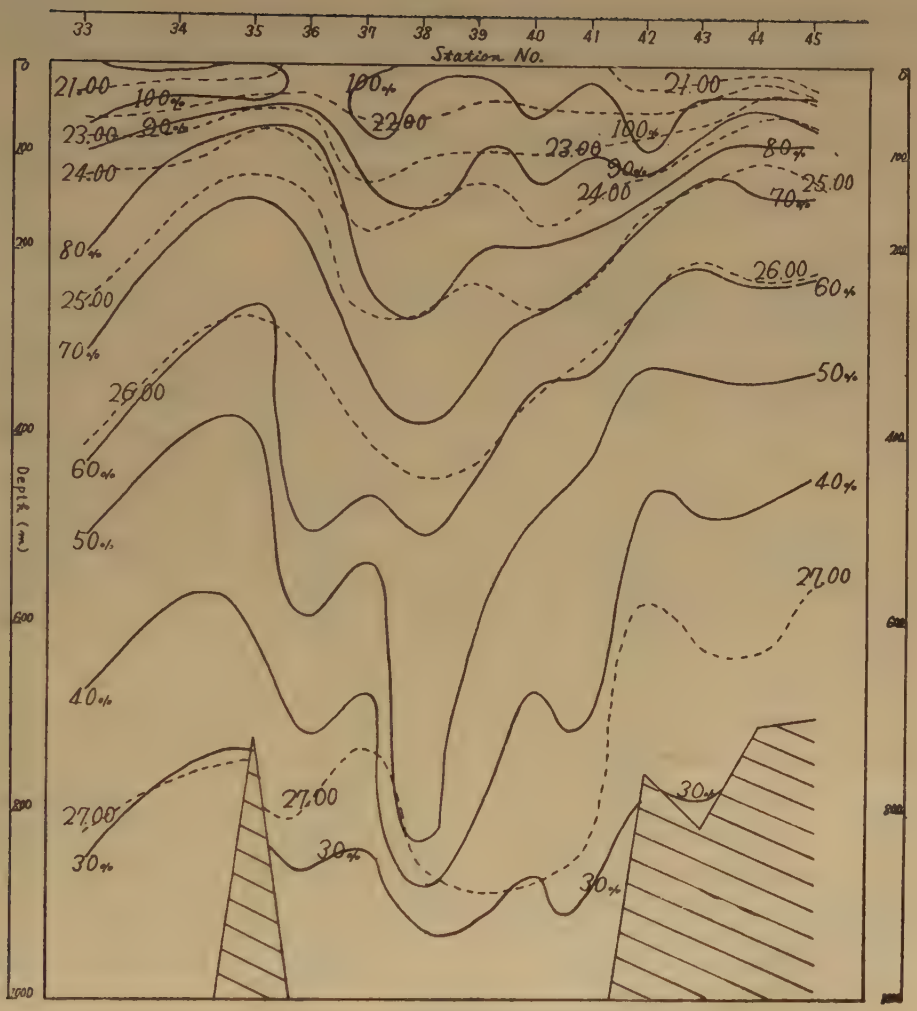

Fig. 4-B. Hydrographic section-iso-lines of $0_2/0_2'(\%)$, isophycnic lines-in the Formosa-Satsunan Kuroshio Region. Real line···$0_2/0_2'$ Dotted line···σ_t

Records of Oceanographic Works
in Japan, Vol. 2, No. 1,
March 1955

Preliminary Report on the Kuroshio in the Eastern Sea of Japan (Currents and Water Masses of the Kuroshio System III)

By Jotaro Masuzawa
(Central Meteorological Observatory, Tokyo)

§ 1 *Preface*

The oceanographic conditions in the eastern sea of Japan have been investigated in order to obtain one of the methods for prediction the weather in summer which influences upon the rice-crop in Northeast Japan and also to find good fishery grounds. The most systematic observations were carried out by the cooperation of many research-ships belonging to the Fishery Authorities in Japan from 1933 to 1941. From these observational data, general features on the Kuroshio and the Oyashio in this region has been made fairly clear by Uda (1935, 1938a, 1938b) and others. Recently Y. Saito (1952) analyzed in detail water masses in the North Pacific and interpreted their mixing in the frontal zone between the Kuroshio and the Oyashio.

After the World War II, the sectional observation along the so-called "C-line" east off Kinkazan (Lat. 38°15′N) had been carried out on board weather ships of the Central Meteorological Observatory almost twice a month from 1948 to 1953. These continuous observations show frequently rapid changes of the sectional distribution of different water masses in the shorter period and also several kinds of seasonal fluctuation of the Kuroshio and the Oyashio appeared in this section (Nannichi 1951, Fukuoka 1953, Ichiye 1953 and Masuzawa 1954).

Since 1951 the communicative meating has been held every year by the Tohokukaiku Fishery Institute, Hakodate Marine Observatory, Marine Safty Agency, the Central Meteorological Observatory and the other marine organizations for the cooperative research on the oceanographic conditions in the eastern sea of Japan.

§ 2 *The general current system of the Kuroshio in summer*

It is only in summer to be obtained oceanographic observations which were carried out by the Fishery Authorities enough extensively to see the general distribution of currents and water masses in the eastern sea of Japan. But, to our regret, these data are not so satisfactorily accurate for dynamic calculation that it is intended to see an outline of current pattern from the distribution of the depth of 10°-isotherm. The 10°-isotherm is a representative one of those showing the largest inclination across a strong current and also is regarded as

the layer dividing briefly the warm upper water from the cold intermediate water (Masuzawa 1951).

It has been often reported that the Kuroshio Current which leaves the coast of Japan at Cape Inubo-zaki (Lat. 35°40′N) flows east-or northeast-wards in projecting branching currents to the north and back currents to the south

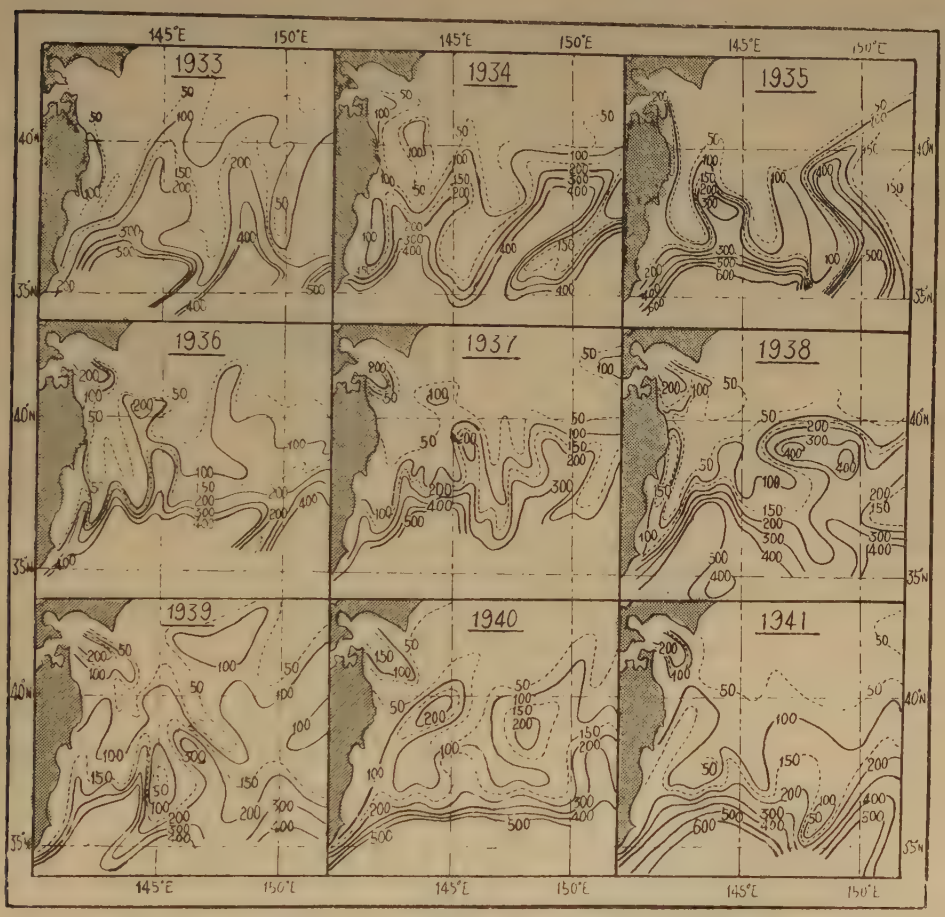

Fig. 1 Distributions of the depth (m) of 10°-isotherm in August

which become an origin of the Kuroshio Countercurrent. But as shown in Fig. 1, the Kuroshio Current in this region presents various trajectories. Namely, in 1933 ~1935 the Kuroshio Current flows in a wavy form with the larger amplitude between Lat. 35° and 40°N,but in the next three years the main stream-axis moves to the north, in 1937 to Lat. 37.5° N, and then in 1940~1941 it again moves back southwards, in 1940 the main current flowing eastward to Long. 150°E along Lat. 36°N. These meandering of main currents or loop-shaped branches stand comparison in the scale with those of the Gulf Stream (Fuglister and Worthington 1951). That is, the north-south width of the meandering sometimes

amounts to 200 or more nautical miles and there exist generally two northward projections of the Kuroshio water in the interval from the coast to the region east about 500 nautical miles off. These northward-projected warm waters are frequently cut off from the Kuroshio warm water and become anticyclonic eddies with various sizes.

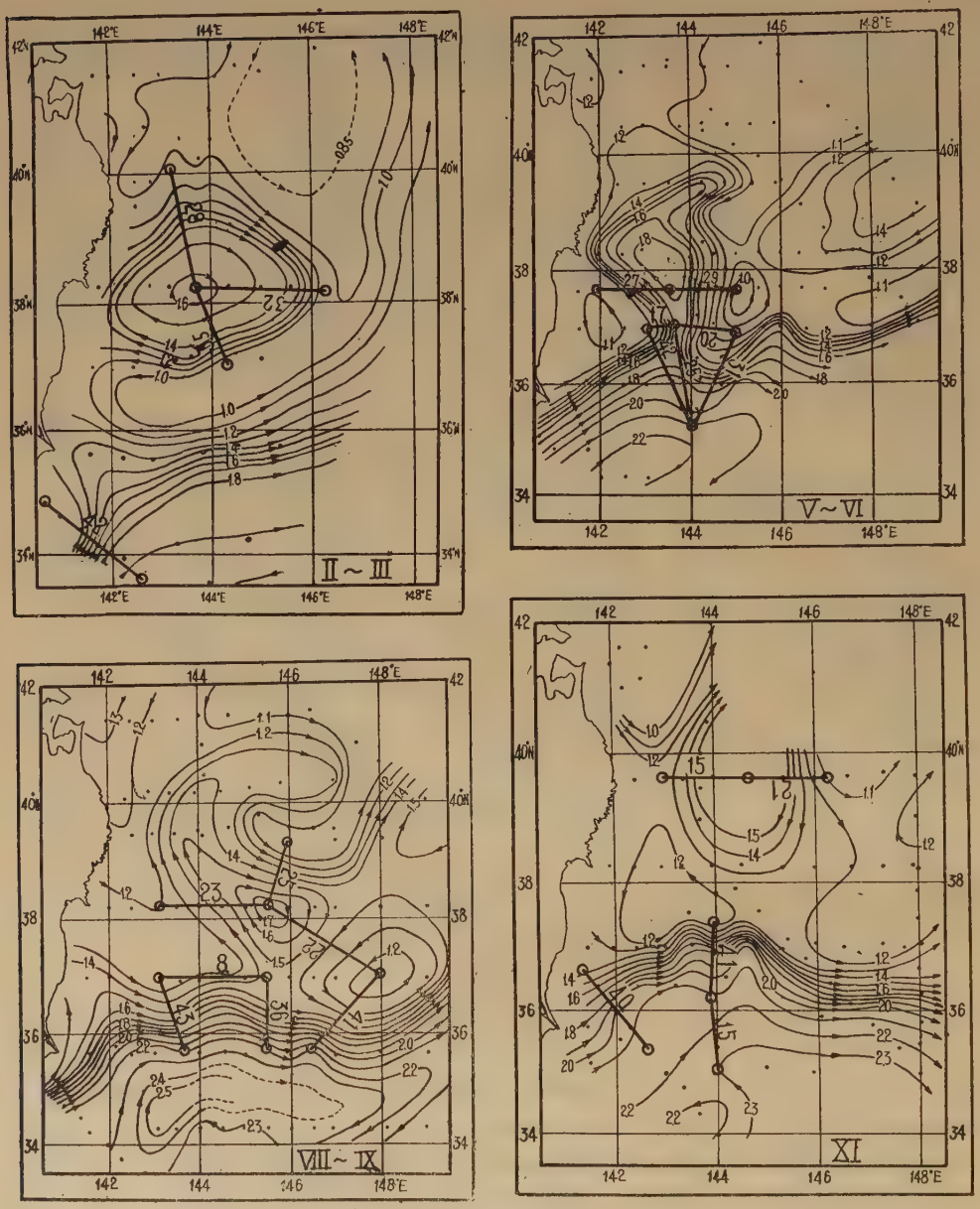

Fig. 2 Geopotential topography of the sea surface in dynamic meters referred to the 1000-decibar surface (800-decibar only in February~March) and large figures attached to thick lines show the volume transports ($10^6 \times m^3/sec$) across the sections from surface to 1000m depth

It is noteworthy in Fig. 1 that the warm water is a little thicker in the limited region to the southeast of Cape Erimo-misaki of Hokkaido owing to the inflow of the Tsushima Current through Tsugaru Strait between Hokkaido and Honshu, and also that the second northward-branch of warm water is abnormal in both 1934 and 1941 when it was cooler in summer in Northeast Japan.

§ 3 *The main stream of the Kuroshio Current away from the coast*

We do not yet have any satisfacotry knowledges on the general structures of the main stream which leaves the coast of Japan for lack of suitable cross-current observations. We could obtain for the first time a reliable example of seasonal fluctuations of the Kuroshio in this region from seasonal observations carried out in 1954 on board R.M.S. "Ryofu-maru" of the Central Meteorolgical Observatory and R. M. S. "Yushio-maru" of the Hakodate Marine Observatory.

The main stream of the Kuroshio flows almost eastwards in a meandering course and its stream-axis moves gradually northwards between Long. 143°E and 145°E from late winter to autumn. There exists a ribbon of hot water at the just south side of the stream-axis as well in the eastern sea of Japan as in the Gulf Stream and the Kuroshio Current in the southern sea of Japan (Dietrich 1937, Uda 1943) (Fig. 3). In summer the salinity-lower surface water

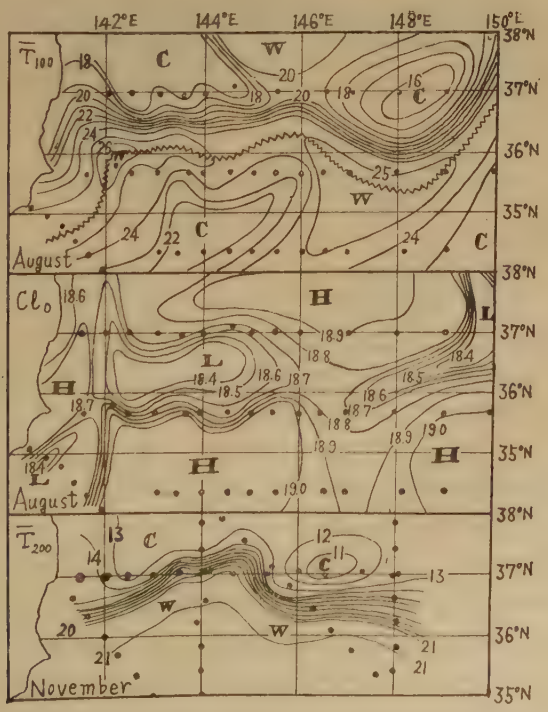

Fig. 3 Distributions of the mean temperature in the upper 100 m layer ($\overline{T}_{100}$) and the surface chlorinity (Cl_0) in August and the mean temperature in the upper 200 m layer in November ($\overline{T}_{200}$)

extends in a band along the main stream of the Kuroshio Current. As suggested already in the Kuroshio south off Cape Shiono-misaki (Masuzawa 1954), this surface water seems to originate from the fresher coastal waters in summer and to be carried by the Kuroshio without any remarkable mixing in the course of the current.

The section "Z_1" in November on which ten observational stations were occupied in the interval of about 25 nautical miles along the meridional of Long. 144°E, shows a typical cross-current structure of the Kuroshio Current east off the coast of Japan (Fig. 4). The vertical distribution of calculated velocity in

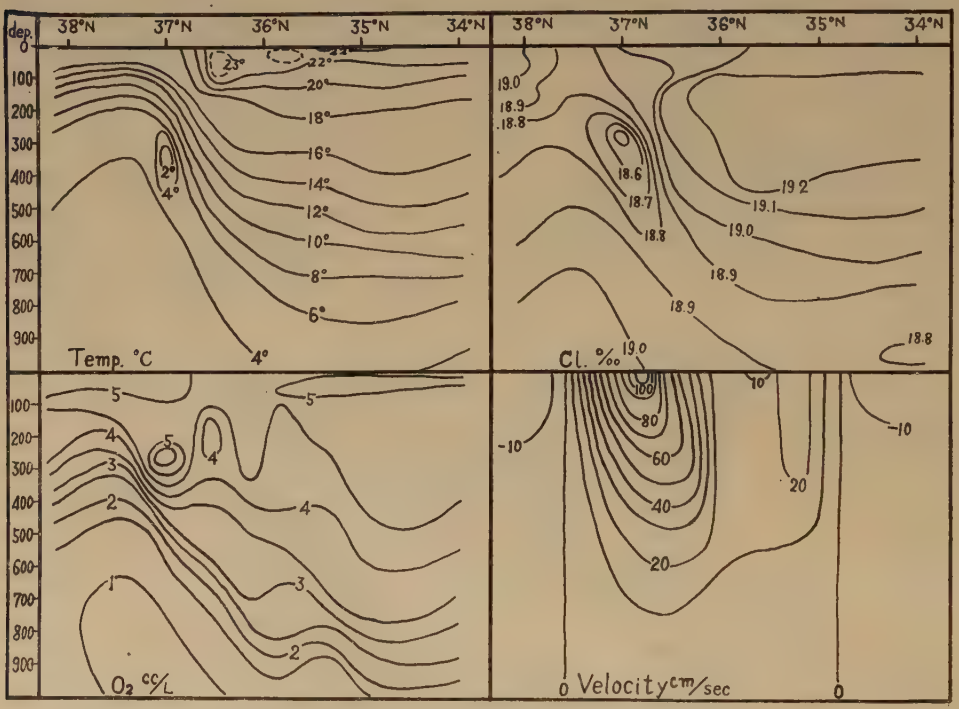

Fig. 4 Vertical distributions of the water temperature, chlorinity, dissolved oxygen and calculated velocity in the section "Z_1" along Long. 144°E

this section is such similar to those in the southern sea of Japan that the eastward stream is about 160 nautical miles wide, a half of its width showing the velocity over 20 cm/sec and its maximum velocicity amounts to 120cm/sec. The warm core reaching down to 150m depth is situated as usual immediately to the south of the stream axis of the upper layer and above the stream-axis of the deeper layer. It is typically indicated in the vertical distributions of water temperature, chlorinity and dissolved oxygen that the deeper water ascends to the upper layer at the northern margin of the eastward-stream, while the upper water reaches to the lower layer at the southern margin. Furthermore the

most characteristic in this section is that there exists in the intermediate layer of the Kuroshio Current a water mass which is cold, salinity-low and rich in dissolved oxygen. When such cold intermediate waters originated from the Oyashio water flow southward and arrive at the Kuroshio Current region, they do not continue their southward-movement in sliding down under the Kuroshio warm water, but flow generally eastward with the Kuroshio Current.

In spite of the above-mentioned change of the stream-axis, we cannot any significant differences in the volume transport of the stronger current, which amounts to about forty million cubic meters per second all the year round in

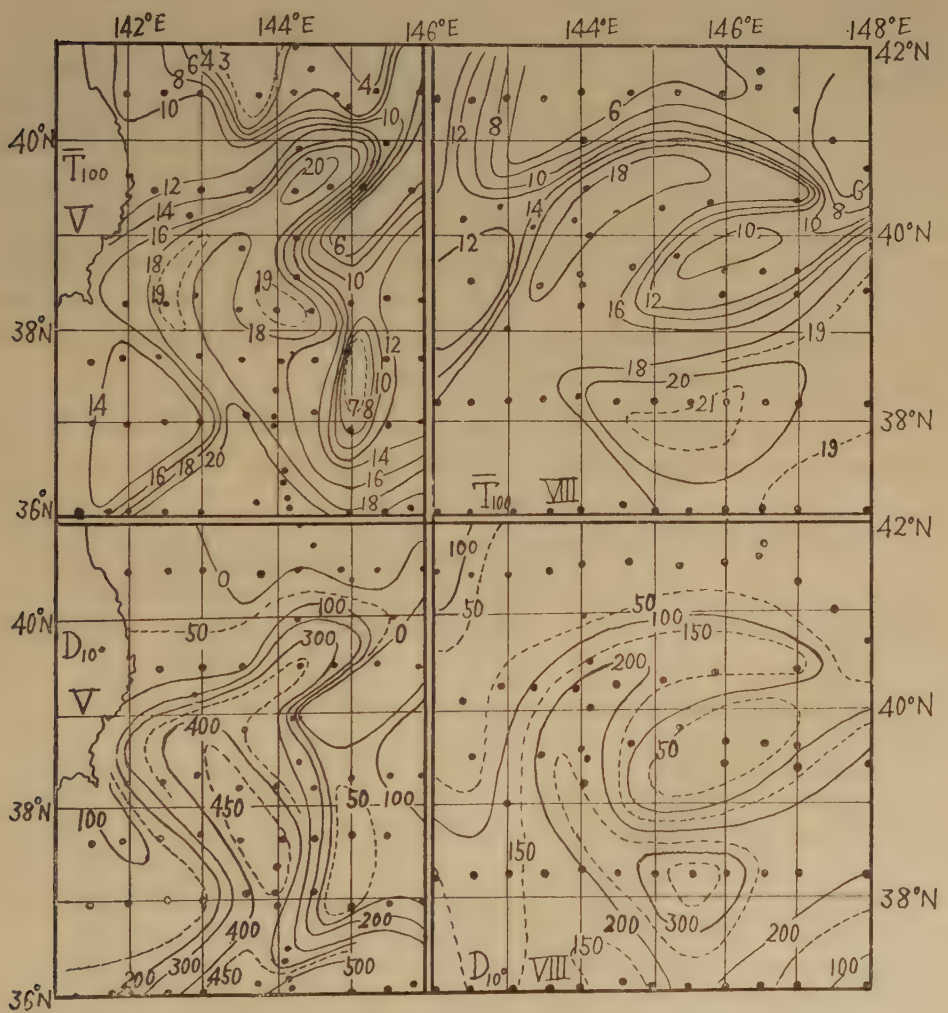

Fig. 5 The mean temperature and thickness of a warm water mass in spring (left) and summer (right)
upper : mean temperature in the upper 100 m layer
lower : depth (m) of 10°-isotherm

the layer from surface to 1000m depth (Fig. 2). The total eastward-transport is equal to $53\times10^6m^3$/sec in the section southeast off Katsuura in summer and $55\times10^6m^3$/sec in the section along 144°E in autumn. These values are comparable to the mean values ($37.9\times10^6m^3$/sec and $48.3\times10^6m^3$/sec respectively) calculated for the Kuroshio south off Cape Shiono-misaki. But this fact does not at once mean tht there exist no significant exchange of water mass between the Kuroshio and its surroundings in the course along the south coast of Japan.

§ 4 *The branching current of the Kuroshio and a warm eddy*

As often pointed out already, a northward-current branches out from the main stream of the Kuroshio away from the coast of Japan between Long. 143° and 145°E, at Lat. 37°N. While there may perhaps no remarkable branch-currents in late winter, in spring the strong branching current turns to the northwest from the position, Lat. 37°N, Long. 143°.5 E and its branching trasport ($17\times10^6m^3$/sec) amounts to about forty percents of the total trasport ($42\times10^6m^3$/sec). In summer this branching current becomes weaker, that is, its volume transport ($8\times10^6m^3$/sec) does not reach to about twenty percents of that total. This branchcurrent flows round anticyclonically and generally joins in the main stream but a part of it turns to the northeast on the way of the anticyclonic course. The boundary zone on which these branchcurrents come in contact with the Oyashio water may be the "Subarctic convergence" pointed by Uda (1935) or the "Oyashio front" called by Kawai (1953).

There exists a remarkable warm water mass in the region enclosed by the above-mentioned branching current. This anticyclonic warm eddy is inclined to

	Feb.~Mar.	May~June	Aug.~Sep.	Nov.
position of its center	38°N 143.5°E	38°N 143.5°E	38°N 145.5°E	39.5°N 144.5°E
max depth at T=10°(m)	520	460	360	400
max depth at Cl=19‰(m)	540	470	300	350
max thickness over Cl=19.15‰(m)	370	380	140	50
max chlorinity (‰)	19.22~.25	19.19~.26	19.10~.20	19.05~.18
max mean temp. in the upper 200 m layer (°C)	16.2	18.1	18.7	15.4
volume transport ($\times10^1m^3$/sec)	28~35	27~29	22~25	15~21

Table 1 Seasonal variations of characteristic properties of a warm water mass

become weaker in the period from winter to autumn, that is, both the volume transport and the thickness of the warm water mass decrease with lowering of the maximum chlorinity (Table 1). As the anticyclonic eddy is communicated closely to the main stream of the Kuroshio in May～June, this warm water mass rather shows such fine structures similar to the those of the main stream that the warmest band in the upper layer streches along the immediately left side of the branching current. In summer, it is expanding eastwards or northwards in decreasing the thickness of the upper warm layer without any remarkable supply of warm water from the main stream.

But the pattern of this anticyclonic eddy in summer is considerably similar to one in spring and this eddy moves eastwards in the rate of 25～35 nautical miles per month in this period. And then the center of this eddy moves to the northeast by about 100 nautical miles in the period from the begining of September to the end of November. These mean moving speeds of the stream-axis are comparable to the value obtained in the Kuroshio south off Shiono-misaki (Masuzawa 1954) but, of course, though they do not give the actual speed in the shorter period (Fuglister and Worshington 1951), its changing speed more than ten nautical miles a day may not continue uniformly during several weaks.

Aknowledgement

The auther wishes to express his hearty thanks to Dr. K. Hidaka, Dr. M. Nakano and Dr. Y. Fujii for there kind advice and encouragement and also to Messrs M. Yasui, T. Nakai and T. Tsuchida for their asistance.

References

Dietrich, G. (1937) : Über Bewegung und Herkunft des Golfstromwassers. *Veroff. Inst. Meereskunde Univ. Be lin* N. F. Reihe A **33**.

Fuglister, F. C and L. V. Worthington (1951) : Some results of a multiple survey of the Gulf Stream. *Tellus* **3** (1).

Fukuoka, J and T. Tsuiki (1953) : On the variation of the oceanographic condition of the sea near the Fixed Point "Extra„. *Records Ocean. Works in Japan* N. S. **1** (1).

I chiye, T (1953) : On the variation of oceanic circulation (IV). *Ocean. Mag.* **5** (1).

Kawai, H. (1953) : On the relation between the bad rice-crop in Northeast Japan and the fluctuation of the ocean polar front in the northeastern sea of Japan (*not printed*).

Masuzawa, J. (1951) : On the intermediate water in the northeastern sea of Japan (First paper). *Ocean. Rep. C. M. O.* **2** (1) (in Japanese).

Masuzawa, J. (1954) : On the Kuroshio south off Shiono-misaki of Japan. *Ocean. Mag.* **6** (1).

Masuzawa, J. (1954) : On the Kuroshio east off Kinkazan of Japan. *Ocean. Rep. C. M. O.* **3** (4) (in Japanese).

Nannichi, T. (1951) : On the fluctuation of the Kuroshio and the Oyashio. *Pap. Met. Geophy.* **2** (1).

Saito, Y. (1952) : On th Oyashio Current (Part 1). *Jour. Inst. Polytechnics, Osaka City Univ.* **3** (2)

Uda, M. (1935) : The results of simultaneous oceanographical investigations in the North Pacific Ocean adjacent to Japan made in August, 1933. *Jour. Imp. Fish. Exp. St.* No. **6** (in Japanese).

Uda, M. (1938a) : Hydrographical fluctuation in the north-eastern sea-region adjacent to Japan of the North Pacific Ocean. *Jour. Imp. Fish. Exp. St.* No **9** (in Japanese).

Uda, M. (1938b) : Researches on "Shiome" or Current Rip in the seas and oceans. *Geophy. Mag.* **11** (4).

Uda, M. (1943) : On the structure of the boundary zone of different water masses. *Jour. Ocean. Soc. Japan* **2** (4) (in Japanese).

Records of Oceanographic Works
in Japan, Vol. 2, No. 1,
March 1955

On the Subtropical Convergence and the Currents in the Northwestern Pacific

Michitaka Uda

(The Tokyo University of Fisheries)

It is already known that the Subtropical Convergence is located in the middle latitudes in which the density in the upper layers increases rapidly towards the poles and is noted by the sinking of the heavy water along it.[1] However, hitherto the details of its characteristic feature and position in the Northwestern Pacific are not exactly investigated.

Fig. 2. Kuroshio Counter Current
(Drift Bottle Expt)

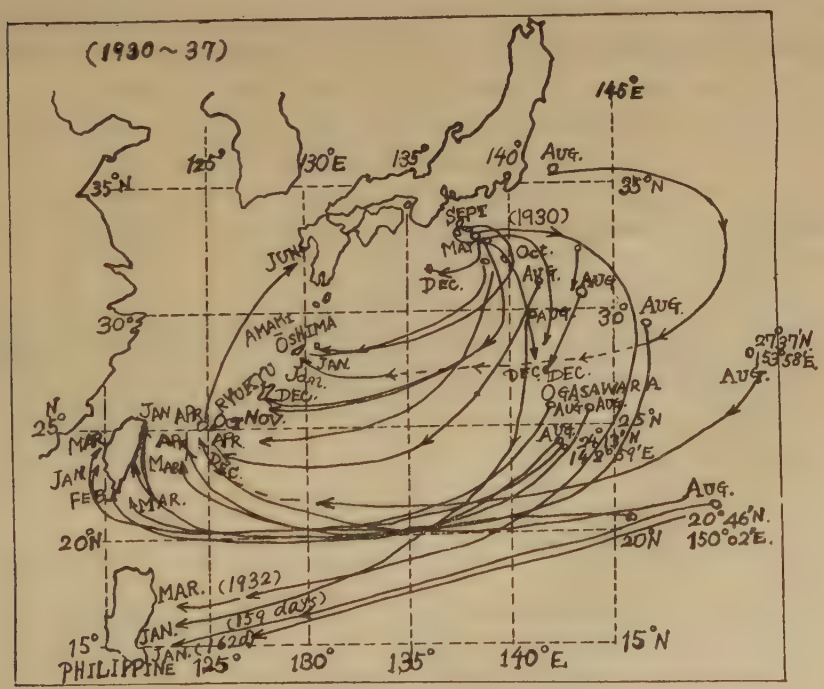

Now, by means of the current-bottle experiments[2] we can show roughly the pattern of the Kuroshio Counter Current (see Fig. 1), which flows in the SW-WSW direction with the average velocity of 15 sea-miles per day i. e. about 0.6 knot (drifting from Aug. thrown in southern Kuroshio waters off Idu Islands to Jan. picked up at Yaeyama- and Miyako Islands south of Ryūkyū).

The adrift of bottles on the coast of those Southwestern Islands is almost limited in the period of winter monsoon from Nov. to April and May (see Table 1).

Table 1. Recovery of Curret Bottles. (Data from the Semiannual Reports of Oceanographical Investigation 1930~37).

Thrown in		Picked Up	Jan.	Feb.	Mar.	Apr.	May.	Jun.	Jul.	Aug.	Sept.	Oct.	Nov.	Dec.
off Iwate	May.	Ogasawa-	2	–	–	–	–	–	–	–	–	–	1	6
〃 Ibaragi	July.	ra	–	–	–	–	–	–	–	1	–	–	–	–
〃 Chiba	Aug.	Kyushu	10	5	5	9	9	4	5	5	3	3	8	5
〃 Tokyo	Sept.	Okinawa	–	–	1	–	–	–	–	–	–	1	–	1
〃 Kana-gawa	Oct.	S. China	1	–	–	–	–	–	–	–	–	–	–	–
〃 Siduoka	Nov.	Philippi-nes	–	–	–	–	–	–	–	–	–	–	–	2
〃 Mie		setc.												
Sum			13	5	6	9	9	4	5	6	3	4	9	14

Table 2. Transparency of Sea Water (D in meter, Secchi's Disc) and the Color of the Sea (F in Forel's Scale).
(Data obtained from Hydr. Bulletin etc. 1935~52.) in the NW-Pacific.
(130°~160°E. 5°S~35°N)

130°–160°E	Amp.	Jan.	Feb.	Mar.	Apr.	May.	Jun.	Jul.	Aug.	Sept.	Oct.	Nov.	Dec.	Mean.	Range
	Max–Min.	m	m	m	m	m	m	m	m	m	m	m	m		
N 35°	D	12.8	19.9	12.8	20.6	14.0	16.2	7	22	7.6	12.8	13	11.5	–	–
	(F)	(1.2)	(1.3)	(1.4)	(1.5)	(1.7)	(1.1)	(1.1)	(1.1)	(1.3)	(0.8)	(1.7)	(1.3)	–	–
30°	D	22.3	20.8	21.3	18.0	22.6	20	32	29.5	32.1	27.0	22	24	24.3	14.1
	(F)	(2.6)	(3.0)	(2.7)	(3.0)	(2.7)	(2.5)	(2.5)	(1.8)	(2)	(2.3)	(3.2)	(2.6)	(2.6)	(1.4)
25°	D	24.7	25.6	20.5	23.3	31.5	29	38.5	39	30.7	29.0	31.3	31	29.5	18.5
	(F)	(2.8)	(2.8)	(2.9)	(2.6)	(2.2)	(2)	(2.6)	(1.4)	(1.4)	(2.2)	(2)	(2.3)	(2.3)	(1.5)
20°	D	34.7	38.0	30.0	30.7	33.8	34.2	32	31.6	32.8	31.9	21	30.8	32.5	17
	(F)	(2.2)	(2.2)	(2.0)	(1.8)	(1.7)	(1.8)	(2.7)	(1.5)	(1.6)	(2.0)	(2)	(1.3)	(1.9)	(1.4)
15°	D	31.4	40.7	33.3	34.6	34.8	37.3	33	35.3	35.2	29.3	30.1	26.6	33.5	13.4
	(F)	(1.8)	(1.7)	(1.8)	(1.8)	(1.7)	(2)	(2.4)	(2)	(1.6)	(1.5)	(1.8)	(2)	(1.9)	(0.9)
10°	D	35.1	36.0	30.3	32.1	32.3	33.7	39	40.8	31.6	39.8	28	30.2	34.1	12.8
	(F)	(1.6)	(1.8)	(1.7)	(1.8)	(1)	(1.9)	(2.1)	(1.7)	(1.5)	(1.6)	(1.5)	(2)	(1.7)	(0.6)
5°	D	27.3	30.8	30.8	38.6	36.1	35.2	34.3	47	38.3	31.1	34	34.5	34.8	19.7
	(F)	(2.2)	(1.8)	(1.5)	(1.5)	(1.9)	(1.4)	(1.6)	(2)	(1.6)	(1.6)	(2)	(2)	(1.8)	(0.8)
0°	D	29.3	29.8	32.0	31.3	36.6	36.2	32.4	25	33.4	32.5	31.5	35.5	32.1	11.6
	(F)	(1.8)	(2.3)	(2.0)	(2.3)	(2.6)	(1.9)	(1.9)	(2.5)	(2.7)	(2.1)	(1.5)	(2)	(2.1)	(1.1)
5°S	D	–	–	–	–	28.0	33.3	36.2	30	–	–	–	–	31.9	–
	(F)	–	–	–	–	(3.2)	(2)	(2)	(2.5)	–	–	–	–	(2.4)	–
Mean (0°~30°N)	D	29.3	31.7	28.6	29.8	32.5	32.2	34.5	35.5	33.5	31.5	28.3	30.4	31.5	–
	(F)	(2.1)	(2.2)	(2.1)	(2.1)	(2.0)	(1.9)	(2.3)	(1.8)	(1.8)	(1.9)	(2.0)	(2.0)	(2.0)	–

Accordingly the Kuroshio Counter Current in the waters south of Kuroshio appears to flow southerly more strongly as the winter monsoon becomes stronger.

The distribution of the transparency of sea water and the color of the sea in the NW-Pacific are shown in Table 2, which indicates a sharp boundary at about 25°N. latitude in the season from Jan. to April. The relatively cold water (more turbid and of low salinity) of Kuroshio Counter Current meets to the warm Central Pacific water (more transparent and saline) in the North Pacific Ocean locating at the northern border of the North Equatorial Current near the Subtropical Convergence.

Several eddies are formed on the undulated line of the Subtropical Convergence. A conspicuous cyclonic eddy in the waters adjacent to Ogasawara Islands (see Fig. 2 a-f) is observed in winter and spring (from Feb. to May), corresponding to the well-known whaling grounds (nearly in the rectangle of 26°-27° N. 143°-144°E).[3] The eddy constituted by the narrow band of the southward intrusion of the cold current from N-NNE direction along the longitudes of 143°-144°E. and its sharp contact to the warm current on both sides of it may be related to the bottom configuration around Ogasawara Islands and Iwōzima. Contrary to the southgoing cold current developing on the Japan Trench the northgoing warm current develops along the west off Ogasawara (on the left hand side)

Fig. 2. Distribution of Water Temp., Warm (W) and Cold (C) Curr.
Surface Isotherms ×·····Whaling Ground.

a. Early March. 1948 b. Middle Mar. 1948 c. Late March. 1948

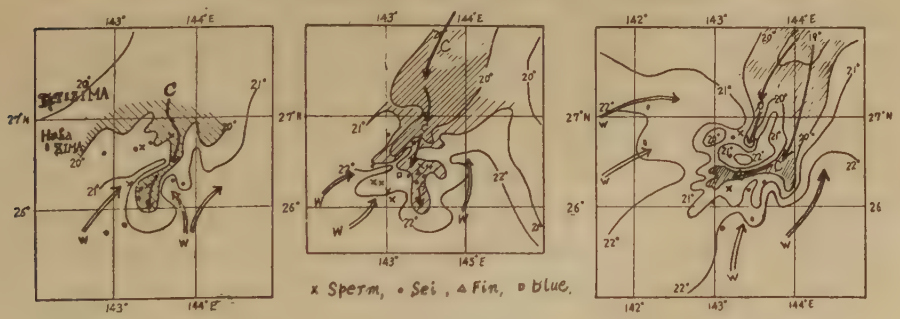

d. Middle March. 1951 e. Late March. 1951 f. Early April. 1951

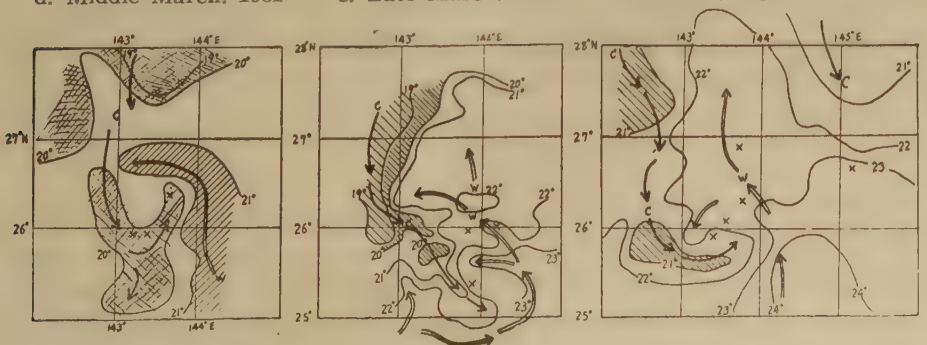

and along the transversal ridge east off Iwōzima (on the right hand side). (See Fig. 3).

Fig. 3. Warm and cold currents related to the Topographical Conditions.

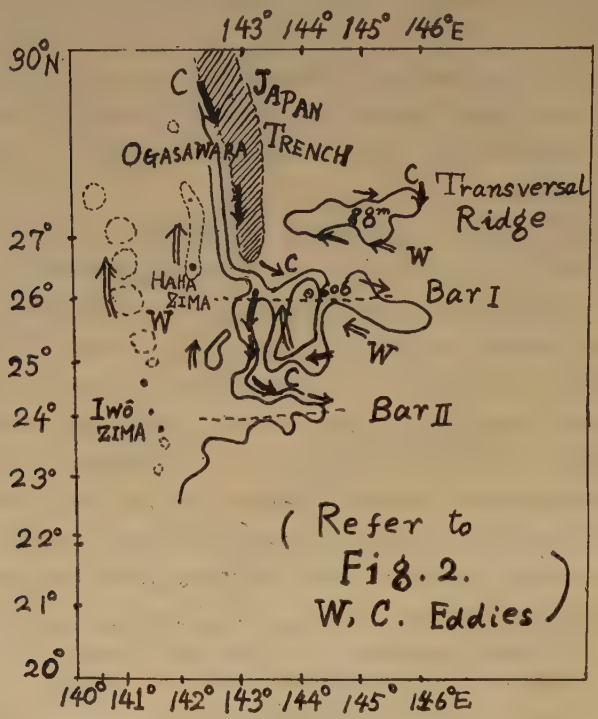

As a rule, in the northern hemisphere generally (except the topographical counter currents) we can find the tendency of the currents around an island or a ridge flowing in the clockwise direction and the currents around a trough or a basin flowing in counter-clockwise direction, since because the deflecting force due to earth's rotation deflect the direction of the current always to right hand in the northern hemi-sphere. We can easily see those examples. i. e. for the former case around Ryūkyū, Japan, Kurile, Aleutian Islands etc. and for the latter case the currents in the Japan Sea, Okhotsk Sea, Bering Sea and Pacific Ocean. The so-called "Ogasawara Current", being the northward flowing branch (west off Ogasawara Islands) of the North Equatorial Current near the Subtropical Convergence seems to develop in spring temporarily in accompany with the decay of the winter monsoon and accordingly of the Kuroshio Counter Current.

Basing on the data in the Hydrographical Bulletins of the Japanese Hydrographic Department[4] and the Semiannual Reports of the Japanese Fisheries Experimental Station[5] the distribution of the water temperature and salinity at the depth of 50 m. in winter, spring and summer (in the year 1939) and

Fig. 4. Water Temp. at 50m. Depth in Winter

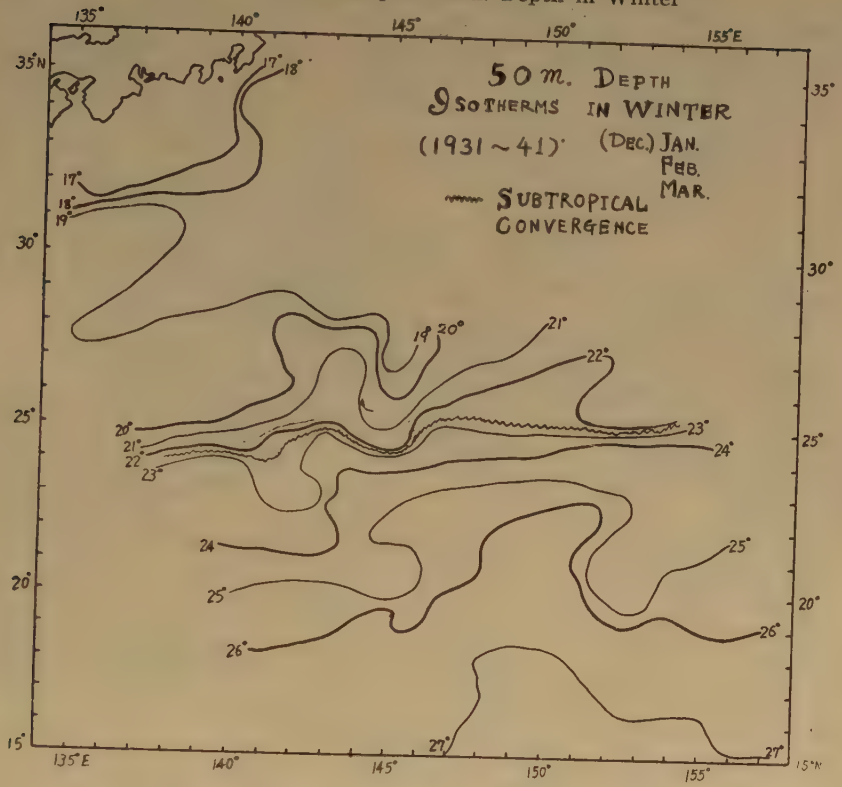

Fig. 5. Water Temp. at 50 m Depth in spring.

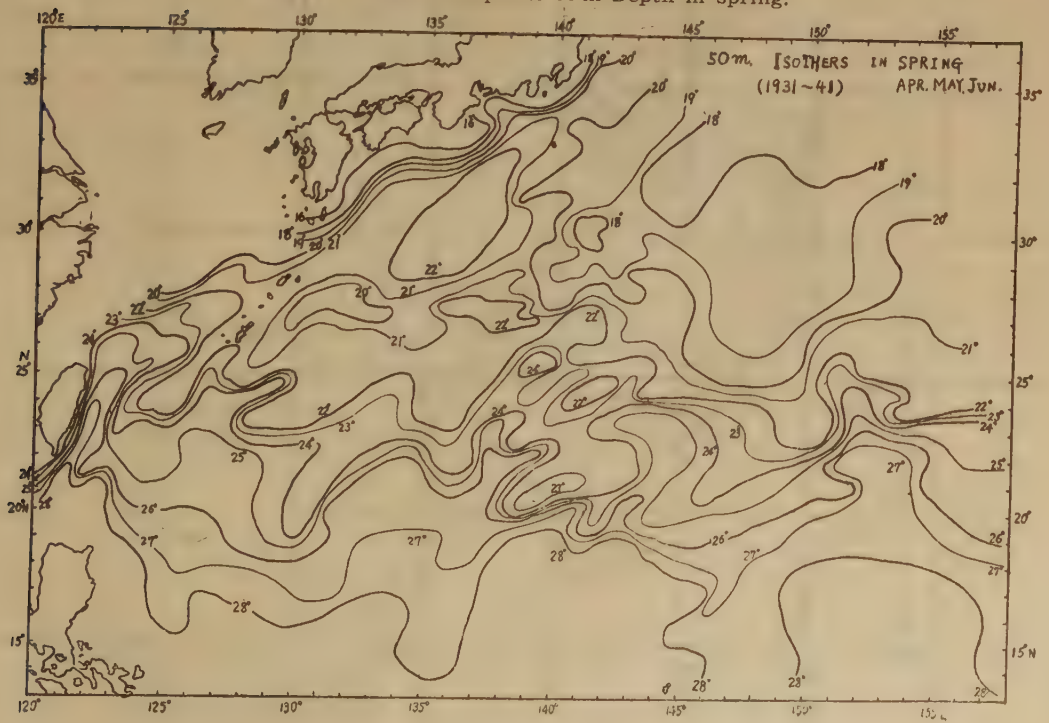

Fig. 6 a. Salinity at 50 m. Depth in Summer (1939).

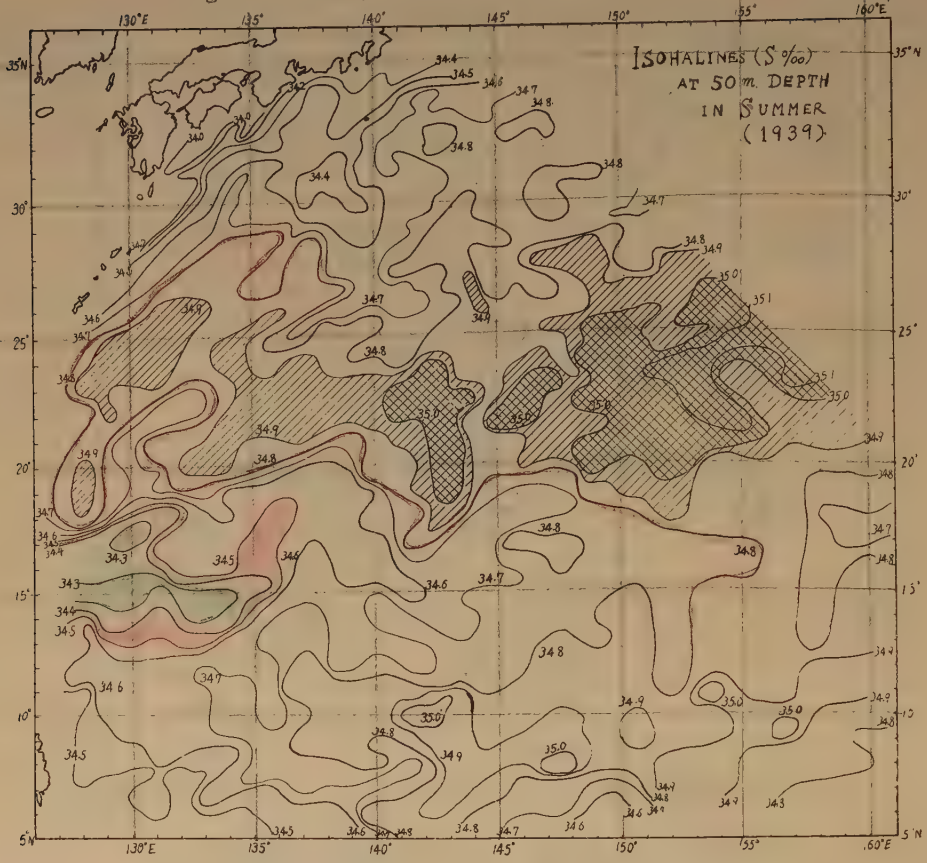

Fig. 6 b. Water Temp. at 50m. Depth in Summer (1939).

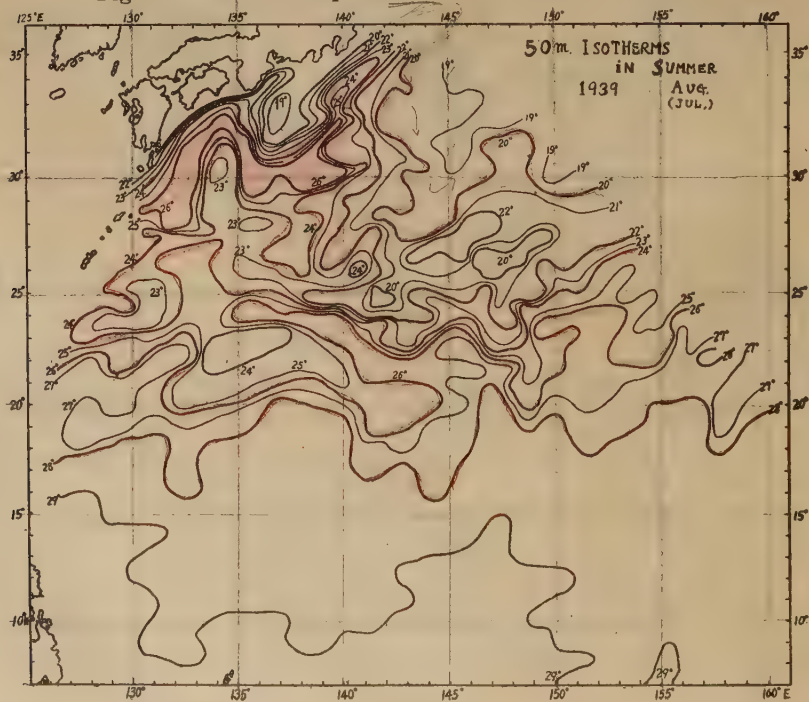

Fig. 7. Chart of Dynamic Isobaths showing the Current Fields at the Surface (Summer, 1939).

Fig. 8. The Location of the Suptropical Conv. in the NW-Pacific.

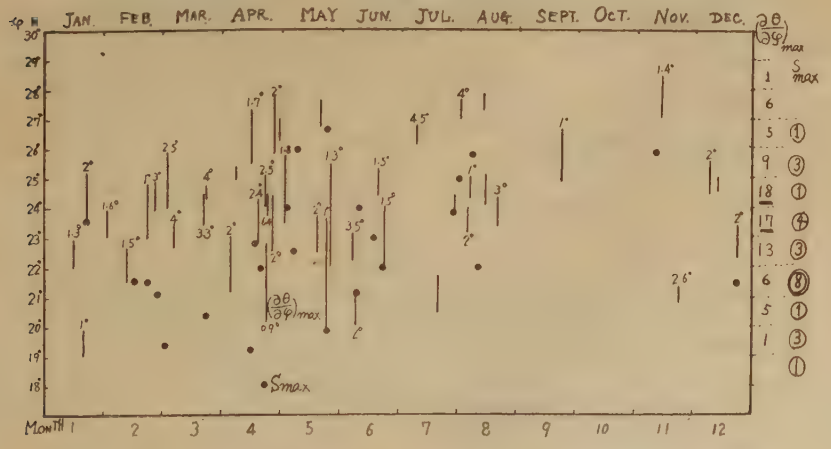

dynamic depths are shown in Fig. 4, 5, 6, a, b and 7. Isotherms of 20°-26°C are crowded near the line of Subtropical Convergence and in somewhat undulated form in latitudes of 20°-27°N.

Statistics on the hydrographic profiles show that the average position of the line of Subtropical Convergence is about in latitudes of 23°-25°N. (see Fig. 8) and the meridional temperature gradients near the line of Convergence are in the range of 1°-4°C per 1° latitude (60 seamiles) or 0.1°-0.7°C per 10 seamiles. The line of the Subtropical Convergence moves seasonally, i. e. from autumn to winter translating to south, and coming to north from spring to summer (the northern extremum in the surface layer above the 25m. depth about at 28°N. and in the subsurface layer below the 50 m. depth about the same position as in winter. The pattern of the Subtropical Convergence is most pronounced in winter throughout the year and comparatively obscure in summer.

The axis of salinity maximum (above 35‰) which is the core of the North Pacific Central Water mass (centred at about 24°-26°N. 165°-180°E.) lies very near to the line of Subtropical Convergence but generally locating a little south of it. (See Fig. 6b, 8).

The sinking of the heavy water masses (oblique descent) near the line of Subtropical Convergence may be perhaps due to the increase of density in winter by the active evaporation on the sea surface. Thus the sunken water mass in winter at the depths of 50-200 m., spreading to south constitutes the core waters of the North Equatorial Current and of Kuroshio as its extension. (Fig. 9)

Fig. 9. Temp. and Salinity Section (SSE off C. Nozima)

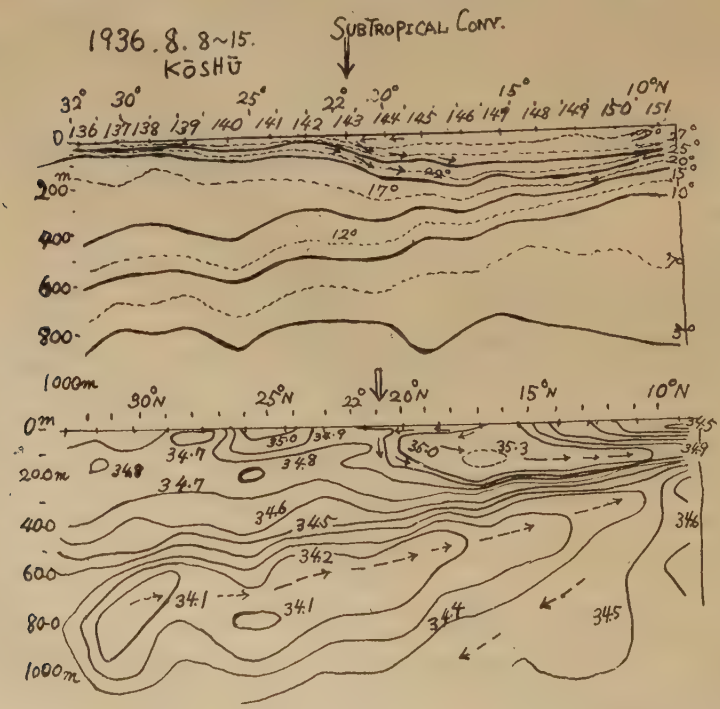

Fig. 10 a. Isopycnals (σ_t-Profile).

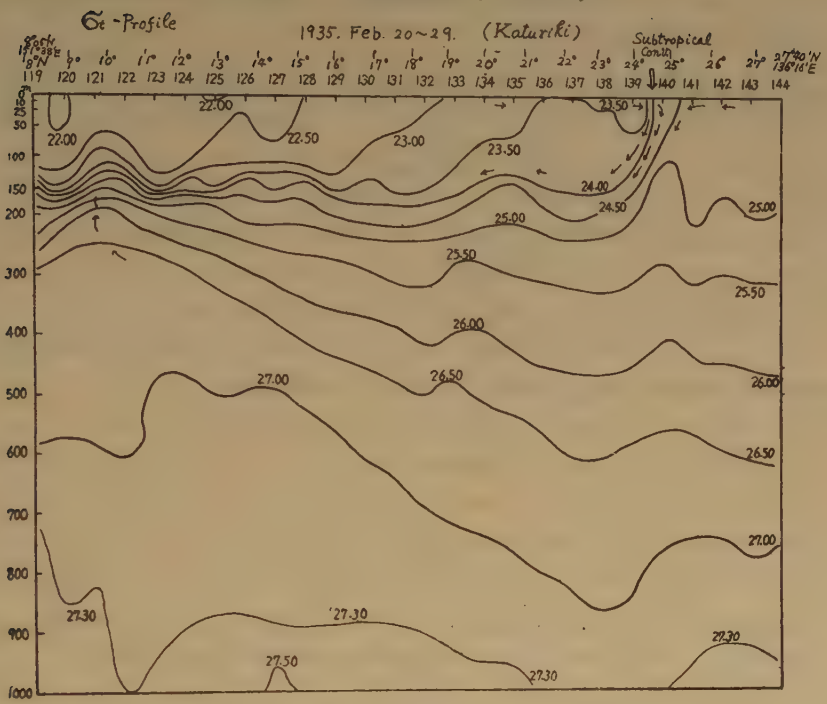

Fig. 10b. Isopycnals (σ_t).

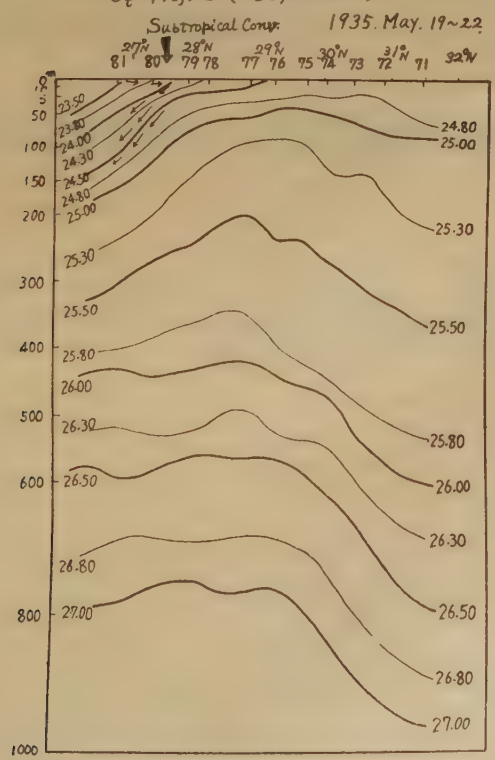

The isopycnal profiles (Fig. 10) indicate the meridional discontinuity of σ_t on the Subtropical Convergence.

In conclusion, we have studied of the nature and its associated characteristics (eddies etc.) of the Subtropical Convergence, showing its discontinuous distribution of water temperature, salinity, turbidity and currents (particularly in winter and spring) in the North Pacific Ocean which is important as an border line of the marine biological environment and also as the southernmost fishing grounds of whales[3], albacore[6] and yellowfin tuna[7] etc. Further in future we should study its yearly and secular variation. Also it is required the direct measurements of the actual state of current fields by means of GEK and current-meters etc. in the vicinity around the Subtropical Convergence.

Literatures

1) H. U. Sverdrup et al : The Oceans. 1948.
2) M. Uda : Rep. of Hydrography in the Pacific. (1933, 34~37). J. Imp. Fish. Expt. St. No. 6. 9. 1935, 38.
3) M. Uda : Studies of the Relation betw. the Whaling Grounds and the Hydrographical Conditions. (I). The Sc. Rep. the Whales Res. Inst. No. 9. 1954.
4) Hydrographic Bulletins. No. 8. 9. 13. (1935~41). 1951, 52, 54. Japanese Hydr. Dept.
5) Semiannual Reports of Oceanogr. Investigations. Imp. Fish. Expt. St. 1935~41.
6) M. Uda, E. Tokunaga : Bull. Sc. Fish. Japan. 5. 5. 1937.
7) M. Uda: On the Rel. betw. the Var. of the Imp. Fish. Cond. and the Oceanogr. Cond. in the adj. Waters of Japan I. J. Tokyo Univ. of Fisheries. Vol. 38. No.3 pp. 384–386. 1952.

Records of Oceanograghic Works
in Japan, Vol. 2, No. 1,
March 1955

A Note on Forecasting Ocean Waves Caused by Typhoons

By

Sanae Unoki and Masito Nakano
(Meteorological Research Institute)

§ 1. Introduction

The ocean waves which give the greatest damage to Japan are those caused by typhoons, and any quantitative discussion has scarcely been made hitherto on this problem. This seems to be due to the fact that there has been no precise wave observation hitherto and that it is difficult to apply the new theories of wave forecasting to these waves, owing to the fact that the typhoons move very rapidly and the variation of the direction and speed of wind in typhoon area is violent. Indeed the theory of ocean wave forecast has made a remarkable progress recently, but these theories rest on many assumptions, and in practising wave forecast, much empirical knowledge is required. In the present paper, a consideration is made concerning what kind of ocean waves is generated by typhoons and how about the method of forecasting of these waves, taking the case of waves at Hachijo Island (Fig. 3) as an example.

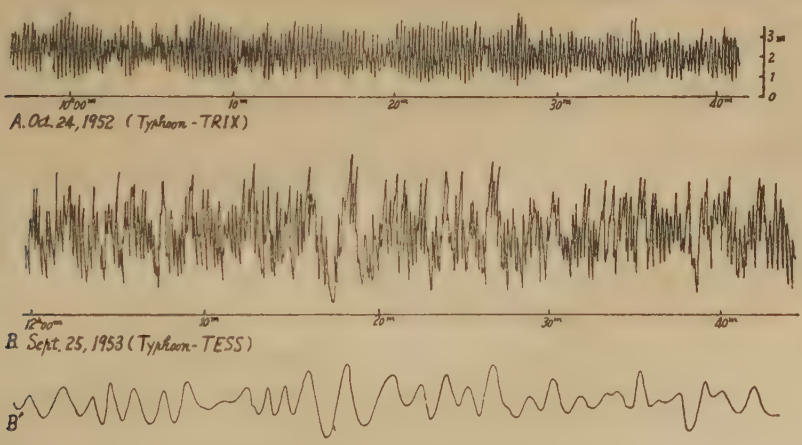

Fig. 1. Two examples of wave records in the case of typhoons. B′shows a peculiar long wave obtaied by smoothing record B.

The case may be conveniently divided into two cases as follows : Namely, (1) the case where a typhoon moves westward far to the south of Japan and passes through Formosa and the Philippines (Fig. 3), and (2) the case where a

typhoon comes up north and then leaves eastward describing a parabolic path approximately (Fig. 6). Indeed waves are, of course, higher in the latter case, but in the former case, too, conspicuous swells surge upon the Pacific coast of Japan and frequently give considerable damages. Moreover, the forerunner of swells which comes out from typhoon area has been known by Japanese people as "doyōnami", and has been utilized in weather forecast as a warning of the coming typhoon. Besides, an example of wave records and that of variation of waves for respective cases are shown in Figs. 1 and 2, respectively.

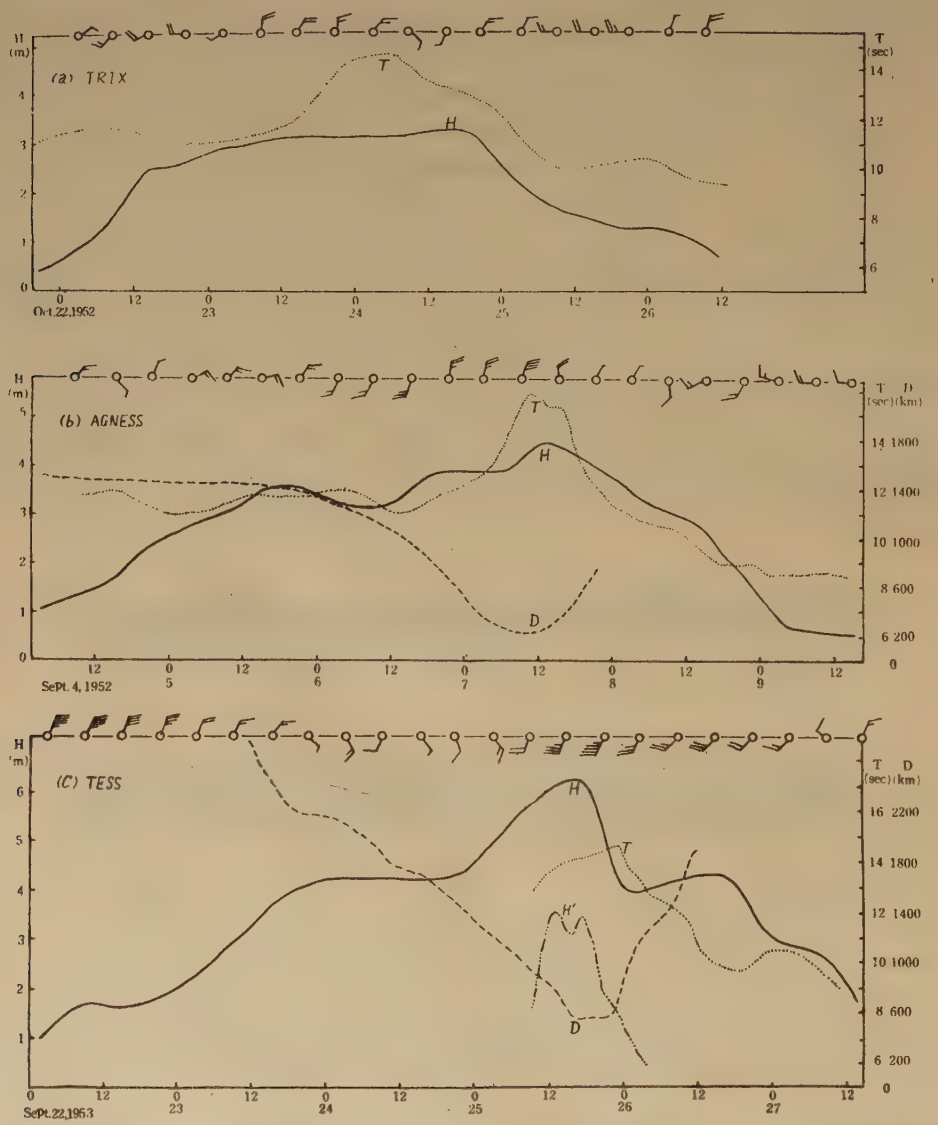

Fig. 2. Some examples of variation with time of wave-height and wave-period. The full line, H, represents the variation with time of wave-height, and the dotted line, T, that of wave-period ; the broken line, D, represents the distance from Hachijo Island to the center of typhoon.

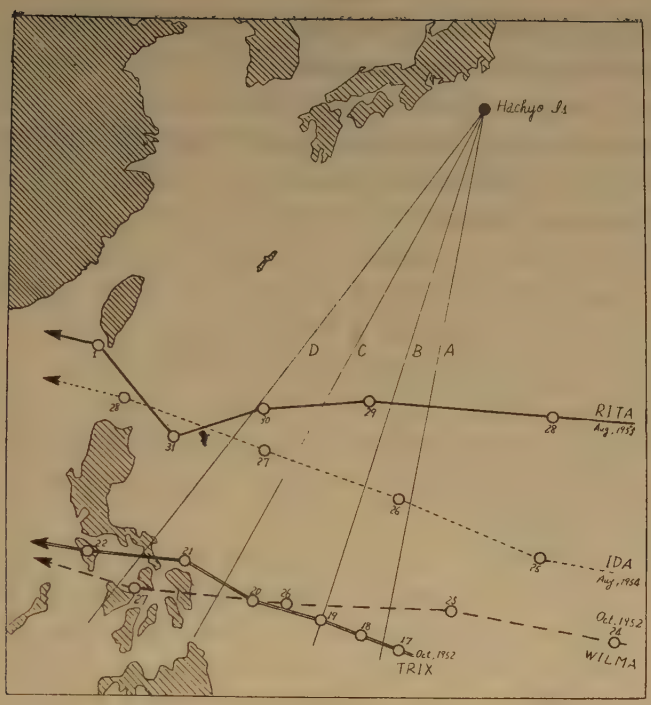

Fig. 3. The tracks of four typhoons which moved westward. Small white circles represent the position of the center of each typhoon at 09h of the date shown by the numeral beside it.

§ 2. The case where a typhoon moves westward far to the south of Japan

Four typhoons were investigated as examples belonging to this case. Fig. 3 shows their paths and Table 1 their elements, from which we can see the following facts :

(1) It is remarked that high waves with wave-height of 3~4m are occurring,

Table 1

Name of typhoon Date	TRIX Oct. 1952	WILMA Oct. 1952	RITA Aug. 1953	IDA Aug. 1954
Lowest central pressure (mb)	960	930	940	895
Distance of nearest approach (km)	2700	2600	1500	2000
Average speed of typhoon (km/hr)	14	35	29	31
Maximum wave-height (m)	3.3	2.5	2.8	4.2
Maximum wave-period (sec)	14.6	13.5	–	–
Duration of higher waves with wave-height over 2m (day)	2.5	2.0	2.5<	6<
Calculated wave-height (m)	3.0	1.5	2.4	3.4
Calculated wave-period (sec)	15.5	14.5	12.0	14.0
Travel time (hr)	78	84	55	64

though typhoons are apart as far as 2000~3000 km.

(2) Also the wave-period is as large as 13~15 sec, and is far larger in comparison with that of the waves caused by cyclones.

(3) The more intense the typhoon is (for example, the case of Typhoon IDA) and the nearer it approaches to the station (compare the Typhoons WILMA and RITA), the waves are naturally higher.

(4) In the case where a typhoon travels slowly, waves tend to become high. For instance, in the the case of Thphoon TRIX, the waves are very high, though the lowest central pressure is 960 mb and is fairy higher in comparison with other typhoons. This is due to the fact that the duration of wind in this case is vey long, as is made clear by drawing the "wind data diagram". According to T. Ōtani (1940), the height of swell seems to be different for different typhoons, even if the intensity of the typhoon is equal, and this may be explained by the above consideration.

(5) Duration of higher waves is very long, considering their wave-height. This may be a matter of course, if we consider the paths of these typhoons. Accordingly, in this case wave-height curve is rather flat, showing no conspicuous peak, as seen in Fig. 2 (A), which represents the wave-height curve for the case of Typhoon TRIX.

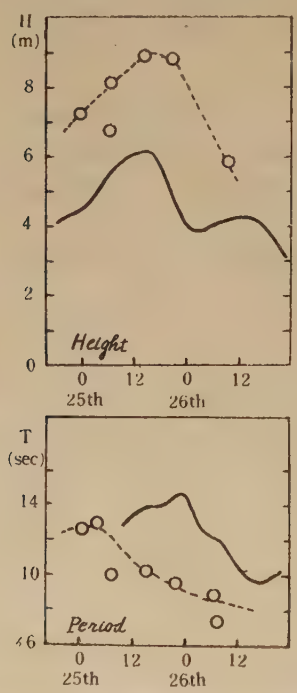

Fig. 4. The comparison between observed (full lines) and forecast values (broken lines) of wave-height and wave-period. (The case of Typhoon TESS)

Method of wave forecasting.

In the case of typhoons, the direction and speed of wind usually change violently from time to time as well as from place to place, and so it is very difficult to determine mean wind velocity, fetch and duration accurately from mere weather charts and compute waves, and accordingly the result is not good. For instance, Fig. 4 shows an example of the results of wave forecasting by means of Sverdrup-Munk's method, and from this figure it is seen that the calculated values are decidedly larger for the wave-height and decidedly smaller for the wave-period, in comparison with the observed ones. Hence the present authors constructed "wind data diagrams" (Darbyshire, 1952), and then applied Sverdrup-Munk's method of wave forecasting. In the following this method of treatment will be briefly described for the case of Thphoon TRIX.

Several straight lines were drawn radially at suitable intervals from the forecasting point (Hachijo Island), as shown by the straight lines A, B, C, D in Fig. 3, and radial component of wind velocity was computed for each point on each of these straight lines using successive weather charts, where the sign of the component was taken as positive or negative according as it is directed toward or away from the forecasting point. Thus, the "wind data diagram" as shown by Fig. 5 (upper) (diagram for C-line) is obtained for each straight line. From

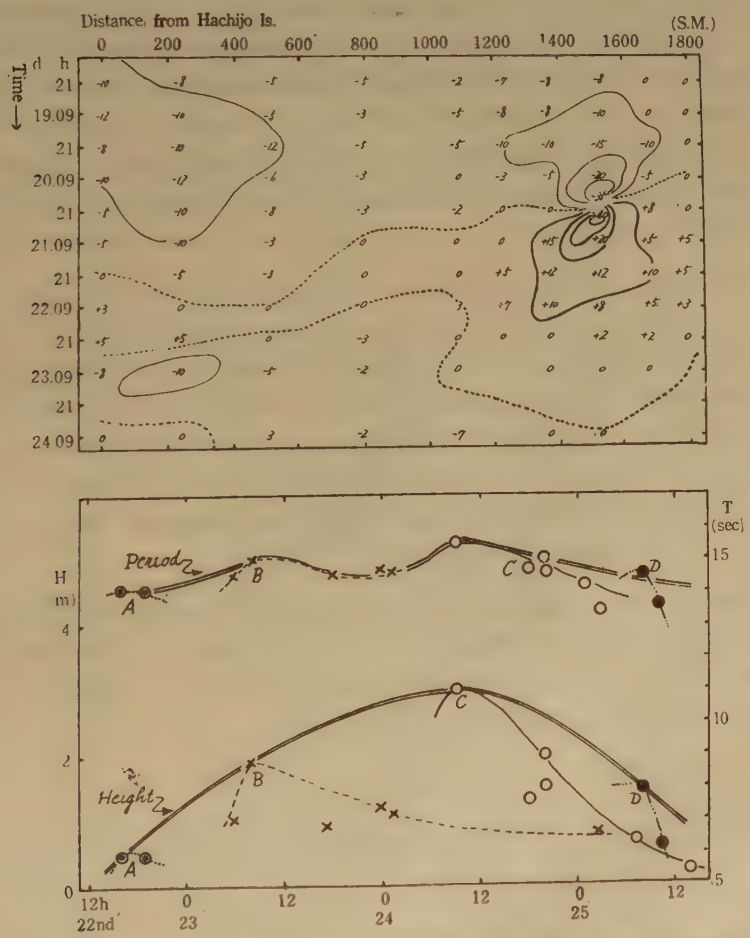

Fig. 5. The upper figure shows the wind data diagram for C-line in Fig. 3; the numerals denote the radial component of wind velocity in m/s. The lower figure shows the forecast values of wave-height and wave-period.

these diagrams the elements of wind can be determined with less arbitrariness. The waves generated along these straight lines and come to the forecasting point were calculated by Sverdrup-Munk's method, the result of which is shown in Fig. 5 (lower).

The height- and period- curves indicated by A, B, C, D are due to winds along straight lines A, B, C, D, respectively. The envelopes of these curves may be regarded as representing the theoretical height- and period-curves of the waves due to the typhoon in question, and if we compare these theoretical curves with actual ones shown in Fig. 2 (A), we can recognize the following facts ; namely, as regards the wave-height the theoretical and actual values agree in substance with each other in their absolute magnitude as well as their tendency of variation. And such is the case with the wave-period, except the parts with lower wave-height where the effect of local wind waves is large. For other typhoons likewise, the maximum values of the calculated wave-height and wave-period are given in Table 1, and if we compare these theoretical values with observed ones, it is seen that although the former is somewhat smaller than the latter for wave-height and contrary for wave-period, yet the two are in satisfactory agreement for practical purposes, provided that the "refraction effect" is taken into account.

Besides,Sverdrup-Munk's method has, indeed, its drawbacks, viewed in the light of wave spectrum etc., but since the result of calculation agrees with observation in such a degree as mentioned above, and its operation is also simple in comparison with other methods, it may be said to be a very effective method. Moreover, it is here added that recently K. Kajiura (Kajiura et al, 1954) have applied the method of wave forecasting by Pierson, Neumann and James (Pierson et al, 1953) to a typhoon, using wind data diagrams, and have obtained a result which is in good accord with observations.

§ 3. The case where a typhoon comes up north and then leaves eastward.

Nine typhoons as shown in Table 2 were investigated as examples belonging to this case. Fig. 6 shows the paths of these typhoos, and Fig. 7 an example of weather charts for the case of Typhoon TESS.

Tabie 2

Name of typhoon	POLLY	ROSE	AGNESS	CARMEN	DELLA	TESS	VIOLA	ALICE	GRACE
Date	Oct. 1952	Oct. 1952	Nov. 1952	Nov. 1952	Nov. 1952	Sept. 1953	Oct. 1953	Oct. 1953	Aug. 1954
Lowest central pressure (mb)	975	985	920	962	998	900	967	915	940
Distance of nearest approach (km)	−230	−350	−200	−470	+100	+300	−700	−600	+350
Maximum wave-height (m)	(3.5)	2.0	4.5	2.4	(2.5)	6.1	2.4	3.9	5.8
Maximum wave-period (sec)	15.0<	10.7	15.8	12.0	–	14.6	–	16.7	–
t_2 (day)	–	0.1	4.0	0.6	0.9	4.5	0.3	4.8	7.3
t_3 (day)	(1.5)	0.0	3.0	0.0	0.0	3.6	0.0	1.3	7.0

t_D-t_B (day)	–	–	3.3	1.3	1.5	3.7	1.3	1.5	7.4
t_H-t_D (hr)	+5~13	−9	+3	+2	+2	−1	+0~22	+1	−12
t_T-t_D (hr)	–	+12	+1	+7	–	+5	–	+6~10	–
t_C-t_D (day)	2.3	0.2	1.9	1.5	1.4	2.1	1.9	–	(1.0)

(Note)

t_B : Time when the waves began to grow.

t_C : Time when the waves have disappeared.

t_D : Time when the typhoon approaches nearest to the station.

t_H : Time when the maximum wave-height appeared.

t_T : Time when the maximum wave-period appeared.

t_2 : Duration of higher waves with wave-height over 2m.

t_3 : Duration of higher waves with wave-height over 3 m.

The + or − sign of the "distance of the nearest approach" of a typhoon corresponds to the case where a typhoon passes on the northern or southern side of Hachijo Island, respectively.

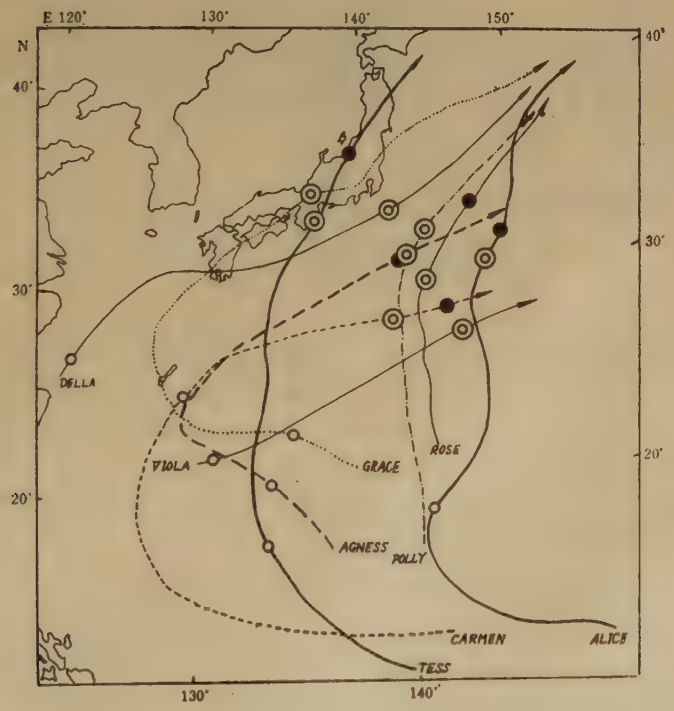

Fig. 6. The tracks of typhoons which come up north and then leave eastward.

(1) Beginning of growth of waves.

In Fig. 6, the points marked with ○ on the paths of the typhoons show the position of the centre of each typhoon at the time when waves begin to grow

at Hachijo Island, and from this figure we can recognize an interesting fact that waves begin to grow at Hachijo Island when a typhoon approaches within a certain distance (about 1500 km), almost regardless of the intensity and the path of the typhoon.

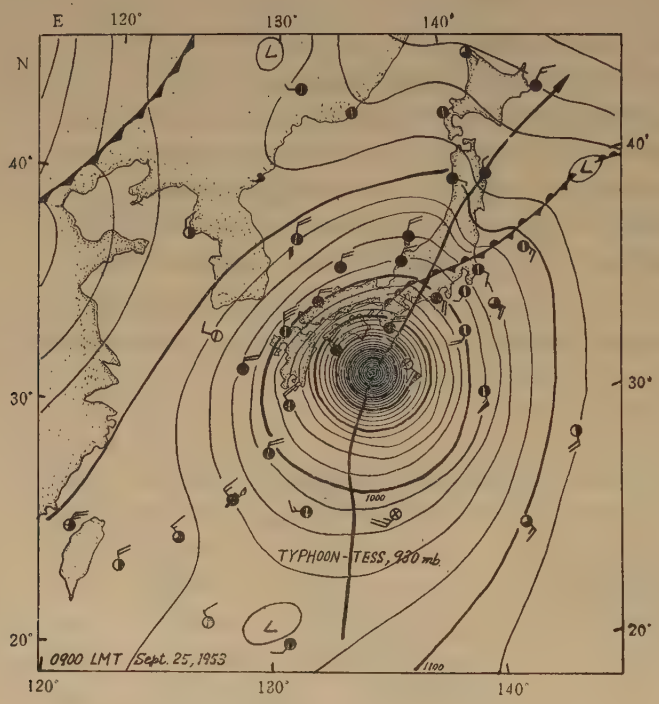

Fig. 7. An example of weather maps.

Referring to Table 2, the value of $t_D - t_B$ (the time interval from the time when waves begin to grow at Hachijo Island to the time when the typhoon approaches nearest to the station) changes from about 1 day to 7 days. This time interval is mainly affected by the speed and the path of the typhoon ; namely, it is generally large when the path of the typhoon fetches a large compass to the west of Hachijo Island.

(2) The maximum of wave-height.

In Fig. 6, the points marked with ◎ on the paths of the typhoons show the position of the centre of each typhoon at the time when the wave-height at Hachijo Island becomes maximum, and it is seen that the maximum wave-height occurs toward the time when the typhoon approaches nearest to this Island. (See the values of $t_H - t_D$ in Table 2)

Now, from Table 2 a diagram as shown in Fig. 8 (left-hand side) was constructed on the consideration that the maximum wave-height depends upon the intensity and the distance of the nearest approach of a typhoon. The compari-

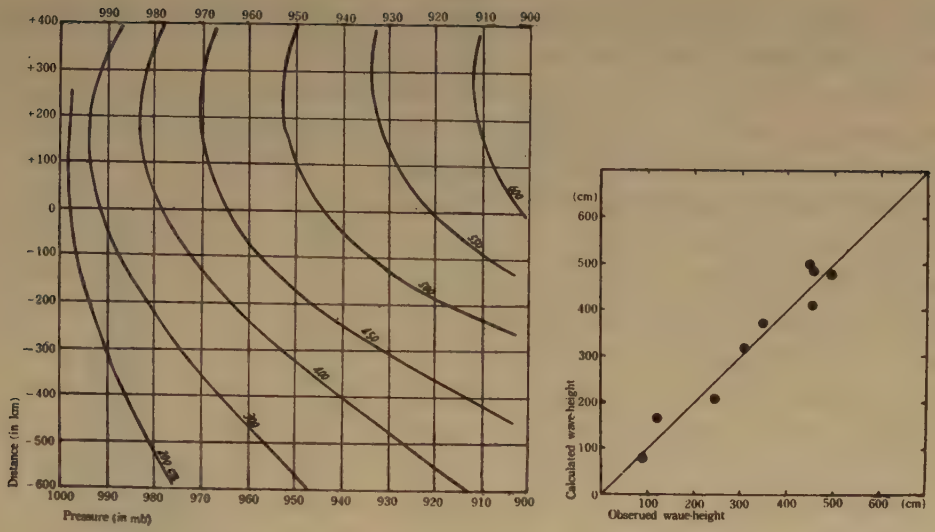

Fig. 8. Left: Relation among the wave-height, the lowest central pressure of a typhoon and the distance of nearest approach. Right : Comparison between observed and calculated wave-height.

son of the values read off from the curves in Fig. 8 (left-hand side) with those observed is shown in Fig. 8 (right-hand side), from which we can see that Fig. 8 (left hand side) gives a satisfactory result in practice. Although Fig. 8 (left-hand side) may require some amendment with further accumulation of observed data, yet this experimental diagram will be useful in wave forecast, at least for the first approximation. In this figure, it is remarked that waves tend to become higher in the case when a typhoon passes northwest of Hachijo Island than in the case when it passes southeast of it, and this can be easily understood if we consider that in the former case the island lies in the dangerous semi-circle of the typhoon and that the observing station is situated on the southwestern coast of the island.

(3) The maximum of wave-period.

In Fig. 6, the points markd with ● on the paths of the typhoons show the position of the centre of each typhoon at the time when the maximum wave-period occurred at Hachijo Island. Again, in Table 2, the quantity $t_T - t_D$ gives the time interval from the time of the nearest approach of a typhoon to Hachijo Island to the time of occurrence of the maximum wave-period. From these we can see that the maximum wave-period occurs several hours later than the time of the nearest approach of the typhoon.

In the case of strong typhoons, the wave-period frequently becomes over 15 sec. Moreover, according to Table 2, a tendency is seen such that the wave-period is larger in the case where a typhoon passes on the southern side of Hachijo Island than in the case where it passes on the northern side of it, and

this is natural if we consider that in the former case swells are predominant, while in the latter case "wind waves" are predominant.

Besides, in the case of Typhoon ALLCE, it was reported that swells with the period of 20~25 sec surged upon the coast of Ito, Shizuoka Prefecture, for about a day, one or two days after the typhoon left over ocean to the east of Japan, and destroyed a mole several dozen metres long. At that time the weather was clam in the vicinity of Ito, and waves were scarcely seen on the surface of the sea as far as several hundred metres off shore, except in the immediate neighbourhood of the coast where unusually high swell was surging, according to report. At any rate, it is to be remarked that such long swells sometimes appear in the case of typhoons. Fig. 9 shows an example of frequency distribution of the period of waves due to typhoons, and it is seen that the distribution is nearly of normal type and that there exist long swells with wave-period of 20 sec or more as mentioned above.

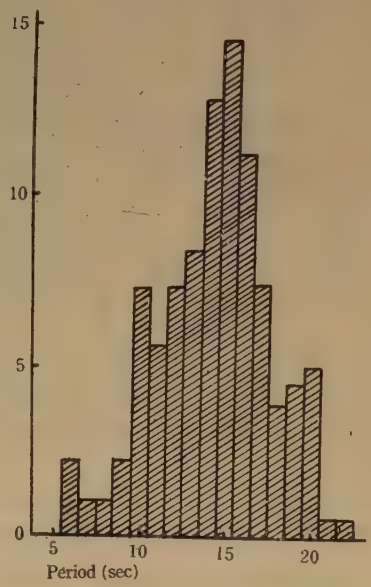

Fig. 9. The frequency distribution of wave-period at Yayene (Hachijo Is.) from 13h to 16h of 25th, Sept. 1953. (The case of Typhoon TESS)

(4) Subsidence of waves.

In Table 2, the quantity $t_C - t_D$ represents the time interval from the time when a typhoon approaches nearest to Hachijo Island to the time when waves have disappeared and it is seen that the waves usually subside after a day or so, in the case of a weak typhoon, or about two days and a half, in the case of a strong typhoon, from the time when the typhoon approaches nearest to the station, Again, if we compare $t_H - t_B$ (the time interval from the time when waves begin to grow to the time when the wave-height becomes maximum) with $t_C - t_H$ (the time interval from the time when the wave-height becomes maximum to the time when the waves have disappeared), we can see that, in the case where the typhoon passes on the northern side of Hachijo Island, the former is larger than the latter, while on the contrary, in the case where the typhoon passes on the southern side of Hachijo Island, the latter is rather larger. This will be due to the fact that in the case where the typhoon passes on the northern side of Hachijo Island, it frequently fetches a large compass westward, and mostly strikes the Japan Island, and so waves will not be newly generated.

(5) Duration of higher waves.

As for the duration of higher waves for different intensities and paths of

typhoons, we can form a probable estimate from the values of t_2 or t_3 in Table 2.

(6) Waves with long period near the coast.

In the case of Typhoon TESS, as seen in the wave record of Fig. 1 B and B′ waves with especially long period as long as 2～3 minutes appeared, in addition to ordinary waves. The variation of these wave-heights with time is shown by the curve H′ in Fig. 2 (C); the maximum wave-height of these long waves attained as much as 3.5 m. And it has already been shown that these waves are not a mere "surf beat" (Munk, 1949) but a kind of oscillation of water in the vicinity of the coast, produced by a water-drift due to southwesterly winds with speed over 30 knots blowing right against the coast of Yayene, together with mass transport due to high wave (Daidoji, Unoki and Kajiura, 1954). At any rate, it is not a negligible matter in practical wave forecast that waves with very long period and with wave-height over 3 m superpose themselves upon high "wind waves".

Acknowledgments

The authors wish to express their hearty thanks to Mr. S. Daidoji, director of the Hachijojima weather Station, and the members of that station who have heartily cooperated with the authors in making wave observations for a long time. Equal thanks are due to Mr. K. Kajiura of the Tokyo University and Mr. J. Sugiura of the Central Meteorological Observatory for their kind help and valuable informations. Further the authors are indebted to the Special Committee on Marine Resources, Japanese National Commission for UNESCO for financial aids.

References

(1) Daidoji, S., S. Unoki and K. Kajiura, 1954 : Waves at Hachijo Island caused by Typhoon TESS and ALICE in 1953 (in Japanese). Journ. Meteor. Res. Vol. 6, pp. 221-229.

(2) Darbyshire, J. 1952 : The generation of waves by wind. Proc. Roy. Soc. A. 215, pp.229-328.

(3) Kajiura, K., H. Miyoshi and K. Takano, 1954 : On the waves at Hachijo Island (unpublished).

(4) Munk, W. H., 1949 : Surf beats. Trans. Amer. Geophys. Uni. Vol 30, No. 6.

(5) Ōtani, T., 1940: "Bofū-u or Storms" (in Japanese). Iwanami Book Co.

(6) Pierson, W. J., G. Neumann and R. W. James, 1953: Practical methods for observing and forecasting ocean waves by means of wave spectra and statistics. Dept. of Met. Oceanogr., New York Univ. Tech. Rep. No. 1.

(7) Sverdrup, H. U., and W. H. Munk, 1947 : Wind, sea and swell ; theory of relations for forecasting.

Records of Oceanographic Works
in Japan, Vol. 2, No. 1,
March 1955

Markings on a Tidal Flat in Uranouchi Bay, Shikoku

Kotora Hatai and Hideo Mii

(Department of Geology, College of Education, Tohoku University)

Introduction

As stated elsewhere,[1] there are several large tidal flats in Uranouchi Bay, Usa-Machi, Takaoka-gun, Shikoku. These tidal flats have been described with regard to their molluscsn infauna and varied ripple marks found thereon. The general oceanographical conditions as relationship between currents and bottom sediments, and the depth distribution within the bay have also been described. In this report, the writers deal with markings found on the tidal flats, that is to say, the castings of *Balanoglossus* and the trails of *Astriclypeus manni* Verrill. These markings are dealt with particularly because similar castings are known to occur in sedimentary rocks of various geological ages, and trails similar to the one made by the echinoid may be found on stratification planes of geological formations.

Acknowledgements

The writers express their thanks to Professor Yuji Kanbara, Director of the Marine Biological Station of Kochi University, where the writers had an opportunity to visit for oceanographical observations during the spring of 1954, for kindly making necessary arrangements during their stay at the station. Acknowledgements are also due to Mr. Takeye Araya of the Committee for the Advancement of Scientific Research in Japan, for the opportunity of making this study.

Remarks on the Castings of *Balanoglossus*

The excreta or castings to be described are those of *Balanoglossus,* which is commonly seen on the tidal flats and at several meters depth below low tide level in the northern eastern half of Uranouchi Bay. The castings are commonly seen on the marginal portions of the tidal flats consisting of sand, but not on those built of coarse materials as pebbly sand, pebbles, or gravels. They are found in areas overgrown with sea-grasses and in areas consisting only of sand. The sand may or may not be more or less carbonaceous.

The animal responsible for the casting is an undetermined species of the

genus *Balanoglossus,* similar to *Balanoglossus misakiensis* Kuwano,[2] a species which lives in the tidal and subtidal regions along the Pacific coast of Japan.

The undetermined species of *Balanoglossus* makes a burrow of U-shape, the distance between the oral and anal holes measures about 32 cm in average, and the depth of the middle part of the burrow is about 40-50 cm from the sand surface. The diameter of the burrow at the anal part is 11-13 cm and that of the oral end was not measured owing to its being at the bottom of a shallow cup-shaped depression. The burrow is lined with a thin mucous membraneous film and its outer side is agglutinated with sand, whereas the inner side is very smooth, although no concentric rings were observed.

The oral end of the burrow is readily noticed by a small, funnel shaped depression in the sand surface, and the anal end by the dome shaped mound of sand with spiral castings on top. In general, the sand grains are coarser at the margins of the mound than above, probably due to that the sorted surface sand is first excreted.

The diameter of the casting is always less that of the burrow, for example, a casting measuring 11 mm in diameter is ejected from a burrow having a diameter of 13 mm, which is that of the outer diameter of the tube. The casting just described, is spiral in shape, clockwise in arrangement, and has numerous concentric rings, each separated by a distance of about 2 mm. The concentric rings may be due to the parting of sand grains by tension caused by the spiral arrangement, and less probably to partial contraction of the anus.

The casting is ejected as a continuous stream, thus the clock-wise spiral accumulation will continue until it breaks owing to having reached a point where no more piling can be continued. When the spiral arrangement is broken, the pieces will accumulate on or around the sand mound. Thus, when the process is continued, the independent parts of the original spiral will be piled up without definite orientation.

The castings are rather firm owing to the mucous membrane or very thin film covering, but easily crumble when picked up by the fingers. They retain their original shape under water for a considerable length of time, at least a day, where current action is not strong. On the tidal flats, the original form is often retained during the period of tides, thereafter the majority are destroyed by the strong bay currents of the tidal and ebb tide. Probably wind also plays a part in their destruction.

If the burrows of *Balanoglossus* were filled with sediment after the animal died, it would be possible that a U-shaped sand or mud pipe would be the result. Should only the two vertical burrows be filled and preserved, the result would be two erect pipes perpendicular to the surface, or bedding plane in geological sense. Providing that only the burrow connecting the two vertical ones is preserved, the result would be a pipe parallel with the surface or

bedding plane and at a distance of about 40-50 cm below it.

Sand pipes are a common phenomenon in sedimentary rocks, but their origin is not well known. The writers believe that observations on recent burrows of different animals may aid in solving the problem. In this respect the works of I. Hayasaka,[3] K. Hatai[4] and W. Häntzschel[5] are well known and further remarks are here unnecessary.

The purpose of taking the casting into consideration is because similar markings have been described from sedimentary rocks of various ages. Some authors even establish generic and specific names for castings of unknown nature. The naming is thereby a procedure in nomenclature, thus suggesting that the zoological relationship with known animals is understood. The writers hold the view that to increase our knowledge on the recent castings and other features as found on tidal flats and in tidal zones is of prime importance. Without such data the true nature of fossil castings is difficult to interpret.

Trails of *Astriclypeus manni* Verrill

Markings such as trails of gastropods and annelids are not rare phenomena in geological formations; burrows of pelecypods and of crustaceans have also been described from sedimentary rocks, but the writers are unaware of markings made by sand dollars in sedimentary rocks. Of the mentioned burrows and trails, those of the former have been reported to occur in the form of sand-pipes in broad meaning, and those of the latter are rather common in rocks older than the Cambrian. Although trails of sand dollars have not been reported as yet, it seems possible that they may be found on stratification planes, but oblitered to a degree by which their original form could not be interpreted.

In several square meters of surface sand of the marginal portion of the largest tidal flat in Uranouchi Bay, a total of four specimens of *Astriclypeus manni* Verrill were found crawling on the sand, leaving behind them interesting trails. The depth of the water at the marginal portion was about 20-30 cm at low tide.

Astriclypeus manni has a discoid shell provided with five holes at its marginal part. The disc measures about 13 cm in diameter of a moderate size specimen and about 14 mm in height. Its spines are very short, measuring only about 2~3 mm in length. By moving these spines the animal is able to crawl on the surface of the sand. It is during this activation that the animal feeds on benthonic organisms.

When crawling, the disc advances forward very slowly, pushing up sand by the bluntly rounded test margin. By this procedure, sand is pushed up and over the test, thus hiding the animal completely. Simultaneously, small levees of sand are built on the lateral sides of the test as the animal moves forwards.

These levees are only about 5 mm to nearly 1 cm in height and separated from one another by the width corresponding to the diameter of the test.

The slow movement of the sand dollar and its own weight appear to serve for its partial submergence in the sand. The depth to which the animal is burried seems to be related to the weight of the whole animal and to the compactness or hardness of the sand. In the present case, very deeply burried tests were not seen, and furthermore, the animal was not found where the sand was very soft, due probably to water saturation and air bubbles as on the eastern side of the easternmost tidal flat.

I. Hayasaka[6] has presented a review of previous literature concerning the mode and rate of locomotion of echinoderms, and has furthermore, described his own observations on *Arachnoides placenta* (Linné). That species is said to be living on a tidal flat in Taiwan, and I. Hayasaka has described the mode and rate of locomotion of that species and also the method by which it submerges into the sand.

Although markings identical with those made by *Astriclypeus manni* and *Arachnoides placenta* or other echinoderms are unknown to the writers, their occurrence seems to be possible. It may be added that observations on the different kinds of markings found on tidal flats may prove to be of importance in interpreting the various kinds of makings found on stratification planes in sedimentary rocks.

Literature Cited

1) K. Hatai and H. Mii, Observations on the Tidal Flats in Uranouchi Bay, Kochi Prefecture, Shikoku, Japan : Rec. Oceanogr. Wks. Japan, New Series (for publication).

2) Illustrated Encyclopedia of the Fauna of Japan : p. 553, fig. 1610, 1949 (Revised edition). Published by the Hokuryukan Co., Ltd., Tokyo.

3) I. Hayasaka, The Burrowing Activities of Certain Crabs and their Geologic Significance : Amer. Midl. Naturalist, vol. 16, no. 1, 1935.

4) K. Hatai, Further Notes on Sand-pipes: Jour. Geol. Soc. Japan, vol. 45, no. 45, no. 543, pp. 873-875, 1938.

K. Hatai, A Problematical Fossil from Yamagata : Short Papers, IGPS, no. 3, pp. 41-45, 1951.

K. Hatai, On a Sand-pipe from near Sendai : Short Papers, IGPS, no. 3, pp. 46-51, 1951.

S. Nomura and K. Hatai, Preliminary notes on Some Sand-pipes : Saito Ho-on Kai Mus., Res. Bull., no. 13, pp. 147-153, 1937.

S. Nomura and K. Hatai, On the Occurrence of Peculiar Shaped Concretions Probably due to Certain Decapod Crustacens : Jap. Jour. Geol. Geogr., vol. 13, pp. 57-61, 1936.

5) W. Häntzschel, Die Lebensspur *Ophiomorpha* Ludren in Miozän bie Hamburg, ihre weltweite Verbreitung und Synonymie : Mitt. Geol. Staatsinstitut in Haburg, Heft 21, 1952.

6) I.Hayasaka, On the Locomotion of an Echinoderm, *Arachnoides placenta* (L) : Kwagaku, vol. 23, no. 9, 5 text-figs., 1953.

Explanation of Plate

Figs. 1-6. Castings of *Balanoglossus* cf. *misakiensis* Kuwano on the tidal flat in Uranouchi Bay, Shikoku. Fig. 1-note the spiral arrangement and the concentric rings. Fig. 2-partly broken spiral casting. Fig. 3-partly broken and the mucous covering is almost lost. Fig. 4-completely broken spiral casting. Fig. 5- initial stage of spiral arrangement. Note the arrangement of grains on the basal part of the mound in comparison with that above. Fig. 6-spiral casting destroyed partially by wind and current action.

Figs. 6-7. Trails made by *Astriclypeus manni* Verrill. Fig. 8-four specimens travelling in different directions within an area of several square meters. Fig. 7-trail and levees of a moderate size specimen.

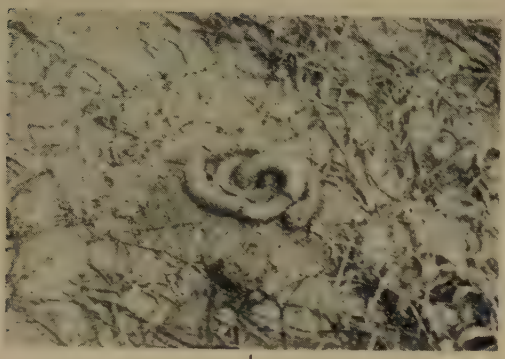

1

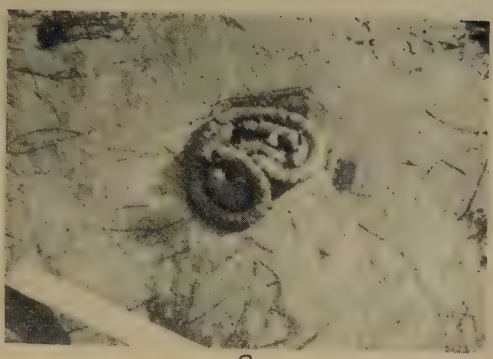

2

3

4

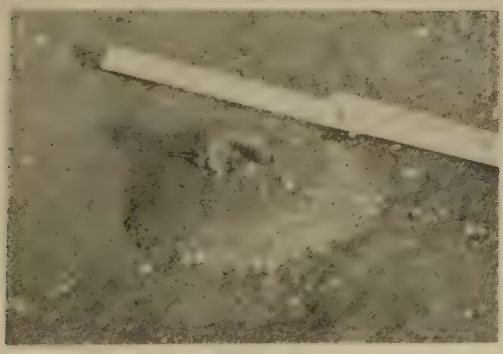

5

6

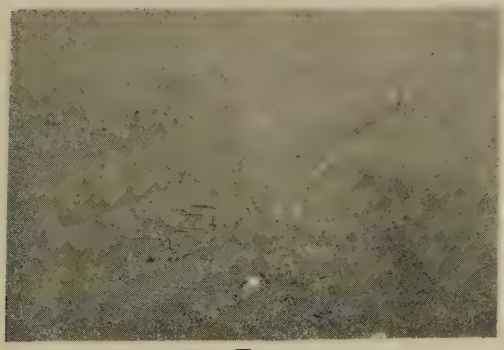

7

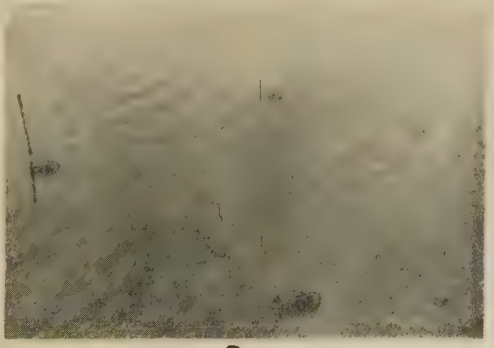

8

Records of Oceanographic Works
in Japan, Vol. 2, No. 1,
March 1955

Observations on the Tidal Flats in Uranouchi Bay, Kochi Prefecture, Shikoku, Japan.

Kotora Hatai and Hideo Mii

(Department of Geology, College of Education, Tohoku University)

Introduction

During the spring of 1954, the writers visited the Marine Biological Station of the Kochi University, with the purpose to make observations on the tidal flats in Uranouchi Bay, and to find, if possible, the relation existing between the distribution of marine invertebrates to bottom sediment and currents. The work is part of a project initiated by the Japanese National Commission for Unesco with relation to oceanogra- phic resources.

The Marine Biological Station of the Kochi University in Shikoku is situated in the village of Inojiri on the northwestern tip of the eastern extremity of the narrow peninsula by which Uranouchi Bay is separated from the Pacific Ocean at its south. The town of Usa is on the opposite or northern side of the bay, communication between the two places being by a motor boat which is run throughout the day. The Station, which lies about 15 kilometers southeast of Kochi City, can be reached by the City controlled Bus that is run regularly throughout the day, the time required being about one hour.

Acknowledgements

The writers are indebted and wish to thank Professor Yuji Kanbara, Director of the Marine Biological Station of the Kochi University, for making all necessary arrangements and providing Facilities during their stay at the Station. Particular thanks are due to Mr. M. Ueda, teacher of the Takaoka High School, Takaoka-gun, Kochi Prefecture, for his sincere help in many ways. The writers also acknowledge their gratitude to Messrs. Jiro Katto of the Department of Geology and Takeshi Yatsuzawa of the Department of zoology, both of Kochi University, for their help in various ways.

This work was accomplished by funds provided by the Committee on Oceanographic Resources of the Japanese National Commission for Unesco Particular thanks are due to Mr. Buei Araya, for kindly making arrangments for the writers research.

Uranouchi Bay

Uranouchi Bay is situated in the central southern part of Kochi Prefecture facing the Pacific Ocean. It is separated from the open sea at its southern part by the narrow peninsula of NNE-SSW trend, and form the Pacific Ocean at its north-northeastern side by the narrow canal between Usa Town and Inojiri Village. The Bay shows a typical submergence topography, both its northern and southern coasts being richly indented with inlets of various sizes and shapes throghout its length. The Bay measures about 8,800 meters in NNE-SSW length, 2,200 meters in maximum width, and about 500-600 meters in width of its canal.

On the seaward side adjacent to the bay-mouth, the bottom consists of sand that is easily shifted by the strong inflow and outflow currents, waves and by winds, thus that area is very shallow and subject to change in depth distribution. The easily shifted sands has caused shallowing of the bottom and constructions are now being prosecuted to keep a narrow waterway for fishing vessels. The bay side part adjacent to the bay-mouth is also shallow and near it are found several large tidal flats.

There are no rivers emptying into the bay and the only freshwater it receives is from the overflow of paddy-fields supplied by four or five small streams, and from rain fall. Thus one would expect stratification within the bay.

There are no sand beaches in Uranouchi Bay, and the flat areas of the valleys consist of muddy material derived by disintegration of the country rocks of Jurassic age. Paddy-fields are distributed chiefly on the northern side of the bay, owing to that side having broader valley-bottoms than that of the southern side where they are narrower, less extensive, fewer in number and with water supplied only by several natural springs.

1) Topography of the Bay.

The topographical features of Uranouchi Bay display a submergence characteristic in the northern and southern coast lines being richly indented with many inlets, small bays or coves, of which Uranouchi and Haigata can be referred to the latter, and Donoura and several without names to the former category. In general, narrow and deeply indented inlets are lacking on the northern side, but are common on the southern, the contrary can be said for the small bays.

Where cliffs are found along the coast-line, the shore descends abruptly to the bay-bottom. Below these cliffs under water, it is noticed that angular boulders and somewhat rounded cobbles predominate and it is interesting to find that fine grained sediments as mud, very coarse sand or pebbles, do not fill the interspaces of the mentioned boulders, particularly along the southern coast from Uzuga to Osaki.

Where paddy-fields are made on either the northern or southern coasts, there have been build concrete or artificial walls to prevent destruction of the fields by bayward flow of the soft muds. In such areas the bottom material consists of soft, dark colored muds, primarily disintegrated from the country rock and subsequently deposited from the materials transported by overflow of the paddy-fields and other artificial agencies.

Although no sand beaches occur, except for tidal flats within the bay, there are several narrow beaches consisting of pebbles, cobbles, rarely of boulders, and granules with mud. All of these materials crumble by weathering and water saturation and the smaller ones can be easily crushed by the fingers, thus showing that the country rocks readily disintegrate by weathering.

The small bays of Uranouchi and Haigata are distinguished from the others by their larger size, having large valleys at their heads which are broad and extensive, and by that they trend southeast and southwards, respectively. All other inlets or indentations on the northern shore of the bay are not prominent and their directions are varied, ranging from southeast, south to southwest. The narrow but deeply indented inlets on the southern shore of the bay are directed to the north or northwest. Thus, it can be recognized that the arrangements of the more outstanding indentations, breadth and extensions of the valleys are contrasting, when the northern and southern shores are compared.

A noteworthy topographic feature is that the coast line from Usa Town to Niyodo River is smooth, without indentations and is of the emergence type. However, the narrow peninsula separating Uranouchi Bay from the open sea at the south shows typical submergence topography. The bay itself seems to be a boundary line separating the mentioned two contrasting topographical features.

Although Uranouchi Bay displays a typical submergence topography, there is evidence of recent uplift exhibited by the presence af elevated notches, by the raised land areas between Seiryuji, the village of Ryu and the hill of Sakiyama on the eastern part of the peninsula, and by another such area on which the village of Inojiri is situated, and others represented by the low-level paddy-fields, all on the southern side of the bay. On the northern side of the bay, similar features are shown by the many low level paddy-fields distributed scatterly throughout the coastal area.

Other evidence for recent uplift is shown by the narrow raised shore-platform developed at the foot of the promontories between Fujigasaki at the west to Matsugasaki at the east along the southern shore of the bay.

Also it is known that Uranouchi Bay was uplifted about 1.50 meters to 2.00 meters due to the Nankai earthquake of December 21, 1946.

2) Shoals in the Bay.

The shoals developed in the area between Fukushima at the east to Haigatasaki at the west on the northern shore, and Uzuga at the east toOsaki at the west on the soutern shore, are characteristic features of the eastern potion of Uranouchi Bay. These shoals, particularly the two large ones close to the northern shore becomes exposed about 30 centimeters above sea-level during low tide, but are completely submerged under about 1.30 meters of water during high tide. The one near to the southern shore is covered with about 30-40 centimeters of water during low tide. Both of these tidal flats consist of medium to coarse grained sands, while the smaller shoal is built of a mixture of sand and gravels. Of the two tidal flats, the one in the east is blanketed with medium to coarse grained sand, but is underlain with sand and gravel particularly in its western portion.

The tidal flats as shown on the topographical map (scale, 1 : 25,000) published by the Geographical Institute in December 1947, have changed since then, both in position and size. The one near the southern shore is submerged and its position and shape seems to be as indicated on the map issued by the same institute, but the smaller one very close to the western part of the northern shore indicated on the map just referred to has been destroyed and is now without shape. The largest flat close to the northern shore has become narrower and more elongated in east-west direction. Another one which is situated immediately south of Fukushima at the eastern portion of the northern shore and separated from the one at the west, is not indicated on the map referred to above. This tidal flat is NNE-SSW in distributian, elongated, and more or less quadrate in shape.

From the foregoing it is evident that the shoals are subject to migration, destruction or construction according to currents and probably also assisted by winds. Thus, the westernnmost one on the northern shore has become destroyed, while a new one in the easternmost part of the same shore has been given birth, and the largest of the two tidal flats has changed its shape considerably.

Although outside of the bay, there is another rather large shoal as indicated in the annexed chart, it remains under water during low tide, but its shape can be distinguished by the movement of the water. This shoal consists of sand without gravels, and is thus expected to be subject to variation in shape, size and position.

3) Depth variation within the Bay.

The depth distribution in Uranouchi Bay is as indicated in the chart, in which only the important measurements are given. In general, the depth of the bay is deepest in th area west of the line drawn from Torakimisaki on the

northern shore to Nagasaki on the southern shore. Therefrom eastwards there is a general tendency of the bay becoming shallower, being shallowest in the region of the shoals above referred to. Where the water depth exceeds seven meters or thereabout, there is a tendency of the bottom to be predominated with mud, and where the depth is less than seven meters, in general, the bottom comprises sand or coarser materials.

From the chart and from the depth variation within the bay, it appears that there is a general tendency of the central eastern portion or the area where shoals are developed, to become shallower owing to deposition of sand transported by the strong currents. By this deposition of the transported sands, that area is gradually building up, or in other words, construction seems to be greater than destruction in such areas.

4) Currents and distribution of sediments in the Bay (refer to chart).

During rising tide the current enters the narrow and shallow canal, therefrom continuing strongly along the southern coast to as far west as the line drawn from Fujigasaki on the northern shore to Osaki on the southern shore. From about this line the current changes its direction of flow from westwards to northwards, partially entering the inlet of Haigata, then continues eastward along the southern shore of the northern margin of the bay. Throughout the mentioned route, the current is strong, and it is within this circumscribed area that sands or coarser sediments are distributed.

The bottom sediments near the canal consists of sand, which become coarse to very coarse westwards, and then to gravelly in the southern parts of the shoals. Thereon westwards the sediments gradually become finer, and in the region where the current abruptly trends northwards, the bottom material consists of silt. Silt also prevails in the inlet of Haigata. From about Haigatasaki eastwards the bottom material again changes to sand, which becomes coarse as the shoals are approached. The narrow, shallow pathway between the shoals and the northern mainland consists of very coarse material as very coarse sand, pebbles and cobbles, which again change into sand near the mouth of the bay.

In the region west of the boundary line from Fujigasaki to Osaki, the bottom sediments consist of soft dark mud of slight sulphuric smell. In the two small inlets of Nyuto and Donoura to the southeast of the boundary line above mentioned, the bottom consists of silty mud or of mud of dark color and with peculiar foul smell. The current does not appear to have influence on these two inlets so far as bottom material is concerned. The sulphuric or peculiar foul smell of these bottom muds suggests that benthonic and infaunal invertebrates may not exist there and that the bottom water layer may be stagnant owing to non-circulation of the bottom water.

From the foregoing description it is recognized that the area circumscribed by the inflowing current has a bottom consisting of sand in various grain sizes and also of pebbles or cobbles at places, whereas in the areas not influenced by the currents to any noteworthy degree, the bottom consists of silt, silty mud or of mud. This evidence suggests that the grain-size distribution of the bottom sediments is in close relationship with the strength and influence of the currents which are responsible for their transportation.

Although it was stated that the currents flow abruptly northwards at the boundary line above referred to, it should be mentioned that several pearl oyster-rafts are found slightly west of the said line. From this fact, it is inferred that only the surface waters enter, and since their flow is greatly decreased it appears that the greater part, or the lower part of the moving water body fails to enter that region.

From the evidence afforded by the sulphuric smell of the soft dark coloured mud from the bottom west of the said boundary line, and from the occurrence of similar muds in the aforestated two inlets, it is inferred that although surface currents may have entered there, the bottom currents failed to do so owing, possibly, to the mass of heavy or stagnant water occupying the subsurface of that region. The lack of sandy sediments in those area may suggest that current action was insufficient for their transportaion. It may also be probable that the bottom of the areas provided with unfavorable smelling muds is covered with heavy and stagnant waters.

In this respect, M. Ueda (1950) has reported that Uranouchi Bay "has a characteristic which closely resembles that of the salt lake, in the point that when the rainfall continues the salinity of surface water decreases thus resulting in the formation of direct stratification. On the contrary, however, when the drought continues, mainly during summer, salinity of surface water increases, which consequently sinks down to the bottom, thus causing disappearance of the stratification".

Mechanical analysis of the bottom sediments is now in progress and the result will be published parallel with an analysis of the bottom microfauna contained in them. The annexed chart showing the distribution of the bottom sediments is subject to slight change owing to that the results of mechanical analysis of the sediments is not included herein.

5) Characteristic Features of the Tidal Flats in the Bay.

On the shoals or tidal flats are found asymmetrical ripple marks and short, irregularly spaced, variously directed, undulatory markings that should be given consideration. The following remarks are preliminary owing to that further studies are expected to be advanced in the field.

The asymmetrical ripple marks consists of one having short wave length superposed upon one of much larger wave length, thus suggesting a ripplenorium (Fig. 3 in plate), if the word can be newly introduced. The wave length of the superposed (Fig. 8 in plate) asymmetrical ripples is 15-20 cm. against 1-2 meters of the underlying larger one. The amplitude of the latter ripples is 15-20 cm and that of the former is 1.5-2 cm. The large one is known as giant ripple as recently dealt with by L. M. J. U. van Straaten (1950, pp. 76-81), and has a slope of 20-27 degrees on its steeper part, 3-5 degrees on its larger surface, and about 10 degrees on its gentle sloping part adjacent to the trough. This kind of ripple mark is well developed on the eastern tidal flat (Fig. 3). On the surface of the steep slope just mentioned, there can be observed horizontal laminae which do not extend into the ripple itself, owing to it consisting of homogeneous massive sand (Fig. 5). The successive laminae are though to represent the layers of sand deposited during progressive lowering of the water level due to the ebb tide. The crest line of this giant ripple trends approximately N 30-40°E., although it possesses many irregularities represented by minute bays and horns. However, its characteristics do not conform with the D-Rippeln described by W. Häntzschel (1938, pp 6-7) on the coast of northern Germany.

The general trend of the crest line of the smaller or superposed ripples is parallel with that of the underlying larger one (Fig. 3). Both of these ripples are of different magnitude, but are similar in their form and arrangement of the sand grains. The sand grains are coarser in the troughs than on the crests. In geological sense, the structure resembles an anticlinorium, thus the name of ripplenorium is here proposed for such type of ripples which diverge from those described from northern Europe by W. Häntzschel and L. M. J. U. van Straaten.

From the patterns of the rill marks developed on the surfaces of the ripplenorium, it is evident that the current direction was toward the steep slope of the ripple and not vice versa. Accordingly, it follows that the asymmetrical ripple marks referred to are true current ripples. From the fact that the currents are strongest with the ebb tide and particularly so just before full low tide, it may be inferred that the giant ripples and also those superposed upon it were formed by such phenomenon. It must be added that the small ripples or those superposed upon the larger, were subject to the influence of rippling waves produced by the tidal current and wind which were in harmony, being approximately S 40°E. This general direction of the wind is perpendicular to the arrangement of the ripplenorium.

From the fact that the direction of the steep slopes of the asymmetrical giant ripples developed on the southern part of the eastern tidal flat was opposite to those of the northern part of the same flat, may be ascribed to the effect of clockwise currents from the eastern part of the flat aided by weaker

currents extending northward from the southern part of the bay. The boundary between the ripplenoria of opposite directions is represented by a gentle scarp measuring 30-40 cm., that of the northern part of the flat being higher than that of the southern part (Figs. 4 & 6).

The short, irregularly spaced, variously directed undulatory markings referred to above are well developed on part of the western tidal flat particularly in regions where the above-mentioned giant ripples are lacking or only partially developed (Fig. 7 & 8). The difference in relief of the minimum and maximum undulatory markings is 10-15 cm. No detail measurements were made of the undulatory makings owing to their disconformity in extension, developments, wave length, amplitude and general trends.

The origin of the mentioned undulatory markings which may be called irregular ripple marks (Fig. 7) may be that the prevailing current was not strong enough for the construction of larger and more definite ripples. Also it may be probable that cross-currents was important in the development of the irregularity, and such currents by forming gently flowing eddies may have also contributed in their development. It must also be mentioned that giant ripples or ripplenoria are not developed in regions near to where such irregular ripple marks exist, but they are found not far away. Also it is worth mentioning that the irregular ripple marks are found on the western side of the tidal flats but not on the eastern, a fact that coincides with the strength of the currents which are weaker on the westward and stronger on the eastward sides of the tidel flat. This currents strength may also be explained in part by the breadth of those parts of the bay, being broader in the western and narrower in the eastern.

From the aforementioned evidence it is inferred that these irregular ripple marks may be nothing but the initial stage in development of the ripplenoria, since they are analogous with the initial stage of transverse megaripples described by L. M. J. U. van Straaten (1953, pl. 1A).

6) Areas of deposition and non-deposition.

The areas of deposition is that in which sand is distributed, although within this area there are regions of non-deposition and of erosion. From the nature of the country rocks it is evident that the sand distributed within the eastern part of Uranouchi Bay, or to the east of the line drawn from Fujigasaki to Osaki already referred to, has been carried into the the bay by currents from the open sea.

Within thise large area of deposition, the regions bordering the southern shore at several places can be said to be the regions of non-deposition, there being no sand or no mud deposited on the bottom which consists of boulders and

cobbles as already mentioned. If this area is considered to be one of erosion, then it follows that the boulders and cobbles must be carries away in suspension after being completely disintegrated by water saturation. However, no muddy material was founds mixed with the sand distributed on the bottom to the west or in the near couse of the current direction. Thus the area may be one of non-deposition and of more or less slow precipitation.

Areas characteristic of only current erosion were not noticed during the short survey of the bay, and therefore, the problem will be reserved for the next occasion.

7) Fauna of the Tidal Flats.

The tidal flats are exposed (Fig. 1) in considerably wide distribution, thus affording observations on the infauna flourishing there.

Among the infauna flourishing on largest tidal flat, *Solen gouldi* Conrad is of particular interest, because of its overwhelming numbers, peculiar distribution and relation to the sedements. This species is rare in regions consisting of pebbly sand and also in places overgrown with sea-grass. There is a general tendency of its population increasing from the flat margins towards the central parts. The species is rarely found on the northern, eastern and western marginal portions of the easternmost flat, and is not common at the western portion of the westernmost flat. The distribution as mentioned seems to have relationship whth the tidal currents which carry the larvae and disturb its settling.

To determine the population of *Solen gouldi* Conrad, an area of approximately one square meter and a depth of 30-50 centimeters were dug in various part of western and eastern tidal flats (Fig. 2). Counting was done by two methods, one was by counting all of the inviduals actually dug out, and other by first counting the number of holes seen on the surface and then by number of individuals dug out. The results are as follows for the largest flat (Fig. 1), per one spuare meters.

Northern margin exposed during low tide·····209 individuals
Northeastern margin of shoal ·····154 (average of 6 diggings)
Eastern margin of shoal ····· 37 (average of 5 diggings)
Southeastern margin of shoal ····· 44 (average of 2 diggings)
Southern margin of shoal ····· 93 (average of 3 diggings)
Southwestern margin of shoal ····· 35 (one digging)
Western margin of shoal ·····390 (average of 7 diggings)
Northwestern margin of shoal ·····237 (average of 2 diggings)
Central area of the shoal ·····189 (average of 3 diggings)

In the central part of the largest flat where 78 holes could be counted in 20 square centimeters of surface sand, a total of 58 individuals of *Solen* were

dug out. In another part of the central part of the same shoal where 39 holes were counted in a similar area of surface sand, a similar number of *Solen* were dug out.

This particular species commonly lives at depths ranging from 5-10 centimeters, but it rapidly burrows down to depths as great as 30-50 centimeters. It commonly lives in grayish, yello wish to dark colored sands, being most frequent in medium sand of grayish to yellowish color.

From the population density of *Solen gouldi* Conrad, particularly on the largest flat, it appears that it would serve as a good can-food production, since its taste is excellent. Its reproduction may be remarkable as it is said to have suddenly dominated the flat. Although the flat is visited daily by persons to dig the shell for food purpose, its population remains rather great.

When the shell is lain on the sand surface, soon extends its foot to secure a hold in the sand, then gradually it pulls its body to an oblique position as the foot digs deeper into the sand. After reaching an oblique position, the animal suddenly becomes vertical and then rapidly burrows into the sand. In a few cases when the animal was placed in a similar position, the foot was suddenly extruded and the animal appeared to leap a few centimeters. The burrowing activity of this animal is very quick.

Although *Solen* was the predominant species found living, only rarely were found other genera of infauna. Several specimens of *Circe scripta stutzeri* (Donovan) and of *Grafrarium divaricatum* (Gmelin) were found shallowly embedded in the sand. No other living shells could be found although considersble digging was done. A living species of the pectinid, *Decatopecten striatus* (Schumacher) was found swimming in a shallow sand pool.

Lutraria arcuata Reeve, *Paphia amabilis* (Philippi) and *Chlamys nobilis* (Reeve) were found scattered on the western marginal portion of the largest flat, but no living shells of these species were found. The number of these dead shells decreased towards the eastern margins of both flats. These shells were all carried to their place of discovery by currents.

Of the echinoderms, *Astriclypeus manni* Verrill was found to be most common in the sand area. This species crawls over the sand, leaving a wide trail with leves on each side, and pushes sand up over its test as it moves forward. Many living specimens of this species were collected from the water covered areas of the marginal portions of the western flat. The greatest population observed was five individuals within an area of about four square meters.

Owing to that the writers failed to have a dredge ready for investigating the population of the infauna flourishing in depths below the flats, such a study is expected to be undertaken at the next opportunity so that the distribution

of the livnug aimals can be determined.

8) Distribution of the common shells in the Bay.

Shells as *Siphonaria sirius* Pilsbry, *Littorinopsis scabra* (Linnaeus), *Contumax kobelti* (Dunker), *Nerita polita* Linnaeus, *Turbo granulatus* Gmelin, and *Monodonta labio* Linnaeus are found along the rocky shores of both the northern and southern sides of Uranouchi Bay. These shells flourish in shallow tide pools, live in clusters and are found crawling on rocky shores above low tide. *Chama reflexa* Reeve, *Spondylus cruentus* Lischke, and *Arca navicularis* Bruguiére are found attached by their byssus to rocks as boulders and cobbles at a depth of about several meters along the southern side of the day. *Chicoreus ramosus* (Linnaeus), *Cypreaea vitellus* Linnaeus, and *Strombus luhuanus* Reeve are the common gastropods seen crawling over cobbles and boulders at about several metres depth along the southern side of the bay. These species have not been observed to be living above low tide level. *Ostrea echinata* Quoy and Gaimard is attched to rocks above low tide level and in between its shells are often found gastropods as *Nerita polita, Littorinopsis scabra,* and *Contumax kobelti.* In the dead shells of the mentioned oyster are often found amphineurans.

Among the rocks strewn along the beaches of the southern shore of the bay are often found *Caecella chinensis* Deshayes embedded shallowly, *Venerupis japonica* (Deshayes) to a little deeper position although it may also be found in association at depths as shallow as one or two centimeters. In the tide pools were also fond *Barbatia lima* (Reeve), *Ostrea echinata, Caecella chinensis,* and amphineurans.

Living shells of *Circe scripta stutzeri* (Donovan), *Gafrarium divaricatum* (Gmelin), *Chione squamosa* Linnaeus, and *Decatopecten striatus* (Schmacher) were found on the flats of the southern side of the bay, all expect the last mentioned were shallowly embedded in the coarse grained sand.

Although the number of dead shells collected from the the bay amount to a considerable number of species and genera, living shells were rarely seen, owing to that no dredge operation was undertaken.

Besides the molluscs above mentioned there were found numerous specimens of echinoids whose names have not yet been determined.

On the rocky regions of the northern shore of the bay were found shells similar to those of the southern shore of similar habitat, but the gastropods found below low tide level along the southern shore were not obseved in similar habitats of the northern shore.

The total list of the species collected from Uranouchi Bay are given in the following table, in which those marked with an asterisk are considered to be common.

List of Molluscan Shells from Uranouchi Bay

Pelecypoda

Anadara broughtoni (Schrenck)
Anadara tricenicosta (Nyst)
Anomia lischkei Dautzenbeg & Fischer
Asaphis dichotoma (Anton)
**Barbatia lima* (Reeve)
**Caecella chinensis* Deshayes
Cardita leana Dunker
**Chione squamosa* Linnaeus
**Chlamys nobilis* (Reeve)
**Circe scripta stutzeri* (Donovan)
Corbula erythrodon Lamarck
Decatopecten striatus (Schumacher)
Dosinia bilunulata (Gray)
Fulvia mutica (Reeve)
Gomphina veneriformis (Lamarck)
Grafrarium transversarium (Deshayes)
Macoma incongrua (v. Martens)
Mactra sulcataria Reeve
Mactra sp.
Musculus neglectus Kuroda
**Ostrea echinata* Quoy & Gaimard
Ostrea Gigas Thumberg
Paphia amabilis (Philippi)
Pecten albicans Schrötter
Pinctada margaritifera (Linnaeus)
Pitar japonica (Kuroda)
Promantellum hirasei (Pilsbry)
Sanguinolaria elongata (Lamarck)
Semele carnicolor Hanley
Septifer bilocularis (Linnaeus)
Septifer virgatus (Wiegmann)
Solen gordonis Yokayama
(Spondylus cruentus Lischke
Tellina sp.
Vasticardium enode (Sowerby)
Venus (Antigona) lamellaris Schumacher
Anadara subcrenata (Liscke)
Anodontia edentula (Linnaeus)
**Arca navicularis* Bruguiere
**Atrina pectinata* (Linnaeus)
Barbatia bicolorata (Dillwyn)
Callista chinensis (Holten)
**Chama reflexa* Reeve
Chlamys nipponensis Kuroda
Chlamys irregularis (Sowerby)
Claudiconcha japonica (Dunker)
Cyclina orientalis Sowerby
Donax cuneatus Linnaeus
Excellichlamys spectabilis (Reeve)
Fulvia papyracea (Bruguiere)
**Grafrarium divaricatum* (Gmelin)
**Lutraria arcuata* Reeve
Mactra ornata Gray
Mactra veneriformis Reeve
Meretrix lusoria Röding
Mytilus crassitesta Lischke
Ostrea folium Linnaeus
**Oxyperas bernardi* (Pilsbry)
Paphia vernicosa (Gould)
Periglypta puerpera Linnaeus
**Pinna attenuata* Reeve
Plicatula muricata Sowerby
Protothaca jedoensis (Lischke)
Sanguinolaria olivacea (Jay)
Semele zebuensis (Hanley)
Septifer keenae Nomura
Solecurtus divaricatus (Lischke)
Solen gouldi Conrad
Sunetta menstrualis (Manke)
Vasticardium arenicolum (Reeve)
Venerupis japonica (Deshayes)

Gastropoda

Angaria rugosa (Kiener)
Astraea haematraga (Menke)
Batillaria multiformis (Lischke)
Bulla vernicosa Gould
Calliostoma unicum Dunker
Cellana stearnsi (Pilsbry)
Cellana testudinaria (Linnaeus)
Cellana toreuma (Reeve)
Cerithium pfeifferi Dunker
Charonia tritonis (Linnaeus)
**Chicoreus ramosus* (Linnaeus)
Clanculus margaritarius (Philippi)
Clavus sp.
Clithon sowerbianus (Recluz)
Columbella versicolor Sowerby
**Contumax kobelti* (Dunker)
Conus sp.
Crepidula aculeata (Gmelin)
Cymatium sp.
**Cypraea vitellus* Linnaeus
**Ergalatax contractus* (Reeve)
Erosaria caputserpentis (Linnaeus)
Erronea cf. *interrupta* (Gray)
Erronea chinensis (Gmelin)
Ficus subintermedius (d'Orbigny)
Haliotis discus Reeve
Littonia brevicula Philippi
**Littorinopsis scabra* (Linnaeus)
Mauritia arabica niger (Roberts)
Melampas caffer (Küster)
**Monodonta labio* Linnaeus
Nassarius caelatus (A. Adams)
Nassarius glans (Linnaeus)
Natica maculosa Lamarck
**Nerita polita* Linnaeus
Olivella fulgurata (Adams & Reeve)
Patelloida saccharina Dunker
Phalium strigatum (Gmelin)
Phalium sp.
Pisania ferrea (Reeve)
Pisania ignea (Gmelin)
Polinices didymus Röding
Purpura bronni Dunker
Purpura clavigera Küster
Pyrene cf. *impolits* (Sowerby)
Pyrene cf. *lifouana* (Hervier)
Pyrene varians (Dunker)
Rapana thomasiana Crosse
Semicassis pila (Reeve)
Serpulorbis trimeresurus Oyama
Sinum sp.
Siphonalia fusoides (Reeve)
Siphonalia ornata A. Adams
Siphonalia signum (Reeve)
Siphonaria sirius (Pilsbry)
Siphonalia sp.
Staphylaea limacina (Lamarck)
Strombus isabella Lamarck
Strombus japonicus Reeve
**Strombus luhuanus* Reeve
Tegula argyrostoma lischei (Tapparene-Canefri)
Tegula pfeifferi (Philippi)
Tegula rustica Gmelin
Tegula xanthostogma (A. Adams)
Terebra cf. *hirasei* Vredenberg
Terebra cingulifera Lamarck
Tonna luteostoma Küster
Trochus pyramis (Born)
Trochus rota Dunker
**Turbo granulatus* Gmelin
Turbo cornutus Solander
Umbonium costatum (Kiener)
Umbonium giganteum (Linnaeus)
Umbonium sp.

Unfortunately no scaphopod molluscs were found in the bay at the time of collection, although several species probably occur. Of the molluscs, the amphineurans (chitons or loricates) have not yet been determined, and the octopods were not touched. The above number of molluscs is certain to be increased should dredge operation be undertaken.

Summary

1. Uranouchi Bay represents an area or submergence topography, but there is evidence of recent uplift as shown by the raised shore platforms and low level terraces.
2. Uranouchi Bay of general east-west direction marks the boundary between emergence and submergence topography, that of the former being shown by the smooth and simple coast line north of the bay, and that of the latter is well displayed by the richly indented coast line provided with numerous inlets.
3. The eastern portion of the bay is shallower than its other parts in general, as shown by the annexed depth distribution chart.
4. Shoals are distributed in the eastern part of the bay. Their distribution, size and shapes have changed since 1947.
5. The tidal flats are predominated by *Solen gouldi* Conrad, a species which occurs so abundantly as to be utilizable for can food production.
6. Two types of ripple marks are found on the shoals or tidal flats, one is the irregular ripple and the other is herein named ripplenorium. The newly proposed name is to distinguish it from types previously described from northern Europe.
7. Areas of deposition and non-deposition were recognized within the bay, that of the former occupies the eastern part of the bay east of the line drawn from Fujigasaki to Osaki, and that of the latter is recognized at several places along the southern shore of the bay.
8. It is felt that further studies in the field must be advanced before conclusive remarks can be given.

References Cited

Geological Map of Kochi in the scale of 1 : 50,000. Issued by the Geological Survey of Japan, 1952.

Häntzschel, W., 1938, Bau und Bildung von Gross-Rippeln in Wattenmeer. Senckenbergiana, Bd. 20, No. 1-2, pp. 1-42.

Katto, J., 1952, Studies on the Undifferentiated Mesozoic Complex in the Outer Zone of Shikoku. Kochi Univ., Nat. Sci. Rep., Vol 2, No. 2, pp. 37-46, 2 pls.

Straaten, L. M. J. U. van, 1950, Giant Ripples in Tidal Channels. Tijdschr. Kon. Ned. Aardr. Gen., 2e reeks, 67, pp, 76-81.

Straaten, L. M. J. U. van, 1953, Megaripples in the Dutch Wadden Sea and in the Basin of Arcachon (France). Geol. Mijnbouw, N. S., No. 1, pp. 1-11, 1 pl., 7 text-figures.

Ueda, M., 1948, Hydrobiological Observation on the Uranouchi Bay, Kochi Prefecture, Japan. Jour. Fish. Soc. Japan, Vol 15, No. 4, pp. 190-198.

Ueda, M., 1950, On the Hydrobiological Conditions of Uranouchi Bay as considered from Limological Viewpoint. Res. Bull. Kochi Prefecture, Ed. Res. Ist., No. 1. pp. 1-26.

Explanation to Plate

Fig. 1-A part of the largest tidal flat in the Bay. Ripple marks are well exposed. The people are digging for *Solen*.

Fig. 2-A hole dug into the sand to find the density populatoin of *Solen*.

Fig. 3-Giant ripple marks on the eastern tidal flat. The name of ripplenorium is here proposed for such ripples. The general trend of the crest line of the small superposed current ripples is parallel with that of the underlying larger one.

Fig. 4-Giant ripple marks on the southern part of the eastern tidal flat. These are found on the southern part of the northern part of the same flat.

Fig. 5-Profile on the giant ripple mark shown in Fig. 3.

Fig. 6-Profile of the giant ripple mark shown in Fig. 4.

Fig. 7-Irregular ripple marks on the western tidal flat. These ripples may be the initial stage in development of the ripplenoria.

Fig. 8-Superposed ripple marks on the irregular ripples on the western tidal flat.

1

2

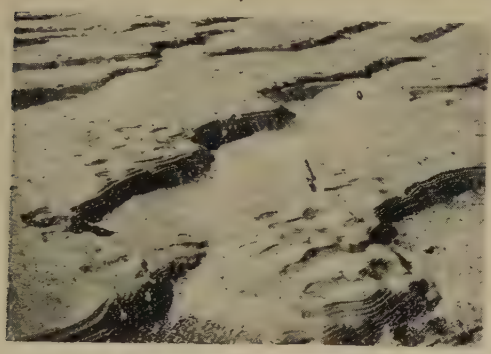

3

4

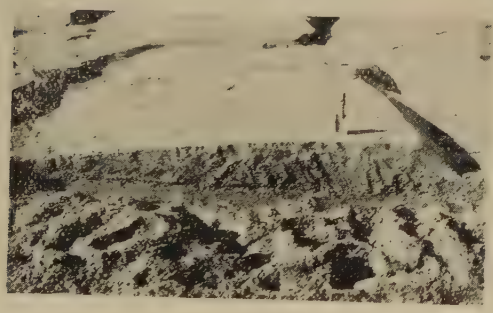

5

6

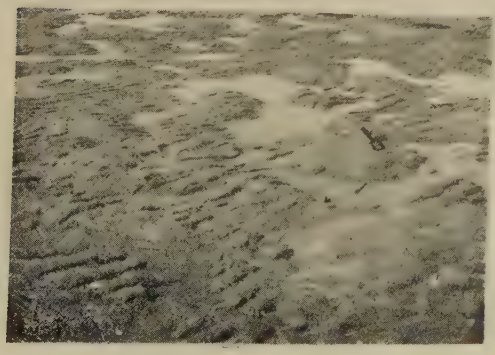

7

8

Bathymetric and Sediment Chart of Uranouchi Bay

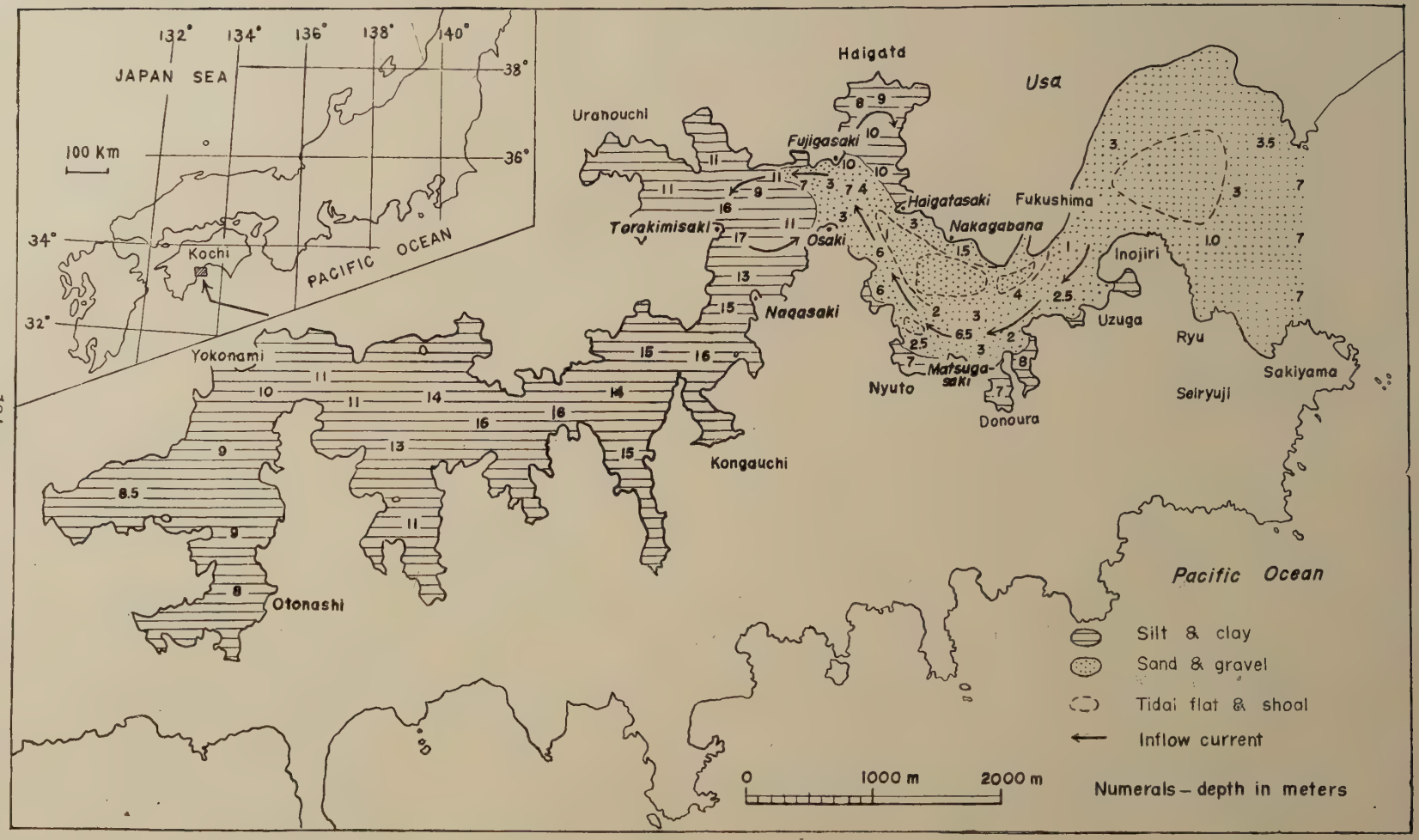

Records of Oceanographic Works
in Japan. Vol. 2, No. 1.
March 1955

On a new Pacific flying-fish, *Prognichthys sealei*, retaining five unbranched fin-rays above in the pectoral throughout life

Tokiharu Abe

(Tokai Regional Fisheries Research Laboratory, and Zool. Inst., Fac. Sci., Tokyo Univ.)

When Seale (1935) described a new species of flying-fish, *Cypselurus zaca*, based on the holotype (No. 5504, Mus. Calif. Acad. Sci., Ichthyol.) from Suva (Fiji Islands) and the single paratype (No. 5505, Mus. Calif. Acad. Sci., Ichthyol.) from Bellona (Solomon Islands), he mentioned passingly about the peculiarity of the pectoral fins of the latter specimen as follows: "The latter specimen seems to have its pectorals malformed, therefore I have taken the one of smaller size for the type." The holotype was 116 mm long, and the paratype was 142 mm long. Comparison of the figures of these two specimens reveals that they are different from one another in the structure of the pectoral fins, and suggests that they may represent distinct species.

Among the flying-fishes presented or sent on loan from many friends of the present writer have been found several young examples and a single mature male resembling the paratype of *zaca* in having about five * unbranched fin-rays above in the pectoral. The writer can not tell for sure if the adult male iust mentioned is identical with the paratype of *zaca*, nor if the latter is conspecific with the young examples just mentioned. However, it is considered necessary to give a new name to the flying-fish retaining five unbranched fin-rays above in the pectoral in the adult. In order not to lead to confusion, the writer describes here *Prognichthys sealei*, new species, taking the adult male (Cat. No. 50474, Zool. Inst., Fac. Sci., Tokyo Univ.) for the type.

***Prognichthys sealei*, new species**

"Daruma-tobi" (new Japanes name)

? *Cypselurus zaca* Seale, 1935, p. 349; *partim*; pl. 21, fig. 2 (Bellona Island, Solomon Is.).

***Holotype*:** Cat. No. 50474, Zool. Inst., Fac. Sci., Tokyo Univ. Fig. 1. Mature male.

* The uppermost fin-ray of the pectoral is difficult to see without removing the skin which covers the pectoral base. The presence of the uppermost rudimentary fin-ray of the pectoral in flying-fishes was overlooked by predecessors and the present writer himself till 1954. It is assumed here that the paratype of *zaca* has this rudimentary fin-ray and that Seale did not count it.

Taken *ca.* 30 miles east of Miyako Island (southern part of the Riukiu Islands) during 0: oo-3: oo a. m., May 11, 1953, by the "Shinshio-maru", a tuna boat. Collected by Mr. S. Kigawa (Nankai Regional Fisheries Research Laboratory). Total length 238 mm; fork length 195 mm; standard length 183 mm.

Proportional measurements. The following measurements are given in hundredths of the standard length: Greatest depth of body (at midway between hind margin of opercle and ventral origin) 19.7, greatest breadth of body (at pectoral base) 15.3, least depth of caudal peduncle 7.7, preventral length (measured parallel to longitudinal axis of body) 58.5, distance between hind margin of opercle and anterior end of ventral base (measured parallel to longitudinal axis of body) 35.5, distance between anterior end of ventral base and base of lower anteriormost rudimentary caudal fin-ray (measured parallel to longitudinal axis of body) 41.0, predorsal length (measured parallel to longitudinal axis of body 73.5, preanal length (measured parallel to longitudinal axis of body 79.2, length of head 24.0, horizontal diameter of eye 7.4 (left) and 7.1 (right), length of snout 6.0 (left) and 6.3 (right), bony interorbital breadth (above centers of orbits) 8.7, length of longest (right 7th*) pectoral fin-ray 63.9, length of longest (3rd from outside) ventral fin-ray 33.3 (left) and 33.9 (right), length of longest (2nd) anal fin-ray 6.8, length of longest caudal fin-ray in upper lobe *ca.* 25.7, length of longest caudal fin-ray in lower lobe *ca.* 32.2; dorsal fin damaged.

General appearance, and color in formalin. The body is rather robust, and the belly is angular along the lateral line. The ventral side of the body is almost flat, or slightly convex, and diminishes in breadth towards the isthmus. The pectoral fin is rather short, its posterior tip reaching the base of the last dorsal fin-ray. The uppermost fin-rays of the pectoral increase in length downwards till the 7th ray (counted from top). The ventral fin, though reaching further back than the pectoral fin, does not reach the base of the anteriormost rudimentary fin-ray of the caudal and ends at midway between the latter and the base of the hindmost fin-ray of the anal. The anal fin begins below the interspace between the 4th and 5th fin-rays of the dorsal, and the base of the hindmost anal fin-ray is below the interspace between the bases of the penultimate and antepenultimate fin-rays of the dorsal. The interorbital space is very slightly concave, and some of the scales there bear minute tubercles which are often observed in the adult of some other species of flying-fishes. The head and eyes are of moderate size. The tongue is rather broad and rounded anteriorly.

The color in formalin is brownish violet, much lighter below. The upper (or inner) side of the pectoral fin is brownish down to the 11th* fin-ray

* The left pecforal fin has been partly damaged; length of the left 8th ray (the uppermost rudimentary fin-ray of the pectoral being counted) is 60.1.

excepting for the postero-dorsal corner (near the posterior parts of the 6th* and 7th* fin-rays) which is hyaline, and the lower part of the fin is hyaline like the narrow area of the proximal part of the upper fin-rays. The ventral fin are mostly hyaline, the dorsal side of the 3rd and 4th fin-rays being dark grey. The dorsal and anal fins are hyaline. The caudal fin is light brownish, the posterior margin being a little darker. The resemblance in coloration with *Prognichthys tringa* Breder is striking.

Meristic characters. The total number of vertebrae (examined by X-rays) is 44 (*ca.* 29+*ca.* 15) or 43 (*ca.* 28+*ca.* 15). The number of vertebrae before the hind margin of the pelvic girdle (examined by X-rays) is *ca.* 21. The number of vertebrae before the lower limb of the 1st interneural is (examined by X-rays) 25 (or 24), namely, the latter is inserted between the neural spines of the 25th and 26th (or, 24th and 25th) vertebrae.

D. 11 (=i+10, the last fin-ray thick). **A.** 8 (=i+7). **P.** left and right 19 (=*i*+iv+14). **V.** left and right 6 (all segmented and branched).

The number of predorsal scales is 28; that of preventral scales 18; number of scale rows from the upper angle of the gill-opening to the caudal base *ca.* 49; number of scales in a backward oblique row from the dorsal origin to the scale just above the lateral line 1/2 8; number of scales in a forward oblique row from the anal origin to the scale just below the lateral line 3 1/2.

The left branchiostegal membrane covers proximally the right one; the number of the branchiostegals is *ca.* 9 on each side. The number of the gill-rakers on the 1st arch on the left side is 7/1/20; the right ones have not been counted.

Dentition. Teeth are present only in the jaws, arranged in a single row, low, conical, and fairly widely apart from one another. The length of the teeth have not been measured, but it may be said that they are of moderate size.

Paratypes :* Cat. No. 50475, Zool. Inst., Fac. Sci., Tokyo Univ. **Fig. 2.** Total

* It should be repeatedly mentioned here that the uppermost rudimentary fin-ray of the pectoral, which is covered by the skin and hardly visible without removing it, is always counted as one fin-ray in the present paper.

** Besides the two paratypes here listed, the following four small specimens borrowed from Nankai Regional Fisheries Research Laboratory and Nagasaki Prefectural Fisheries Experiment Station are believed to represent the same species:

3 specimens, total length 24.5–31.0 mm, fork length 21.0–26.5 mm, standard length 18.5–24.0 mm. Taken by a surface larva net of "No. 3 Kuroshiwo-maru" at 2°39′N, 128°23′E, during 12 : 40–12 : 55, February 9, 1953. Collected by Mr. S. Ueyanagi.

1 specimen, total length *ca.* 51 mm, fork length *ca.* 45 mm, standard length 42 mm. Taken by a larva net near Hirato I. (near Nagasaki), on June 12, 1954. Collected by some of the staff members of Nagasaki Prefectural Fisheries Experiment Station.

These specimens were returned to their owners some time ago, and the writer wishes to propose not to regard them as the paratypes. The number of vertebrae have not been counted of these specimens which bore no catalogue number.

length 68 mm; fork length 56 mm; standard length 52 mm. Taken at Ōmuro-dashi (south of Bōsō Peninsula), a famous fishing ground for the two forms or species of the Japanese mackerels, during night of May 20-21, 1953. Collected by Mr. M. Igarashi.

Cat. No. 50476, Zool. Inst., Fac. Sci., Tokyo Univ. **Fig. 3.** Total length 50 mm; fork length *ca.* 42 mm; standard length 38 mm. Taken near Izushichitō probably in 1952. Collected by Mr. Y. Kurata.

In the absence of medium-sized juveniles, the writer is not confident of the identity of these young examples with the mature male described just above, yet, as will be seen below, it is highly probable that the former represent young stages of the present new species. The following measurements are given in hundredths of the standard length, and those for the smaller paratype are enclosed in parentheses: Greatest depth of body (a short distance in advance of ventral origin) 20.2 (21.8), greatest breadth of body (at pectoral base) 18.3 (20.0), least depth of caudal peduncle 9.2 (9.2), preventral length* 55.7 (56.6), distance between hind margin of opercle and anterior end of ventral base* 33.7 (32.9), distance between anterior end of ventral base and base of lower anteriormost rudimentary caudal fin-ray* 44.2 (42.1), predorsal length* 71.2 (70.3), preanal length* 76.9 (78.9), length of head 22.1 (23.7), horizontal diameter of eye 10.6 (10.5) on both sides, length of snout 5.8 (5.3) on both sides, bony interorbital breadth (above centers of orbits) 13.5 (13.2), length of longest (7th or 8th) pectoral fin-ray 59.6 (56.6) on left side (both sides), length of longest (3rd from outside) ventral fin-ray 41.3 (38.2 and 39.5) on left side (left and right sides), length of longest (2nd and 3rd) fin-rays 15.0 (*ca.* 15.3), length of longest [2nd (3rd)] anal fin-ray 11.9 (*ca.* 12.6), length of longest caudal fin-ray in upper lobe *ca.* 18.3, length of longest caudal fin-ray in lower lobe *ca.* 29.8.

General appearance, and color in formalin. Compared with the holotype, a mature male, the paratypes differ considerably from it in general appearance; body is more robust, snout much shorter, eyes larger (impinging on upper profile of head), bony interorbital space much wider and more deeply concave, pectoral fins shorter, ventral fins longer, and upper and lower lobes of caudal shorter than in the holotype.

The coloration of the paratypes also differs from that of the holotype; paired fins dark brown, leaving outer margin of upper part of pectoral white, posterior part of dorsal brownish distally, caudal hyaline anal lightly brown (not shown in figs. 2 and 3) posteriorly, and belly darker than back.

Meristic characters. The counts for the smaller paratype are enclosed in

* Measured parallel to the longitudinal axis of body.

Fig. 1

Fig. 2

Fig. 3

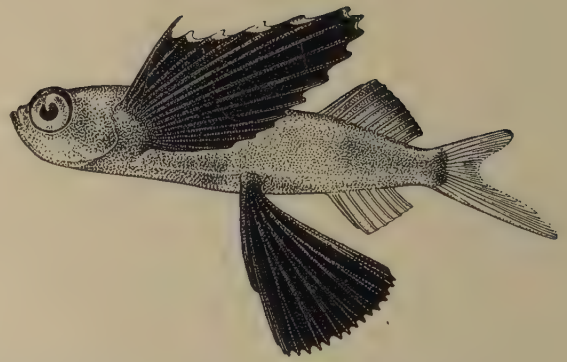

Fig. 1. *Prognichthys sealei*, new species. Holotype (Cat. No. 50474., Zool. Inst., Fac. Sci., Tokyo Univ.), 238 mm in total length. Fig. 2. The same species. Paratype (Cat. No. 50475, of the same institute), 68 mm in total leng th. Fig. 3. the same species. Paratype (Cat. No. 50476. of the same institute), 50 mm in total length. All drawn by M. Shirao.

parentheses. Total number of vetebrae (examined by X-rays) *ca.* 44 (44 or 45).* Number of vetebrae before hind margin of pelvic girdle (examined by X-rays) *ca.* 21 (21 or 22).

D. 11 (11). **A.** 8 (8 or 9). **P.** 19=*i*+iv+14** on both sides (19=*i*+*ca.* iii+15** on left side; 20=*i*+*ca.* v+14** on right side). **V.** 6 (6) on both sides.

Number of predorsal scales *ca.* 26 (ca. 25); that of preventral scales *ca.* 19 (ca. 18); number of scales in a backward oblique row from dorsal origin *ca.* 1/2 8 (ca. 1/2 8); number of scales in a forward oblique row from anal origin *ca.* 3 1/2.

Dentition. Though seemingly a little larger, the jaw teeth are similar in form and arrangement to those of the holotype.

Relationships. The present species is undoubtedly more closely related to *Prognichthys tringa* Breder of the eastern Pacific than to *P. gibbifrons* (Valenciennes) of the Atlantic. The first differs from the second in the retention of five unbranched fin-rays above in the pectoral and in the position of the longest pectoral fin-ray. In the type of *tringa,* measuring 205 mm in total length and 163 mm in standard length, the number of the uppermost unbranched fin-rays in the pectoral is three,† having the 5th† and 6th† pectoral fin-rays longest. The total number of vetebrae in *tringa* is not known.

The present new species resembles *gibbifrons* in the total number of vertebrae, the number of caudal vertebrae and many other characters. They agree to each other in attaining maturity at a small size. In the holotype of the former, the total number of vertebrae (examined by X-rays) is 44 (or 43), and the number of caudal vertebrae (examined by X-rays) is *ca.* 15; in the latter species, according to Bruun, 1935, the total number of vertebrae is 42 (=26+16) and 43 (=27+16;=28+15). Among the apparent differences between the two species are the number of the dorsal and anal fin-rays (smaller in the former species), the number of the uppermost unbranched fin-rays of the pectoral (smaller in the latter species) and body proportions (*cf.* Breder. 1928, p. 22).

On the other hand, the paratype of Seale's *zaca* has five† unbranched fin-rays above in the pectoral, and the 2nd† fin-ray from top of the pectoral is longer than the three unbranched fin-rays below it. In the two paratypes of the present new species, *sealei,* the relative lengths of the uppermost fin-rays of the pectoral differ from those of the paratype of *zaca* and the depth of body seems greater in the former specimens, but speaking generally, the pectoral fins of

---

* Number of caudal vertebrae in the smaller specimen is *ca.* 15.

** Number of the lowermost unbranched rays is uncertain.

† The presence of the uppermost rudimentary fin-ray of the pectoral is assumed here and counted as one.

the paratypes of *sealei* are suggestive of the fin of the paratype of *zaca*. In view of the remarkable changes with advancing age of the structure of the pectoral fin in *Prognichthys* (Fowler, 1944; Herre, 1952), *Hirundichthys* (Bruun, 1935; Breder, 1938; Imai, 1952, 1954) and *Danichthys* (Breder, 1938), the present writer is somewhat doubtful as to the adequacy of always regarding the number and relative lengths of the uppermost fin-rays of the pectoral as the dicisive keys to the genera of flying-fishes. If the remarkable situation of the holotype of *zaca* (which is smaller than the paratype), namely, the number of the uppermost unbranched fin-rays of the pectoral is four (assuming that the uppermost rudimentary fin-ray exists and that it was not counted by Seale) and the length of these fin-rays increase in length downwards, or, if peculiarity of the structure of the pectoral fin in the paratype of *zaca* mentioned above, will prove to be due to individual variation during the development of the pectoral fin, then *tringa, zaca* and *sealei* might turn out to be conspecific.

In this paper the writer assumes that the paratype of *zaca* may be distinct from the holotype of *zaca* and that the adult male of *sealei* first described in the present paper is distinct from the latter. It is not certain whether another new name should be given to the paratype of *zaca* or not.

In regard to the affinity of *sealei* with the members of the so-called *Cypselurus* or the other genera of flying-fishes, it may be stated that *Cypselurus starksi* Abe comes nearest to *sealei*, especially resembling in the form of body, number of vertebrae (in *starksi* total number of vertebrae 43 or 44; number of caudal verbebrae 15) and the position of the hind margin of the pelvic girdle (in *starksi* below the 20th vertebra). If the two small specimens described above represent young stages of *sealei*, this species agrees with *starksi* in the absence of barbels at the standard length of some 40-50 mm. Obvious differences between the two species are the dentition, position of the 1st interneural, number of gill-rakers on the 1st arch, number of pectoral fin-rays, number of uppermost unbranched fin-rays of the pectoral and distribution range. It may also be added here that *starksi* is a coastal form whereas *sealei* seems to be an oceanic one.

Acknowledgments

The study of the flying-fishes of the Pacific and Indian Oceans have been supported by grants-in-aid from the Japanese National Commission for UNESCO. The present writer takes great pleasure in expressing here his thanks to this organization and to Dr. S. Hatai, Dr. K. Hidaka, Dr. W. Nagai and Mr. B. Araya who have enabled the writer to continue the study for their kindness. It is also a pleasing duty of the writer to express here his thanks to Mr. T. Fujita (Chief, Nagasaki Prefectural Fisheries Experiment Station), Mr. Y. Kurata (Tokyo Prefectural Fisheries Experiment Station), Mr. M. Igarashi (Ōshima Branch, Tokyo

Prefectural Fisheries Fxperiment Station), Mr. H. Kan-no (Chief, Hachijo Branch, Tokyo Prefectural Fisheries Experiment Station), Mr. T. Kusakari (of the same branch), Mr. S. Kigawa (Nankai Regional Fisheries Research Laboratory, Kochi), Mr. S. Ueyanagi (of the same laboratory) for their courtesy extended to him in collecting and examining the specimens of the fishes.

References

In addition to the publications referred to by Abe, 1954, the following have been consulted:

Abe, T. 1954. Notes on the flying-fishes of Hachijo Island, with nomenclatorial remarks on the flying-fishes of the mainland of Japan. II. *Cypselurus pinnatibarbatus japonicus*. (With additional notes on *Prognichthys agoo*). Jap. Journ. Ichth., iii, pp. 192-202, 209-222.

——1954a. In Tomiyama and Abe's "Figures and descriptions of the fishes of Japan", vol. 50, pp. 983-996, pls. 196, 197. Tokyo.

Breder, C. M. Jr. 1928. Scientific results of the Second Oceanographic Expedition of the "Pawnee" 1926. Nematognathi, Apodes, Isospondyli, Synentognathi, and Thoracostraci from Panama to Lower California. Bull. Bingham Oceanogr. Coll., ii, art. 2, pp. 1-25.

Herre, A. W. C. T. 1951. Twenty-six noteworthy Philippine fishes. Philip. Journ. Sci., lxxix, no. 2, pp. 137-154.

Imai, S. 1952. Life-histories of the flying-fishes of the genus *Hirundichthys*. Bull. Jap. Soc. Sci. Fisher., xviii, no. 1, appendix p. 2. In Japanese. Abstract of the paper read before the Annual Meeting of Jap. Soc. Sci. Fisher. held in April, 1952.

——1954. On two flying-fishes of the genus *Hirundichthys* Breder and their juveniles from Japan. Kagoshimadaigaku Suisangakubu Kiyo, iii, no. 2, pp. 62-72. In Japanese, with summary in English.

Seale, A. 1935. The Templeton Croker Expedition to western Polynesian and Melanesian islands, 1933. Proc. Calif. Acad. Sci. 4th ser., xxi, no. 27, pp. 337-378. pls. 20-23.

Addition

After the foregoing went to press, a fine frozen example of the adult male of the present new species was presented by Mr. M. Hata, wireless operator of the "Dai-ichi Tōsui-maru", through courtesy of Mr. M. Yamaguchi of the Tōto Suisan Co. The writer wishes to express here his thanks for their kindness. The specimen sailed on deck of he boat just mentioned at 16° 08′ S, 169° 00′ E (east of the New Hebrides) on January 19, 1955. The surface tempeature there was 28°. 0 C～28°. 2 C. The total length 235 mm; fork length 195 mm; standard length 182 mm. Greatest depth of body 34 mm; greatest breadth of body 28.5 mm.

D. 10 (=i+9). **A.** 8 (=i+7). **P.** 19 (=*i*+iv+14) on both sides.

Number of predorsal scales (counted from the one just above the posterior horns of supraoccipital) *ca* 28; number of preventral scales (counted from the one just before the line connecting the ventral origins) *ca.* 19. Number of gill-rakers on 1st arch 5/1/20. Number of branchiostegals on left side 12. Ratio of length of jaw tooth to standard length *ca.* 0, 0011-0. 0013. Jaw teeth are fairly widely apart from one another, and pointed. Color prior to preservation is greyish blue above, silvery below. Pectoral fin-rays are silvery outside (from the 5th ray downwards), and the membranes are dark violet. Postero-dorsal corner and lowermost part of the pectoral are hyaline. Caudal fin dark violet. Dorsal fin light milky white (rays dark grey). Anal fin hyaline. Ventral fin-rays dark violet excepting for the innermost and outermost rays. The membrane of ventral fin partially light violet.

The catalogeu number of this specimen is Abe No. 10195. It is one of the three paratypes of the present new species.

Records of Oceanographic Works
in Japan. Vol. 2, No. 1,
March 1955

Further Notes on the Brachyuran Crustacea of the Hachijo Island

By
Tsune Sakai

(Faculty of Liberal Arts and Education,
Yokohama National University)

The faunal and bio-geographical research of Decapot Crustaceans of the Hachijo Island has been carried out during three exploring tours; the first was in July, 1952, the second in August, 1953; and the third in May, 1954. The result of the first tour was published in an article in 1954,* in which 62 species of crabs, referable to 41 genera and 11 families were enumerated as the principal fauna of this Island. The present paper is concerned with the result of the second and the third exploring tours, and deals with 24 species of crabs, of which one is new to science. Although these species were not obtained in the first tour, they seem not uncommon on this Island ; most of them are tropical and some of course cannot be seen on the Japanese mainland.

The author's gratitude is due to the authorities of the Japan Society for the promotion of Scientific Research, under whose auspices these investigations have been carried out. The author is also grateful to Mr. S. Gamo, the assistant of the Iwa Marine Laboratory attached to the Yokohama National University, through whose constant efforts, many important specimens were collected.

Fam. Calappidae.

Calappa gallus (Herbst).

Cancer gallus Herbst, Krabben, III, iii, p. 46, pl. 58, fig. 1.

Calappa gallus, Sakai 1939, pl. XVII, fig. 2 (lit.).

Material: 1 ♂, Yaene, on the coast near the Tōkaiku Fisheries' Experimental Station.

Distribution : This species mainly ranges along the continental coast of Asia, from the Red Sea to the Far East. In Japan it is known, but locally, from Kagosima to the Izu Peninsula.

Fam. Majidae.

Micippoides angustifrons A. Milne-Edwards.

* Records of Oceanographic. Works in Japan, vol.1, No. 2, New Series, 1954.

Micippoides angustifrons A. Milne-Edwards, 1865, Journ. Mus. Godeffr. I, Crust. p. 254 ; Rathbun 1911, p. pl. , fig. : Sakai 1943, The Zoological Magazin, vol , p. .

Material 1♂, Yaene, near the coast of the Tokaiku Fisheries' Experimental Station.

Distribution : Coetivy, Bonin Isls. and Hachijo Island as reported here.

Fam. Portunidae.

Thalamita admete (Harbst).

Cancer admete Herbst, Krabben, III, iii, p. 40. pl. 57, fig. 1.

Thalamita admete Sakai, p. 321, pl. LXXXV, fig. 1 (lit.).

Material : 1 ♂, Ohkago.

Distribution : This species widely rages in tropical Indo-Pacific ; the northern limit of distribution of this species in Japan is Miyazaki Prefecture.

Fam. Xanthidae.

Xantho (*Leptodius*) *cavipes* (Dana).

Chlorodius cavipes Dana 1852, Proc. Nat. Sc. Philad. p. 79.

Xantho (*Leptodius*) *cavipes* Sakai, 1939, p. 463, pl. XCI, fig. 3 (lit.).

Material: 1 ♂, Sokodo.

Distribution : This species also ranges in tropical Indo-Pacific ; in Japan it has been recorded from Miyazaki, Kagoshima and Bonin Islands.

Paraxanthias elegans (Stimpson).

Xanthodes elegans Stimpson 1858, p. 33 : 1907, p. 47, pl. 5, fig. 3.

Paraxanthias elegans, Sakai 1939, p. 470, pl. LX, fig, 1 ; pl. XCI, fig. 7 (lit).

Material : 3 ♂♂, 2 ♀♀, Ohkataura.

Distribution : A common Japanese species, which ranges on the Pacific side of Japan, from Sagami Bay to Kyushu. It has also been reported from South Formosa and Australia.

Paraxanthias notatus (Dana).

Xanthodes notatus Dana 1952, p. 178, pl. 8, figs. 12 a-b.

Paraxanthias notatus, Sakai 1939, p. 470, text-fig. 33.

Material : 2 ♂♂, 3 ♀♀, Ohkataura.

Distribution : The known localities of this species are : Hawaii, Andaman Sea, Palk Strait, Ceylon and New Caledonia ; in Japan, it has been recorded from Tosa Bay.

Lachnopodus subacutus (Stimpson).

Liomera subacuta Stimpson 1858, p. 32 ; 1907, p. 39, pl. 5, fig. 1.

Lachnopodus subacutus, Odhner 1925, p. 83 : Balss 1934, p. 509 ; 1938, p. 480 (no new locality).

Material : 3 ♂♂, .2 ♀♀ Sokodo ; 3 ♂♂, 4 ♀♀, Borawazana.

Distribution : The known localities are: Loo Choo (type locality), Tahiti, Amboina and the East Coast of Africa. It has not yet been recorded on the Japanese mainland.

Actaea ruppellii(Krauss), juv.

Aegle ruppellii Krauss 1843, p. 28, pl. 1, fig. 1.

Actaea ruppellii, Sakai 1939, p. 491, pl. XCIII, fig. 6.

Material : 1 ♂, Ohkaura.

Distribution : A common tropical Indo-Pacific species ; in Japan, it has been recorded from Sagami Bay, Kôbe, Nagasaki and Bonin Islands.

Etisus (Etisodes) anaglyptus (H. Milne-Edwards)

Cancer anaglyptus H. Milne-Edwards in Cuvier's An. Crust., pl. 11, fig. 4.

Etisus (Etisodes)anaglyptus, Sakai 1939, p. 499, pl. XCVI, fig. 2 (lit.).

Material : 1 ♂, Yaene.

Distribution : This species ranges on the continental coast of Asia, from the Red Sea to Japan ; the northern limit of distribution in Japan is Izu Peninsula.

Etisus (Etisodes) electra (Herbst).

Cancer electra Herbst, Krabben III, ii, pl. 51, fig. 6.

Etisus (Etisodes) electra, Sakai 1939, p. 500, text-fig. 40.

Material : 1 ♂, Ohkataura ; 1 ♂, Sokodo.

Distribution : A common tropical Indo-Pacific speceies ; in the vicinity of Japan, it has only been recorded from Loo Choo.

Chlorodopsis nigrocrinita (Stimpson).

Pilodius nigrocrinitus Stimpson 1858, p. 34 ; 1907, p. 58, pl. 7, fig. 1.

Chlorodopsis nigrocrinita Sakai 1939, p. 504, pl. LXII, fig. 2 ; pl. XCVII, fig. 2.

Material : 1 ♂, Sokodo ; 1 ♀, Ohkataura.

Distribution : This species was originally recorded from Simoda by Stimson, but now it is known from various localities in Indo- Pacific regions.

Chlorodopsis granulata (Stimpson).

Pilodius granulatus Stimpson 1858, p. 34 : 1907, p. 58, pl. 7, fig.2.

Chlldopsis granulata, Sakai 1939, p. 503, pl. LXII, fig. 1 : pl. XCVII, fig. 6 (lit.)

Material : 1 ♀, Borawazawa.

Distribution : This species was also originally recorded from Simoda, and

afterwards from Kagosima and Yakuzima ; it ranges in various localiteis in Indo-Pacific.

Psudozius caystrus (Adams & White).

Panopeus caystrus Adams & White, Samarang Crust., p. 42, pl. 9, fig. 22.

Pseudozius caystrus Miers 1886, p. 142 : Alcock 1898, p. 181 (lit.) : Sakai 1939, p. 514 (no new locality).

Material : 3 ♂♂, 3 ♀♀, Sokodo : Many ♂♂, ♀♀, Ohkataura.

Distribution; The known localities are: Wake Is., Paumotu Isls., Andamans, Laccadive, Mauritius, Bombay and Mekran coast; in the vicinity of Japan it has only been reported from Bonin Isls. by Stimpson.

Epixanthus corrosus A. Milne-Edwards.

Epixanthus corrosus A. Milne-Edwards 1873, p. 241, pl. 9, fig. 1 : Sakai 1939, p. 519, text fig. 48.

Material : 1 ♂, Ohkataura : 1 ♀, Borwazawa.

Distribution : The known localities are : Malay Archipelago, Red Sea, New Caledonia; in Japan it has been recorded from Manazuru in Sagami Bay, Simoda and Kagosima.

Pilumnus scabriusculus Adams & White.

Pilumnus scabriusculus Adams & White 1848, p. 44, pl. 9, fig. 5 : Sakai 1939, p. 533, pl. C, fig. 5 (lit.)

Matetial : 1 ♀, Ohkataura.

Distribution : The known localities are : Philippine, Samoa, Malay Archipelago, Andamanes, coast of India; in Japan it has been recorded from Simoda, Tosa Bay and Kagosima Bay.

Trapezia cymodoce areolata Dana.

Trapezia areolata Dana 1852, p. 259, pl. 15, fig. 8.

Trapezia cymodoce areolata Sakai, 1939, p. 552, pl. C, fig. 5 (Lit.)

Material : 3 ♂♂, 2 ♀♀, Ohkataura.

Distribution : This species ranges widely in tropical Indo-Pacific ; in the vicinity of Japan, it has been reported from Kii Peninsula, Kagosima Bay, Loo Choo and Northern Daitô-zima.

Fam. Ocypodidae

Ocypoda cordimana Desmarest.

Ocypoda cordimana Desmarest, 1825, Conside, Génér. Crust., p. 121 ; Sakai 1939, p. 613, pl. CIV, fig. 1 (lit.)

Material : 4 ♂♂, 3 ♀♀ (all juvenile), Borawazawa.

In the first exploring tour, no representative of sand crabs (Ocypodidae)

was obtained, because the lack of sand beach or estuarine area on this island seems to provide no proper habitat for such crabs. Contrary to our expectations, however, we obtained 4 ♂♂ and 3 ♀♀ specimens of *Ocypoda cordimana* on the beach of Borawazawa, during the second tour. These were all juvenile specimens, the length of the carapace being less than 5 mm, and were found on a very small area of coarse sand deposited temporarily by the shore waves.

In such a small, narrow area, it is probably difficult for the sand crabs to survive until the adult stage. Whether these young crabs originate from the adult females living on the beach of Hachijo Island itself or from those of other localities was not certain to us at that time. Afterwards, however, the clue to the origin of these young crabs was somewhat revealed to us. It does not seem unnatural to cosider that they were conveyed from the Kochi or Kii district (the south west part of Japan) by means of the warm current "Kurosiwo".

According to the information of Asst. Prof. S. Nomura of the Geological department of Yokohana National University, a large quantity of floating timber drifted ashore on to Miyake Island (which is located about 10 miles west of Hachijo Island) during the few days between 13th and 16th of August 1953. This floating timber had obviously come from Kii Peninsula, where a great amount of timber and wood had been carried as a result of the typhoon and heavy rains of 18th August of that year. According to the information of the authorities on Hachijo Island, some such floating timber was also seen on the beach of Hachijo Island at the same period.

It is very probable that the waters near Shikoku and Kii Peninsula join thoes of Hachijo and Miyake Islands by means of the warm current in a period of about 30 days.

Now, the *Ocypoda cordimana* is not uncommon on the coast of Shikoku and Kii peninsula, and some of the larvae of this crab, which are spawned in these areas are probably conveyed to the Hachijo area by the said current. The duration of the larval, pelagic period of the sand crab (*Ocypoda*) is not yet exactly known but that of the shore crab (*Grapsidae*)is, according to Hart (1936)*, 4 to 5 weeks ; the data concerning Grapsidae and Ocypodidae probably do not greatly differ.

It is again probable that some of young crabs after reaching Hachijo Island may try to land on the beach and pass beyond the tidal line, but in the case of the Ocypodidae, such ones find it difficult to survive on the hard beach of the island.

---

* Hart, J. F. L. 1935 : The larval development of British Columbia Brachyura. In Canad. Journ. Res. 12.

Fam. Grapsidae

Metopograpsus messor (Forskal).

Cancer messor Forskal, Descrip. Anim. in itin. Orient. p. 88

Metopograpsus messor, Sakai 1939, p. 654, pl. CVII, fig. 3 (ubi lit.).

Material ; 1 ♂, Ohkataura.

Distribution: This species ranges widely in Indo-Pacific regions. In Japanese mainland, it has not yet been reported. (Balss's locality (1922)-Aomori Bay is doubtful.)

Pachygrasus plicatus (H. Mine-Edwards).

Grapsus plicatus H. M.-Edwards, 1837, Hist. Nat. Crus. II, p. 89.

Pachygrapsus plicatus Sakai, 1939, p. 657, pi. CVIII, fig. p. 4 (ubi lit.).

Material : 1 ♀. Ohkataura.

Distribution: This species also ranges widely in tropical Indo-Pacific regions. It has not yet been reported in the vicinity of the Japanese mainland.

Ptychognathus barbatus A. Milne-Edwards.

Gnathograpsus barbatus A. Milne-Edwads. 1873, p. 316, pl. 17, fig. 4.

Ptychognathus barbatus Sakai, 1939, p. 659, text-fig. 113 (lit.).

Material : 1 ♂, Ohkago ; 1 ♂, 3 ♀♀, Borawazawa.

Distribution : The coast of India and Burma, various localities in Central Pacific. In the Far East it has only been reported from Loo Choo.

Ptychognathus takahasii Sakai.

Ptychognathus takahasii, Sakai 1939, p. 661, text-fig. 115.

Material : 1 ♂, Sokodo ; 4 ♂♂, 2 ♀♀, Borawazawa.

Distribution : Formosa (type locality), Hayama in Sagami Bay, and Hachijo Island as reported here.

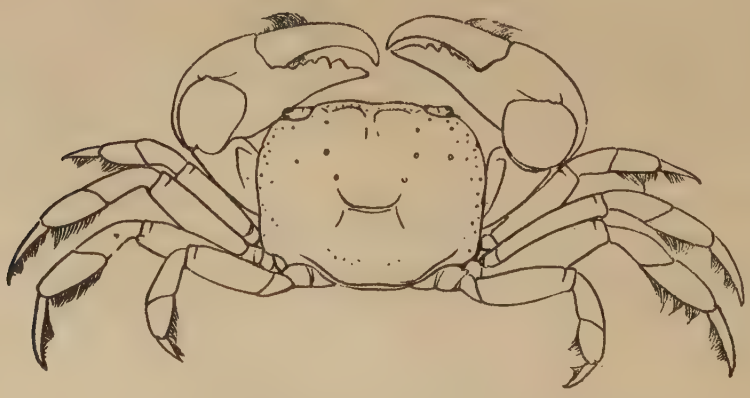

Text-fig. 1. *Ptychognathus hachijyoensis* sp. nov.
Dorsal aspect of male holotype. (×2)

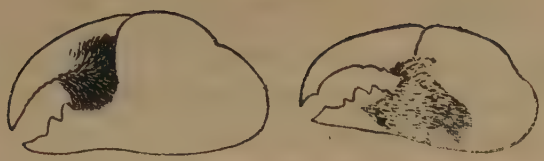

Text-fig. 2. Chela of :
a, *Ptychognathus hachijyoensis* sp. nov.
b, *Pt.* ishi Sakai.

Ptychognathus hachijoensis sp. now.

Material: 3 ♂♂ (one of which is designated as male holotype), 1 ♀ (allotype).

Description of the male holotype : The carapace is perfectly flat and glabrous but the surface near the frontal and lateral borders is obscurely punctate. The frontal margin is sinuate, not much produced beyond the level of the orbits; the two epigastric ridges are obscurely demarcated just behind the frontal border.

The antero-lateral borders are somewhat crested, with a vestige of incision behind the external orbital tooth. The postero-lateral borders are convergent posteriorly; the surface of the carapace near these bordersis depressed but not clearly demarcated. The epibranchial ridge is also very obscure.

The infraorbital ridge bears 10 to 11 tubercles, which are depressed and obscure ; in *Pt. ishii*, which is the nearest kind of this species, it is furnished with 10 to 12 pearl-shaped tubercles.

The external maxillipeds are almost identical with those of *Pt. ishii* in general aspects, the exognath being foliaceous in shape, distinctly broader than ischium, and the merus extremely auriculated at antero-external angle, mueh broader than long.

Chelipeds are stout and symmetrical, the arm and wrist are unarmed, the inner angle of the latter blunty cristate but never forming a tooth. The chela is furnished with a tuft of hair on the outer proximal surface, the hair does not extend toward the inferior surface of the palm. The fingers are not much gaping, the immovable finger bears four blunt teeth, of which the proximal two are very small, the movable finger bears about nine small, blunt teeth, of which the distal 3 or 4 are indistinct. The tip of both fingers is slightly hooked.

Length of the Carapace 12.5mm, width of same 10.5mm.

Relationship : The new species is closely related to *Pt. Ishii*, Sakai and *Pt. glaber*, Stimpson. From *Pt. Ishi* the new species is distinguished by the much more obscure antero-lateral incision and by the different shape of the chela as shown in text-fig. 2. From *Pt. glaber*, it is distinguished by having a tuft of

hair at the base of the chela.

Pseudoguapsus albus Stimpson.

Pseudoguapsus albus, Stimpson 1858, -. 104 : 1907, p. 127. Tesch 1918, p. 99 (lit.) : Sakai 1939, p. 666 (no new locality).

Material : 2 ♂♂, 3 ♀♀, Borowazawa, under stones on upper tidal zone.

Distribution : Kikaisima, Loo Choo (type locality), East coast of Indian Archipelago, New Caledonia and Fiji Isls. It has not yet been recorded in Japanese mainland.

Fam. Gecarcinidae.

Epigrapsus notatus (Heller).

Grosodes notatus Heller 1865, p. 58, pl. 5, fig. 2.

Epgrapsus notatus, Tesch 1918, p. 134 (lit.).

Material : 1 ♀, Borowazawa. This species lives in the crevices or the rock, not far from the beach where the fresh water is dropping down.

Distribution : The known localities are : Nicobar Isls. (type locality Heller, and Alcock), Pulu weh, north of Sumatra (Tesch), Morotai, near Halmahera (de Man), and Samoa (Miers). The record of occurrence of this species in the Far East is new!

Literature cited

ADAMS, A. & WHIT, A. 1848 : Zoology of the voyage of H. M. S. Samarang. Crustacea. Part 1.

BALSS, H. 1922 : Ostasiatische Decapoden. In : Arch. Naturg. Bd. 88. IV. Die Brachyrhynchen (Cancridea), 1922.

_____ 1934 : Die Krabben der Reise J. W. Harms nach der Christmas Insel und dem Malayischen Archipel. In : Zooi. Anz. Bd. 106.

_____ 1938 : Die Decappoda Brachyura von Dr. Sixten Bocks Pazifik-Expedition 1917-1918. In : Götebotgs Kungl. Vet. Vitterg.-Samh. Handlingar. Femte Föjjden, ser. B. Bd. 5, no. 7.

DANA, J. D. 1852 : United States Exploring Expedition, Crustacea.

EDWARDS, A. M. 1873 : Faune carcinologique de la Nouvelle Calédonie. II. Portuniens, Cancériens, Catometops. In : Nouv. Arch. Mus. tome 9.

HELLER, C. 1865 : Die Crustaceen. In ; Reise der oesterr. Fregatte "Novara" um die Erde, Zool Teil Bd. 2, Adt. 3, Wien

HERBST, J. W. 1790 : Versuch einer Naturgeschichte der Krabben und Krebse. Bd. 1.

ODHNER, T. 1925 : Monographierte Gattungen der Krabbenfamilie Xanthidae, 1. In : Göteborg. Vet. Handl. vol. 29, no. 1.

RATHBUN, M. J. 1911 : The Percy Sladen Trust Expedition to the Indian Ocean in 1905, vol, 3, no. 11. Marine Bracyura. In : Trans. Linn. Soc. London, Zool. (2), xol 14.

SAKAI, T. 1937 : Studies on the Crabs of Japan, II. Oxyrtamata, in Sc. Rep. Tokyo Bunrika Daigaku, vol. 2, Suppl. No. 1.

_____ 1938 ; Ibid, III. Brachygnatha, Oxyrhyncha, Yokendo, Tokyo.

_____ 1939 : Ibid, IV. Brachygnatha, Brachyrhyncha, Yokendo, Tokyo.

STIMPSON, W. 1858 ; Prodromus descriptionis animalium evertebratorum, 4. In ; Proc. Ac. Nat. Sc. Philad. 1858.

_____ 1907 : Report on the Crustacea, Bdacyura and Anomura collected by the North Pacific Exploring Expedition 1858-1856. In : Smiths. Misc. Coll., Vol. 49.

Records of Oceanographic Works
in Japan. Vol. 2, No. 1,
March 1955

Distribution of Mopalioid Chitons in the Pacific

by Isao Taki

(National Science Museum, Tokyo)

I. Systematic considerations on the Mopalioid chitons in the Pacific.

The Mopalioid chitons consist of *Mopalia* in the north, *Plaxiphora* in the south Pacific and *Hachijomopalia* in the intermediate region between them.

Thiele (1929) embraced 3 subgenera in *Mopalia,* such as *Dendrochiton, Semimopalia* and *Mopalia* s. str. Of these subgenera, *Dendrochiton* (Berry, 1911) was regarded as a subgenus of *Chaetopleura,* because its features characteristic of the girdle armatures are of similar nature to *Chaetopleura.* Dall (1919) established *Semimopalia* as a subgenus of *Mopalia,* but it should be a member of *Plaxiphora,* because of its minutely decussate tegmental surface and slit-less tail valve. Oldroyd (1927) placed *Basiliochiton lobium* into *Mopalia,* but it seems to be natural to treat it as a member of *Ploiochiton,* which is a subgenus of *Lepidochiton.* Therefore the genus *Mopalia* is so restricted in this paper as to exclude the members of those subgenera as mentioned above.

Plaxiphora is the representative of the Mopalioid chitons in the south Pacific, as having the intimate relationships with *Mopalia* in many points of characteristic features, and divided into 7 subgenera, such as *Aerilamma, Guildingia, Diaphoroplax, Poneroplax. Maorichiton, Frembrya* and *Vaferichiton.* A greater part of them have been treated as distinct genera by certain authors, but it may be acceptable to regard them all as subgenera of *Plaxiphora,* because they are so closely related to one another that they are separable by the mere differences of the mucronal position on the tail valve, the more or less developed apophysis of the median valves and the number of setae and their arrangements on the perinotum. And the setae are all characterized similarly in those subgenera.

As mentioned above *Semimopalia* should belong to *Plaxiphora,* therefore, which consists of 8 subgenera.

II. Distribution of *Mopalia.*

Mopalia is peculiar to both sides of the north Pacific and contains 30 species. There can be classified the possible types of distribution into 6 regions, such as the sub-arctic, the cold temperate, the warm temperate, the wide

northern, the wide southern, the wide ranging and the common northern regions.

1. The sub-arctic region is the environs of lat. 55°N on the Alaskan coasts with the adjacent islands and on the coasts of Saghalien and Primorskaya Province.

There occur 2 species of *Mopalia* on each side of the north Pacific, such as *M. ciliata* and *celetoides* from Alaska and Forrester Island. *M. middendorffi* and *schrencki* are known from the west coast of northern Saghalien and from its opposite coast of Primorskaya Province. These 4 species tend to be cold-tolerant stenothermal chitons, and find their principal development in the cold seas.

2. The cold temperate region is restricted to the coast of Washington on the east, especially to the environs of lat. 45°N with one species, *M. laevior,* while on the west, it extends from lat. 41°N to lat. 45°N, embracing one species, *M. hirsuta.* They are both the stenothermal and the cold-limited forms.

3. The warm temperate region extends from lat. 25°N to lat. 40°N, that is Californian coast on the east, where is rich in species, such as *M. porifera* (Bolinas Bay), *acuta* and *chloris* (Santa Barbara to San Diego), *lionotus* and *lowei* (San Pedro), *phorminx* (Point Pinos) and *chacei* (La Jolla). No species is know from the west side of this region.

4. The wide northern region extends from lat. 45°N to lat. 55°N on the east side, ranging from the Pacific coast of Alaska to Washington of United States. Three species were recorded from this region, such as *egretta* and *elevata* (Forrester Island to Puget Sound), and *goniura* (Port Althrop to Puget Sound). On the western side no species has ever been reported from the region. They are eurythernal, enduring rather cold waters.

5. The wide southern region ranges from lat. 30°N to lat. 50°N, that is the area, extending from Vancouver Island to Lower California on the east side. One species, *M. ciliata,* is only known from the region with a wide range of its distribution. Any species has not ever been reported from the region on the west side.

6. The wide ranging region extends from lat. 25°N to lat. 55°N on the east side, ranging from Alaska to Lower California, where occur 7 species, such as *muscosa* (Shumagin Is. to Rosario), *hindsi* (Sitka to Gulf California), *lignosa* (Sitka to Magdalena Bay), *swani* and *kennerlyi* (Shumagin Is. to Monterey), *imporcata* (Forrester Is. to San Pedro) and *sinuata* (Forrester Is. to San Francisco). On the west side *M. retifera* ranges from Amur Bay, through Tingtao, China, Honshū and Shikoku to the southern end of Kyūsyū. They are all the evident representatives of eurythermy.

7. The common northern region extends from the coast of North America

to Japanese shores. Out of 30 species of *Mopalia,* one is common to the two sides of the northern Pacific, i. e. *M. wosnessenski* has been known from Santa Rosa Island (lat. 38°N), California, through Alaska (lat. 55°N) and Unalaska to Hokkaido (lat. 41.5°N), and cannot extend much more southward on the west side than on the east side, even though it is tremendously vast ranging species in the cold water. Then the ecological conditions, which limit the southward extention of this species at lat. 38°N on the east and at lat. 41.5°N on the west, seem to be similar for this species at both the limiting points of its distribution.

III. Distribution of *Plaxiphora.*

A greater part of *Plaxiphora* have been reported from the southern Pacific and a very few from the Indian and the southern Atlantic. The fauna of *Plaxiphora* in the southern Pacific consists of 19 species and of 4 distributional regions.

1. The tropical region extends from lat. 10°S to lat. 20°S. There occur a few species of *Plaxiphora* in the southern tropics. Three species of *P. primordia*-group have been reported from the Indo-Australian region. One of them, *P. primordia* is only species from northern Queensland on the west side of the tropics.

2. The temperate region extends from lat. 30°S to lat. 45°S. Three species are known from the region on the east side, such as *frembryi* (Valparaiso, lat. 33.6°S), *fernandezi* (Juan Fernandez Is., lat. 33°42′S) and *tricolor* (Lobos Id., lat. 33°S).

On the west side, 12 species have been recorded from the region, such as *P. mixta* (Kermadec Is., lat. 29°15′S), *biramosa, egregia, obtecta, murdochi, caelata, schauinslandi* and *metonomaza* (New Zealand), *costata, albida, paeteliana* and *conspersa* (east, south and west Australia and Tasmania). Those western species are much more variously differentiated in shape and distributed much more widely than those eastern representatives.

3. The sub-antarctic region extends from lat. to. 50°S to lat.55°S, including those areas from southern Chile to Magellan Straits on the east side, but on the west, there is not only a habitat, but also without any species in the region. There occur 2 species, such as *P. setiger* and *grisea* from Cape Horn, Magellan Straits.

4. The common southern region, that is the circum-antarctic region, ranges from lat. 35°S to lat. 55°S. *P. aurata* is only species common to both sides of the southern Pacific, occurring from New Zealand, southern terminal region of South America, Falkland Islands and southern end of Africa, Cape of Good-Hope.

IV. The intermediate zone between the 2 distributional areas of *Mopalia* and *Plaxiphora,*

There has been a vacant zone between the north and the south Pacific in distribution of Mopalioid chitons until *Hachijomopalia* is found from the zone. Thus the southern limits of *Mopalia* in its distribution are lat. 25°N on the east and lat. 31°N on the west, and *Plaxiphora* is permitted its northward extention to lat. 10°S. *Hachijomopalia integra* is only species, known from the area where the warm current washes, and related intimately both with *Mopalia* and *Plaxiphora* in many features characteristic of them. Therefore this is very important not only in its systematic position but also in its distribution.

V. Faunistic consideration of Mopalioid chitons.

A. General considerations.

1. Mopalioid chitons consist mostly of littoral species, which may be regarded as faunistic indicators in the littoral region.

2. The faunistic regions employed in this paper do not accord just the same with those of general mollusks, arranged by the previous authors. That may be regarded as Mopalioid chitons are so peculiar in their distributions that they are more sensible for their ecological conditions than any other mollusks. Then the finer conditions of the marine fauna are perceivable by Mopalioid chitons than by any other mollusks.

3. *Mopalia* and *Plaxiphora* are distributed discontinuously in respective habitats, leaving intermediate zone between them.

B. The northern Pacific distribution.

4. Out of 30 species of *Mopalia,* 26 are on the east side, while 5 on the west, then the east side species are about 4.3 times as abundant as the west ones in number.

5. The number of species on the west side is much less than that on the east side, even though there are longer, more irregular coast lines on the west. Then the topographic nature of the coasts seems not to effective upon the distribution and the richness of the species of *Mopalia.*

6. The east coasts of the northern Pacific are richer in species of *Mopalia* as well as in subspecies than the west, therefore there seems to furnish the most favourite a home of *Mopalia* in the east.

7. The east coasts of the northern Pacific are dividuous into 7 regions in their distributions, and of these regions, the west coasts are devoid of the warm-temperate, the wide northern and the wide southern regions.

8. Out of 7 regions on the east coasts, the warm-temperate and the wide ranging regions are by far the richest in species in the northern Pacific, as having 7 in each region. On the west coasts none was found from the warm-

temperate region and only one from the wide ranging region. The differences in fauna between both sides of the northern Pacific are perfectly clear in those 2 regions.

9. Basing upon these facts mentioned above, the faunistic differences between both sides of the northern Pacific may not rather be caused by the topographic nature of the coasts but by the marine conditions.

10. One species of *Mopalia* is certainly common to the 2 shores of the north Pacific.

C. The southern Pacific distribution.

11. Out of 19 species of *Plaxiphora,* 13 species occur in the west Pacific, while 6 in the east. The number of species is about 2.2 times in the west as abundant as in the east, and the coastal lines are much more irregular in the west than in the east, that may be caused by the different distribution of the continents at approximately the same latitude.

12. The characteristic species in the east consist of those which confined to the sub-antarctic region, while those in the west to the tropical region.

13. The temperate region is by far the richest in species on both sides of the southern Pacific, but the species are large disparity in number on both sides, thus 11 on the west, while 3 on the east. Then there can be found some evolutional differences in *Plaxiphora* between 2 coasts of the southern Pacific.

14. One species and one subgenus, out of 9 subgenera of *Plaxiphora*, is only commn to both sides in the common southern region.

15. *Plaxiphora* is strikingly differentiated into peculiar subgenera at Neozelanic coasts.

16. Two subgenera of *Plaxiphora* are known from the east coast, one of which, *Semimopalia,* is highly specialized of all the subgenera of *Plaxiphora.*

17. *Aerilamma* is the most primitive group of all subgenera of *Plaxiphora* and confined to the tropical region.

D. Comparison between the southern and the northern Pacific.

18. *Mopalia* is peculiar to the northern and *Plaxiphora* to the southern.

19. No common species or even a genus to both the hemispheres can be found, then 2 genera thrive better particularly in each habitat.

20. *Plaxiphora* may be regarded as a little more specialized genus than *Mopalia,* and *Semimopalia* is the highest expression of all subgenera in *Plaxiphora.*

21. Both genera may be considered better fitted for life in the temperate region than any other area.

22. *Hachijomopalia* is a peculliar genus, as having some common features characteristic of *Mopalia* and *Plaxiphora*, and more highly specialized than 2 genera, occurring at the intermediate zone between them.

23. *Plaxiphora* exceeds in morphological characteristics more than *Mopalia*, which is richer in species (30) in the northern Pacific than the former (19), but, which flourishes better in subgenera in the southern Pacific than the latter.

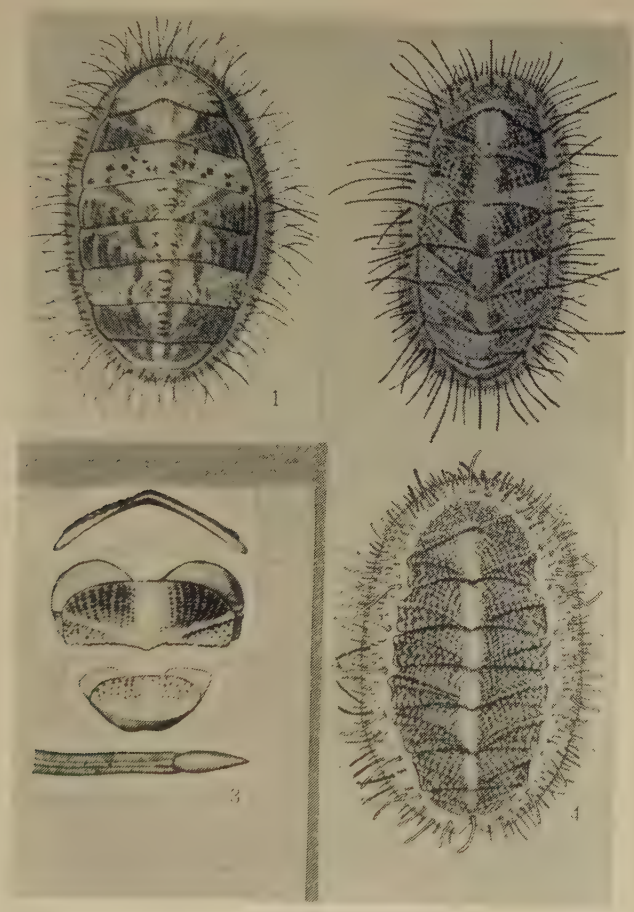

Text-figures

Mopalia of the western Pacific.

1. *M. middendorffi* (Schrenck), Bay of Castries, Primorskaya Province, about 75 m in depth; body 14 mm in length.
2. *M. hirsuta* Taki, Mutsu Bay. Japan, about 60 m in depth; body 9 mm in length.
3. *M. schrencki* Thiele, Gulf of Geduld, Saghalien, 45–60 m in depth; 5th and tail valve, bristle of perinotum, boby 20 mm in length.
4. *M. retifera* Thiele, Inland Sea of Seto, Japan, at about low tide mark; body 27 mm in length.

24. Five species are known from the west shores in the northern Pacific, while 6 from the east in the southern Pacific. North American seas have 26 species, whereas Austro-Neozelanic region 13. Then North American and Austro-Neozelanic regions are plentiful in species, standing at the diagonal positions through the Pacific, while Japanese seas and South America are poor in species, situating at another diagonal positions in the Pacific.

25. All the points mentioned above should be the faunistic features characteristic of Mopalioid chitons in the Pacific.

North Pacific Ocean (*Mopalia*)

region	West coast (Asian)	East coasts (N. American)
sub-arctic (lat. 55°N)	*middendorffi* *schrencki*	*cirrata* *celetoides*
cold temperate (lat. 41°–45°N)	*hirsuta*	*laevior*
warm temperate (lat. 25°–40°N)		*porifera* *acuta* *lionota* *phorminx* *lowei* *chloris* *chacei*
wide northern (45°–55°N)		*egretta* *goniura* *elevata*
wide southern (30°–50°N)		*ciliata*
wide ranging (25-55°N)	*retifera*	*muscosa* *hindsi* *lignosa* *swani* *kennerlyi* *imporcata* *sinuata*
common northern	*wosnessenski*	
sum	5	26
Intermediate region (31°N)	*Hachijomopalia integra*	

South Pacific Ocean (*Plaxiphora*)

region	West coasts (Austro-Neozelanic)	East coasts (S. American)
tropical (lat. 10°–20°S)	*primordia* (*Aerilamma*)	
temperate (lat. 30°–45°S)	*biramosa* (*Diaphoroplax*) *egregia* (*Fremblya*) *obtecta* (*Guildingia*) *murdochi* (*Vaferichiton*) *caelata* (*Maorichiton*) *schauinslandi* (*M.*) *mixta* (*M.*) *metonomaza* (*M.*) *costata* (*Poneroplax*) *albida* (*P.*) *paeteliana* (*P.*) *conspersa* (*P.*)	*frembryi* (*Plaxiphora*) *fernandezi* (*P.*) *tricolor* (*P.*)
sub-antarctic (lat. 50°–55°B)		*setiger* (*Plaxiphora*) *grisea* (*Semimopalia*)
commom southern (lat. 35°–40°–55°S)	*aurata* (*Plaxiphora*)	
sum	14	6

Table showing species of Mopalioid chitons in their distributional regions in the Pacific.

Literature Cited

Allee and Schmidt 1951 Ecological animal geography.

Cooke, A. H. 1927 Distribution of marine Mollusca, Mollusca, Cambridge Natural History, vol. 3, pp. 360–377.

Cotton and Godfrey 1940 Plaxiphoridae, The Molluscs of South Australia, part 2, pp. 541–544.

Iredale and Hull 1926 Plaxiphoridae, A monograph of the Australian Loricates, Australian Zoologist, vol. 4, pt. 3, pp. 164–169.

—— ——1932 Plaxiphoridae, The Loricates of the Neozelanic region, Austr. Zool.. vol 7, pt, 2, pp. 119–136.

Oldroyd, I. S. 1927 Mopaliidae, The marine shells of the west coast of North America, vol. 2, pt. 3, pp. 300–317.

Pilsbry,H. A. 1892 Mopaliidae, Manual of conchology, vol. 14, pp. 293–333.

Schrenck, L. v. 1867 *Mopalia middendorffi*, Reis. Forsch. Amur-land, Bd. 2, S. 259–976.

Taki, Is. and Iw. Taki 1929 *Mopalia retifera*, Studies on Japanese Chitons, (2), Venus vol. 1, pp. 141–153.

Taki, Is. 1938 *Mopalia hirsuta*, Studies on chitons of Mutsu Bay, Sci. Rep. Tohoku Imp. Univ., ser. 4. vol. 12, pp. 323–423.

—— 1953 *Hachijomopalia integra*, Rec. Oceanogr. Works Jap., N. S. vol. 1. no. 2, pp. 60–65.

Thiele, J. 1909 *Mopalia retifera. M. schrenckii*, Revision des Systems der Chitonen, Zoologica, Bd. 22, Hf. 56, S. 30–31.

Records of Oceanographic Works
in Japan, Vol. 2, No. 1,
March 1955

Marine Plankton Copepods from the Hachijo Island, Idzu Is., with Special Reference to their Vertical Distribution

By Sigeru Motoda and Masateru Anraku

(Faculty of Fisheries, Hokkaido University, Hakodate, Japan)

The present studies are based on the materials collected off Kamiminato(33° 12, N, 139° 49' E), east coast of Hachijo Island on August 22nd, 1953. The collection was made by simultaneous serial horizontal tow with ten small nets (12 cm in mouth diameter, 50cm in length and made of bolting cloth equivalent to Nr. 5 Müllergaze), (Motoda & Anraku, 1952) for one hour at about noon under bright sky. The rope carrying a series of nets inclined about 45 degrees and therefore, the depths at which nets were towed were calculated to be about 0, 7, 14, 21, 28, 35, 42, 50, 57 and 64 metre depth respectively.

The nets used were so small in size that large agile plankton animals were not expected to be sufficiently sampled. The plankton animals of medium size were obtained in considerable quantity, the majority of which, by bulk, consisted of copepods, the remainder being a few member of hydromedusae, amphipods, euphausiids, mysids, ostracods, crab larvae, chaetognaths, polychaete larvae, salps, appendicularians, fish eggs and fish larvae. None of phytoplankton was included in the samples.

Seventy-two species of copepods were identified in total (table 1). On their occurrence brief mention will be made referring to the previous reports on the copepod fauna of the present area given by Honjo (1951), Matsue and Komaki (1953), Tanaka (1953) and Anraku (1954a). Three genera, *Gaidius, Gaetanus* and *Pleuromamma* which have been recorded in these previous collections were not found from the present samples probably because of their preference of comparatively deep water (Anraku, 1954a). *Eucalanus elongatus* has been reported from California coast by Johnson (1938) and from Bonin Islands by Anraku (1954a), but the present collection has missed this species. *E. bungii californicus* was not found in the present collection, though it was collected by Tanaka (1953) in the Idzu region. In the present collections four species of *Eucalanus* were obtained, among which *E. attenuatus* was by far prevalant. Both *Haloptilus oxycephalus* and *H. mucronatus* which have been known to be those inhabiting warm water (Mori, 1937) were found in the present collections though small in number. The former species has been also reported from off Sanriku (Anraku, 1952) and near the Aleutian Islands (Anraku, 1954b). Many species of *Corycaeus, Sapphirina* and *Copilia* that are characteristically warm water forms

were found in the present samples.

Individual numbers of copepods occurring at different depths were calculated by grouping into species, or into genera when exact identification was too laborious to make quick estimation (table 2). The distribution of total sum of the copepods through vertical range is given in figure 1. The temperature and salinity curves inserted in figure 1 are those cited from the oceanographic data at the station, 33° 06′ N, 139° 21′ E, on July 9th, 1950 (Tokai Reg. Fish. Res. Lab., 1952, p. 42). Table 2 indicates that most of copepod species generally inhabit the water below about 30 metre depth, very few individuals dispersing above this depth, as shown in the general type of distribution of total copepods in figure 1. The discontinuity of density of water, if present, might result in the upper or lower limit of vertical distribution of plankton, but the temperature and salinity gradient showed that there was no discontinuity within the range from the surface to at least about 60 metre depths. The type of vertical distribution of plankton copepods in general might be largely affected by intensive day light under bright sky, as many previous investigations have proved, the majority of them probably being forced to sink below about 30 metre depths. Some of copepods, however, such as *Calanus vulgaris, Paracalanus, Clausocalanus, Acrocalanus, Oithona, Setella, Oncaea* and *Corycaeus anglicus* were present in considerable number in shallow water as well as in the deep, but the largest concentration was seen in 40-50 metre depth.

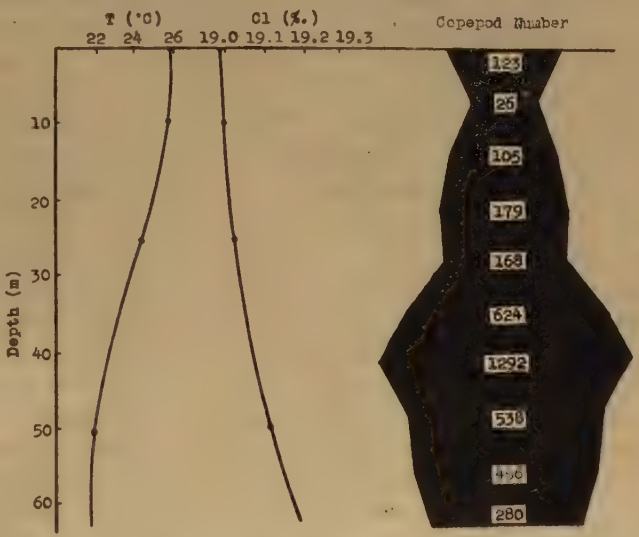

Fig. 1. Relative abundance of total copepods in vertical range

The present observation is confined to show the distribution of copepods in a daytime of particular season, and therefore, no general information on their migratory behaviour can be given, but it is felt to be useful in relation to the feeding depth of some fish which subsist upon copepods.

The present work was rendered possible through the financial support of a grant-in-aid for Fundamental Scientific Research from the Ministry of Education. The authors are much indebted to Drs. S. Hatai and K. Hidaka for giving

facilities for the work. They also thank Mr. H. Kanno of the Hachijo Fishery Experimental Station for his kindness in providing facilities in the sampling. To Mr. H. Takano thanks are due to for help in the sampling at sea.

Table 1. List of copepod species collected

Calanus tenuicornis Dana
C. minor (Claus)
C. vulgaris (Dana)
C. darwinii (Lubbock)
C. pauper Giesbrecht
C. gracilis (Dana)
C. sp.
Eucalanus attenuatus (Dana)
E. mucronatus Giesbrecht
E. subcrassus Giesbrecht
E. crassus Giesbrecht
Rhincalanus sp.
Mecynocera clausi Thompson
Paracalanus parvus (Claus)
P. aculeatus Giesbrecht
Acrocalanus gracilis Giesbrecht
Calocalanus sp.
Clausocalanus arcuicornis (Dana)
C. *furcatus* (Brady)
C. pergens Farran
Aetideus giesbrechti Cleve
Euchaeta marina (Prestandrea)
E. longicornis Giesbrecht
Scolecithricella bradyi (Giesbrecht)
S. orientalis Mori
Scolecithrix danae (Lubbock)
Phaenna spinifera Claus
Centropages violaceus (Claus)
Temora stylifera (Dana)
T. discaudata Giesbrecht
T. sp.
Lucicutia flavicornis (Claus)
L. ovalis Wolfenden
Heterorhabdus papilliger (Claus)
Haloptilus oxycephalus (Giesbrecht)
H. mucronatus (Claus)
Candacia bispinosa Claus
C. bipinnata Giesbrecht
C. truncata (Dana)
Pontellina plumata (Dana)
Acartia erythrea Giesbrecht
A. negligens Dana
A. danae Giesbrecht
A. clausi Giesbrecht
Labidocera acuta (Dana)
Oithona nana Giesbrecht
O. fallax Farran
O. plumifera Baird
O. setigera Dana
O. rigida Giesbrecht
Setella gracilis Dana
Microsetella sp.
Clytemnestra scutellata Dana
Oncaea venusta Philippi
O. conifera Giesbrecht
O. media Giesbrecht
Lubbockia squillimana Claus
Sapphirina stellata Giesbrecht
S. gastrica Giesbrecht
S. gemma Dana
S. opalina Dana
Copilia mirabilis Dana
C. quadrata Dana
C. longistylis Mori
Corycaeus speciosus Dana
C. anglicus Lubbock
C. concinnus Dana
C. longistylis Dana
C. agilis Dana
C. flaccus Giesbrecht
C. catus F. Dahl
C. latus Dana

Table 2. Occurrence of each species of copepods at ten depth zones

Length of rope (m)	0	10	20	30	40	50	60	70	80	90
Depth (m)	0	7	14	21	28	35	42	50	57	64
Calanus tenuicornis							5	4		
C. minor		1	2	3	2	7	41	13	8	6
C. vulgaris	11						8	38	6	1
C. darwinii				1	1	6	15			
C. pauper					2	4	10	5	4	6
C. gracilis				1						
C. sp.							8	3	6	5
Eucalanus spp.				10	4	22	60	23	15	11
Rhincalanus sp.										1
Mecynocera clausi					2	25	22	7	2	3
Para-Clauso-Acrocalanus	20	3	35	55	70	260	440	130	80	75
Aetideus giesbrechti							2	15	20	3
Euchaeta marina						3	3	6		
E. longicornis						6	5	3	6	1
Scolecithrix danae						2	8	3	2	4
Phaenna spinifera					1	1	3	3	1	2
Centropages violaceus			1							
Temora stylifera						1				
T. discaudata				2	2	1	5	2	4	1
T. sp.								1		
Lucicutia flavicornis							11	3	8	
L. ovalis							5	4		3
Heterorhabdus papilliger							2	1		
Haloptilus oxycephalus							3	1	1	
H. mucronatus								1	1	
Candacia bipinnata						4	4	3		
C. bispinosa	1				1	1	4	10	9	
C. truncata						1	4	2		
Pontellina plumata								1		
Acartia spp.	1		3	1	4	6	20	4	2	4
Labidocera acuta					1					
Oithona spp.	3	4	13	7	10	70	70	50	30	20
Setella gracilis	3		9	7	1	7	9	6	4	5
Microsetella sp.	2									
Clytemnestra scutellata							5	3	2	2
Oncaea spp.	27	17	35	75	60	125	400	190	190	85
Lubbockia squillimana						4	2	3	4	2
Sapphirina stellata						1	2			3
S. gastrica						1				1
S. gemma					1	3	1	1	1	

Sapphirina opalina					1				
Copilia mirabilis		3	2		2	5	1		
C. quadrata							2		2
C. longistylis							3		
Corycaeus anglicus with a few other species of *Corycaeus*	55	4	15	6	52	80	25	55	35

Individual number obtained by one hour tow with 12cm net

References

Anraku, M. (1952). Plankton copepods collected by R. S. "Yushiwo Maru" in Pacific waters to the east of northern Japan during her cruise in November 1948. Bull. Fac. Fish., Hokkaido Univ., *3* (1), 31-39. (in Japanese).

——— (1954a). Copepods collected on the whaling grounds off northern Japan and around Bonin Islands. *Ibid., 5* (1), 1-8.

——— (1954b). Gymnoplea copepoda collected in Aleutian waters in 1953. *Ibid., 5* (2), 123-136.

Honjo, K. (1951). Distribution of Copepoda in the adjacent seas of the Izu Islands during winter and spring. Jour. Oceanogr. Soc. Jap., *7* (3-4), 77-87. (in Japanese).

Johnson, M. (1938). Concerning the copepod *Eucalanus elongatus* Dana and its varieties in the northeast Pacific. Bull. Scripps Inst. Oceanogr., *4* (6), 165-180.

Matsue, Y. & Komaki, Y. (1953). The feature of the plankton found in the surrounding area of Myojin-sho. Report on the submarine eruption on Myo-jin-sho. Jour. Tokyo Univ. Fish., *40* (2) Special Number, 22-25.

Mori. T. (1937). The pelagic copepoda from the neighbouring waters of Japan. 150p., 80 pls., Tokyo.

Motoda, S. & Anraku, M. (1952). Observations on the plankton of Funka-Bay, Hokkaido. I. Vertical distribution of plankton at the mouth of the bay in August, 1950. Bull Hokkaido Reg. Fish. Res. Lab., 5, 17-20.

Tanaka, O. (1953). The pelagic copepods of the Izu region. Rec. Oceanogr Wks. Japan, N. S., *1* (1), 126-137.

Tokai Regional Fisheries Research Laboratory (1952). Oceanographical Investigation. (January-December, 1950 collected). No. 74, 1-143.

Chuwa Printing Co. Ltd.